



UNIVERSITÀ  
DEGLI STUDI  
DI PADOVA

UNIVERSITA' DEGLI STUDI DI PADOVA

**Dipartimento di Ingegneria Industriale DII**

Corso di Laurea Magistrale in Ingegneria Meccanica

Progettazione di un sistema stampo per la sinterizzazione e l'estrazione  
senza attrito di una micro ruota dentata in alluminio attraverso processo  
FAST – Field Assisted Sintering Technology

Relatori:

Chiar.ma Prof.ssa Stefania Bruschi (DII)

Ing. Mogens Arentoft (IPU)

Ing. Emil Krabbe Nielsen (IPU)

Emanuele Cannella mat. 1081882

Anno Accademico 2015/2016

## Abstract

Micro-part manufacturing has seen an increasing demand in recent decades. The use of micro components has spread to several fields, from industry applications to instruments of everyday need. Thus, the focus of the producers would be an increase in production with reduced costs of manufacturing processes. In this way, several forming processes have been improved in the last decades; in most cases, the “inspiration” has been taken from the macro-forming processes. However, the adaptation of macro processes into micro has been affected by several problems related to micro size. Size-effect is the definition associated to the scaling down of macro-manufacturing technologies to micro ones. Among several existing-forming processes, sintering represents the best solution to prevent loss of material; thus, the final part is produced by pressing and heating metallic powder. FAST - Field Assisted Sintering Technology is one of the results related to the improvements of the traditional sintering technique. Good quality and net-shape of the sintered part are the main purposes. Among the different problems related to the sintering of micro components, the ejection force represents an important influencing factor. After the process, the friction between the sintered component and die increases the force required in ejection and produces cracks and/or defects on the workpiece. Lubrication is one solution in decreasing friction; however, the part contamination related to the use of lubricants should be taken into account. This project aims at developing and designing a new die-system capable of reducing the ejection force after sintering, which is based on the functional principle of a Micro-FAST sintering process. The system is based on the shrink-fit principle from cold forging; thus, the die results in a pre-stress condition during sintering. The experimental phase has involved the production of a large number of gears either with or without the shrink-fit principle. Then, the resulting-ejection forces have been compared. The experiments also include gears produced in unlubricated condition.

## Preface

*This thesis reports my project work carried out in DTU – Danmarks Tekniske Universitet, Lyngby. The project duration has been 5 months, October 2015 - February 2016. It has represented my final requirement to the Master's degree in Mechanical Engineering. This experience has been possible to me thanks to the University of Padua and the Erasmus+ programme, which allowed me to come in Denmark and have a so wonderful experience. My thanks go to my family: my father Franco, my mother Cettina and my sisters, Miriam and Eleonora, that supported me and my choice of coming here for this long period. In particular Miriam, who had her B.Sc. defence in Industrial Engineering in Catania, while I was here. Sorry for my missing! Thanks to Dr. Mogens Arentoft, for having accepted to be my supervisor, allowing me to have my master's project with IPU group. Thanks to MSc. Emil Krabbe Nielsen, who has helped me everytime, also when he was very, very busy; it was great having you as a co-supervisor. Thanks also to the remaining IPU group, here at the 2<sup>nd</sup> floor of the building 425: MSc. Nikolas Paldan, Jesper Mørkhøj, Dr. Rasmus Eriksen, and Dr. Torben Tang, I have appreciated a lot your cordiality and willingness whenever I have asked you some information or help. On the Italian side, I want to thank my supervisor, Prof. Stefania Bruschi, for helping me to find the right contacts and the support about this project work in Denmark; Prof. P. F. Bariani for the opportunity of carrying out my thesis abroad. I am very thankful to all these people who have welcomed me when I arrived in Lyngby. Finally, I would thank my girlfriend, Livia, who has helped and supported me all this period; thanks also for accepting my choices and the help with the written part of the thesis. Thanks also to her family, Pippo, Loredana, and Gaetano, for the support given from Italy during this period.*

# SUMMARY

---

ABSTRACT .....	1
PREFACE.....	2
SUMMARY .....	3
1. INTRODUCTION .....	6
2. SINTERING .....	8
2.1. Overview .....	8
2.2. Sintering of Metal Powder .....	9
2.2.1. Powder Production .....	9
2.2.2. Pressuring Phase.....	13
2.2.3. Compact Characteristics and Influencing Parameters .....	17
2.2.4. Sintering .....	20
2.2.5. Other Sintering Processes .....	24
2.3. Advantages and Disadvantages .....	26
3. MICRO-FAST .....	28
3.1. Introduction.....	28
3.2. Micro-Scale Overview .....	29
3.3. Micro-FAST Process.....	30
3.3.1. Sintering Process Analysis.....	31
3.3.2. Effects of Coupled Multi-Fields Activation .....	33
3.4. Literature Survey: Main Application of Micro-FAST Sintering .....	34
3.4.1. Forming of Copper Micro-Gears (Dong Lu et al. 2013).....	34
3.4.2. Forming of Micro-Components Using Different Types of Powder (Jie Zhaoa et al. 2015).....	37
3.4.3. Fabrication of MnZn ferrite (Qin 2015).....	39
3.4.4. Fabrication of Hard Alloy: Hardness Investigation (Qin 2015).....	41
4. SINTERING OF A MICRO GEAR .....	43
4.1. Introduction to the Project .....	43
4.2. Project Definition and Boundaries.....	44
4.2.1. Micro Gear Geometry.....	44
4.2.2. Sintering Process .....	45
4.3. Residual Radial Pressure .....	46
4.3.1. Residual Stress due to Powder Compaction .....	46

4.3.2. Residual Radial Pressure due to Thermal Expansion .....	50
4.3.3. Residual Pressure Consequences .....	52
4.4. Problem Solving to Residual Pressure .....	55
4.4.1. Split Die and Thread Forming .....	55
4.4.2. Pre-stressing Tools .....	56
5. CONCEPT MODELLING .....	60
5.1. Introduction.....	60
5.2. Analytical Results on the Gear Expansion.....	61
5.3. Conical-Die Concept .....	65
5.2.1. Tools Analytical Model .....	66
5.4. Die-Ring Design .....	68
5.4.1. Interference Radius Influence .....	70
5.4.2. External Ring Radius Influence .....	73
5.4.3. Interference Influence.....	75
5.5. Die-system 3D modelling.....	77
5.5.1. Gear Punches.....	80
5.5.2. Die-Ring Punches.....	83
5.5.3. Thread Cover.....	85
5.5.4. Ejection Ring.....	86
5.5.5. Other Tool Components .....	87
5.6. Force Estimating .....	89
5.6.1. Analytical Model on Assembling and Disassembling Forces.....	89
5.6.2. Die-Ring Assembling and Releasing .....	90
5.6.2. Compaction Forces and Buckling of the Punches .....	96
5.7. Material Selection .....	98
5.7.1. Die and Ring material.....	98
5.7.2. Other Components Material.....	99
6. EXPERIMENTS AND RESULTS .....	102
6.1. Overview .....	102
6.2. Experimental Set.....	102
6.3. Parameters Optimising .....	104
6.3.1. 1 <sup>st</sup> Series of Experiments .....	104
6.3.2. 2 <sup>nd</sup> Series of Experiments .....	111
6.4. Ejection Force Analysis .....	116
6.4.1. Simplified Conical Concept.....	116
6.4.2. Experimental Procedure.....	119
6.4.3. Force Analysis: Results and Comparison.....	122

6.5. Macro- and Micro-Structure Analysis .....	125
6.6. Unlubricated Samples .....	131
7. CONCLUSIONS.....	134
BIBLIOGRAPHY .....	136
APPENDIX 1: Spring-Die Design	
APPENDIX 2: Datasheets	
APPENDIX 3: Technical Drawings	

# 1. Introduction

Micro-manufacturing engineering indicates a general term which comprises a series of relevant activities within the chain of manufacturing micro/nano-products. The main relevant activities are related to manufacturing methods, technologies, equipment, organizational strategies and systems. Over the last 15 years, there has been an increasing demand on micro-systems and components, e.g., MEMS (Micro Electro-Mechanical Systems), micro-reactors, fuel cell, micro-mechanical devices, micro-medical components, etc., popularly used in vehicles, aircraft, telecommunication, home facilities, medical devices and implants application. Globally, the predicted growth in micro-components demand until 2019 will be around 20% (Qin 2015). In micro-manufacturing, a large variety of processes can be described. Typical processes can be classified into subtractive (Micro-EDM; Micro-ECM; Laser beam machining; Photochemical machining; etc.), additive (Surface coating; Micro-casting; Micro-injection moulding; Sintering; etc.), deforming (Micro-forming, e.g, stamping, extrusion, coining, etc.; Micro-nano imprinting; etc.), joining (Micro-mechanical assembling; Laser welding; Bonding; etc.) and hybrid (Micro-laser-ECM; LIGA combined with laser machining; Micro-EDM and laser assembly; Laser-assisted micro-forming; etc.) (Qin 2015). Among the different micro-manufacturing processes, powder sintering represents a good solution to the manufacturing of components with complex shape and geometry, especially in mass production. Sintering process mainly consists of two general steps: compacting and heating the powder. The most important result is the possibility of obtaining a net-shape part characterised by high quality and shape accuracy. A secondary process, like machining, is not required in most cases. As a consequence, the loss of material and the manufacturing costs will be reduced. In this field, Micro-FAST sintering process is a new developing technique, capable of joining the advantages related to the traditional sintering with a reduced lead time of production. The development of this process starts from FAST sintering, defined as Field Assisted Sintering Technology. The manufacturing field of this one is related to the macro-components. The aim of Micro-FAST is taking the functional principle of this one into the micro-account. This possibility has to be related to the size-effect, which considers the changing of the process parameters due to scaling down of the components, from macro to micro-account. The main characteristic of Micro-FAST sintering, compared to the classical sintering process, consists in the simultaneous applying of heat and pressure. As a consequence, a coupled multi-fields activated forming process (Qin 2015) allows the micro part manufacturing in a reduced time, holding the same

advantages of a sintering process. Additionally, a better part density could be achieved, with the optimisation of the main process parameters, such as temperature, pressure, and heating rate. Different scientific researches have focused on Micro-FAST, in particular on the process parameters, different applications, and main advantages compared to the other manufacturing processes. The forming capability of a copper micro gear has been investigated, with particular regards to the process parameters related to heating rate (Dong Lu et al. 2013). A feasibility study on the different metallic and ceramic powders aims to analyse the capability of the process related to the micro-manufacturing of components made of different material (Jie Zhaoa et al. 2015). Other researchers have investigated on the possibility of obtaining good magnetic property at the end of the sintering by using MnZn ferrites (Qin 2015). Additionally, the capability of sintering due to manufacture components characterised by a high hardness has been investigated. (Qin 2015). This project wants to study, design, and realise a die-system based on the Micro-FAST sintering process due to manufacturing a micro-component. For experimental reasons, a micro-gear has been designed. The compacting phase generates residual pressure to the die-wall interface due to different influencing parameters. As a consequence, frictional forces occur during the ejection phase. The focus of this project is on decreasing these kind of forces through an optimised tooling design, and possibly avoiding any kind of lubrication due to part contamination related to this one. Different solutions have been analysed. After designing phase, a series of different experiments have been realised, in order to verify the compatibility between the theoretical and experimental results. The effects of the main influencing parameters during the process have been analysed, by referring to the results shown by scientific papers as well. During the thesis period, the entire project has been developed with the structures and instruments of the Mechanical Department in Danmarks Tekniske Universitet – DTU, and supported with the technical knowledge and experience of the IPU team (Institute of Product Development – IPU).



## 2. Sintering

### 2.1. Overview

Sintering is one of the most recent technologies in manufacturing processes. The functional principle consists in pressing and then heating powder to obtain the final part. The workpiece does not reach the melting temperature, but the heating allows to generate cohesion between the pressed powder particles due to decreased surface energy and atomic diffusion processes among these ones. A large variety of materials can be sintered; for example, metals, ceramics, and plastics. The process is classified into the powder metallurgy (PM), as a moulding process; however, it has to be considered that sintering comprises also different characteristic from other kind of manufacturing processes. As with forming process, plastic deformation of material is involved. In these terms, the design of the whole mechanical system (die, punches, ejectors..) should be optimized to reach the wanted outcome. Furthermore, the correct sintering temperature should be employed as to optimize the final part quality. Sintered parts result in improved density, strength, electrical, and thermal conductivity. Porosity can be decreased through new sintering technology. During the process, these effects have been increased with a very fine atomization of powder due to a reduced free surface among particles.

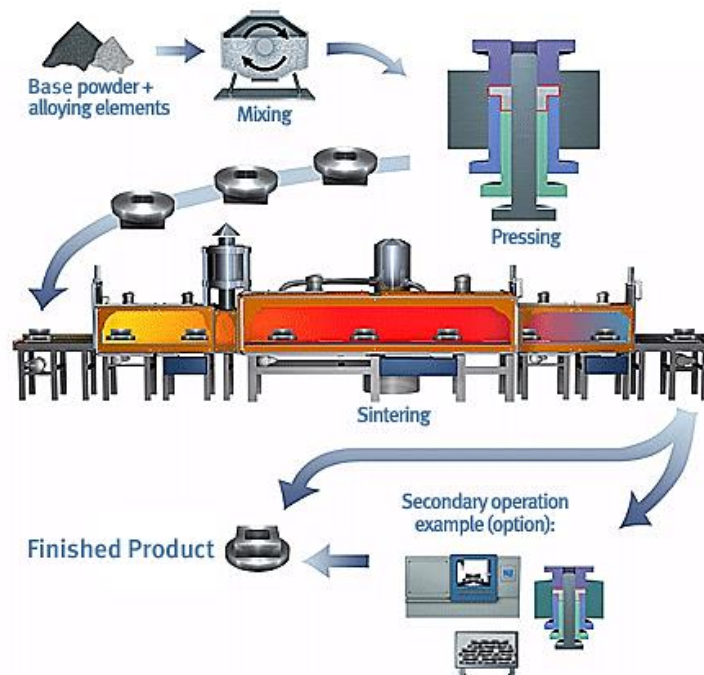


Figure 2.1: Schematic sintering process for a stainless steel workpiece.  
*Note.* From *Aluminium PM Process* (gkn.com).

## 2.2. Sintering of Metal Powder

The process, *figure 2.1*, starts from raw material, metallic powder, in its elemental or alloyed state, with needed shape and size particles. The different density, heat treatments and alloying are the most effective factors of different final products. Not all metallic materials can be sintered; it depends on their contamination resistance between particles surfaces. The use of protective gas or vacuum is useful to avoid contaminations or corrosion under atmospheric pressure.

### 2.2.1. Powder Production

Powder particles are classified according to their chemical properties, size, shape, purity, granulation, and structure of the part. It is possible to classify a variety of mechanical processes relating to powder production, as mechanical comminution, electrolytic method, oxide reduction, and atomization (Colombo 2000). These different methods allow to generate metal powder from different metallic materials as not all can be reduced in granules with the same method.



Figure 2.2: Results of mechanical metal comminution (Colombo 2000).

Mechanical comminution processes consist in the reduction of the materials size. Often directly derived from the extraction place, the raw material is worked through crushing and/or grinding, with an energy-intensive process, thus obtaining smaller sized particles, *figure 2.2*. Crushing machines are influenced in wear and pollution generated by powder; so, they need great strength and resistance.

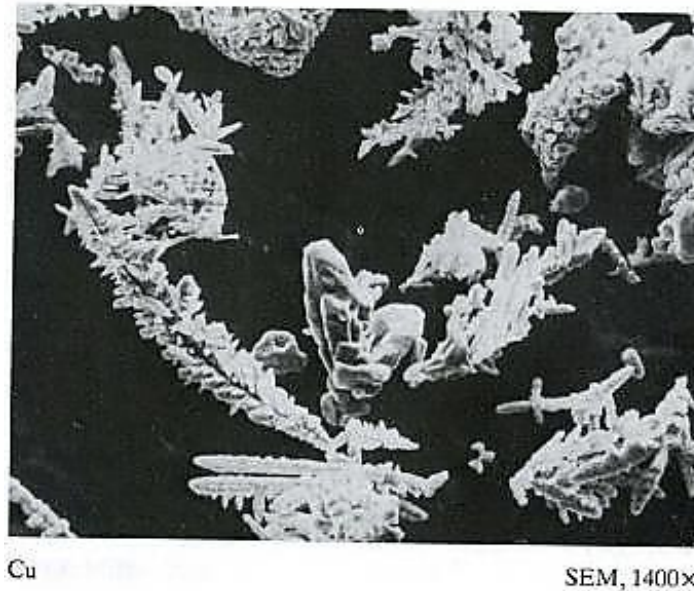


Figure 2.3: Metallic particles due to electrolytic process. (Colombo 2000).

Electrolytic method is based on the metal powder precipitation action from a water solution through a displacement. The incoherent particles, *figure 2.3*, can be easily grinded afterwards.

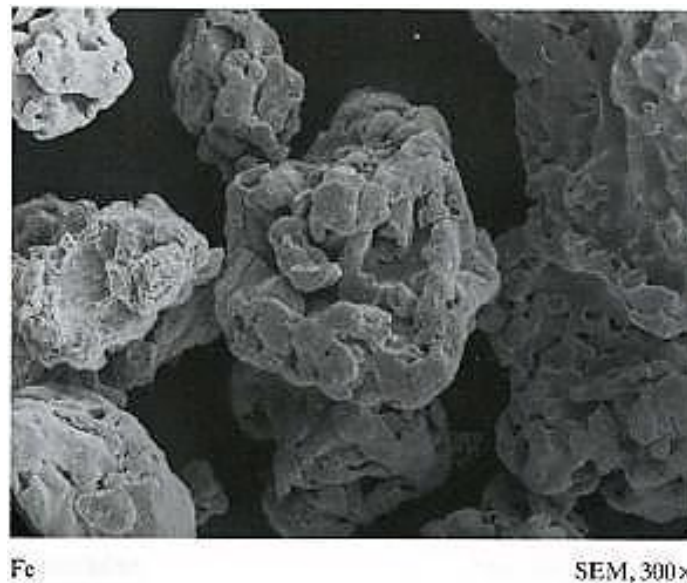


Figure 2.4: Particles produced using oxide reduction (Colombo 2000).

Oxide reduction is possible by using hydrogen, carbon, and carbon oxide. The reduction role of these elements allows to realize chemical reactions. Then, the produced vapour is fast condensed over a cold surface; thus obtaining particles, *figure 2.4*.

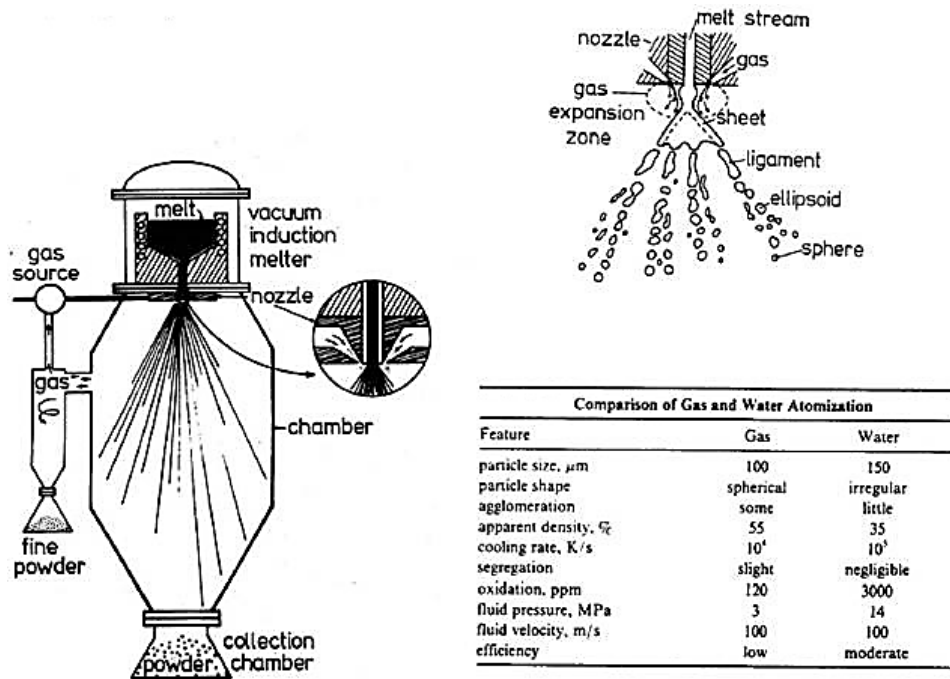


Figure 2.5: Traditional atomization process for metallic powder (Colombo 2000).

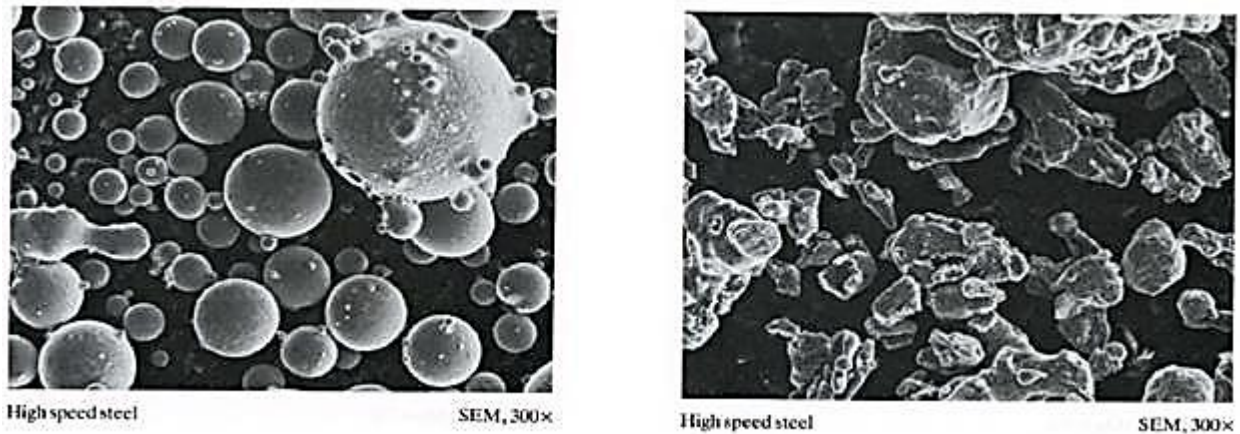


Figure 2.6: Differences in atomization results, gas atomization on the left, water on the right (Colombo 2000).

Atomization is the most widespread method of obtaining metallic powder particles. The process consists in a dispersion of a liquid row using water or inert gas at high pressure. Firstly, the liquid is directly shot by a fluid stream, and secondly, particles falls on the bottom of a container, *figure 2.5*. It is possible to see the final atomization particle depending on the stream type, in *figure 2.6*.

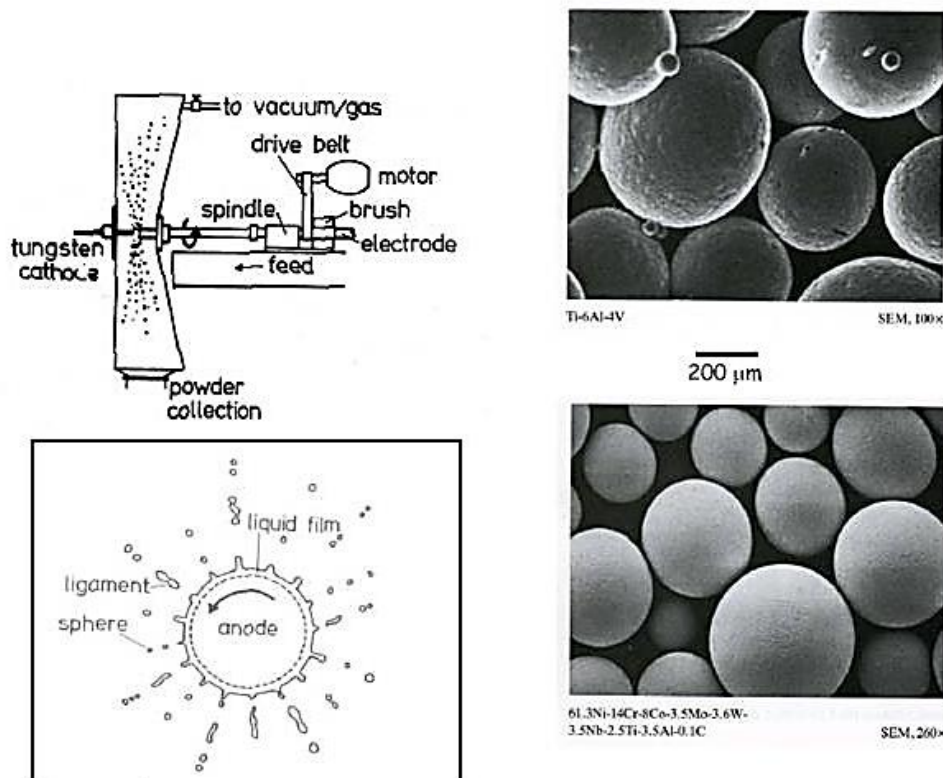


Figure 2.7: Functional principle and final results of centrifugal atomization (Colombo 2000).

A different atomization system based on centrifugal force is also used. The functional principle is based on the high-rotational speed of the rod, while its surface has been heated to the melting temperature, *figure 2.7*. Particles are driven off the rod and collected in a container.

The powder produced can be classified into three different categories:

*Admixed powders;*

*Partially-alloyed powder;*

*Pre-alloyed powders.*

*Admixed powders* are used when there is a requirement of metal particles with a high rate of purity. The word “admixed” indicates the presence of elemental powders, like copper, nickel, and graphite added to the based powders, like iron or copper. Decreased yield strength allows an improvement in green density. However, the homogeneity reached after sintering is worse than the pre-alloyed one. *Partially-alloyed powders*, composed of two or more elements, enhance the compressibility of the base powders. The main characteristics of these ones are represented by the presence of different micro-structures and non-homogeneity. Phase diagrams are useful to control different micro-structures when temperature

varies. Mixing base powders makes possible to obtain a wide range of mechanical properties. *Pre-alloyed powders* are similar to the last ones. The main difference is the production. Instead of mixing different elemental powders, particles are directly produced through atomization, or another PM production process of the alloyed rod. As a consequence, the micro-structure is homogenous and each micro-particle has the same properties. Excellent fracture toughness is possible with this procedure. Other particular properties can be enhanced with the use of supplementary additives.

### 2.2.2. Pressuring Phase

At the beginning of pressing, the powder particles are characterized by their apparent density. The vacancies among particles can reach values of 50-70%. The pressing phase allows to generate the part near its real density. The compact generated is called “green”. Depending on the applied pressure and die/punches material, different final green characteristics can be obtained.

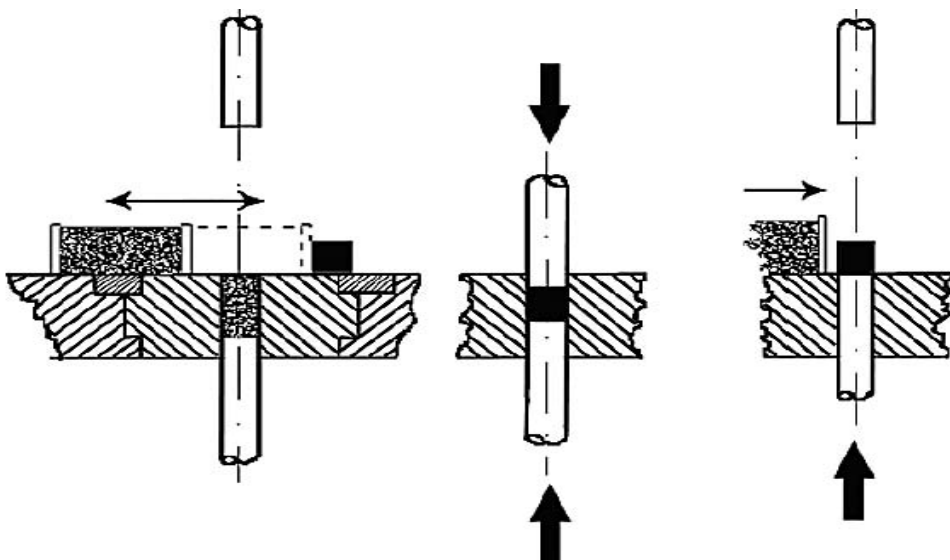


Figure 2.8: Schematic representation of the three stages in compacting powder (Höganäs 2013).

The compaction cycle, *figure 2.8*, can be divided into three stages (Höganäs 2013):

*Filling the dies;*

*Densifying the compact;*

*Ejecting the part.*

The correct relative movements among different tools has to be assured to achieve the final correct piece. In the first filling step, powder falls into the die due to gravity through a feeding shoe or similar system. A wider cross-section facilitates the process. In these terms, a correct filling is done considering the size particles. Commercial powder sizes go from 0.15 mm to 0.2 mm. Experience advices to design

the smallest die feature five times larger than the largest metal particle (Höganäs 2013). Filling problems are related to segregation and inhomogeneous densification, in particular with a complex die concept. After filling, the punches start to compact powder. A “neutral” plane zone is defined as the middle section of compression in which the powder has the lowest density. This is a consequence of compacting process, as powder is better compressed in near punch location. Friction and inhomogeneous filling density does not allow an isostatic pressing. Different kind of pressure system are described in literature.

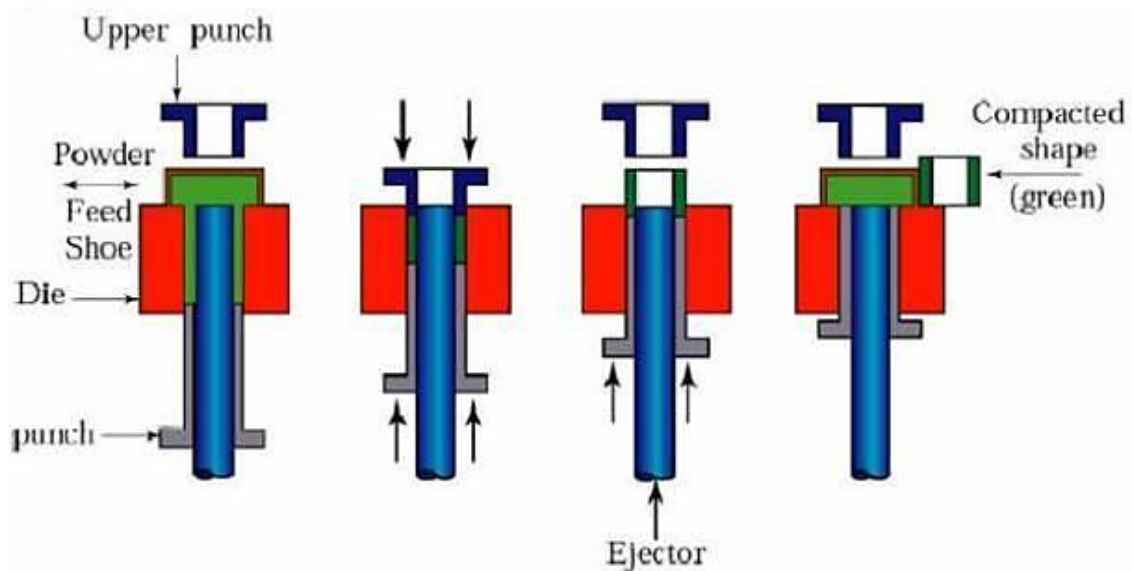


Figure 2.9: Description of a bilateral pressing system (Colombo 2000).

A preliminary classification can be done between unilateral and bilateral pressing. In unilateral pressing, a single punch presses the powder until generating the compact; while in bilateral pressing, *figure 2.9*, there is a simultaneous action of two punches.

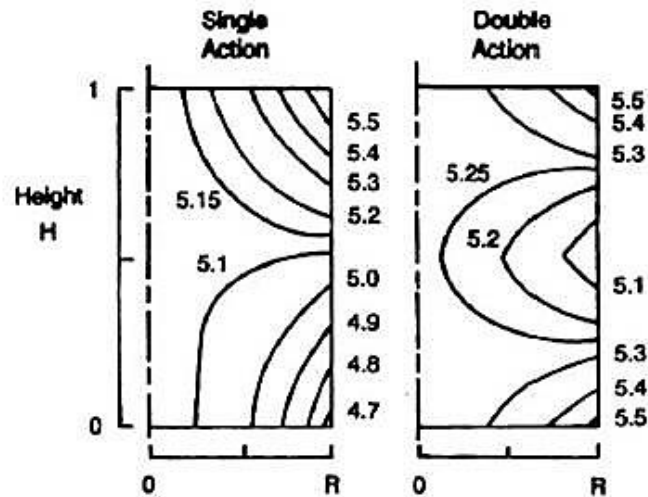


Figure 2.10: Different density homogeneity between single and double punching action (Höganäs 2013).

This second system generates a more uniform density part, *figure 2.10*, in spite of a more complicated punching mechanism. It is worth underlining the different location of the neutral zone for the two different systems; in the bottom of the die for the unilateral punch system and in the middle between punches for the second system, *figure 2.10*.

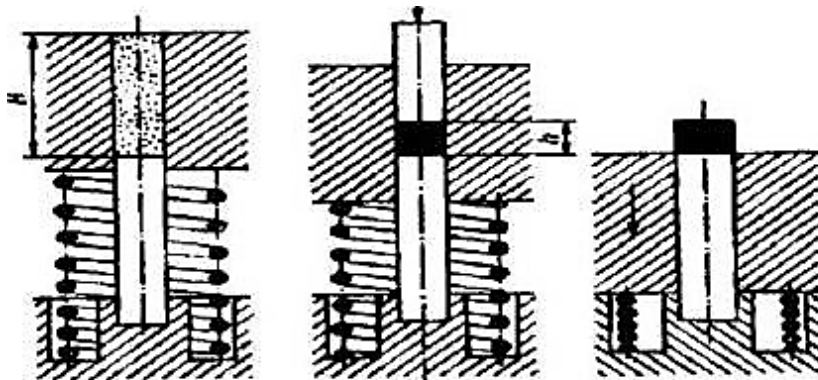


Figure 2.11: Floating die mechanical principle (Höganäs 2013).

A similar two-punches system consists of a floating die, *figure 2.11*, which functional principle is based on moving the die. During the compaction of the powder, the die will be moved against the force exerted by an elastic element, for example a spring. The result is high homogeneity of the compact, without using two different punch mechanisms. This system is not suitable for parts with different height features. A correct design of elastic element is compulsory. As a guideline, it should be noted that a more complex part requires a complex system, too. Multiple-tool system associated with electrical control allows big improvements from this point of view. For a hollowed part, an internal core rod is designed, *figure 2.9*.



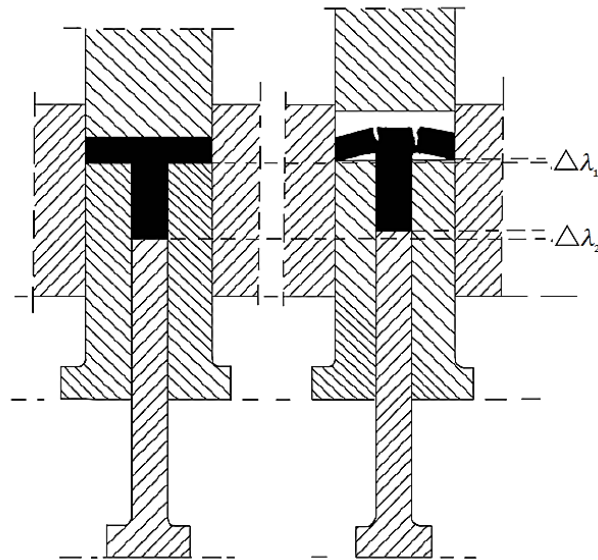


Figure 2.12: Crack occurred due to relative movement between die and punch. Residual force are a consequence of the different thermal expansion (Höganäs 2013).

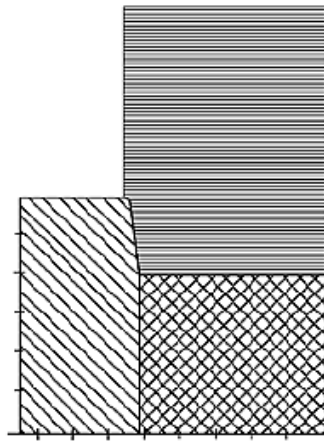


Figure 2.13: Chamfer used to compensate the elastic expansion at the end of ejection (Höganäs 2013).

In the final compacting phase, the part has to be removed from the die. The functional principle is based on the same movement between the die and the compact, but in the opposite direction. Residual stress, friction, and micro-voids are the main crack factors. A homogeneous ejection pressure might be applied on the part in order to withstand any residual pressure inside the die. An eventual relative movement between the die and the part may result in crack, *figure 2.12*. Principally, residual radial pressure implies elastic expansion during the ejection of the part, the so-called spring-back effect. As a consequence, cracks may occur close to the die corners. Chamfers at the top of the die can avoid this kind of problems, *figure 2.13*.

### 2.2.3. Compact Characteristics and Influencing Parameters

During the compaction phase, the different plastic mechanisms involved during powder deformation has to be controlled to obtain a higher material density of the part. In general, three steps can be described (Colombo 2000):

*Powder densifying through redistribution of the particles;*

*Elastic phase;*

*Plastic deformation.*

In the starting step, a feeder shoe provides the correct amount of powder into the die. Then, the punches start compressing; therefore, the particles are reallocated in free space depending on their shape and size. After reallocation, the elastic deformation starts; if pressure will be released in this period, the powder will return to its starting configuration. After elastic deformation, beyond the yield strength limit, plastic deformation starts.

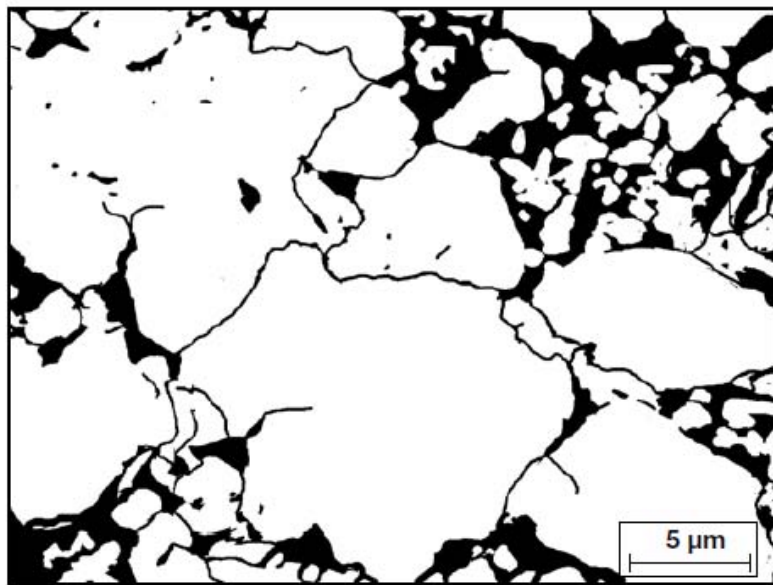


Figure 2.14: Adaptation of surface contours due to plastic deformation, copper powder (Höganäs 2013).

The particles surface continues adapting to each other, *figure 2.14*, and reduces during the process, as a consequence of the shear-stress decreasing. According to the theory of elasticity, considering a hollow sphere under isostatic pressure  $p$  and characterised by its yield strength  $\sigma_0$ , a plastic deformation occurs when the maximum shear stress  $\tau_m$  exceeds the shearing yield stress  $\tau_0 = \sigma_0/2$  ( $\tau_m \geq \sigma_0/2$ ) at the outer surface of the hollow sphere. Considering the Mohr's circles theory at the outer diameter, shear yield strength can be described by  $\tau_0 = |(\sigma_r - \sigma_t)/2|$ .

$$|\sigma_r - \sigma_t| \geq \sigma_0 \quad (2.1)$$

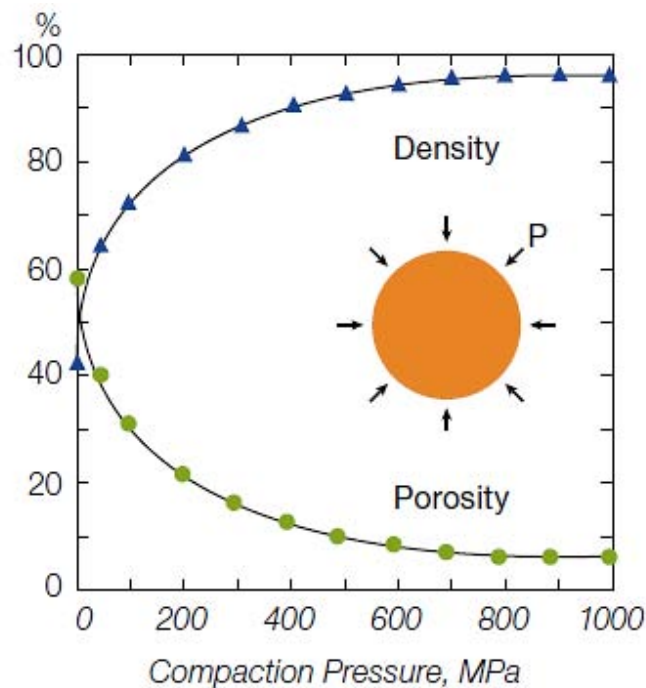


Figure 2.15: Relation between compaction pressure and final density (Höganäs 2013).

The occurred force increases during compaction because of plastic effects, like strain hardening and continuous decreasing of the volume particles. In order to obtain the maximum density, testing the applied pressure is very important. Higher pressure means higher density, *figure 2.15*. However, cost considerations have to be done, in particular about tooling and cycle time. Other influencing factors are encountered by environment, polishing of surfaces, friction, lubrication condition, and tooling design. A controlled environment, using inert gas or vacuum, protects the green from external-undesired-contaminating elements that might compromise the quality of the part. Interface surfaces have to be manufactured with a strict roughness tolerance in order to reduce friction and obtain a high quality. It may be considered that a high roughness is the main contributor in sliding friction, while a very low value of roughness can determine adhesive friction, especially when contact materials has the same characteristics.

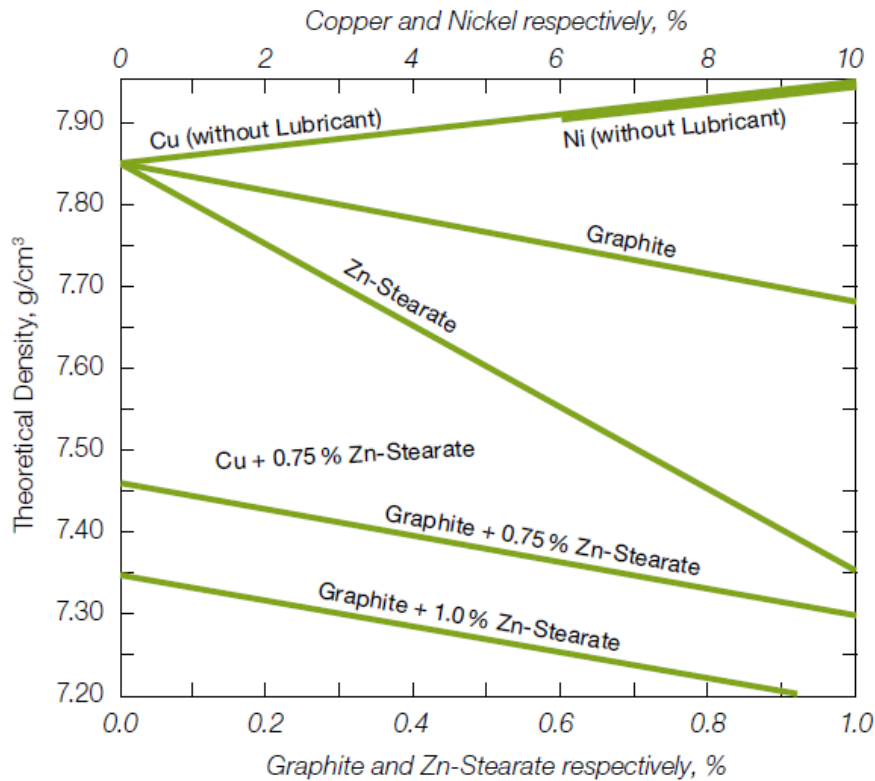


Figure 2.16: Influence of added alloying elements and lubricants on the theoretical (pore-free) density of iron powder mixes (Höganäs 2013).

Lubrication is the best-known solution in decreasing die-wall friction. However, the main disadvantages are represented by the lubricant-fluid infiltration inside the green. The total amount of lubricant cannot be expelled by the part after the sintering process; therefore, the residual quantity might be entrapped inside pores, thus contaminating and compromising the final quality of the part, *figure 2.16*. Tooling design consists in designing the correct geometry, choosing the correct tolerances, and using the correct material. Optimising these parameters is the best way to improve a die configuration, possibly avoiding lubrication or any other additive. The design of a tool has to reach a trade-off with cost, especially if the system need to be employed in series production. Working tools also has to withstand very difficult conditions, due to high pressure, wear, residual stress, and temperatures, in some cases. Whenever is possible, using a symmetrical tool concept ensures a homogeneous applied pressure. Advantages of a correct tool design are linked to time stability of the system, to maintained clearance during several work processes, and to avoided bending of the components. In particular, the parallelism between the die cross-section and punch pressing surface has to be guaranteed. Heat treatments allow the production of fatigue-resistant tools.

#### 2.2.4. Sintering

Sintering is the last part of the process, where compressed powder particles are bound together through different diffusion and atomic mechanisms (Höganäs 2013). Typically, the classic cycle consists in heating the part up to a very high temperature into a furnace; however, depending on the material, temperature has to be below the melting point. Activated from high temperature, the energetic and chemical interactions among particles generate a strong cohesion culminating in mechanical properties improvements. The typical parameters involved in this process can be classified in powders and process dependent. Process parameters are temperature, time, and environment atmosphere. Increasing temperature allows decreasing time, but too high temperature need more maintenance, and machine costs are higher. Standard condition in the example of iron sintering can be 1120-1150 °C for 15-60 minutes. A controlled atmosphere of furnace is the best solution to control oxidation, and avoid residual oxides in the part. Carburization and decarburization control is also important, depending on material (carbon or non-carbon containing material). The most used elements are endogas, hydrogen, cryogenic nitrogen, and cracked ammonia. On the other hand, powder properties, such as particle size, density of the green, and composition, have the same influence. Although it might result more difficult to compress particles for the reasons explained before, see *paragraph 2.2.3*, small-sized ones are preferred for a better sintering process. High density improves mechanical properties, but plastic deformation involved slows the process. Generating a mix of powders improves the properties of the part; but, different microstructures, melting temperature, and chemical properties between the alloyed elements, imply inhomogeneity and longer-process time. Therefore, the conclusion is that main parameters has to be chosen in a way that ensures the right trade-off. Two different kinds of sintering can be distinguished (Colombo 2000):

*Solid Phase Sintering (SPS);*

*Liquid Phase Sintering (LPS).*

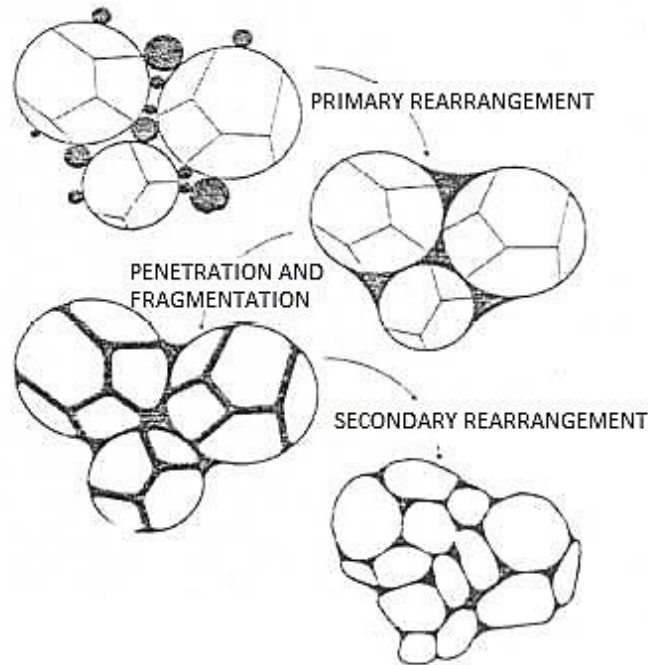


Figure 2.17: Main steps in Solid Phase Sintering (SPS), (Colombo 2000).

Particles are characterized by a high-total-free surface, related to the free surface energy. As it tends to decrease ( $\Delta G_{surface} < 0$ ) during the process, this kind of energy represents the driving force. In solid-phase sintering, it is possible to identify three principle steps, *figure 2.17*. In the first step of *Solid Phase Sintering (SPS)*, grains increase their contact surface in spite of a reduction of pores surface. These ones start getting rounded.

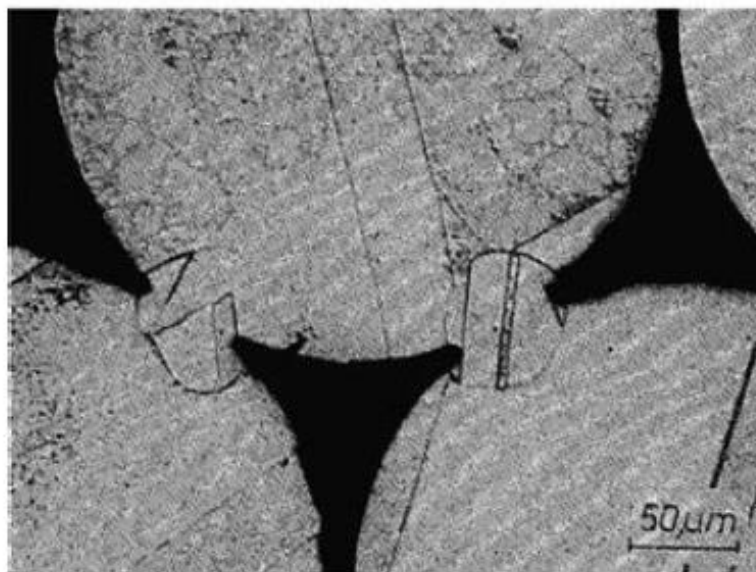


Figure 2.18: Neck formation in sintering process (Höganäs 2013).

Then, powder particles will result joined each other. As showed in *figure 2.18*, neck formation is visible. Experimental studies over necks have been conducted in order to identify the predominant sintering mechanism, for example, volume, grain-boundary or surface diffusion, viscous or plastic flow, and evaporations/condensations of atoms.

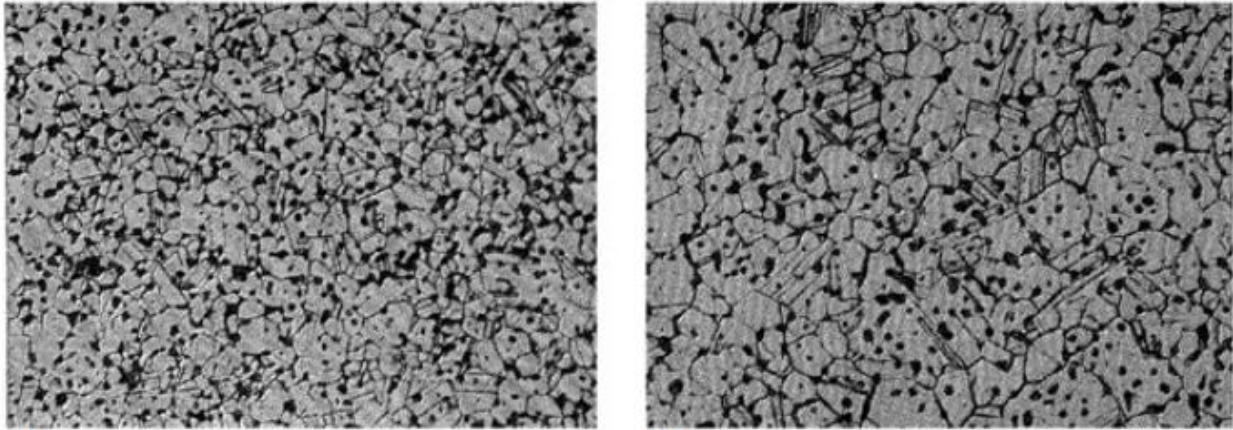


Figure 2.19: Grain size and pore size during iron sintering at 1000 °C. Times: 4 and 8 minutes (Höganäs 2013).

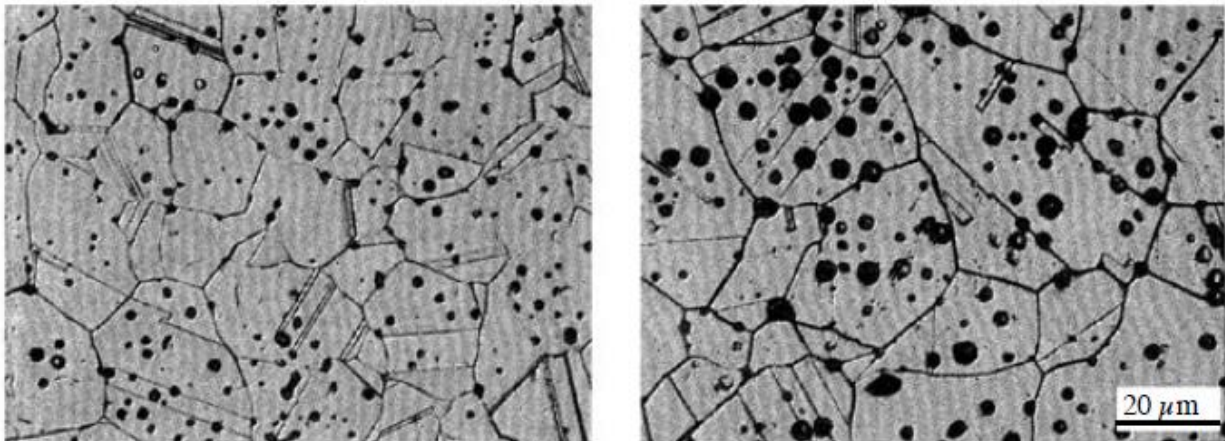


Figure 2.20: Grain size and pore size during iron sintering at 1000 °C. Times: 30 and 120 minutes (Höganäs 2013).

After diffusion, pores starts to join with grain boundaries. When the grain growth increases, pores tend to leave and starts to locate itself alone; this is the so-called “closed porosity”. In the meantime, smaller neighbour pores are included by bigger ones, joined by grain boundaries, or condensed on the surface, *figure 2.19 & 2.20*. The last description has to be considered for homogeneous powder. Due to different particle properties, different considerations have to be done about heterogeneous powder. Difference in particle size has to be considered, too. So, at the beginning of sintering, the distribution of the particles inside the compact is completely unknown. Over the next steps, bounding and homogenization take place at the same time, thus generating a more homogeneous part. The homogenization rate depends on the material diffusion coefficient.

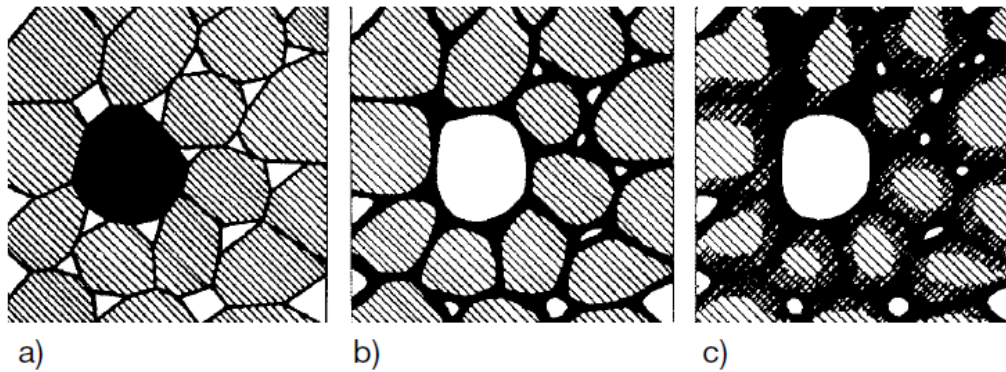


Figure 2.21: Liquid Phase Sintering. Penetrating, alloying and solidifying (Höganäs 2013).

With the presence of a liquid phase, *Liquid Process Sintering (LPS)* takes place. Mixed additives/elements have usually different melting temperatures. One or more among them melts at the sintering temperature; therefore, this is the reason of the presence of the liquid phase. Due to capillarity, the liquid goes around solid particles, thus penetrating the grain boundaries and so as to generate a fast densification. The final part is quite similar to SPS, with growing and fixing of pores. Liquid phase will slowly disappear. *Figure 2.21* represents the main LPS activities. Depending on diffusional mechanism, the part may result increased or decreased in volume. In order to accelerate the process, activated sintering is based on this functional principle. This method is also suitable for these elements presenting difficulties in sintering.

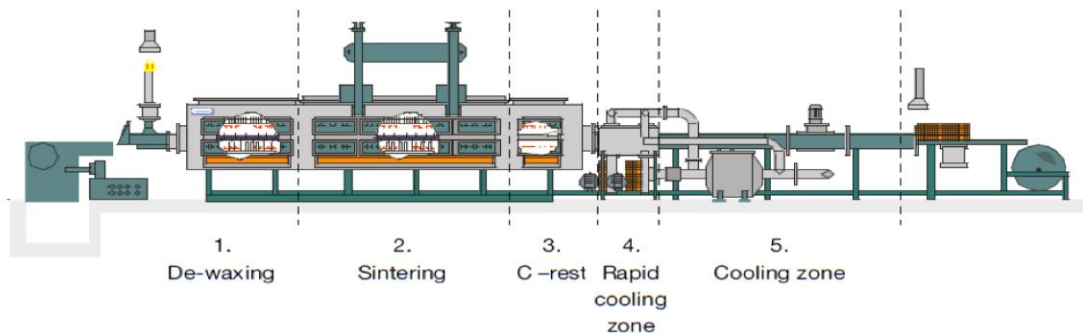


Figure 2.22: Drawing of a sintering furnace (Höganäs 2013).

The whole process is performed inside a furnace. This last is divided into different sectors in order to heat, reach the sintering temperature, ensure the sintering process, and allow the cooling down of the part, *figure 2.22*.



### 2.2.5. Other Sintering Processes

As described before, the two main phases in a sintering process, compacting and heating are designed to be operated separately. Scientific researches and discoveries have determined the possibility to enhance the quality of a sintering process by operating the two phases simultaneously.

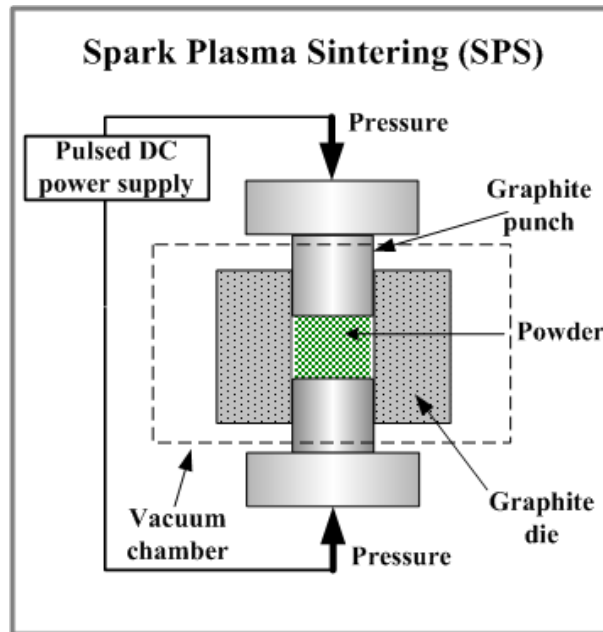


Figure 2.23: Spark Plasma Sintering working scheme. *Note.* From: [www.substech.com](http://www.substech.com).



Figure 2.24: SPS work station. *Note.* From: [www.ifam.fraunhofer.de](http://www.ifam.fraunhofer.de).

The functional principle is based on an electrical field operating among the two punches, through which it is possible to heat the part via Joule effect, *figure 2.23*. The generation of heat is “inside” the part. In order to vary the operating temperature of the part, it is possible controlling the operating electric parameters. If compared to a conventional sintering process, sintering time is decreased; rather than hours, only few minutes are required. Simultaneous application of high temperature and pressure allows a high densification of the part. Metallic powder is directly fed on the sintering chamber. After die closing, punches start to press the part and temperature grows related to a defined heating rate. Less holding time and high-rate temperature allow the reduction of any undesired reaction and contamination. Nano-structures and nano-composites can be generated with a high densification rate and a small number of defects. As a consequence, they result in improved mechanical properties. Spark Plasma Sintering (SPS) is the name associated to this process. Most recent improvements, based on the same functional principle, are represented by Field Assisted Sintering Technique (FAST) and Pulsed Electric Current Sintering (PECS).

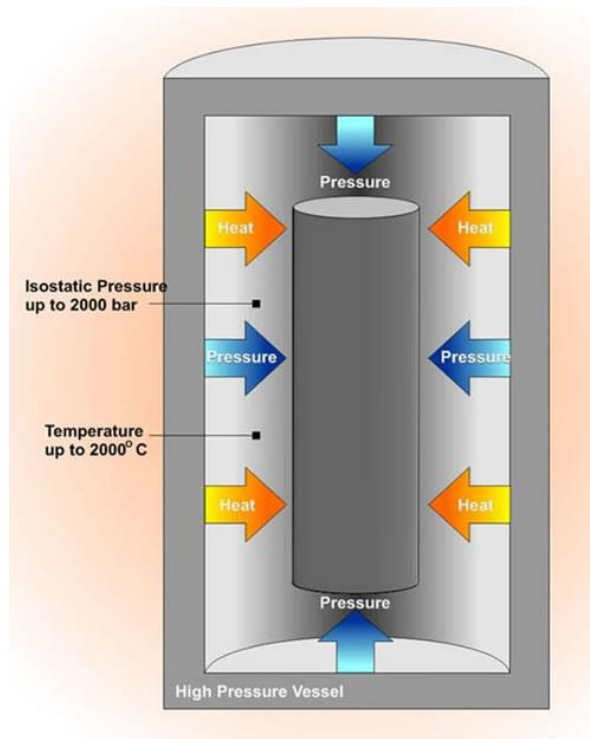


Figure 2.25: Hot Isostatic Pressure scheme. *Note.* From: [www.azom.com](http://www.azom.com).

Another solution is represented by Hot Isostatic Pressing (HIP), where the heat generation is applied “outside”. A pressure chamber provide an equal pressure from all directions (“isostatic”), *figure 2.25*. The main advantages of these processes consist in reduced sintering time, low temperatures, reduced porosity of the final part, and improved fatigue limits of the part.

### 2.3. Advantages and Disadvantages

The main advantages related to sintering process consist in obtaining a net-shape-part, thus avoiding any next secondary-manufacturing process, decreasing the lead time of product, and reducing costs, at least. High surface finishes and tolerance can be achieved.



Figure 2.26: Geometry complex sintered parts. *Note.* From: [www.tuwien.ac.at](http://www.tuwien.ac.at).

The production of complex parts, formed by feature with different height and thickness, is improved, *figure 2.26*. The loss of material due to manufacturing process will be reduced if compared to classic metal forming process. For example, producing a single gear by sintering will avoid the scrap generated by a machining process. The repeatability and reliability of this process allows to conduct production on large scale. Considering this aspect, the savings of material would be considerable. Surely, a correct design of tools is a key factor in order to obtain several production cycles, considering the most fundamental concept rules, based on symmetry, parallelism of surface during compaction, and minimum thickness allowed. The manufacturing capability of a complex geometry allows to reduce assembling components after sintering, thus producing the whole final part. Continuing to describe the sintering process advantages, the characteristic of sintering temperature below the melting temperature of the sintered elements reduces the risk of generating impurities, contamination, oxidation, and grain burn. Considering the part quality, sintering allows to produce parts with a large variety of material composition, depending on the final results desired. Other manufacturing processes need to start from the pre-alloyed rod or billet with a defined composition. Correct pressure allows

to obtain the part density desired. The inner porosity can be an interesting solution for vibration dumping control. Cost considerations are related to the definition of sintering as a very efficient-rapid-prototyping method, allowing functional and geometrical test on the real part, before start of production. The aim of this new sintering method is a large-scale production, not only prototyping. However, some disadvantages has to be encountered. In sintering, a mass consideration is not possible because raw material consists of powders. Prediction of mass should be done depending on the initial and final volume, by trying to take into account all the possible influencing factors, like thermal expansion, residual pressure, and the spring-back of material during ejection, for example. As a consequence, a wrong concept or varied environment conditions may result in cracks or not perfect final-size related to nominal geometry. On the cost side, sintering tools can be more expensive than classic forming tools. A correct prediction of wear and the possibility of withstand several manufacturing cycles are key factors in production investment.

## 3. Micro-FAST

### 3.1. Introduction

Field Assisted Sintering Technology (FAST) is a very recent technology developed by the functional principles of sintering process. The main difference consists in the advantages that this process can achieve by operating simultaneously heating and pressing. Less holding time and higher heating rate are the key factors, see *paragraph 2.2.5*. This results in high-quality component and net-shape parts with full density achieved. A large variety of metallic and ceramic materials can be worked.



Figure 3.1: Micro-FAST logo ([www.micro-fast.eu](http://www.micro-fast.eu)).

Micro-FAST ( $\mu$ -FAST) aims at reaching the same results of FAST process, applying the same functional idea in micro-components, *figure 3.1*. It can be possible to take characteristics which are designed for macro-account into micro-account; but, only considering a large variety of parameters, like using powder produced with a smaller particles size (nano-sized), density model different from macro-parts, different considerations in heating of the part, contamination derived from the use of lubricants and additives, die-wall friction, and handling of micro-components inside the operating machine. In general, macro-scale parameters could not be directly converted into micro-scale parameters. This theory is called Size-Effect. Micro-FAST project wants to focus on this aspect in order to develop a common manufacture process suitable for large-scale production.

## 3.2. Micro-Scale Overview

Depending on the size of the part, it is possible to define different size process manufacturing (Qin 2015):

*Miniature-scale* ( $< 10\text{ mm}$ );

*Micro-scale* ( $< 1\text{ mm}$ );

*Nano-scale* ( $0.1 - 10\ \mu\text{m}$ ).

The last few decades have underlined a continuous need for micro part fabrication in a wide variety of areas, such as microsystems, micromechanics devices, and biotechnology products. Microelectromechanical systems (MEMS) market grew about 19.8 % per year during 2010-2015 (Dong Lu et al. 2013). In particular, improvements and developments are requested on size accuracy of the final part due to required tolerance specifications. Forming, injection, casting processes are the most common among large mechanical components due to the great experience developed over time, researches, and tested mechanical systems. In most cases, these solutions are not affordable for micro-parts, however. For example, considering powder injection, the complete die filling is not assured due to viscosity of the melted material, friction generated at the interface, thinner injection feeds than macro-ones. Different manufacturing processes have been studied and developed, such as soft lithography, x-ray radiation lithography (LIGA), electro-discharge machining ( $\mu\text{EDM}$ ), laser machining, electro-forming (Dong Lu et al. 2013). Powder sintering starts being employed in macro-scale; then, it is scaled down to micro-forming. Conventional sintering seems to be suitable for the purpose. The most relevant disadvantages related to this solution consist in time and accuracy. Normal sintering needs some considerable time to achieve the final shape; during this time, the workpiece can be contaminated, and size control is difficult. In general, the process is slow and without control; therefore, the risk of faulty parts is very high. The development of FAST process allows to cross these disadvantages, ensuring high accuracy of the part.

### 3.3. Micro-FAST Process

The main process can be considered similar to the FAST process, with the only difference in micro-scale. Loose powder is weighted with a precision balance according to the calculated weight: it might be assured the accuracy of the final volume of the part, in spite of influencing process parameters. Then, the powder is filled into the die.

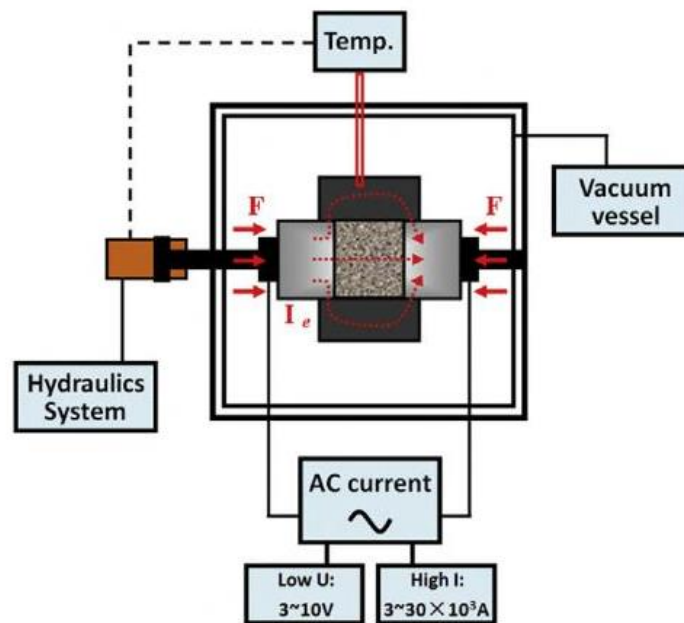


Figure 3.2: Drawing of a Micro-FAST set configuration (Qin 2015).

A schematic representation of die-set equipment is shown in *figure 3.2*. Powder is compressed between two punches. A thermal simulator, such as Gleebe-1500D (Jie Zhaoa et al. 2015), generates an AC current passing between punches and powder. The generated electrical field heats the powder. Typical electrical parameters are low voltage and high electrical current, controlled during the process. These parameters represents a difference between FAST and SPS process. In SPS, high-voltage-current discharges heat the powder, enhancing temperature (Dong Lu et al. 2013). Experimental analysis have been conducted without any additive used (Jie Zhaoa et al. 2015), allowing high value of purity. In the meantime, pressure is applied in order to compact the powder, generating plastic deformation and densifying. Common values of pressure are around 100 MPa. Heating rate can vary from 50 to 200 °C/s, the total time of process from few seconds to few minutes, depending on the part volume.

### 3.3.1. Sintering Process Analysis

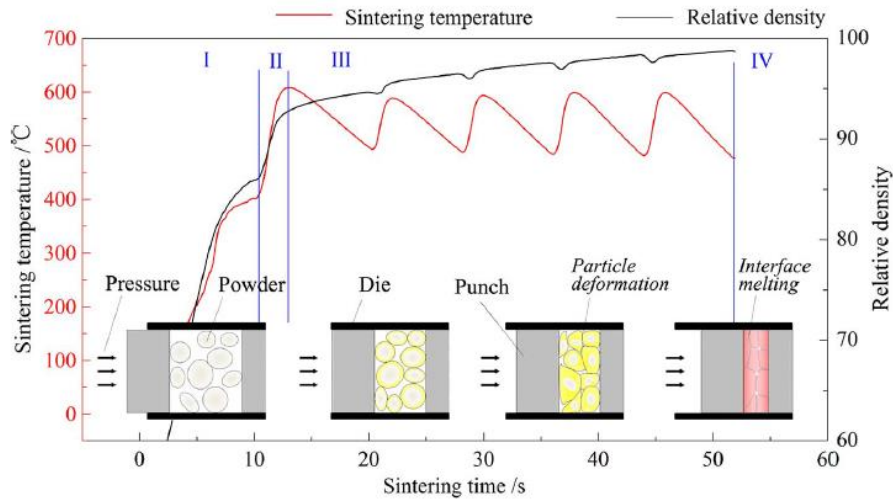


Figure 3.3: Diagram illustrating the main Micro-FAST sintering phase (Dong Lu et al. 2013).

Generally, Micro-FAST sintering process can be described as a four-stages process, *figure 3.3*, (Qin 2015):

*Pre-heating period (stage I)*, also characterised by a low-temperature heating period. Electric current is transferred to the powder; then, because of the Joule heating, the temperature rises up to 200-400 °C. The use of a vacuum chamber ( $p < 10^{-4}$  Pa), high temperature, and pressure applied on the powder, held for a certain time, enhances the solid diffusion of particles, increasing part density ( $\approx 86\%$  of relative density in experiments described by literature) (Dong Lu et al. 2013). The gas trapped inside the powder is also driven out. The electric current contributes even in densifying powder, through a number of phenomenon involved, generated by electrons flux (Munir 2000);

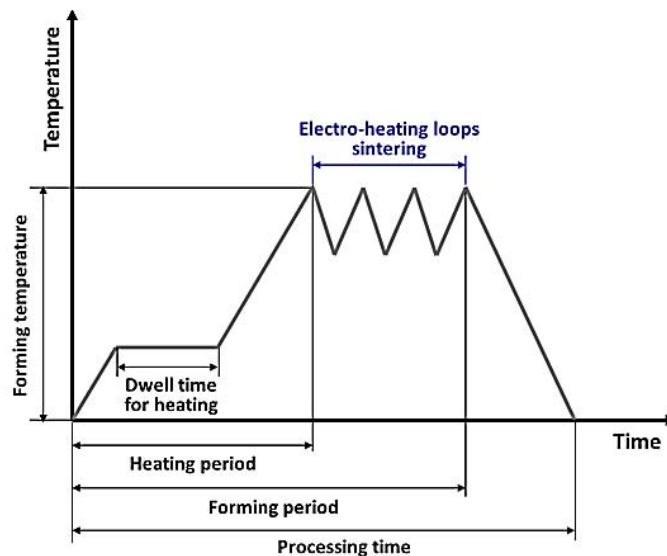


Figure 3.4: Temperature diagram related to a Micro-FAST sintering process (Yi Qin 2015).



*Calefactive period (stage II)*, also characterised by high-temperature heating period. Pressure is maintained and temperature rises up to sintering temperature. The amount of necessary heating depends on the final temperature of the end of stage I. The simultaneous effects of pressure applied and sintering stress enable a combination of particles deformation and breaking (Munir et al. 2000).

*Sintering period (stage III)*, where heating cycles are performed. Typically, the temperature range is between the sintering temperature and 100-200 °C below, *figure 3.4*. The number of performed cycles is an experimental parameter. A higher number of cycles enhances the density of the part and allows a lower pressure. Fluctuating temperature enables electrical and density flux that generates a high value of heat energy into the interface among particles (Chen 1998). The incremented contact surface among particles decreases the resistance. As a consequence, micro-melted points are generated and particles are joined. Surely, a trade-off based on cost consideration and maximum allowed cycle time has to be considered;

*Cooling period (stage IV)*, the electric current is switched off, the temperature part is decreased until room temperature.

It is worth considering that the general division into a four stages-process has to be considered only by a general point of view. Depending on the specific part or material the process can be described with greater or lower level of details. Considering the cycle time, all the process can be performed from a minimum of some seconds up to a maximum of some minutes. The decreased time, related to a traditional sintering process, is determined by the “continuous” nature of the process capable of simultaneous actions as heating, pressing, deforming, breaking, melting, and joining.

### 3.3.2. Effects of Coupled Multi-Fields Activation

The four-stages process before described has noted the strict relation among pressure, electric field, and generated heat. This relation results in a coupled multi-fields activated forming process, under an external pressure applied (Qin 2015). The starting powder material has an apparent volume due to vacancies between particles. A resistance has to be overcome to compress the part, reduce the porosity, and join the particles inside the compact. The higher temperature is, the lower the yield strength of the particles is, resulting in a decreased resistance and viscosity to the interface. Grain growth can occur with a very high temperature; so, it is important to control the maximum allowable value. The heating flux refers to the Joule-Lenz's law:

$$Q = I^2 R t \quad (3.1)$$

where  $I$  is the electric current intensity,  $R$  is the resistance of the powder to the electricity, considered both among and itself particles,  $t$  is the electricity holding time.

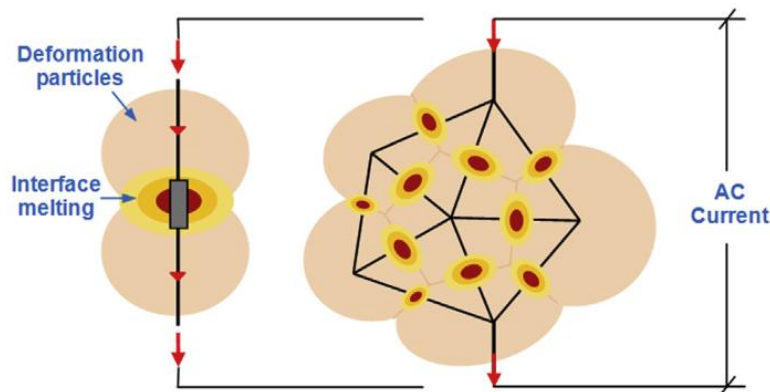


Figure 3.5: Heating process and joining mechanism inside powder (Qin 2015).

The decreasing of  $R$  between particles interface generates a higher temperature due to greater heating. Particles boundaries melt. If compared to a traditional sintering process, where the first pressuring phase consists of neck growth or coarsening, in Micro-FAST process densification is acquired because of plastic deformation. In FAST process densification is obtained with a continuous reducing of surface among particles and following joining. This mechanism is illustrated in *figure 3.5*. It is worth underlining that external pressure field has a great influence on the action of temperature and electricity and vice versa, in micro-forming, in particular. Under high pressure, plastic flow will result accelerated; the Bingham model (C. H. Lee & K. Jiang 2008) describes the inner deformation due to increased internal stress.

### 3.4. Literature Survey: Main Applications of Micro-FAST Sintering

Micro-FAST sintering is the way to obtain high-density and net-shape parts with great savings of material and using loose powder. In literature, different experiments are described, underlining the convenience and the high quality of the part with a series of feasibility experiments. The literature knowledge will result useful to the experimental phase of this project, showing the major parameters involved and the ways to optimise these ones.

#### 3.4.1. Forming of Copper Micro-Gears (Dong Lu et al. 2013)

Raw materials consist of copper powder with an average particle size of  $35\ \mu\text{m}$  and a purity of 99.5 %.



Figure 3.6: Die-system, respectively upper and lower punches, die and generated micro-gear (Dong Lu et al. 2013).

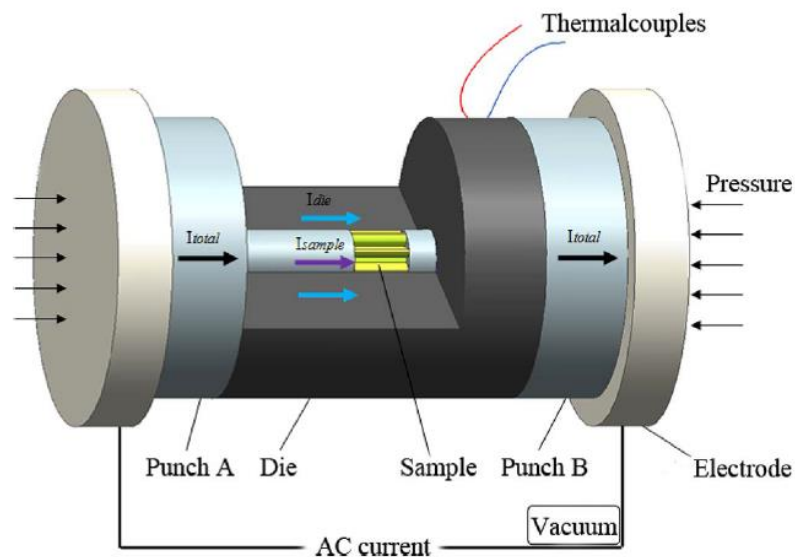


Figure 3.7: Micro-FAST process with a Gleebe-1500D thermal simulator (Dong Lu et al. 2013).

After die-system configuration, *figure 3.6*, the same has been placed in a thermal simulator (Gleebe 1500-D), *figure 3.7*. The heating rate has been fixed at 50 °C/s, the same for the cooling rate. Uniaxial pressure applied was equal to 100 MPa. The entire experiment has been executed inside a vacuum chamber ( $< 10^{-4}$  MPa). During cooling phase pressure has been released. After sintering process, morphology and density have been analysed.

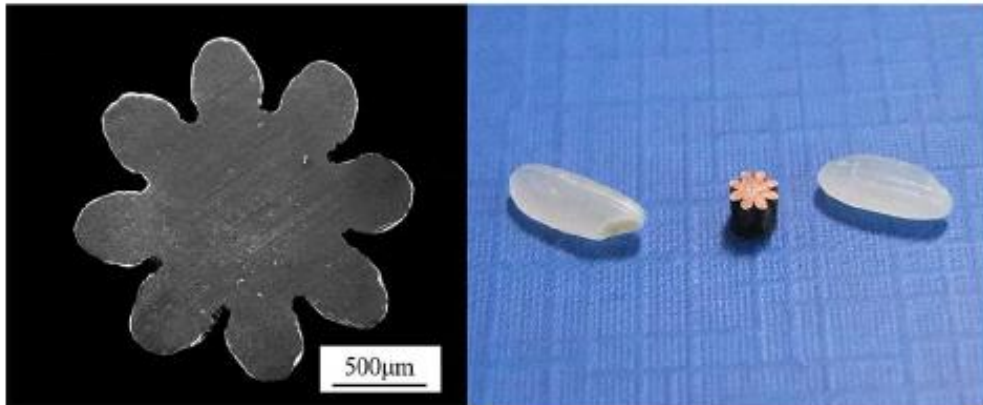


Figure 3.8: Scanning electron micrograph of a sintered micro-gear (Dong Lu et al. 2013).

The *figure 3.8* shows a picture of the final part obtained; the gear is characterised by eight teeth, 1.6 of pitch diameter and 2.0 mm of height. A good shape is resulting from a visual analysis.

PROCESS CONDITIONS AND RELATIVE DENSITY OF THE FORMED SAMPLES

Specimen designation	Heating rate (°C/s)	Sintering temperature (°C)	electro-heating loops* (T~400°C)	Pressure (MPa)	Density (g/cm <sup>3</sup> )	Relative density (%)
1#	50	500	3	100	8.226	92.2%
2#	50	600	3	100	8.491	95.2%
3#	50	700	3	100	8.668	97.2%
4#	50	600	5	100	8.806	98.7%
5#	50	600	1	100	6.680	74.9%
6#	50	600	3	75	8.300	93.0%

Figure 3.9: Experiment results and main process parameters (Dong Lu et al. 2013).

The authors has illustrated the main results in a table, *figure 3.9*. In this case, the main important final result is that of part density. It can be noted that electro-heating loops have the major influence on it.

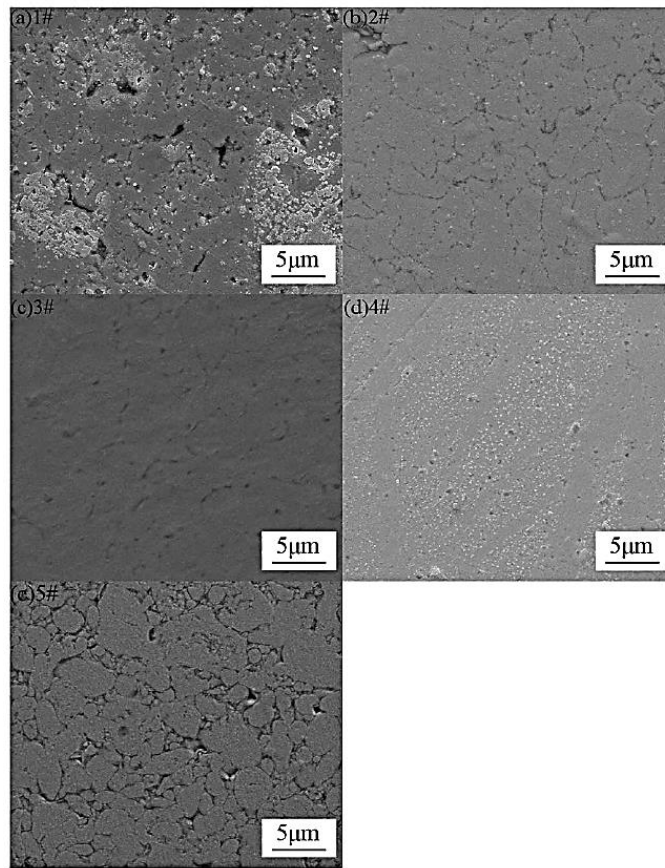


Figure 3.10: Comparing microstructure in different parameter process production (Dong Lu et al. 2013).

Sample 5# results in a lower density although the other parameters result equal to the last experiments. Comparing in particular samples 1# and 5#, it can be seen that the decreasing of the sintering temperature has lower influence in part density than decreasing the number of heating-cycles. In the first case a relative density of 92.2 % is achieved, while in the second case is only 74.9 %. Sample 6# highlights the obtained result with the decreasing of pressure. Sample 3# and 4# have the highest density part: increasing electro-heating loops is more advantageous than increasing temperature. *Figure 3.10* compares the different microstructure obtained. All the processes have been performed with a short time process (< 1 min). SPS process and classic sintering require longer time. Considering all these factors, and results linked to quality of the part, time, and cost FAST process has applied to micro-parts, production results a good way of production.

### 3.4.2. Forming of Micro-Components Using Different Types of Powder (Jie Zhaoa et al. 2015)

In this research experiments, simulations on 13 different types of powder have been executed. The results aim to a feasibility study of the FAST sintering process over the micro components production.

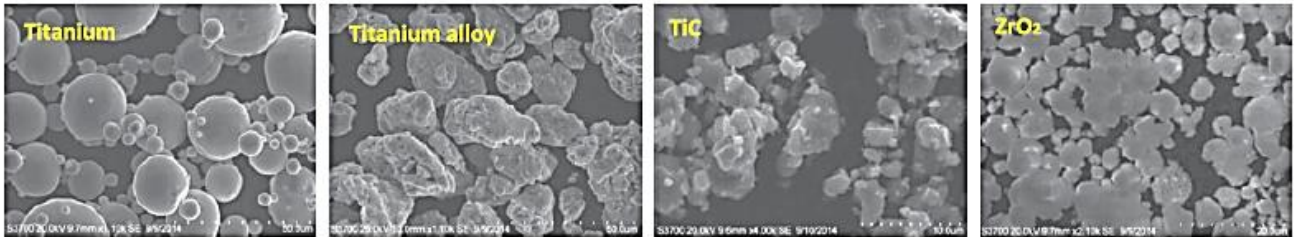


Figure 3.11: Morphology of different powder obtained through a Scanning Electronic Microscope (Jie Zhaoa et al. 2015).

Initially, two main groups have been defined: metallic and ceramic. The main difference among these groups consists in melting temperature, about 1600 °C for metallic powder and 3000 °C for the ceramic ones. Initial powder morphology can be seen in *figure 3.11*.



Figure 3.12: Die-set equipment (Jie Zhaoa et al. 2015).

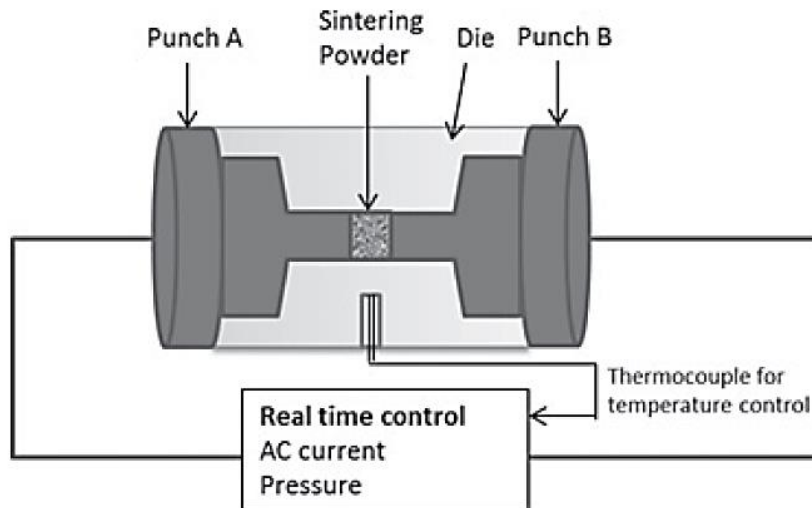


Figure 3.13: Experimental set-up. A Gleebe-3800 is equipped (Jie Zhaoa et al. 2015).

Die-set equipment and thermal set-up are similar to the previous series of experiments described in the last paragraph, *figure 3.12 & 3.13*. A thermocouple in

the middle section has been placed in order to control temperature during the process. The geometrical part has a cylindrical shape, 4.0 mm of height, 4.0 mm of diameter. Initially, the correct powder mass has been weighted in an electronic balance considering the starting and finishing volume, related to density. Then the die has been filled with powder and the experiment set-up has been settled. Process parameters are controlled by a software interface, while thermocouples give instantaneous results during the process. The varied key parameters among different experiments are related to the maximum sintering temperature, heating rate, pressure, and holding time. A vacuum chamber protects the part from oxidation during the high temperature process.

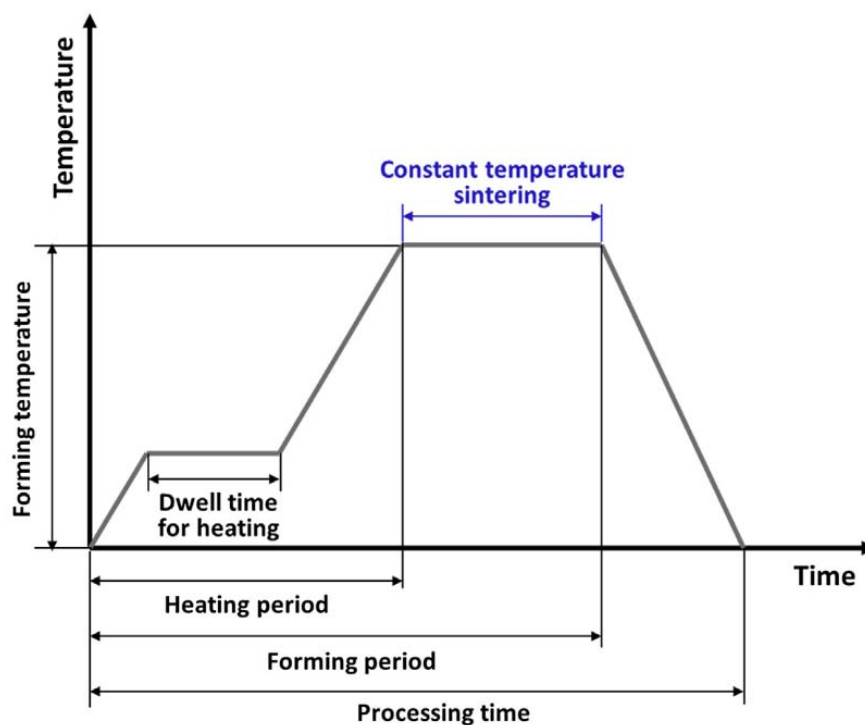


Figure 3.14: Process temperature diagram, with constant sintering temperature (Jie Zhaoa et al. 2015).

About temperature, for metallic powder has been set a sintering temperature of 1100 °C and a heating rate of 100 °C/s. Instead, for ceramic powder has been a sintering temperature of 1300 °C and 50 °C/s of heating rate. Unlike the previous paragraph, it is worth pointing out that in these series of experiments, as soon as the temperature has reached its maximum value, it has been maintained constant, *figure 3.14*.

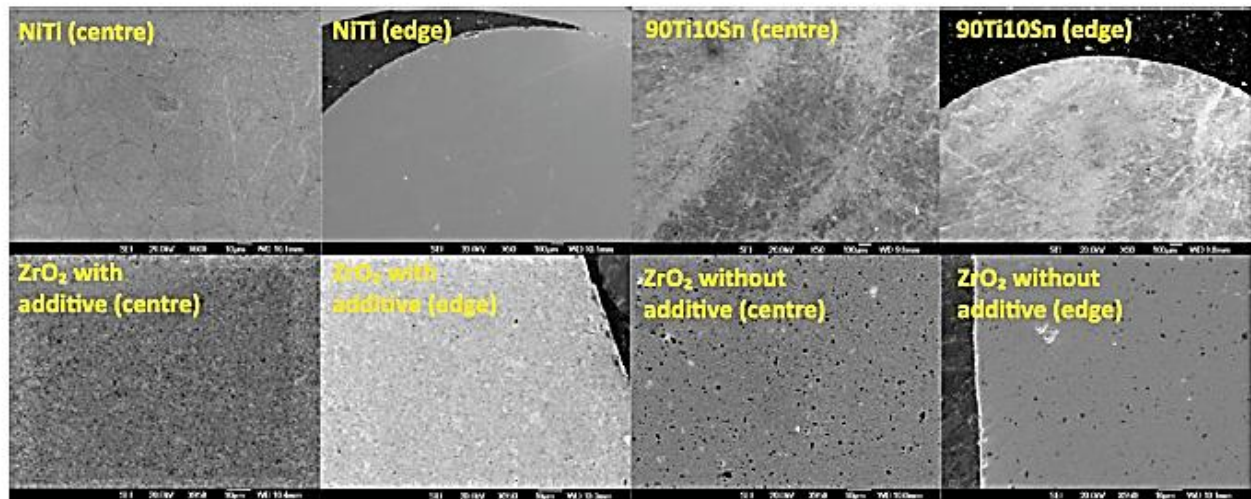


Figure 3.15: Different microstructure morphology after processing. Scanning Electronic Microscope (Jie Zhaoa et al. 2015).

In *figure 3.15* is possible to see the morphology of the different materials. The results obtained confirm the high final part quality. Final part size results compatible with nominal size. Metal powder has achieved up to 99.89 % of relative density, while up to 95 % or above ceramic powder. From microstructure analysis, no large pores are observed, only small residual ones. These results highlight the possibility of quality enhancing through optimizing process parameters, in particular, maximum temperature, holding time, and heating rate. Certainly, although in the article has not been revealed the used value, also the applied pressure has to be considered for process optimization. The higher is the value, the higher will be the density. In general, the same influences described in theory are encountered in experiments. The main advantage over traditional sintering process is that these results are achieved with lower temperature in less time.

### 3.4.3. Fabrication of MnZn ferrite (Qin 2015)

MnZn ferrites are widely used in mini DC – CD converters and inductors. The next-exposed experiments want to demonstrate the capability of Micro-FAST in this operating field. One of the goal of this kind of part is the achieving of good magnetic properties. Operating-die set-up is similar to the last ones described. Thermal simulation is provided by a Gleebe-1500D, sintering temperature is 800 °C with a heating rate of 50 °C/s under a pressure of 75 MPa. The holding time is fixed in 8 minutes; then, the part is cooled down until room temperature. Like the other experiments, a vacuum atmosphere is provided in order to avoid oxidation that may occur at high temperatures.



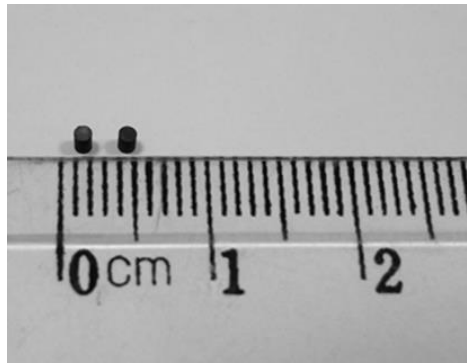


Figure 3.16: Final MnZn part produced (Qin 2015).

Part produced can be seen in *figure 3.16*. The part density reached is equal to  $4.69 \text{ g/cm}^3$ . Nominal size of 1.0 mm height and 1.0 mm of diameter results inside the assigned tolerance. Good magnetic properties are also maintained.

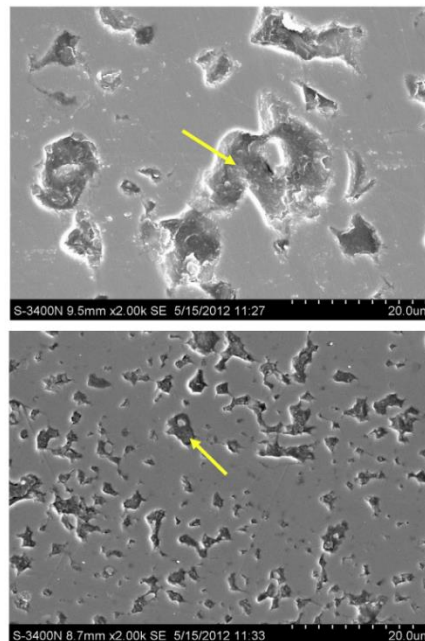


Figure 3.17: Microstructure comparison. At the top traditional sintered part, at the bottom Micro-FAST sintered part (Qin 2015).

A microstructures comparison, *figure 3.17*, wants to point out the main difference between the same part produced through a classic sintering process and another produced through Micro-FAST process. Temperature of  $1280 \text{ }^\circ\text{C}$  and sintering time inside the furnace of 8 hours are the manufacturing parameters for the first sample, characterised by 8.0 mm in diameter and height. The second one is the result of Micro-FAST sintering, obtained with 8 minutes of holding time under a temperature of  $800 \text{ }^\circ\text{C}$ . Results are clearly visible, as a more homogeneous material distribution has been reached in the second sample. The dark parts of *figure 3.17* represent raw material.

Sintering Method	Sample Size/(mm)	$\rho$ /(g/cm <sup>3</sup> )	BH <sub>max</sub> /(GOe)	B <sub>r</sub> /(G)	H <sub>ci</sub> /(G)	Ms/(emu)
Solid-state reaction for 4 h at 1280 °C	Φ 8 × 8	4.74	116.61E+3	6.5790	0.262	7.5522
Micro-FAST for 8 min at 800 °C	Φ 1 × 1	4.69	50.362E+3	52.143	30.152	2.0340

Figure 3.18: Results comparison between the two different sintering methods (Qin 2015).

A summary can be seen in *figure 3.18*. The obtained density is almost similar. On the one hand, focusing on magnetic properties, it can be seen that magnetic saturation is higher in solid-state reaction (classic sintering) with a value of 7.5522 emu, if compared to the one obtained with Micro-FAST of 2.0340 emu. On the other hand, residual ferrite on the sample is lower in the first sample than in the second, 6.5790 G related to 52.143 G. The strength point of Micro-FAST can be seen on the first column, related to the less required lead time.

#### 3.4.4. Fabrication of Hard Alloy: Hardness Investigation (Qin 2015)

Cutting tools and dies have to withstand high pressure and strength. Due to wear and fatigue resistance, high toughness is required. Typical employed materials for this purpose are WC-Co composites. Usually, this kind of elements are worked by sintering processes at temperature comprised within 1400 – 1600 °C. Other alternative techniques, like hot isostating pressing, microwave, SPS are used too. The main problem is the grain growth that is the main responsible of coarse-grained. Controlling grain growth is possible using inhibitor additives, such as vanadium and chromium carbide. Together with fast heating rate and brief time process under high temperature, especially vanadium carbide is the most suitable solution in tools manufacturing. For micro-tools, Micro-FAST process has been investigated as a capable manufacturing process for this purpose.

Specimen Designation	Heating Rate (°C/s)	Sintering Temperature (°C)	Pressure (MPa)	Times of Electro-Heating Loop (T ~ 400 °C)	Relative Density (%)
1#	50	850	75	1	92.90
2#	50	850	75	3	93.30
3#	50	850	75	4	93.80
4#	50	850	75	6	97.80

Figure 3.19: On the left, sintered WC samples; on the right, experimental results on different WC sintered samples (Qin 2015).

The experiments are especially focused on the improvements obtained by the heating-cycle loops, namely the fluctuating of temperature around its sintering value, *figure 3.4*. The advantages have already been described in *paragraph 3.3.1*. The continuous fluctuating of temperature increases the electrical field and the heat flux. As a consequences, the densification process will result faster and increased. About the experiments description, four samples of height and diameter of 4.0 mm, *figure 3.19*, are produced and analysed. Results are visible in *figure 3.19*. It can be seen the increasing of final relative density related to a high number of heating-cycles loops. All the other parameters have been fixed.

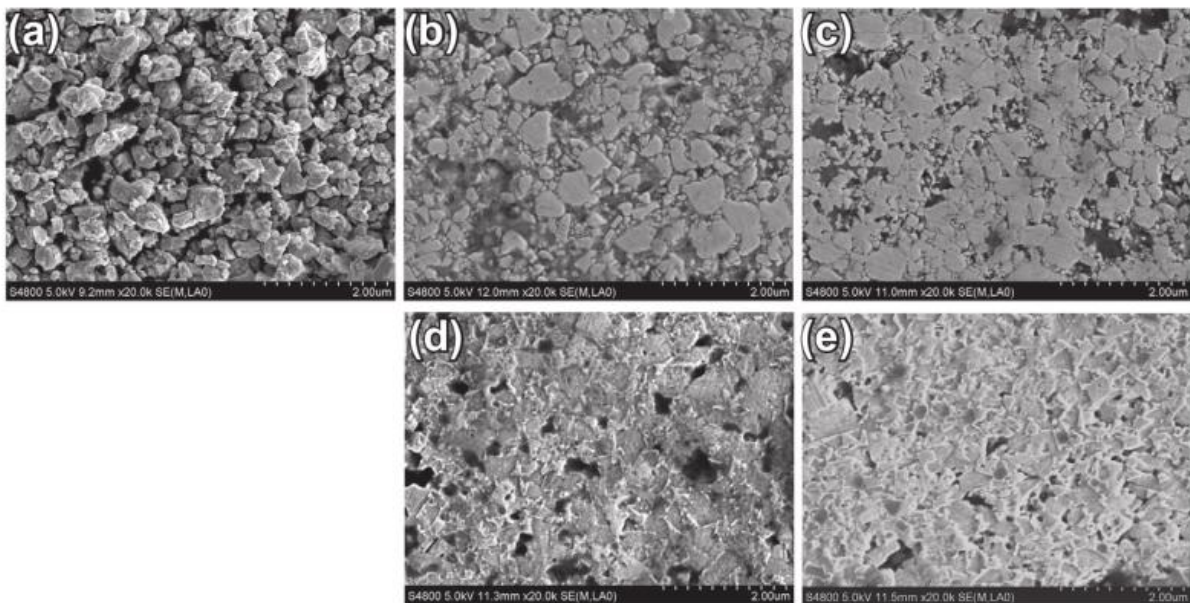


Figure 3.20: Different microstructures obtained, (a) raw materials, (b) 1-loop, (c) 3-loops, (d) 4-loops, (e) 6-loops. Pressure and sintering temperature respectively equal to 75 MPa e 850 °C. Heating rate of 50 °C/s (Qin 2015).

The analysis related to microstructure observation, underline the strong dependence between heating-loops and porosity of the part, *figure 3.20*. Increasing the number of loops, pores will be reduced.

## 4. Sintering of a Micro Gear

### 4.1. Introduction to the Project

After an overview of literature and theory related to this project, this chapter focuses on describing the purposes of this thesis and finding the main suitable solutions. The topic consists in studying and researching an optimised way of a micro-part manufacturing through a Micro-FAST sintering process. In particular, it has been decided to produce a micro gear with pure aluminium powder. The main problem that occurs during production is related to the residual pressure inside the die after the sintering process, which causes the increase of ejection force and deformation due to die-wall friction during the ejection stroke. Therefore, the focus is on reducing the inner residual pressure and ejection force through an optimised-tool design. Surely, net shape, density, and part quality need to be guaranteed at the end of the process. Another parameter worth optimising is lubrication. As described in *paragraph 2.2.3*, lubrication has an important role in decreasing friction; however, the residual quantity of the lubricant increases porosity. As a consequence, density will decrease.

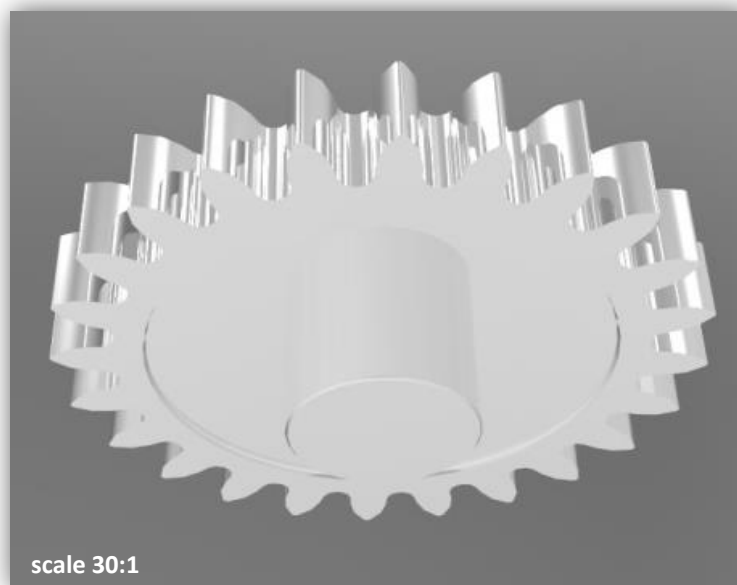


Figure 4.1: Micro gear 3D CAD rendering.

## 4.2. Project Definition and Boundaries

In the following paragraphs, the main characteristics of the project will be described. In particular, it should be noted that all the next-developed concepts idea are based on the following constraints, considered as a starting point.

### 4.2.1. Micro Gear Geometry

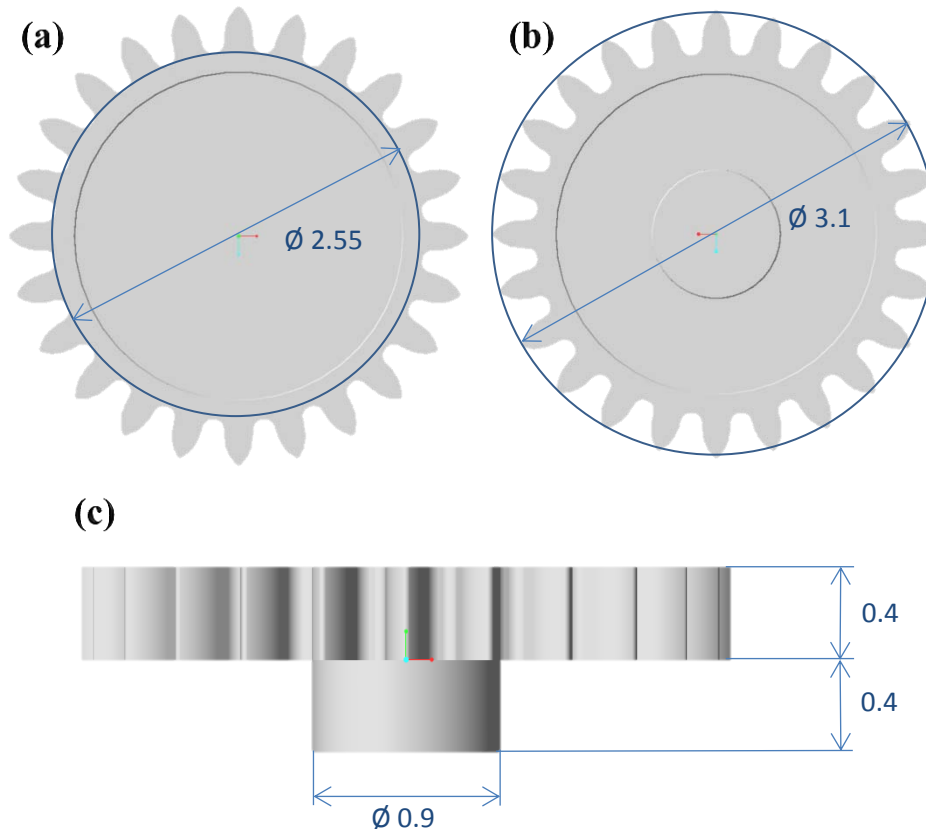


Figure 4.2: Respectively top view (a), bottom view (b) and front view (c) of the 3D model CAD of the gear.

The part geometry consists of a micro gear, *figure 4.1*. This is characterised by 24 teeth, a pitch of 0.4 mm, a total height of 0.8 mm. As it can be seen in *figure 4.2 (c)*, the micro gear is characterised by two part: the upper part, gear, and the bottom part, a cylindrical feature. The external diameter of the gear is of 3.1 mm, while the internal one is of 2.5 mm. The circumscribed-cylindrical shape is 0.4 mm high. A single teeth has a length of 0.3 mm. The bottom feature has a diameter of 0.9 mm and a height of 0.4 mm. The part can be included among the micro-scale components although the main diameter is  $> 1.0$  mm. General characteristics on this application fields, described in *paragraph 3.2*, have to be considered. Classic forming process, like injection or casting, can be very difficult to control during working; moreover, micro-part can contain defects due to density and shape. Micro-FAST sintering seems

to be a suitable manufacturing process, also considering scientific results (Dong Lu et al. 2013), see *paragraph 3.4.1*.

#### 4.2.2. Sintering Process

In Micro-FAST sintering process, described in the last chapter, the heating of the part is provided by a thermal simulator, such as Gleebe machine, which heats the part through an activated electrical field between the up and the bottom punch. The heating direction is axial. By contrast, the heating system used in this project is different, in order to have a safety, less-complex and cost-saving process. These changes do not influence the experimental results regarding ejection, as the functional principle related to simultaneous applying of pressure and heat is still operated. However, axial and radial density may be influenced, because of varied heating direction.



Figure 4.3: Watlow mineral insulated (MI) nozzle heaters.

The heater used, see *Appendix 2: Datasheets*, in these experiments has a cylindrical shape, *figure 4.3*. The die system is placed inside, where the heating is transmitted by the nozzle. The part temperature can grow up to 600 °C. The main difference with FAST is also the heating direction, that is provided in radial direction in this case, instead of the axial one. As a consequence, all the die system is subjected to high temperature, with corrosion and oxidation risks because of high temperature. To control temperature, an electronic system by Allen-Bradley is used (Rockwell Automation). With manual setting of temperature, it is possible to operate heating loops during the process. Thermal conductivity of the tools should be considered in order to have a low value of the temperature difference between the surface in contact with the nozzle and the pressed powder inside the die.

### 4.3. Residual Radial Pressure

The concept-design parameters related to the process and part production are optimised in order to achieve the best quality of the produced part. The greater problem of achieving this result consists in residual radial pressure generated during the process. The main factors related to this one consist of the radial pressure derived from compaction exerted by the punch and the different thermal expansion generated by workpiece, tools, and sintered part during the sintering process. This last factor is caused by the different value of thermal expansion coefficients of aluminium, die material, and punches.

#### 4.3.1. Residual Stress due to Powder Compaction

Compacting powder into the die allows part densification. Simultaneous heating accelerates the process and decreases the yield strength of the material. However, compaction of the part is subjected to plastic deformations limit, see *paragraph 2.2.3*. Higher pressure means not only higher densification rate and lower porosity of the part, but also higher cost involved. A trade-off has to be reached. Another important consequence related to compacting pressure is radial pressure generated into the die.

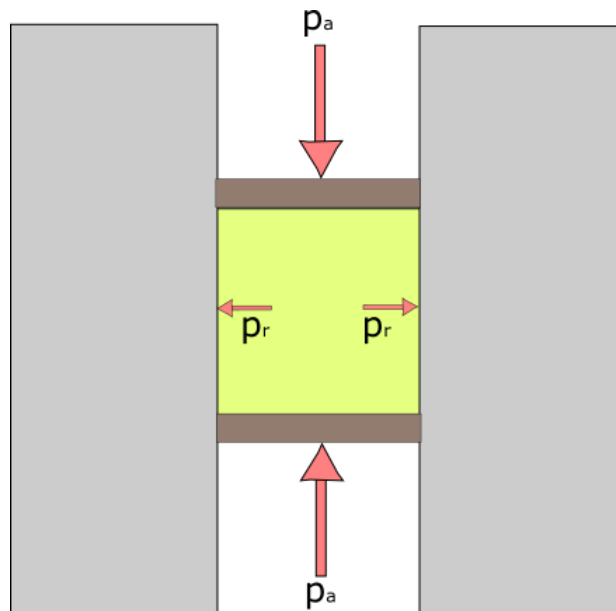


Figure 4.4: Theoretical pressure distribution inside a die.

On a theoretical way, it is worth studying a liquid cylinder inside a die compressed by an axial pressure  $p_a$ , *figure 4.4*, considering a perfect lubricated condition onto the interface die-part. The radial pressure exerted on the wall,  $p_r$ , is equal to  $p_a$ ; the ratio between axial and radial pressure is 1. This theoretical consideration is valid for Newtonic liquid, such as water. Considering powder instead of a liquid, the ratio will

not be equal to 1; this is due to initial allocation of the particles into the compact. The empirical relationship between radial and axial pressure was studied in 1960 by W. M. Long (Long 1960). Long's considerations started from a free-standing cylinder characterised by a Young's modulus  $E$  and a Poisson's coefficient  $\nu$ ; this last coefficient determines the stress ratio for homogeneous parts. A compressive stress  $\sigma_a$ , applied on the upper and lower surfaces of the cylinder, generates a radial stress  $\sigma_r$  due to the elasticity law. Radial deformation occurred is equal to:

$$\varepsilon_r = (\sigma_r - \nu\sigma_r - \nu\sigma_a)/E \quad (4.1)$$

In a second step, the same cylinder is put on a cylindrical die, like the configuration shown in *figure 4.4*. In this configuration, the powder is constrained by die wall during compaction. Assuming a perfect lubrication in order to avoid any die-wall friction, and a Young's modulus of the die larger than the cylinder one, radial expansion  $\varepsilon_r$  can be considered equal to 0. So, the *equation 4.1* becomes:

$$\sigma_r - \nu\sigma_r - \nu\sigma_a = 0 \quad (4.2)$$

$$\sigma_r = \frac{\nu\sigma_a}{1-\nu} \quad (4.3)$$

This result is considered in pressure-loading phase under an elastic field. Particles has not reached yet the yield strength of the material,  $\sigma_0$ . When the maximum-shear stress  $\tau_{max}$  overcomes the yield-shear stress  $\tau_0$ , the material starts to be plastically deformed; according to Mohr's circle theory,  $\tau_0 = \sigma_0/2$  while  $\tau_{max} = |(\sigma_a - \sigma_r)/2|$ . So, in plastic field, under loading condition:

$$\sigma_r = |\sigma_a - \sigma_0| \quad (4.4)$$

When the loading phase is over, the releasing phase is the next one. Axial pressure starts decreasing from the maximum reached value, under elastic condition. Radial pressure can be described as following:

$$\sigma_r = \frac{\nu\sigma_a}{1-\nu} + k \quad (4.5)$$

Where  $k$  is a constant value which considers the starting condition of powder after the compaction phase. This equation can be considered true until the value of axial pressure is higher than the radial one. After this point, it should be considered a plastic deformation according to Mohr's theory:

$$\sigma_r = \sigma_a + \sigma_0 \quad (4.6)$$



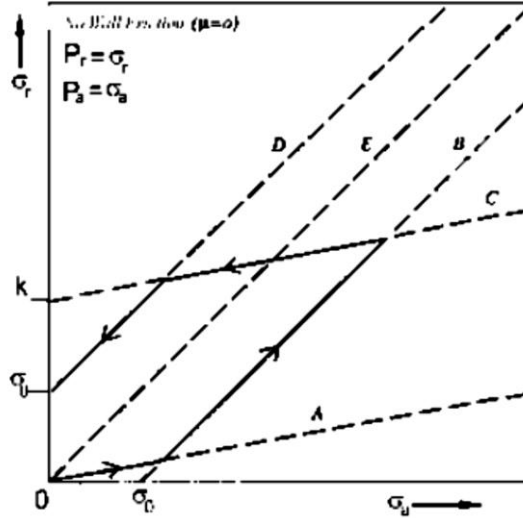


Figure 4.5: Theoretical model disregarding friction (Höganäs 2000).

From these results, it can be noted that all the process is subjected to hysteresis cycle, *figure 4.5*. After the complete releasing of pressure, the residual radial pressure into the compacted part is equal to  $\sigma_0$ . It is worth remembering that these last equations are referred to no-friction condition. A modified model, which takes into account the die-wall friction, was suggested by G. Bockstiegel (Bockstiegel 1965). Frictional forces exerted during compacting and ejecting of the part act in the opposite direction of the compacting punch. The frictional force can be assumed proportionally to the radial pressure which is exerted at the die-wall interface during compaction/ejection of the part. The axial stress can be described as:

$$\sigma_a = p_a \pm \mu p_r \quad (4.7)$$

The positive sign is referred to the compacting phase, while the negative one to the releasing phase. Long's *equation 4.3, 4.4, 4.5 & 4.6* can be written taking into account friction:

$$\text{Elastic loading: } p_r = \frac{\nu p_a}{(1-\nu+\mu\nu)} \quad (4.8)$$

$$\text{Plastic loading: } p_r = \frac{p_a - \sigma_0}{1-\mu} \quad (4.9)$$

$$\text{Elastic releasing: } p_r = \frac{\nu p_a}{(1-\nu-\mu\nu)} + k' \quad (4.10)$$

$$\text{Plastic releasing: } p_r = \frac{p_a + \sigma_0}{1-\mu} \quad (4.11)$$

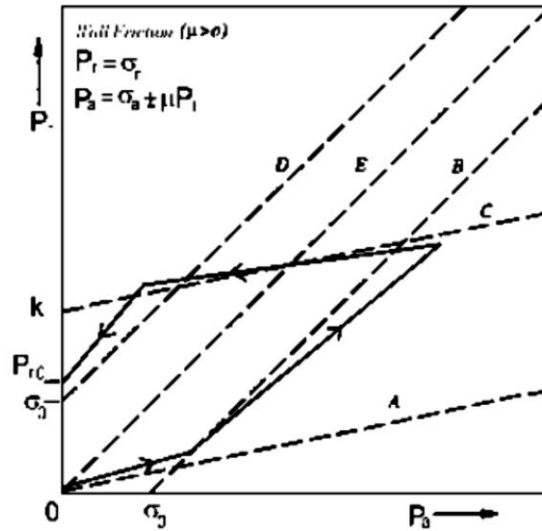


Figure 4.6: Theoretical model considering friction (Höganäs 2000).

These last relations are equals to the Long's equations if friction  $\mu=0$ . They are similar to the starting equations. The only difference which can be noted relates to the hysteresis cycle. The diagram will be distorted with respect to the first one, *figure 4.6*. The importance of the yield-strength value can be observed in the model described. In particular, it is possible to state that a material with a low-yield strength value and negligible tendency to deformation behaves as a hydraulic one during compaction in a rigid die. Vice versa, a metal with a high-yield strength value and with a deformation tendency exerts a higher radial pressure during compaction with respect to the last one. A reduced-yield strength would results in a better densifying of the compact.

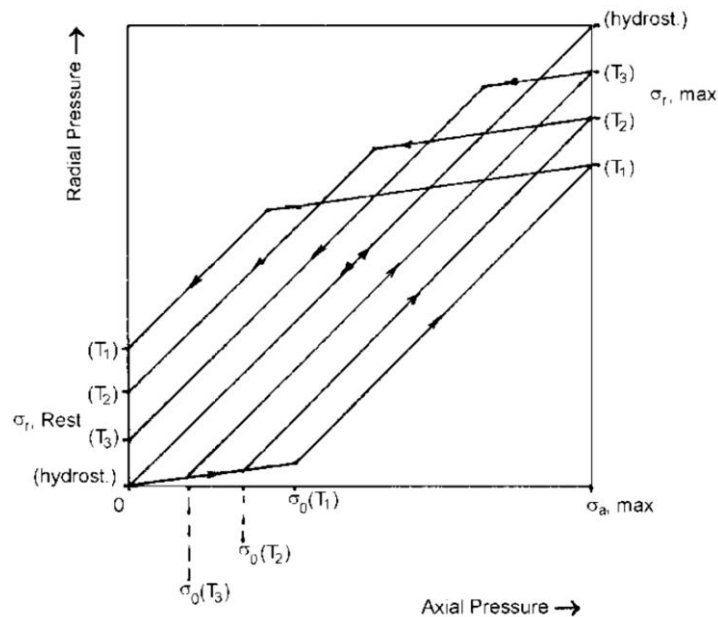


Figure 4.7: Relations between temperature and yield strength ( $T_3 > T_2 > T_1$ ) (Höganäs 2000).

Laboratory experiments have carried out a strong dependency of the yield strength to temperature (Höganäs 2000). Increasing temperature of compacting is possible to decrease the yield strength of the material, *figure 4.7*, thus achieving a better and more homogeneous densification of the part.

### 4.3.2. Residual Radial Pressure due to Thermal Expansion

Temperature is the second influencing factor that should be encountered in radial pressure generated during sintering process.

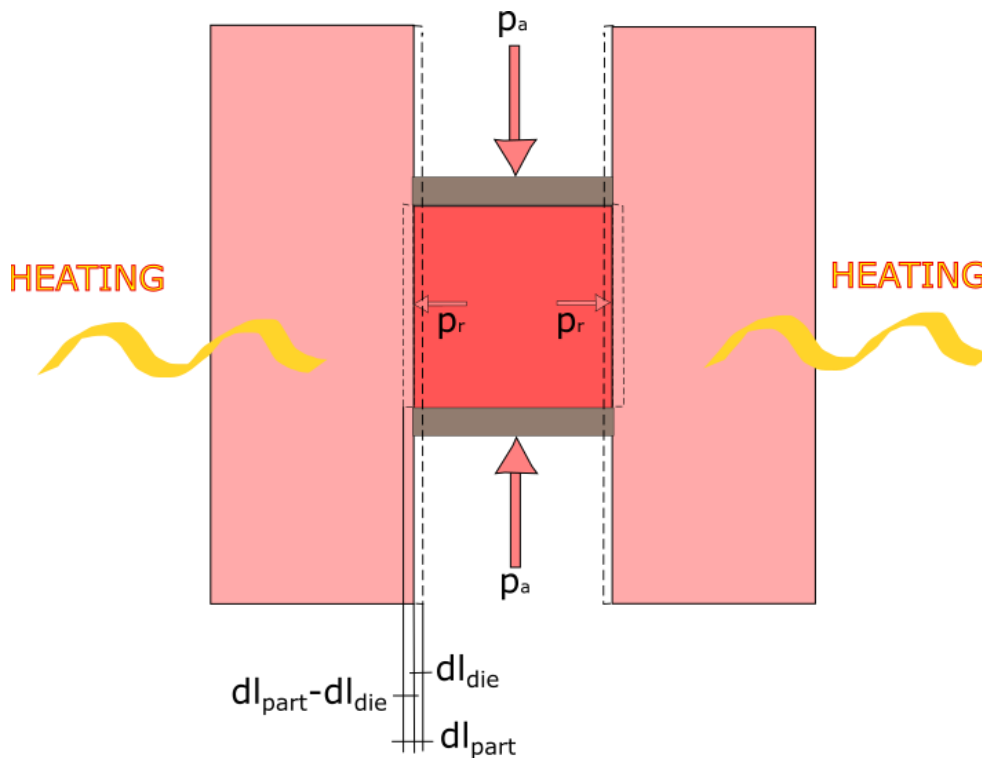


Figure 4.8: Schematic picture referring the pressure generated into the die due to thermal expansion.

Pressure and temperature are applied simultaneously while the compact is still inside the die cavity during the manufacturing process. This problem is not considered in traditional sintering because the two main steps mentioned occur in two different moments; thus, the compact, called “green”, is heated into the oven after being ejected from the die. By contrast, Micro-FAST sintering should take into account also the temperature effect. The radial pressure is generated as a consequence of the different values of thermal-expansion coefficients, one related to the part material, and the other to the die material, *figure 4.8*. The following relation has been used in order to calculate the thermal expansion at a specific temperature:

$$dl = \alpha_{material} \cdot l_0 \cdot \Delta T \quad (4.12)$$

In this equation,  $dl$  is the elongation,  $\alpha_{material}$  is the thermal expansion coefficient of the part,  $l_0$  is the starting length, and  $\Delta T$  is the difference between the sintering temperature and room temperature ( $293.15 \text{ K} = 20 \text{ }^\circ\text{C}$ ). It should be noted that the elongation is referred to the starting-length of the diameter of the cross section; so, the last relation refers to the linear-thermal expansion. When two elements are in contact each other, a differential thermal expansion is measured, on the basis of the different thermal-expansion coefficients involved:

$$dD = dl_{gear} - dl_{die} = (\alpha_{gear} - \alpha_{die}) \cdot D_0 \cdot \Delta T \quad (4.13)$$

The last equation described refers to the gear-sintering case study, considering the two thermal expansion coefficients  $\alpha_{gear}$  and  $\alpha_{die}$ , respectively of the gear and the die, the external diameter  $D_0$  of the gear, equals to the internal diameter of the die, and the  $\Delta T$  related to the sintering process. The thermal expansion of the gear is higher than for the die, so a radial pressure onto the die-wall interface is exerted, according to the linear model theory:

$$p_r = \frac{dD}{D_0} E \quad (4.14)$$

where  $p_r$  is the radial pressure,  $dD/D_0$  is the deformation and  $E$  is the Young's modulus of the gear. If the material used is the same for the two parts, thus with similar thermal expansion coefficient, this pressure could be neglected. In this case study, due to low values of hardness, melting point, and strength of the material, it is not possible to use aluminium for both the gear and the die. An important consideration about the temperature gradient should be done; indeed, as it has been explained before, therein lies the difference between sintering temperature and room temperature. After sintering, the process is completed with the part cooling to the room temperature. Consequently, in order to obtain safer conditions and take into account any hysteresis phenomenon, the calculated pressure will result overestimated related to the real condition.

### 4.3.3. Residual Pressure Consequences

The radial pressure described in the last paragraphs is considered due to consequences connected to final-part quality and tools lifetime. The main problems relating to radial pressure refer to die-wall friction, cracks caused by volume expansion during ejection, welding effects, and flash generation.

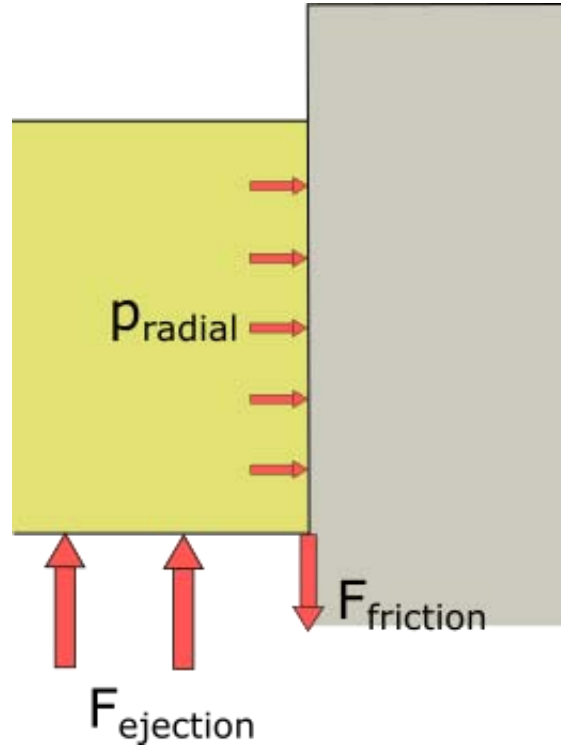


Figure 4.9: Frictional force during ejection of the workpiece.

Frictional force occurs when a radial-pressure field is exerted onto the die-wall interface, *figure 4.9*. The friction direction is always opposite to the punch direction. As a consequence, the force required in order to eject the part will be increased. The ejection force required is expressed by (Höganäs 2000):

$$F_{ejection} = \mu \cdot 2\pi R h \cdot p_{radial} \quad (4.15)$$

The force is calculated as the product between the radial pressure and the lateral surface of the sintered part. In the *equation 4.15*,  $\mu$  is the frictional coefficient,  $R$  is the inner radius,  $h$  is the height of the die, and  $p_{radial}$  is the residual pressure. The pressure exerted over the punch can be calculated as:

$$p_{ejection} = \frac{F_{ejection}}{\pi R^2} = \frac{\mu \cdot 2\pi h \cdot p_{radial}}{\pi R} \quad (4.16)$$

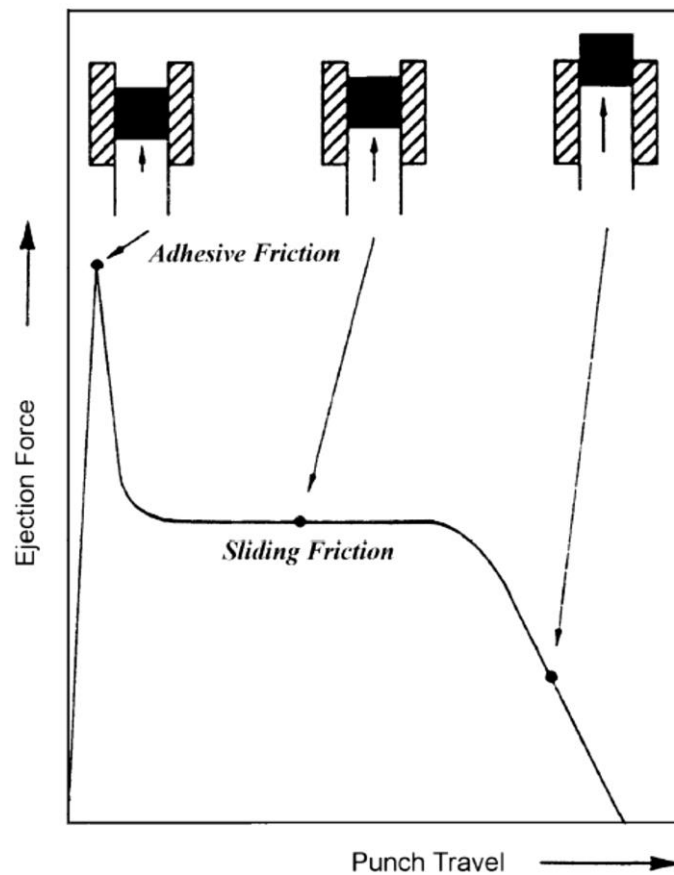


Figure 4.10: Ejection force as a function of the movement of the ejecting bottom punch (Höganäs 2000).

Two different frictional steps can be distinguished during ejection (Höganäs 2000). An initial adhesive frictional step and a second one with sliding friction. The two steps are plotted in *figure 4.10*. According to *equations 4.15 & 4.16*, the frictional coefficient is proportional to the ejection force. Lubrication of the die-wall interface would be the solution to decrease the frictional coefficient. The value of the frictional coefficient for a dry aluminium-steel interface is equal to 0.61. Under lubricated conditions, for example using molybdenum, this last value could decrease down to 0.2 (Engineers Edge). In order to avoid stick-slip behaviour during ejection, a homogeneous lubrication is also required. The problem related to lubrication is the contamination of the sintered part, due to the risk of residual lubricant inside the compact. Different part properties, as magnetism and porosity, can be affected by this problem. It is worth pointing out that lubricant contamination is more relevant for micro-parts due to the small size.

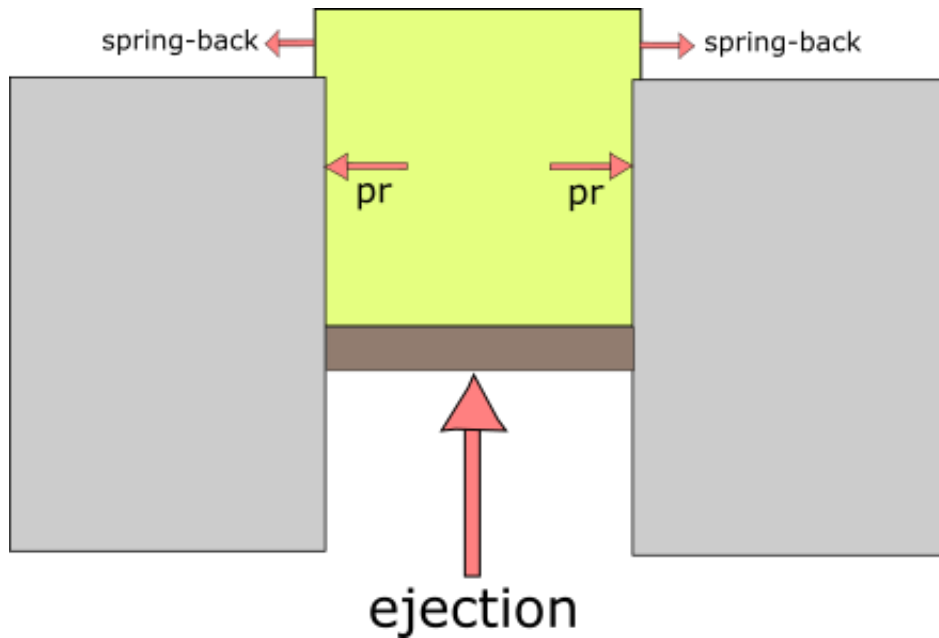


Figure 4.11: Schematic drawing of the spring-back effect during ejection.

Another important problem related to residual pressure consists in the spring-back effect, *figure 4.11*. The sintered part is still compressed during the ejection. When the upper part of the compact sticks out from the die, it expands elastically while the bottom part is still compressed inside the die. The horizontal shearing stress generated by this phenomenon may generate cracks in correspondence of the output corner. In order to avoid this kind of problem, it is possible to have a gradual ejection of the part through a sleeve or using chamfer instead of edges. The spring-back percentage can be calculated according to, (Höganäs 2000):

$$S\% = 100 \cdot \frac{\lambda_c - \lambda_d}{\lambda_d} \quad (4.17)$$

where  $\lambda_c$  is the transversal dimension of the ejected part and  $\lambda_d$  is the transversal dimension of the compressed part inside the die. Spring-back depends on different parameters, like compacting pressure, powder properties, lubricants, alloying additives, and elastic properties of the compacting die.

## 4.4. Problem Solving to Residual Pressure

The last paragraph has pointed out the definition of the residual radial pressure and its effects as the most influencing problems related to micro-sintering, concerning how obtain net-shape parts without any cracks and defects. The focus is on researching and designing a tool-system in order to overcome the problem related to pressure, as described at the beginning of this chapter. As described in *paragraph 4.3.3*, lubrication is a solution to decrease friction and reduce frictional force, consequently. However, this project aims at obtaining no-lubricated condition, perhaps reducing the amount of lubricant, in order to avoid all the effects related to part contamination caused by lubricant infiltration. The effects of residual lubricant inside the compact may be represented especially by a higher rate of porosity and changed mechanical, magnetic, and electrical properties; part inhomogeneity, caused by binders, affects electrical conductance/isolation of the workpiece. Before proceeding to the concept modelling, a preliminary study of different scientific papers has been done to better examine different tool-system solutions involved with radial pressure issue.

### 4.4.1. Split Die and Thread Forming



Figure 4.12: (a) Experimental set for split die (Chen et al. 2007), (b) thread forming die (Andersen & Lund 2008).

A split-die design provides a solution to the residual pressure. The die tool is characterized by different components. Before starting the process, all the components are assembled in order to close the die and sinter the workpiece. After the manufacturing process, the die is disassembled and the part ejected. Two different ways has been studied in order to close the die. The first one consists in closing the die by screwing two halves, *figure 4.12 (a)*. After sintering, unscrewing of the two



halves allows the releasing of the die and the ejection of the part (Chen et al. 2007). The second one consists in thread forming, *figure 4.12 (b)*. The die is split into different jaws that realise a thread on the external surface. An external tool, characterised by an internal thread, is screwed in order to assemble the different jaws (Andersen & Lund 2008). Of course, advantages and disadvantages should be analysed. Particularly in micro-forming, this kind of tools facilitate the ejection of the part, as the tools need only to be disassembled (Fu & Chan 2014). On the other hand, some disadvantages have to be taken into account. Formation of flash at the parting lines, difficulty in alignment of the tools (Fu & Chan 2014), intermittence of the process and feasibility for industrial processes (Ghassemali et al 2013), and difficulty in controlling the axial pre-stress during the process (Groenbaek & Nielsen 1997) are the main disadvantages related to this solution.

#### 4.4.2. Pre-stressing Tools

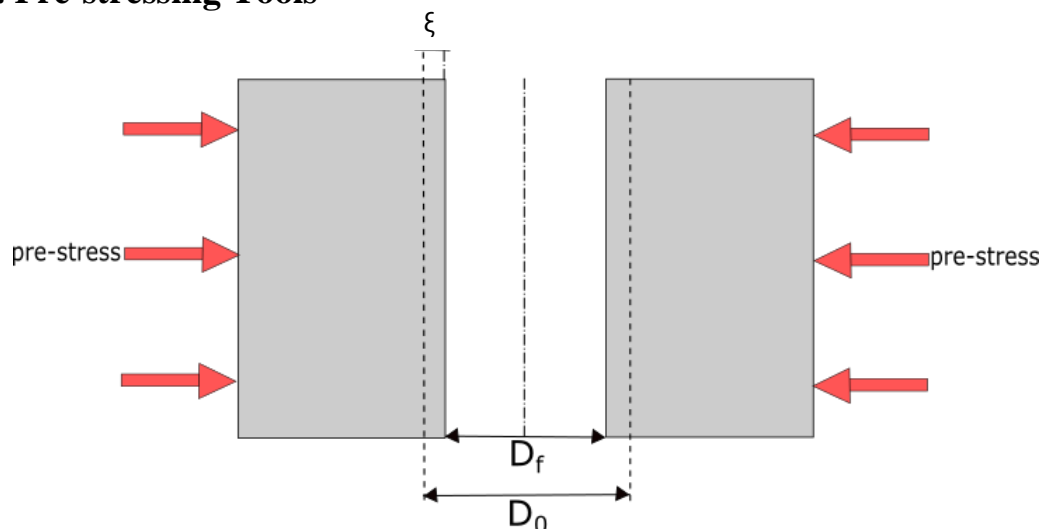


Figure 4.13: Diameter reduction due to a pre-stressed condition.

A different approach to overcome the problem related to residual pressure consists in pre-stressing. The functional principle related to pre-stress consists in reducing the inner size of the die through a compression tool applied on the outer diameter. The inner radius will result decreased by a value equals to  $\zeta$ , depending on the pressure applied, *figure 4.13*. During sintering, the die will be under a pre-stressed condition, the part will generate a compression over the die-wall interface due to powder compaction and temperature, as described in *paragraph 4.3.1 & 4.3.2*. After sintering process, the die will be released by pre-stress and it will expand to its starting size, at last. Simultaneously, the sintered part starts to expand due to spring-back. If the die expansion is higher than the workpiece expansion, a clearance between the two parts will be generated. On a theoretical way, the free-ejection condition is achieved. Different ways has been studied in order to obtain a pre-stressed die.

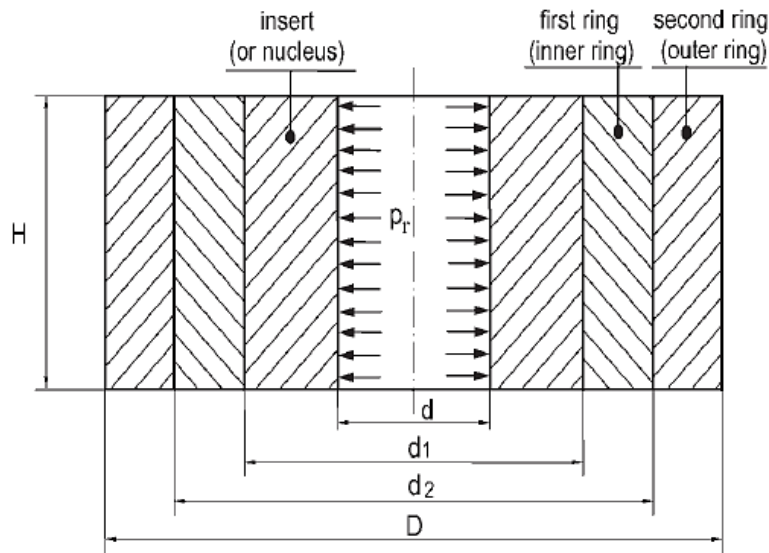


Figure 4.14: Double stress-ring application (Armentani et al. 2012).

The most widespread solution is based on a stress-ring application. The functional principle is based on the assembling of one or two rings on the external diameter of the die, *figure 4.14*. In order to generate a shrink fit, the inner diameter of the stress ring must be lower than the external diameter of the die. A fit pressure is generated, related to the interference value, between the two diameter sizes. This solution represents a cost-savings way to achieve the pre-stress. The stress-rings allows an optimized control of the pressure and a homogeneous stress field (Andersen & Lund 2008). On the other hand, the stress-rings are subjected to longitudinal fatigue cracks (Groenbaek & Nielsen 1997); their use for large and complex products is questionable in terms of economics, practicality, and maintainability (Koç & Arslan 2003).

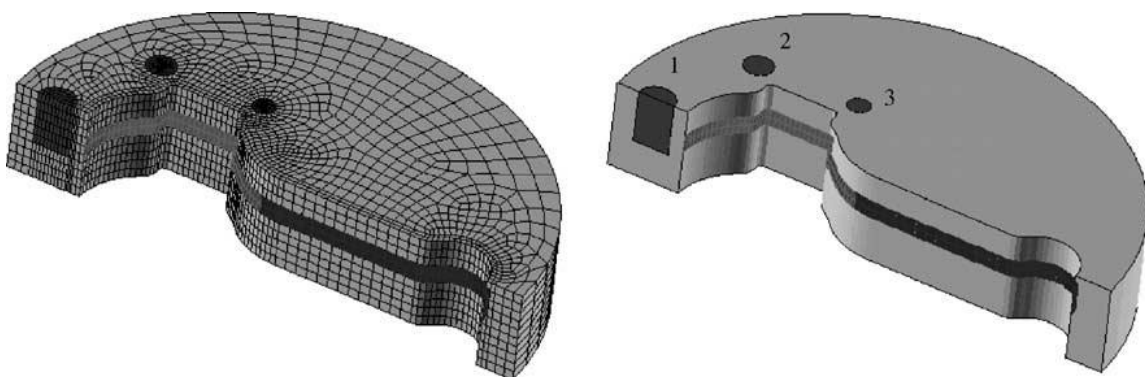


Figure 4.15: Stress pins (Koç & Arslan 2003).

The stress pins, *figure 4.15*, represent a good solution to obtain localized stress-fields. They are placed in critical areas of the die depending on the part complexity (Koç & Arslan 2003). The stress pins improve the tools lifetime and allow the manufacturing of complex sintered parts; moreover, they are easy to install and suitable for cost-

saving. They represent a good alternative whenever stress-ring solution results difficult to apply.

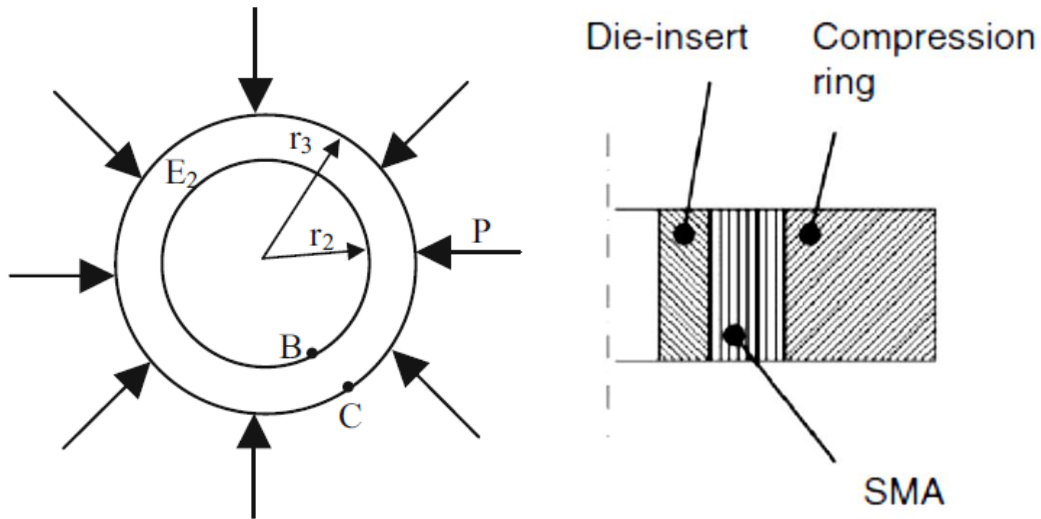


Figure 4.16: (a) Pressure generated by SMA contraction (Pan et al. 2008), (b) Smart Forming-Tool Concept® (Qin 2006).

Shape-memory alloys (SMAs) represent a recent interesting solution. These alloys have a particular property based on recovery capability when they are heated over certain temperatures, called *austenitic temperatures* (Qin 2006). This property can be used in die pre-stressing. After heating the SMAs over their proper austenitic temperature, they start to apply pressure over the die, similarly to a stress-ring, *figure 4.16 (a)*. Currently, researches have been focused on the capability of this material in micro-forming. A concept can be seen in *figure 4.16 (b)*. The most widespread alloy is Nitinol, a NiTi based alloy. The austenitic temperature depends on the phase transformation temperature of the specific alloy; this one depends on its chemical composition and deformation history. Other advantages of SMAs consist in their form-error compensation during the process and their resistance attack to most chemicals. However, SMAs result difficult in pressure control. There is no satisfactory thermodynamic model that adequately describes their behaviour, and its properties may change dramatically with stress strain-temperature cycling if subjected to fatigue lifetime (Johnson et al. 2001).

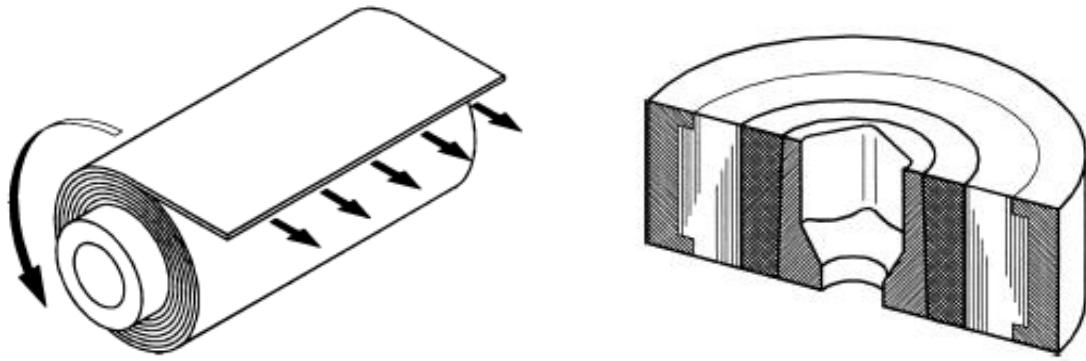


Figure 4.17: (a) Winding principle of STRECON®, (b) STRECON® layout (Groenbaek & Nielsen 1997).

Strip-wound containers produced by STRECON<sup>®</sup> represent the industrial solution to pre-stressing of dies. The pressure is provided by winding a thin strip of high-strength steel around a core of tool steel or tungsten carbide. During the winding process, the steel strip is preloaded with a controlled winding tension, *figure 4.17 (a)*. The stress distribution can be optimised by varying the wind tension to the optimal value. Consequently, the strip-wound containers can be loaded with a higher-internal pressure than a conventional multiple stress ring set before the material would deform plastically (Groenbaek & Nielsen 1997). This solution is the most expensive among the last ones described. However, it represents a good solution for series production due to improved die lifetime.

## 5. Concept Modelling

### 5.1. Introduction

After a general overview of the different solutions studied, see *paragraph 4.4*, the one adopted in this project is based on the stress ring. The reasons of this choice are evaluated in cost consideration, experimental capability, available resources, and chances of success. Stress ring is the best-known solution if compared to the others. Stress pins are not suitable for a part characterised by axial symmetry, as the design would result more complex than a classic stress-ring application. Split-die and thread forming may result difficult to apply due to flash generated at the parting lines, especially with aluminium powder used in this project; furthermore, the alignment of the different tool components may result difficult because of micro-size and final part quality may be compromised. Strecon<sup>®</sup> represents an industrial solution for macro-manufacturing; whose application has not been investigated in scientific literature. Additionally, while an industrial solution does not allow the full design of the tool, stress-ring application allows the complete analysis and choice of the geometrical parameters involved in order to control the pre-stress and the resulting diameter reduction of the die. Firstly, in order to estimate the required-die compression, next paragraph starts evaluating the residual pressure and the volume expansion of the sintered, considering the theory seen in *paragraph 4.3*. Secondly, the details of geometrical characteristics related to the solution adopted have been described. Then, all the analytical models related to the die-system have been explained; thus, the designing phase has been described. On a preliminary phase, the die-ring assembly has been investigated considering all the influencing-geometrical parameters involved. Then, all the other components of the whole die-system have been designed, starting from the geometrical characteristics of the die-ring assembly, and trying to take into account all the main geometrical constraints. Finally, some investigations on forces and materials have been done in order to ensure the functionality of the concept.

## 5.2. Analytical Results on the Gear Expansion

This paragraph aims at estimating the residual stress of the sintered gear, thus the volume expansion. This value allows to understand the required diameter reduction of the die in order to obtain the correct clearance between die and gear. After sintering phase, this clearance could allow a free-ejection condition of the sintered part. Estimations on this paragraph have been calculated according to the theory seen in *section 4.3*.



Figure 5.1: Aluminium powder used in the experiments.

The gear is manufactured with aluminium powder, *figure 5.1*; for the main characteristics see *Appendix 2: Datasheets*.

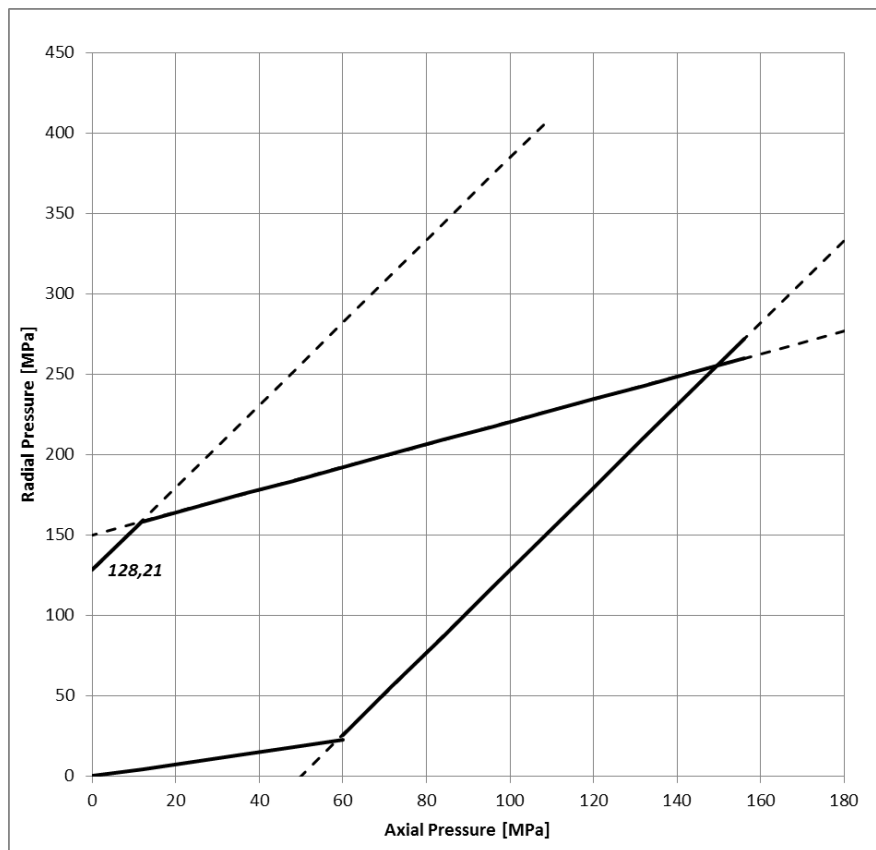


Figure 5.2: Hysteresis during compaction and releasing of the powder.

The powder needs to be compacted in order to obtain the highest density. The purpose is obtaining a value of the final density near the nominal one ( $2.7 \text{ mg/mm}^3$ ). When the powder is compressed inside the die, a radial pressure is generated onto the die-interface, as the radial expansion is not possible. Through Bockstiegel's model it is possible to estimate the value of residual pressure, see *paragraph 4.3.1*. In *figure 5.2*, the hysteresis cycle during powder compaction is shown. Here, the radial pressure generated during the elastic/plastic compaction and releasing of the axial pressure has been calculated according to *equation 4.8, 4.9, 4.10 & 4.11*. By referring to the model, it can be considered that the main parameters related to residual radial pressure consist of the yield strength of the material and frictional condition. The material has to be plastically deformed, otherwise it will recover its starting shape due to elastic condition. The aluminium yield strength, for pure aluminium at room temperature ( $20 \text{ }^\circ\text{C}$ ), can vary from 30 MPa to 150 MPa (Kaufman 1999). An average value of 50 MPa has been considered in this project.

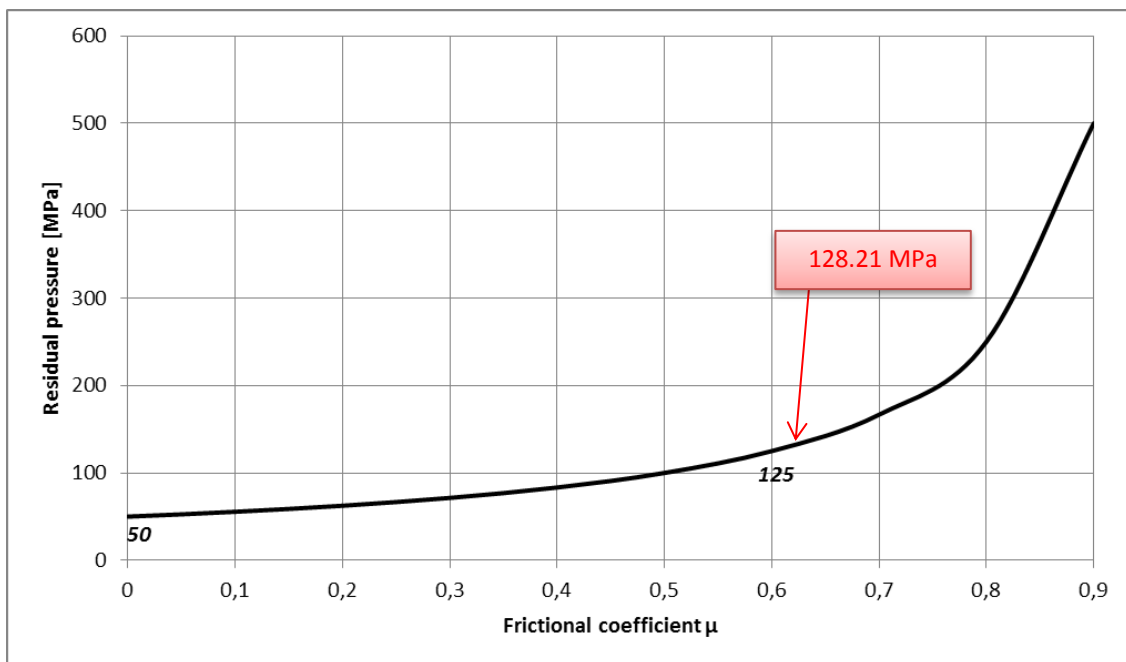


Figure 5.3: Residual stress depending on friction condition.

The frictional coefficient has an important influence on the residual pressure. The pressure value has been calculated according to (Bockstiegel 1965):

$$p_r = \frac{\sigma_0}{1-\mu} \quad (5.1)$$

where  $\sigma_0$  is the yield strength and  $\mu$  represents the frictional coefficient between the die and powder. The *equation 5.1* evaluates the residual radial pressure at the end of hysteresis. From the diagram in *figure 5.3* it is possible to see how the value of pressure results higher with the increase of friction. In this project, one of the purpose

is to avoid lubrication due to related contamination problems. For the analysis the value of 0.61 is used, related to the aluminium-steel friction (Engineers Edge). Analytically, the residual pressure generated by powder compaction is equal to 128.21 MPa.

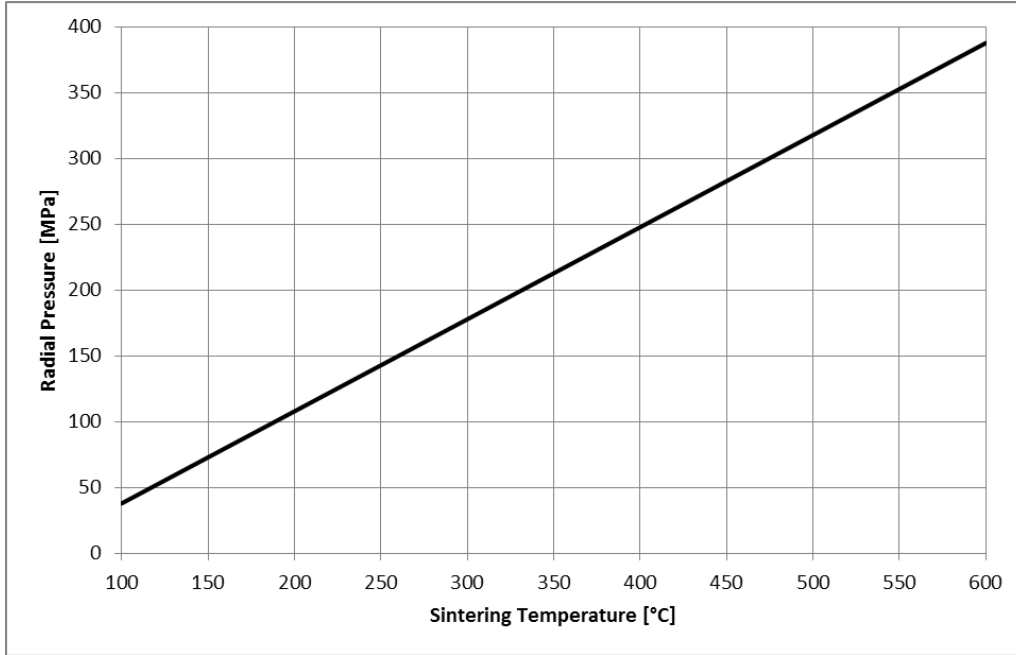


Figure 5.4: Radial pressure generated at the die-wall interface, related to sintering temperature.

The second influencing parameter is the sintering temperature. In this project, the process temperature planned is up to 600 °C; this value represents a trade-off in order to achieve a good densification of the compact and avoid any grain growth because of high temperature, considering that the melting temperature of aluminium is 660 °C. As said in *paragraph 4.3.2*, the different thermal expansions between the part and the die during the whole process generate a pressure onto the die-wall interface. The pressure value can be calculated according to *equation 4.14*:

$$p_r = \frac{dD}{D_0} E = \frac{(\alpha_{gear} - \alpha_{die}) \cdot D_0 \cdot \Delta T}{D_0} E \quad (5.2)$$

where  $\alpha_{gear}$  and  $\alpha_{die}$  are the thermal expansion coefficient of the gear and die,  $D_0$  is the diameter of the circumscribed circle of the gear, equals to 3.1 mm,  $E$  is the Young's modulus, and  $\Delta T$  is the temperature gradient, compared to the room temperature (20 °C). The *Figure 5.4* shows the calculated radial pressure at different temperatures. It is worth pointing out that in the preliminary calculations,  $\alpha_{gear} = 2.4 \times 10^{-5}$  mm/(mm·°C) and  $\alpha_{die} = 1.35 \times 10^{-5}$  mm/(mm·°C); the first value refers to aluminium, the second one, instead, refers to an average value related to the hot-work-steel class under condition of high temperature. This choice has been made because the specific die material has not been chosen yet.



$T_{\text{sint}}$	$\Delta l/l_{\text{gear}}$	$\Delta l/l_{\text{die}}$	$\Delta l/l_{\text{total}}$	$p_{\text{thermal}}$	$p_{\text{compact}}$	$p_{\text{tot}}$	$r_{\text{exp}}$
[°C]				[Mpa]	[Mpa]	[Mpa]	[μm]
100	0.00192	0.0014	0.0006	37.96	128.21	166.17	1.37
200	0.00432	0.0027	0.0016	107.89	128.21	236.10	2.44
300	0.00672	0.0041	0.0027	177.82	128.21	306.03	3.51
400	0.00912	0.0054	0.0037	247.75	128.21	375.96	4.59
500	0.01152	0.0068	0.0048	317.68	128.21	445.89	5.66
<b>600</b>	<b>0.01392</b>	<b>0.0081</b>	<b>0.0058</b>	<b>387.61</b>	<b>128.21</b>	<b>515.82</b>	<b>6.74</b>

Table 5.1: Theoretical value of the total residual pressure and resulting radius expansion of the gear after sintering process.

After pressure calculations, the two main components, which are the one generated after powder compaction and the thermal one, have been added in order to estimate the residual radial pressure. In *table 5.1* the different values obtained are shown depending on the maximum sintering temperature achieved during the process. The last column would show the radius expansion if the gear was not constrained by the internal die-wall. Radius expansions is related to the residual radial pressure according to the next formula, (Long 1960):

$$r_{\text{exp}} = \frac{(\sigma_r - \nu\sigma_r - \nu\sigma_a)}{E} \times r_0 \quad (5.3)$$

where  $E$  is the Young's modulus,  $\nu$  is the Poisson's coefficient,  $r_0$  is the radius of the circumscribed circle of the gear, and  $\sigma_r$  and  $\sigma_a$  the radial and the axial pressure inside the compact, respectively. It is worth underlining that for this calculation an axial-compaction pressure of 150 MPa has been hypothesised, corresponding to the maximum pressure planned for the experiments; this value should be seen according to the yield strength of aluminium described above. Finally, it should be remembered that after sintering process the manufactured part will be cooled down to the room temperature. The final expansion will not be the same calculated at the defined sintering temperature. The die-system geometry would be based on the highest value calculated, corresponding to the sintering temperature of 600 °C. This choice should be seen in behalf of safety, considering the uncertainty related to the theory approximations. After this consideration, the value of 6.74 μm has been used in next calculations, as highlighted in *table 5.1*; the diameter reduction of the die, after pre-stressing, has to be larger than the gear volume expansion in order to ensure the correct clearance after sintering process.

### 5.3. Conical-Die Concept

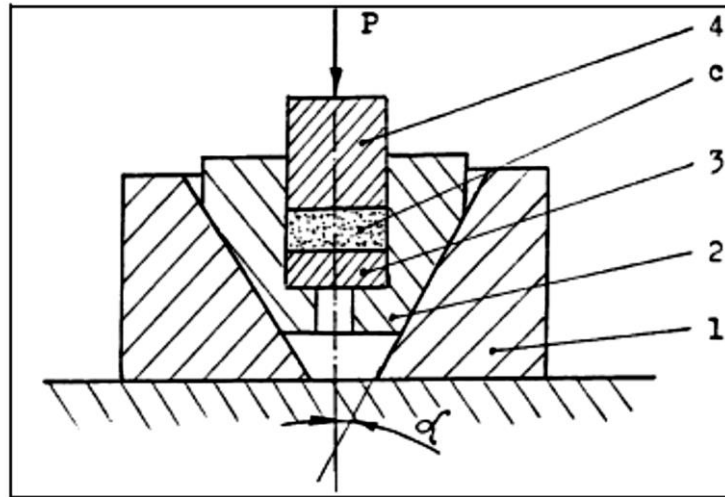


Figure 5.5: Schematic drawing of a conical die concept. 1- container; 2- sleeve; 3-ejector; 4-punch; c-powder compact (Noveanu 2013).

Based on the stress-rings-functional principles, a conical-die concept is designed, *figure 5.5*. The main difference related to a classic stress ring application is referred to the fit shape. A conical shape allows to assemble and release the die-ring system under elastic conditions without compromising the mechanical integrity of the tools. The die can be ejected from the ring by releasing fit-pressure. As described in stress-ring application, see *paragraph 4.4.2*, the purpose of this system is generating a clearance between die and sintered part after pressure releasing in order to have a free-frictional condition during the ejection of the sintered workpiece.

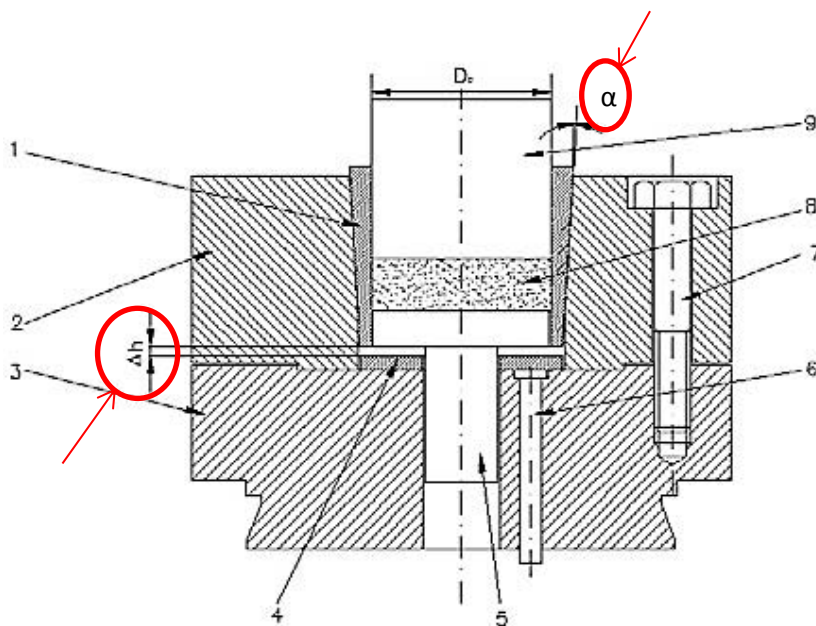


Figure 5.6: Conical die concept. 1-sleeve; 2-die body; 3- lower die body; 4-spacer disc; 5- lower punch; 6-ejection pin; 7- die assembly bolt; 8- part; 9- upper punch (Noveanu & Frunză 2013).

On the basis of literature studies, diameter reduction can be calculated as following, (Noveanu & Frunzã 2013):

$$\Delta D = 2 \cdot \Delta h \cdot \tan \alpha \quad (5.4)$$

where  $\Delta h$  is the interference calculated in the axial direction, and  $\alpha$  is the conicity of the sleeve, *figure 5.6*. The  $\Delta h$  value gives the size of the elastic radial pre-strain. This pre-strain should be at least equal to the relaxation of the part in order to achieve free ejection.

### 5.3.1. Tools Analytical Model

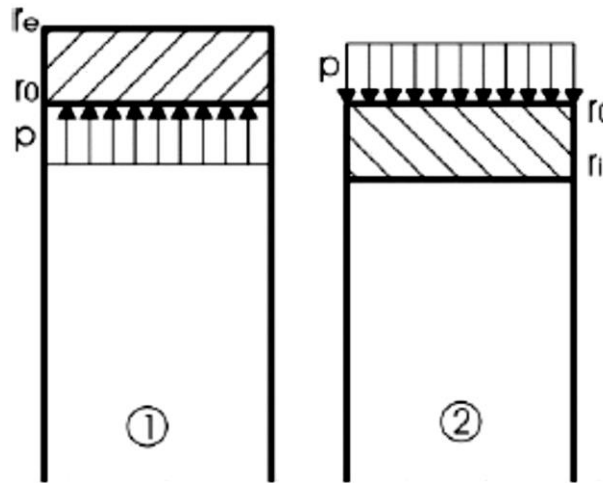


Figure 5.7: Die-ring coupling for the analytical approach (Tovo 2012).

In order to achieve the desired clearance after sintering, it is important to designing the correct sizes of the die and the ring. In this project, the analytical theory is based on the thick-walled hollow cylinder theory (Atzori 2001), *figure 5.7*. The fit-pressure related to the interference die-ring is calculated as following:

$$p_f = \frac{I_\phi E}{4r_o^3} \frac{(r_e^2 - r_o^2)(r_o^2 - r_i^2)}{r_e^2 - r_i^2} \quad (5.5)$$

where  $I_\phi$  is the diameter interference after fitting,  $E$  is the Young's modulus of the materials,  $r_e$  is the outer radius of the ring,  $r_i$  the inner radius of the die and  $r_o$  is the radius after fitting. This relation starts from the hypothesis of plane stress and plane strain.

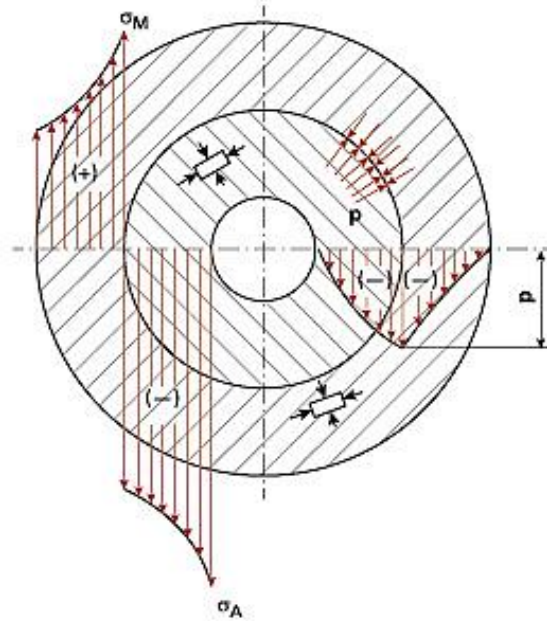


Figure 5.8: Stress field generated due to tools fitting (Crivelli 2013).

The fit-pressure generates a stress field inside the tools, *figure 5.8*. This field is characterised by three main component, radial, tangential, and longitudinal stress. Due to the previous hypothesis related to stress and strain, the longitudinal stress can be neglected. Tangential and radial stresses depend on the applied pressure.

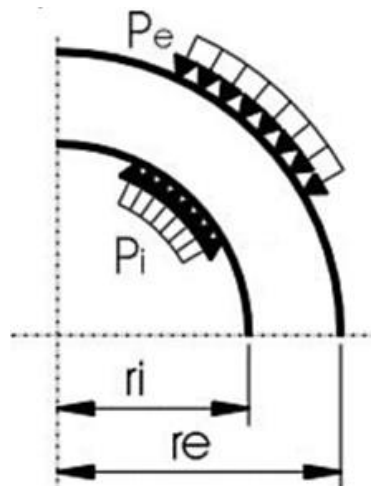


Figure 5.9: Schematic drawing of a tool subjected to internal/external pressure (Tovo 2012).

When the tool is pressed on the outer diameter, *figure 5.9*, as in the case of the die, the radial and the tangential components of the stress field can be calculated with the following formulas:

$$\sigma_r(r) = -\frac{p_e r_e^2}{r_e^2 - r_i^2} \left(1 - \frac{r_i^2}{r^2}\right) \quad \sigma_t(r) = -\frac{p_e r_e^2}{r_e^2 - r_i^2} \left(1 + \frac{r_i^2}{r^2}\right) \quad (5.6)$$

where  $p_e$  represents the external pressure, in this case the fit-pressure,  $r_e$  and  $r_i$  are respectively the external and the internal radius of the die after fitting, and  $r$  is the

generic radius. To calculate the stress components inside the ring, similar equations are described:

$$\sigma_r(r) = \frac{p_i r_i^2}{r_e^2 - r_i^2} \left(1 - \frac{r_e^2}{r^2}\right) \quad \sigma_t(r) = \frac{p_i r_i^2}{r_e^2 - r_i^2} \left(1 + \frac{r_e^2}{r^2}\right) \quad (5.7)$$

where  $p_i$  is the internal pressure, the fit-pressure in this case,  $r_e$  and  $r_i$  respectively the external and the internal radius of the ring after fitting and  $r$  the generic radius. The description of the whole stress field inside the tools is important to calculating the internal diameter reduction of the die and to study the total pressure which the tools have to withstand. The radial reduction, *figure 4.13*, of the internal diameter of the die is calculated as following:

$$\xi = \frac{r_i}{E} [\sigma_t - \nu \sigma_r] \quad (5.8)$$

where  $r_i$  is the internal diameter of the die,  $E$  is the Young's modulus of the die,  $\sigma_t$  and  $\sigma_r$  are respectively the tangential and the radial stress of the die referred to the inner radius. This value has to be compared to the manufactured-part expansion. In order to reach a clearance condition after sintering, it is important to have an elastic relaxation of the part lower than the die one.

## 5.4. Die-Ring Design

The diameter expansion of the experimental micro gear, calculated in *paragraph 5.2*, represents the starting point for the die design.

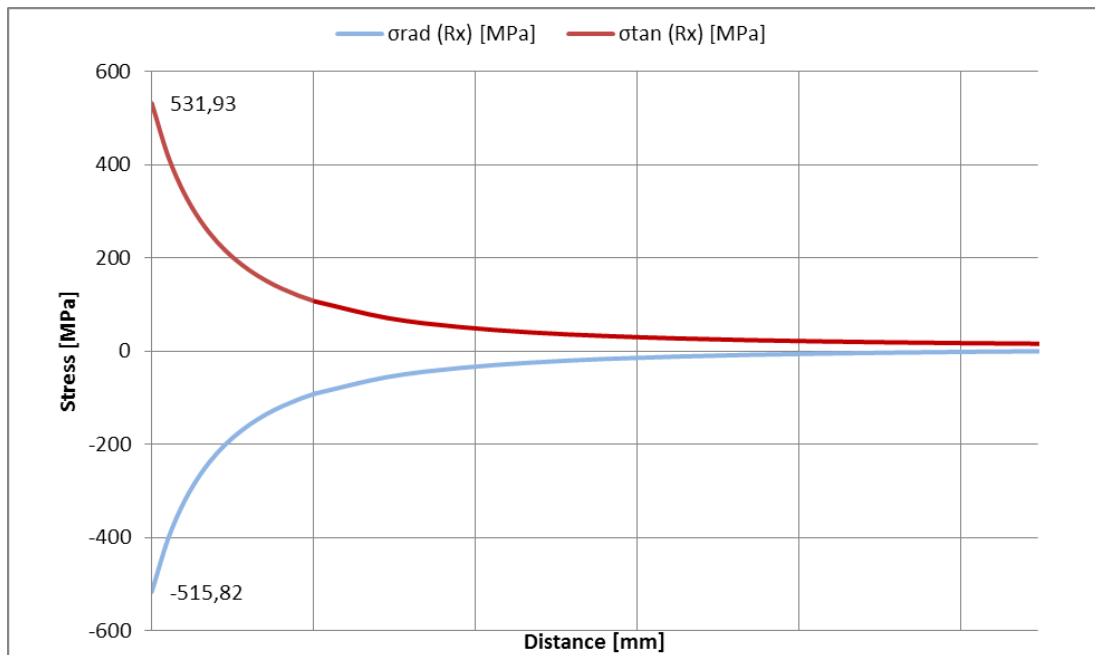


Figure 5.10: Stress field inside tools generated by gear expansion without any pre-stressed die. This field refers to a sintering temperature of 600 °C, see *table 5.1*.

The *Figure 5.10* shows the stress field exerted by the radial pressure of 515.82 MPa ( $T_{\text{sint}} = 600 \text{ }^\circ\text{C}$ ), see *table 5.1*, according to the thick-walled hollow theory, *equations 5.7*. The calculated stress field of *figure 5.10* refers to a simple die without any applied pre-stress. This pressure is exerted onto the internal die-wall surface. As a consequence, the ejection of the gear may result difficult due to friction, and the risk of cracks may be very high. Furthermore, the problem of spring-back during ejection could affect the part quality, see *paragraph 4.3.3*. The die pre-stressing aims at avoiding this kind of problem reducing the internal diameter of the die during the sintering and then expanding it again, at the end of the process. The diameter reduction of the die is allowed by conical-interference fit between the die and an external ring, as already described in *paragraph 5.3*.

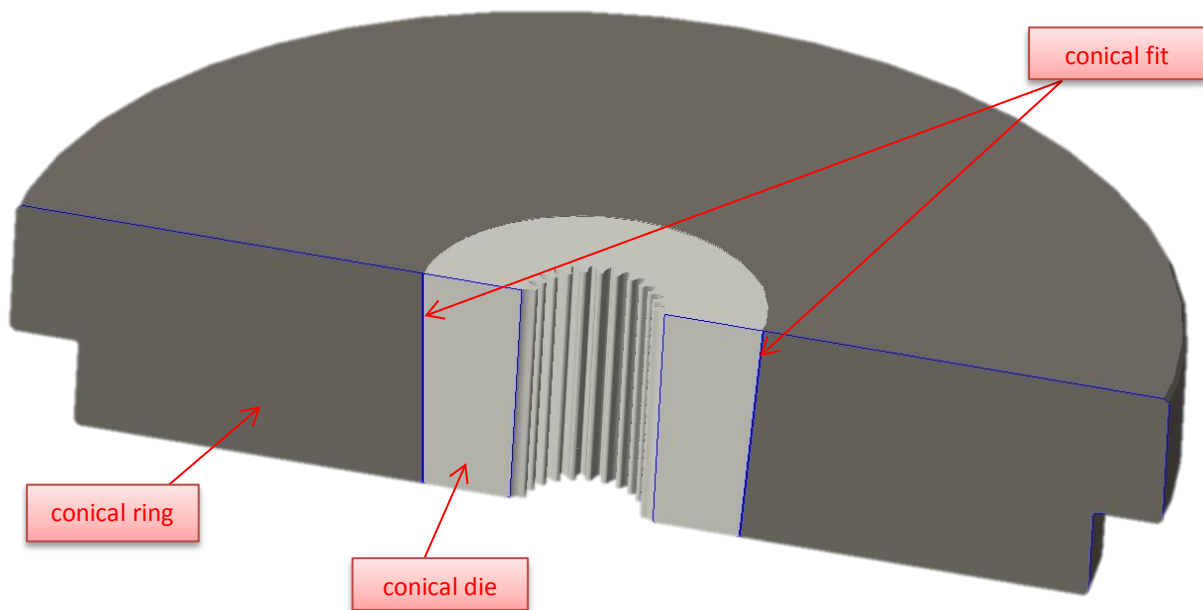


Figure 5.11: Conical die concept section, 3D model cad design.

The conical fit, *figure 5.11*, generates a stress field inside the die and the ring, thus an internal diameter reduction to the die. It is possible to optimise the interference between tools according to the thick-walled hollow theory, described in *paragraph 5.3.1*. After fitting of both the tools, a fit pressure is achieved, according to *equation 5.5*. Then, the calculation of this pressure allows the estimation of the internal pressure fields of the tools, according to *equation 5.6 & 5.7*; in particular, the internal-die-stress field makes the estimation of the internal diameter reduction possible by using the *equation 5.8*. This formula requires the tangential and radial pressure corresponding to the internal diameter of the die, *equation 5.6*. As can be seen from these analytical models, many geometrical parameters are involved in stress calculations. Next paragraphs aims at describing the main influencing

parameters considered in the designing phase of the die-ring assembly; in particular, the influence of the interference radius  $r_0$ , the external radius of the ring  $r_e$ , and the interference value  $I_\phi$ , have been studied and analysed. The choice of these parameters is related to the *equation 5.5*, where the inner radius of the die,  $r_i$ , and the Young's modulus of the tools,  $E$ , are considered fixed; the first one because of the size of the gear, the second one since referred to the tools material, defined by steel. It is worth pointing out that the conicity angle of the fit does not have any influence in the next calculations, as all the formulas described refers to the diameter of the middle-cross section of the tools. With regard to the 3D cad model concept, an angle of  $3^\circ$  has been chosen by referring to scientific literature (Noveanu & Frunzã 2013). The same reasoning can be applied on the height of the tools. A fine optimisation of these latest parameters has been done considering the forces involved in the fitting of the two components, see *paragraph 5.6.2*. Finally, it should be noted that the influencing parameters described above ( $I_\phi$ ,  $r_0$  and  $r_e$ ) have been analysed together during the designing phase trying to achieve a fine optimisation of the tool sizing. The formal division in different paragraphs aims at describing how the single parameter influences the whole system with particular regards to the inner-radius compression of the die. All the calculations have been made by using an Excel<sup>®</sup> datasheet.

#### 5.4.1. Interference Radius Influence

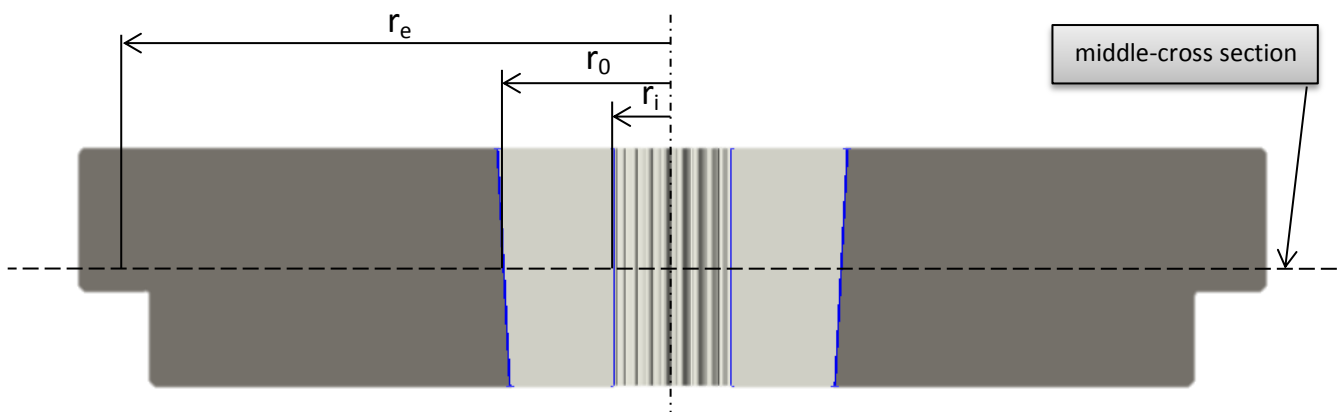


Figure 5.12: Conical die concept, main geometrical size.

Related to the conical fitting, the first analysed element is the interference radius,  $r_0$ . After the fitting phase, the external diameter of the die has been compressed, while the internal one of the ring has been expanded. The radius  $r_0$  is obtained when the die and the ring have been fitted, and evaluated on the middle-cross section, *figure 5.12*. From *figure 5.12* it is also possible to see the other two geometrical sizes,  $r_e$  and  $r_i$ , respectively the external and the internal radius of the whole assembly; in particular, due to alignment requirements,  $r_e$  is considered as the external average radius because of the extrusion designed on the tool.

Poisson $\nu$		0,3							
Young E		190000 MPa							
<b>DIE</b>				<b>RING</b>					
$r_i$	$r_{e\_die}$	$r_{i\_ring}$	$r_e$	$I_\emptyset$	$r_0$	$p_{fit}$	$\sigma_{rad}(r_i)$	$\sigma_{tan}(r_i)$	$r_{red}$
[mm]	[mm]	[mm]	[mm]	[ $\mu m$ ]	[mm]	[MPa]	[MPa]	[MPa]	[ $\mu m$ ]
1.55	7	6.96	10	80	6.98	271.94	0	-572.09	-4.67
1.55	6.2	6.16	10	80	6.18	364.91	0	-778.80	-6.35
1.55	5.6	5.56	10	80	5.58	443.43	0	-961.02	-7.84
1.55	5.04	5	10	80	5.02	524.84	0	-1160.30	-9.47
1.55	4.5	4.46	10	80	4.48	611.51	0	-1389.33	-11.33
1.55	4	3.96	10	80	3.98	698.44	0	-1646.63	-13.43
1.55	3.8	3.76	10	80	3.78	734.41	0	-1765.72	-14.40
<b>1.55</b>	<b>3.57</b>	<b>3.53</b>	<b>10</b>	<b>80</b>	<b>3.55</b>	<b>775.82</b>	<b>0</b>	<b>-1917.10</b>	<b>-15.64</b>

Table 5.2: Radial reduction related to different values of interference radius.

Depending on the gear size, the inner radius has a fixed value, see *paragraph 4.2.1*. According to literature (Bay 1992), the starting outer die radius has been fixed to its maximum value, about 4.5 times larger than the inner one ( $r_i = 1.55$  mm;  $r_{e\_die} = 7$  mm). The hypothesised elastic modulus  $E$  and the Poisson's coefficient  $\nu$  have been referred to the average characteristics of a hot-work steel. The theoretical results of the radial compression of the die, depending on the  $r_0$ , are shown on *table 5.2*. The iteration has been made by decreasing the external radius of the die. As a consequence, the internal radius of the ring  $r_{i\_ring}$  and the interference radius  $r_0$  have been decreased, too. All the other influencing parameters, the external radius  $r_e$ , and the interference value  $I_\emptyset$  have been maintained constant. The fit pressure,  $p_{fit}$ , the tangential and radial pressure at the inner radius,  $\sigma_{rad}$  and  $\sigma_{tan}$ , and the radial-radius reduction due to press-fit,  $r_{red}$  are calculated according to the thick-walled hollow theory, see *equations 5.5, 5.6 & 5.8*.



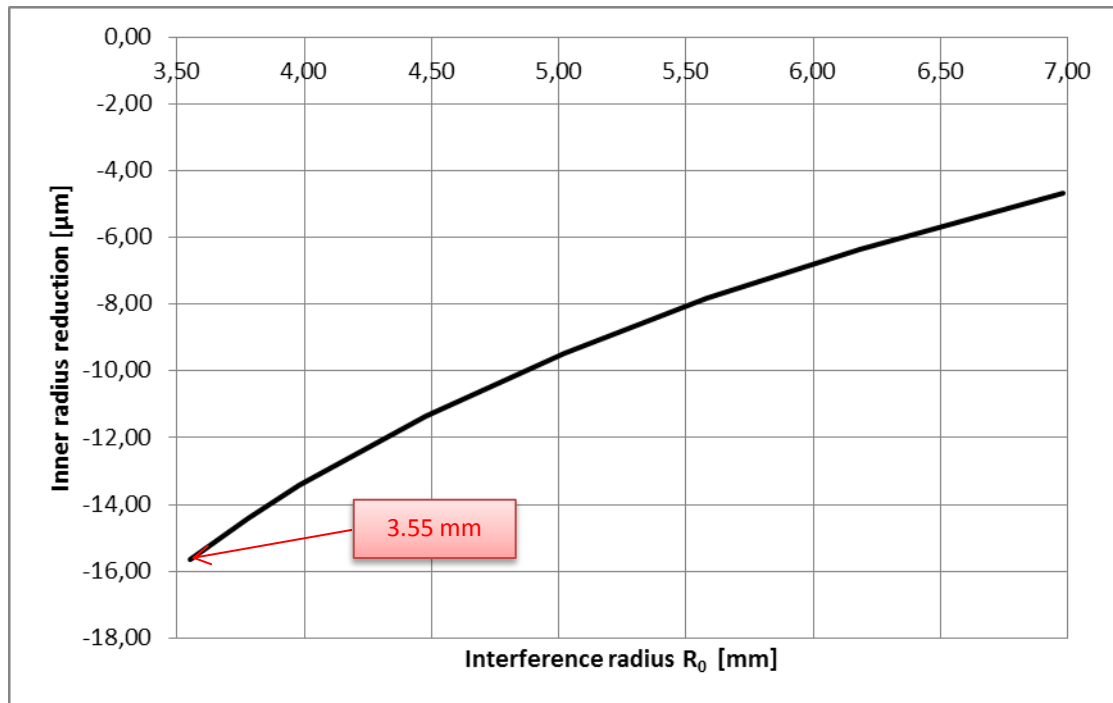


Figure 5.13: Relation between inner radius reduction and interference radius.

By increasing the value of  $r_0$ , it is possible to obtain larger fit pressure, thus higher value of  $r_{red}$ , figure 5.13. It should be observed that the radial stress at the inner radius of the die will be equal to 0 according to the theory, equation 5.6. The reduction is a consequence of the tangential pressure inside the tool. If, on the one hand, the radial compressing of the tool is the purpose, on the other hand the maximum stress value must be kept under control in order to avoid the yielding of the tools. The radius reduction obtained should be a trade-off between the reduction need and technological limits. On this way, with regard of the interference radius, the highlighted solution on table 5.2 represents a trade-off. The choice has been influenced by many geometrical constraints. On the one hand, having a lower value of  $r_0$  allows more compression; on the other hand, if this value is too low there may be some problems related to the higher pressure and difficulty in punches design. A small diameter of the die decreases the available surface to the punches action in order to assemble and release the die from the ring. A small surface means also higher exerted pressure involving other problem related to the buckling of the punches.

### 5.4.2. External Ring Radius Influence

This paragraph aims at analysing the influence of the external radius on the inner-radius compression of the die, while maintaining fixed the other parameters. As described at the end of the last paragraph, the value of the interference radius  $r_0$  is the result of a geometrical trade-off.

DIE		RING							
$r_i$	$r_{e\_die}$	$r_{i\_ring}$	$r_e$	$l_\emptyset$	$r_0$	$p_{fit}$	$\sigma_{rad}$ ( $r_{int}$ )	$\sigma_{tan}$ ( $r_{int}$ )	$r_{red}$
[mm]	[mm]	[mm]	[mm]	[ $\mu m$ ]	[mm]	[MPa]	[MPa]	[MPa]	[ $\mu m$ ]
1.55	3.57	3.53	6	80	3.55	603.34	0	-1490.90	-12.16
1.55	3.57	3.53	7	80	3.55	676.72	0	-1672.22	-13.64
1.55	3.57	3.53	10	80	3.55	775.82	0	-1917.10	-15.64
1.55	3.57	3.53	12.5	80	3.55	808.92	0	-1998.91	-16.31
1.55	3.57	3.53	13	80	3.55	813.32	0	-2009.77	-16.40
1.55	3.57	3.53	17	80	3.55	835.53	0	-2064.65	-16.84
1.55	3.57	3.53	20	80	3.55	844.13	0	-2085.92	-17.02
1.55	3.57	3.53	25	80	3.55	852.17	0	-2105.77	-17.18

Table 5.3: Radial reduction related to different value of the outer ring radius.

Generally, by increasing the size of the external ring radius, it is possible to achieve a larger fit pressure, according to *equation 5.5*. As for the last paragraph, the fit pressure allows to calculate the tangential and radial pressure at the inner radius of the die, *equations 5.6*. Then, the values obtained have been used in *equation 5.8*, in order to estimate the inner radius compression. The correct size has to be chosen also by making reference to the whole die-system geometry. Considering that the heating element used in this project, see *paragraph 4.2.2*, has got a specified maximum diameter of 25 mm, this geometrical constraint has influenced the designed ring. Moreover, in order to avoid any clearance between the heater and the ring, a radius of 12.5 mm has been designed. It is important to consider that an eventual clearance will decrease the heat transmission and will constrain to use metallic strips between the ring and the heater.

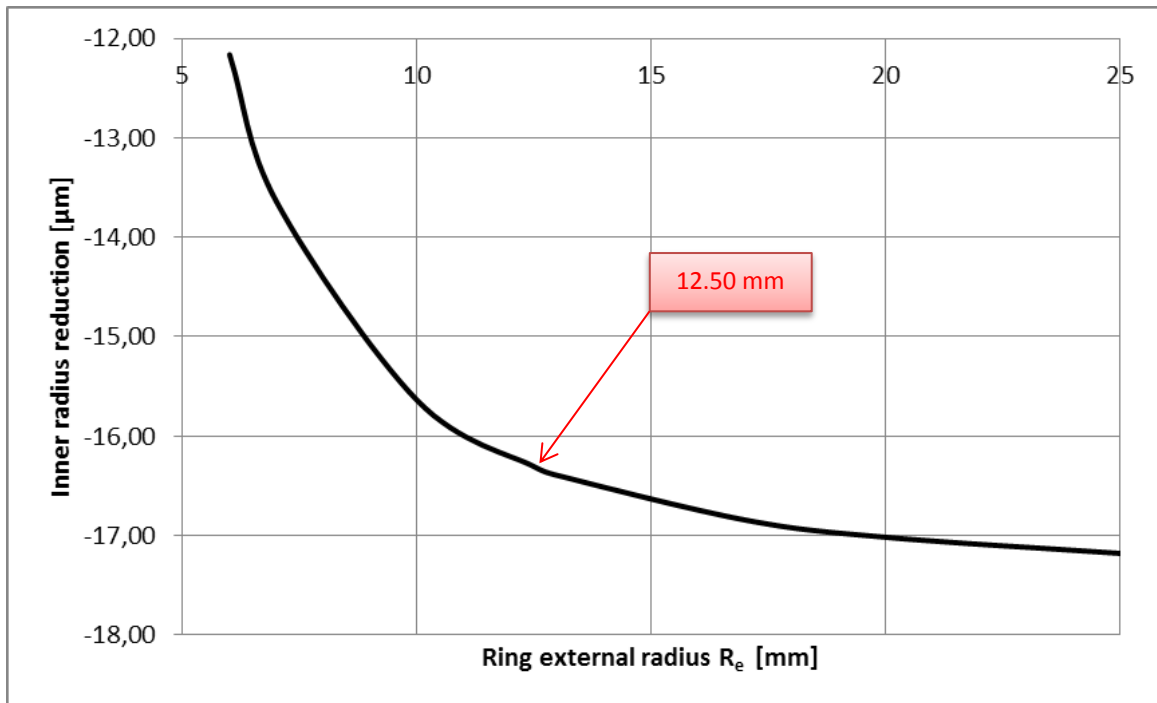


Figure 5.14: Relation between inner radius reduction and external radius of the ring.

Although the maximum allowed radius is 12.5 mm, a theoretical analysis has been done until 25 mm of radius in order to understand the influence of the external radius on the radius compression, *figure 5.14*. Differently from the interference radius, the influence of the outer radius become less influential with its increase; from 6 to 7 mm, there is an increase of 1.48  $\mu\text{m}$  in radius reduction, while from 20 to 25 mm only 0.16  $\mu\text{m}$ . Even if the heater had not been a constraint, the choice of a large  $r_e$  would not be convenient.

### 5.4.3. Interference Influence

The last influencing parameter considered in this project is the interference itself. The other parameters described have been involved in technological and geometrical constraints, as described in the last paragraphs. By contrast, the interference value has not been influenced by geometry. However, the pressure generated is the main element that should be kept under control.

DIE		RING							
$r_i$	$r_{e\_die}$	$r_{i\_ring}$	$r_e$	$l_\emptyset$	$r_0$	$p_{fit}$	$\sigma_{rad}(r_{int})$	$\sigma_{tan}(r_{int})$	$r_{red}$
[mm]	[mm]	[mm]	[mm]	[ $\mu m$ ]	[mm]	[MPa]	[MPa]	[MPa]	[ $\mu m$ ]
1.55	3.57	3.49	12.5	160	3.53	1624.25	0	-4024.43	-32.83
1.55	3.57	3.5	12.5	140	3.54	1419.82	0	-3515.53	-28.68
1.55	3.57	3.51	12.5	120	3.54	1215.79	0	-3008.32	-24.54
1.55	3.57	3.52	12.5	100	3.55	1012.15	0	-2502.78	-20.42
1.55	3.57	3.53	12.5	80	3.55	808.92	0	-1998.91	-16.31
1.55	3.57	3.54	12.5	60	3.56	606.09	0	-1496.70	-12.21
1.55	3.57	3.55	12.5	40	3.56	403.66	0	-996.15	-8.13
1.55	3.57	3.56	12.5	20	3.57	201.63	0	-497.25	-4.06

Table 5.4: Radial reduction related to different value of interference.

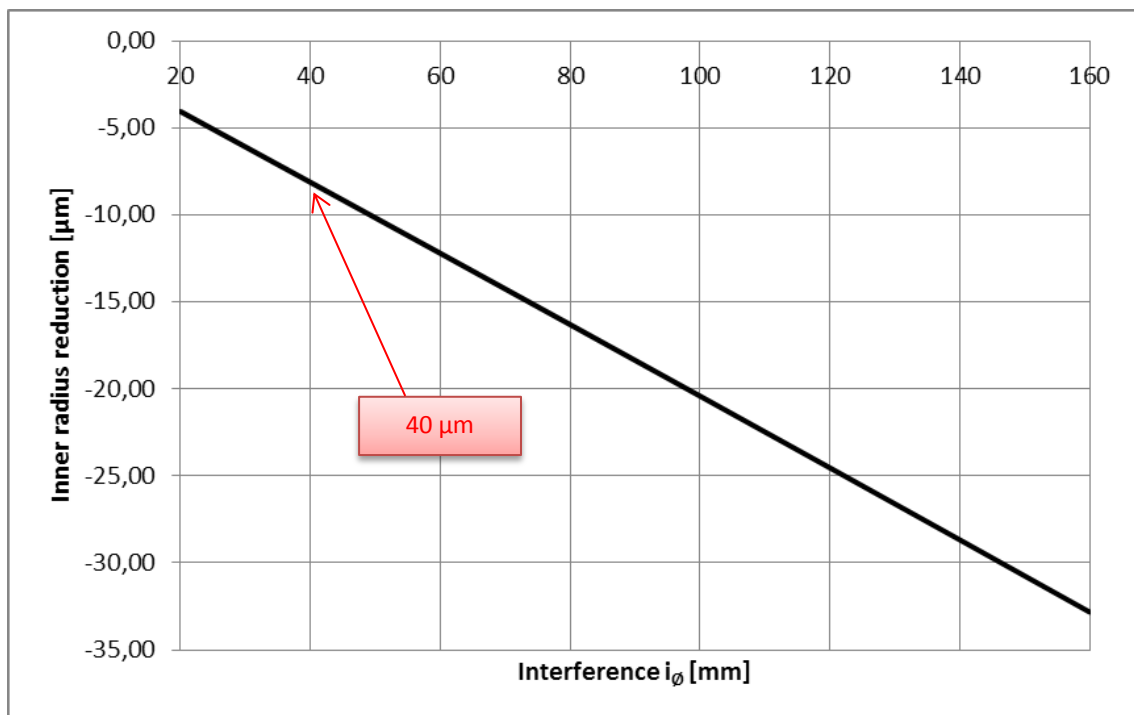


Figure 5.15: Relation between inner radius reduction and the interference value.

Having chosen the interference radius  $r_0$ , and the external radius of the ring  $r_e$ , the calculations aim at describing the influence of the interference value. Table 5.4 shows an overview of the main interferences analysed. The inner-radial reduction has been estimated according to the thick-walled hollow theory as for the last parameters analysed. The influence of the interference value has a linear behaviour with regard to the inner radius reduction, figure 5.15; increasing the interference of 20  $\mu\text{m}$ , allows an increase of about 4  $\mu\text{m}$  in radius reduction. However, an increase of 500 MPa in pressure should be encountered, too. Surely, having a larger compression of the internal radius is better from a functional point of view, but the yield limit of the tool material should be taken into account. Analysing the results shown in table 5.4, 20  $\mu\text{m}$  of interference generates a low value of compression (about 4.06  $\mu\text{m}$ ). Considering that the gear would expand 6.74  $\mu\text{m}$ , as described in paragraph 5.2, this solution is not possible, although the generated pressure may be lower than the yield limit of several tools material. Over 60  $\mu\text{m}$ , the pressure exerted is too high. The process should be reversible to eject more than once, so the risk of plastic deformation of the tools would not be acceptable. The choice is between 40  $\mu\text{m}$  or 60  $\mu\text{m}$ ; respectively, these interference values generate a compression of -8.13  $\mu\text{m}$  and -12.21  $\mu\text{m}$ . In behalf of safety, the value of 40  $\mu\text{m}$  has been chosen, as highlighted in table 5.4. This choice has allowed a larger range of possible tool materials. Moreover, the theoretical compression should be suitable for the gear expansion; the value of -8.13  $\mu\text{m}$  is higher than 6.74  $\mu\text{m}$ , with a predicted clearance of -1.39  $\mu\text{m}$ .

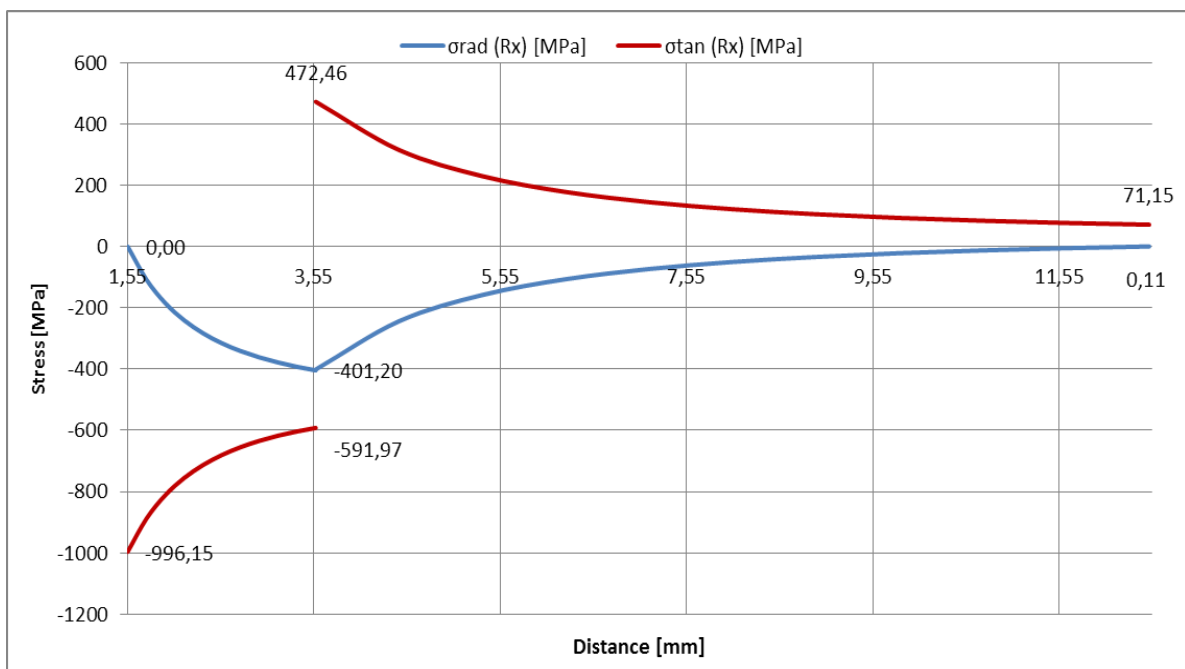


Figure 5.16: Stress field inside the die ( $x < 3,55\text{mm}$ ) and the ring ( $x > 3,55$ ) for 40  $\mu\text{m}$  interference.

According to the thick-walled hollow theory, the pressure field inside the tools, die and ring, has been estimated, *figure 5.16*. Considering the Von Mises failure strength, the equivalent pressure before failure would be  $\sigma_{eq} = \sigma_{tan} - \sigma_{rad}$ . The value calculated is equal to 996.15 MPa, corresponding to the inner radius of the die. So, the material should be chosen with a yield strength  $\sigma_0$  higher than the maximum equivalent stress generated by tools fitting.

### 5.5. Die-system 3D modelling

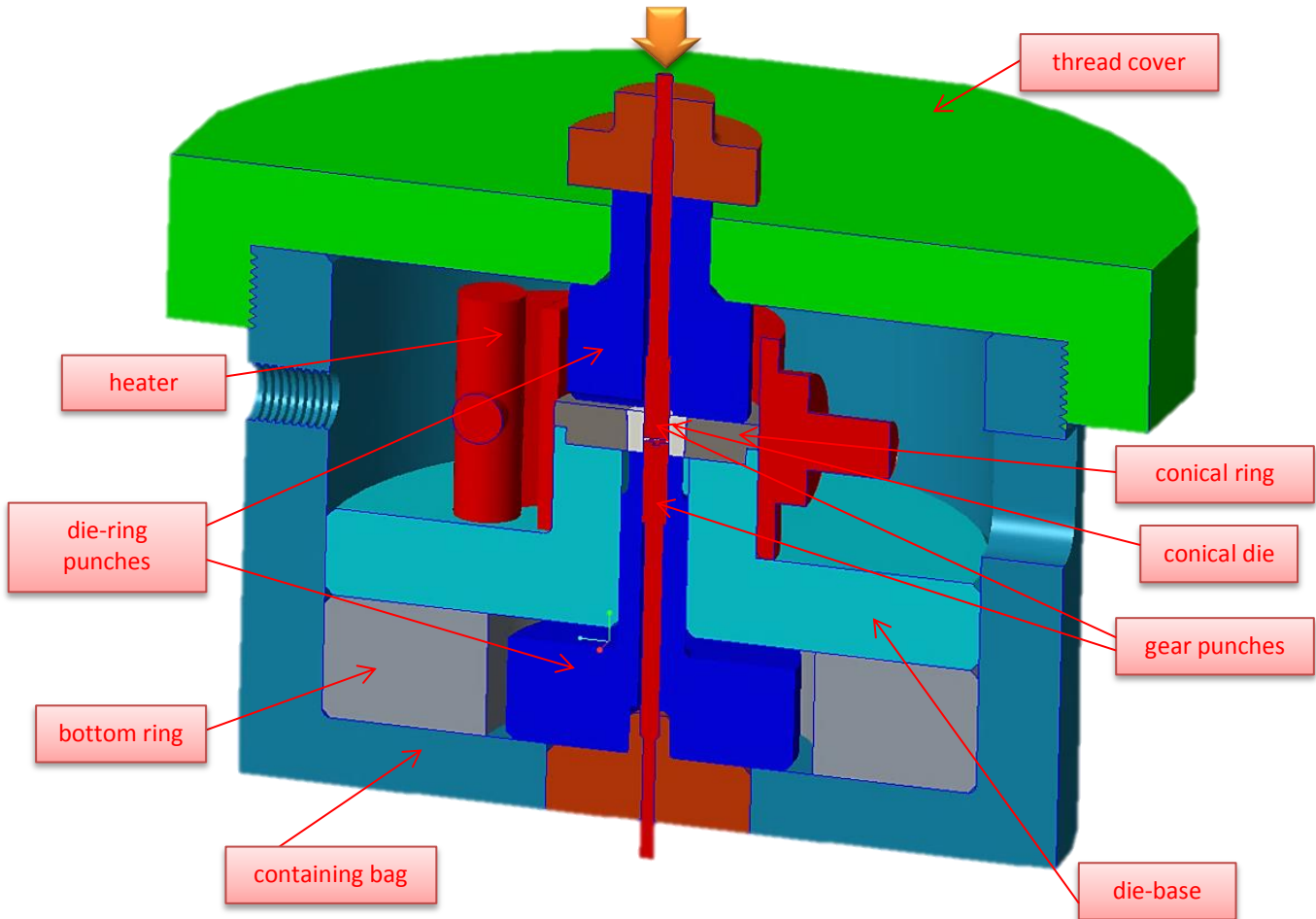


Figure 5.17: Die-system 3D CAD model, section.

After designing the die-ring assembly, the whole die-system has been engineered, *figure 5.17*. Firstly, the design of a system capable of containing the die-ring assembly and ensuring its functionality has been the main aim of this phase. Secondly, it has been studied and designed a system in order to realize the conical fit. The main components of the concept consist of the punches, the containing bag, the thread cover, the die-base, the bottom ring, and the die-ring assembly. In total, the punches are four, two for the gear compaction/ejection, and two for the die-ring coupling/releasing. The gear punches are both composed of two parts because of manufacturing requirements. The containing bag aims at assembling all the

components; the specific sizes are related to geometrical constraints because of the used press. The thread cover is used to apply the correct force exerted by the punch on the die in order realise the conical fit. The force is applied by screwing the cover on the upper thread of the containing bag. It is worth pointing out that the cover is only for coupling; the releasing of the die is operated by the press. The other components, bottom ring and die-base, have been designed only for geometrical need. The details of the components and the functional principle related to the coupling, compaction, and ejection phases will be described thoroughly in next paragraphs. For the specific size of the single tools see *Appendix 3: Technical Drawings*. All the designing phase has been operated by using a 3D cad software, PTC Creo<sup>®</sup>.



Figure 5.18: Mechanical press.

With regard to the maximum dimensions of the system, the external size of the containing bag is defined to the maximum size allowed by the mechanical press, *figure 5.18*. The maximum diameter and height of the system should be not larger than 150 mm and 155 mm, respectively; in addition, the total die-system height should encounter the stroke of the punches.

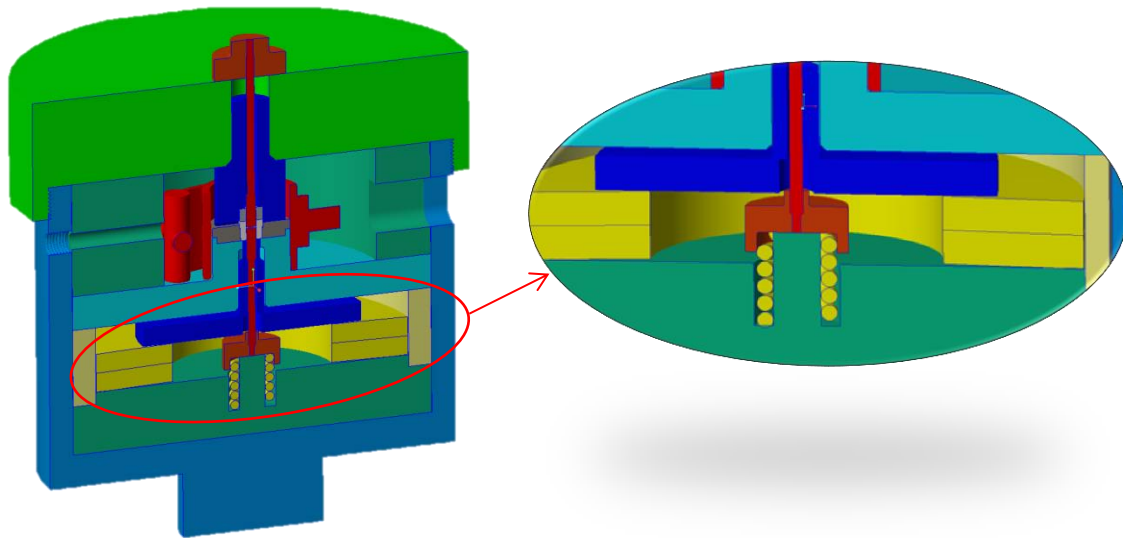


Figure 5.19: On the left, spring-die design developed in the first part of the project; on the right, ejection-springs detail.

It is worth pointing out that during the first work period it had been designed a different concept, *figure 5.19*. The main difference consisted of an ejection system based on a spring concept. This one was difficult to realise due to a more complicate design and the high-required forces. So, this design has not been manufactured. Further details are available on *Appendix 1: Spring-Die Design*.



### 5.5.1. Gear Punches

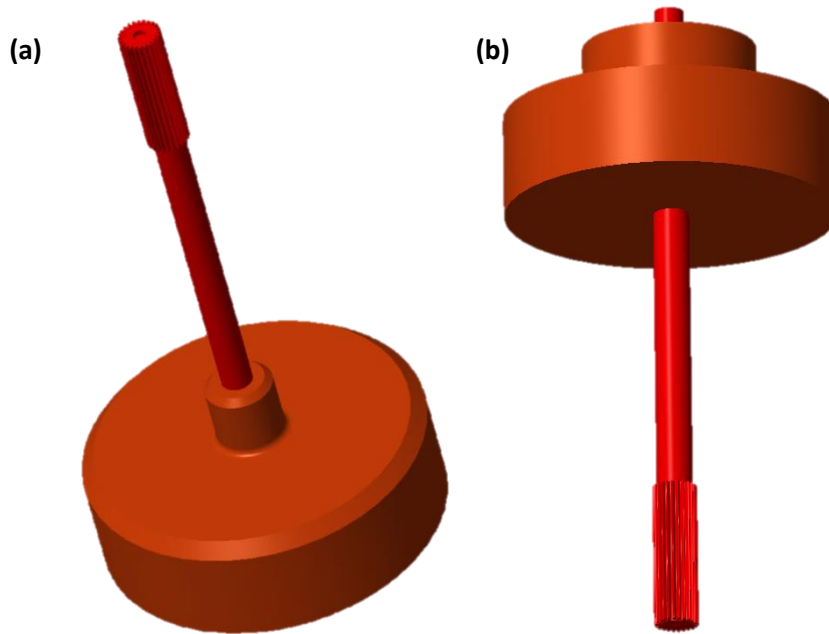


Figure 5.20: Gear punches assembling (a) lower, (b) upper.

The upper- and the lower-gear punches, *figure 5.20*, have been designed, respectively, in order to compact the powder inside the die and eject the gear after the sintering process, respectively. They have represented a critical design phase due to accuracy requirements. The most critical choices have concerned the main geometrical sizes, in particular tolerances related to the die-punch clearance. Although the reduction of the forces during ejection is the purpose of the project, the correct sizing of the gear profile has been done in order to ensure the correct clearance with the die in the assembling phase. In particular, close attention has been paid on the tolerance related to the circumscribed and inscribed circles related to the gear profile, in order to ensure the correct clearance to the die-wall surface.

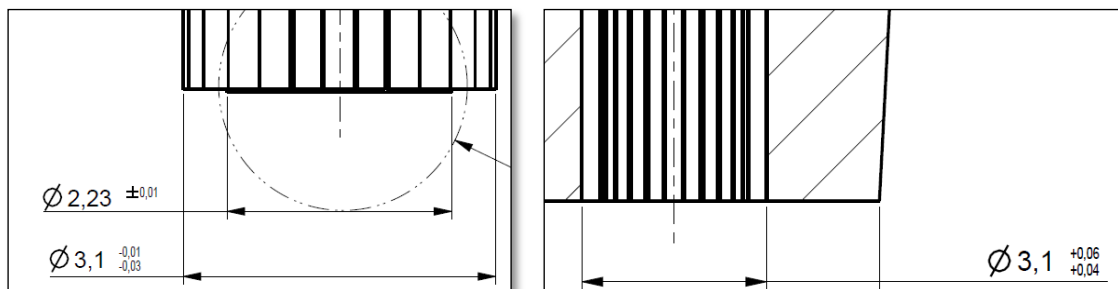


Figure 5.21: Clearance between die and punch, considering the circumscribed circle related to the gear profile.

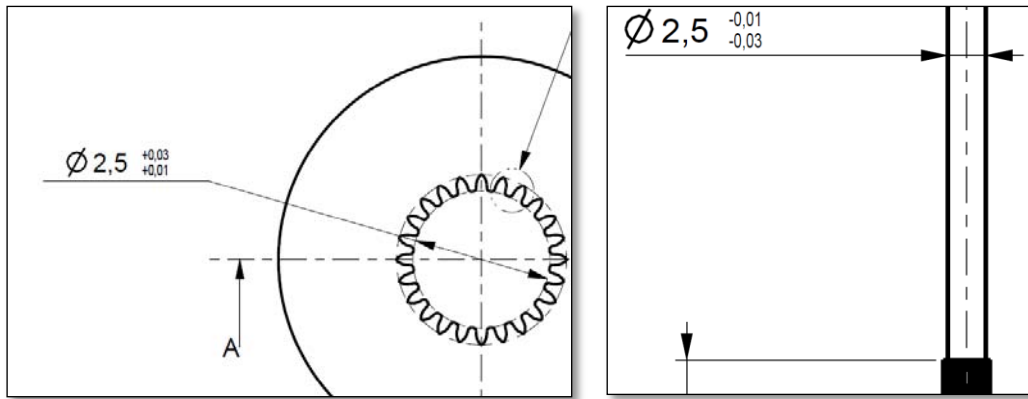


Figure 5.22: Clearance between die and punch, considering the inscribed circle related to the gear profile.

From the specific drawings, attached in *Appendix 3*, is possible to see the designed tolerance with regard to the clearance between die and punches. The minimum clearance corresponding to the circumscribed circle is equal to  $50\ \mu\text{m}$ , *figure 5.21*;  $20\ \mu\text{m}$  to the inscribed one, *figure 5.22*. The choice of these values aims at avoiding any kind of interference fit between the two components during the assembly phase.

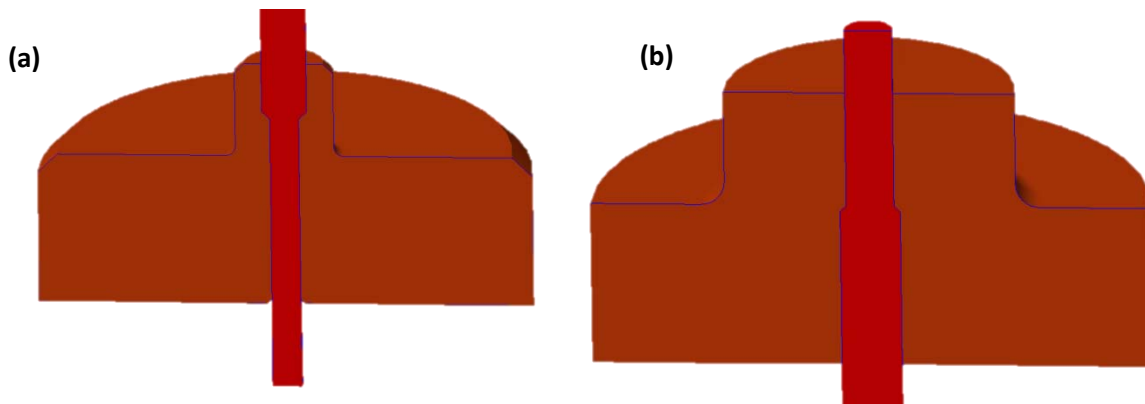


Figure 5.23: Cylindrical-shaped elements (a) lower, (b) upper, coupled to their respective punches.

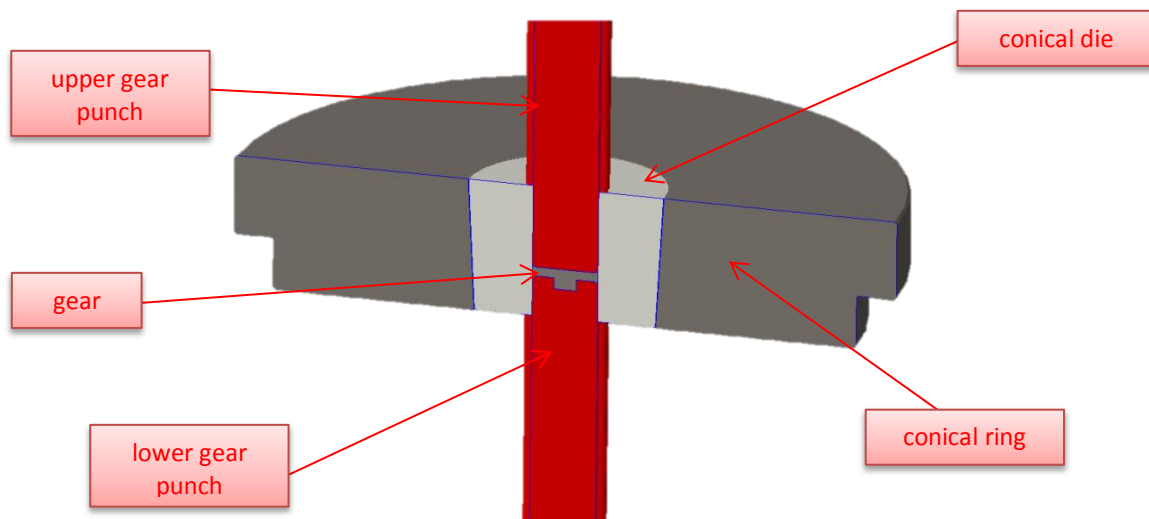


Figure 5.24: Schematic 3D cad of the sintering process.

As said in the last paragraph, the tool geometry of both punches has been divided into two parts, *figure 5.20*, due to manufacturing requirements. The two components consist of the inner element, and the cylindrical-shaped element, *figure 5.23*. The upper-inner punch compacts the powder, *figure 5.24*. The cylindrical-shaped element aims at transmitting pressure to the inner element and aligning this one to the whole die-system assembly. The choice of a larger diameter for this feature should be considered in behalf of an increased surface to the press action, by allowing an homogeneous pressure to the inner component; otherwise, the applied pressure would be exerted directly to this one. Manufacturing capability have not allowed to produce the two components as a single tool because of the high diameter-size difference. In addition, the heights of the cylindrical-shaped elements have an important role in stroke control, both for compacting and ejection phase.

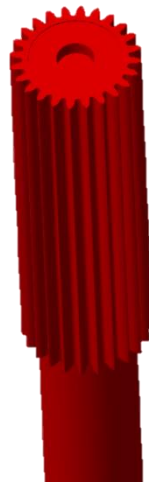


Figure 5.25: Detail of the inner punch profile.

The inner component have a bound geometry, *figure 5.25*, due to specific profile requirements. The main problem of these ones is related to buckling phenomenon because of their slenderness. Specific calculations have been done in order to ensure the correct functionality of the part, see *paragraph 5.6.3*.

## 5.5.2. Die-Ring Punches

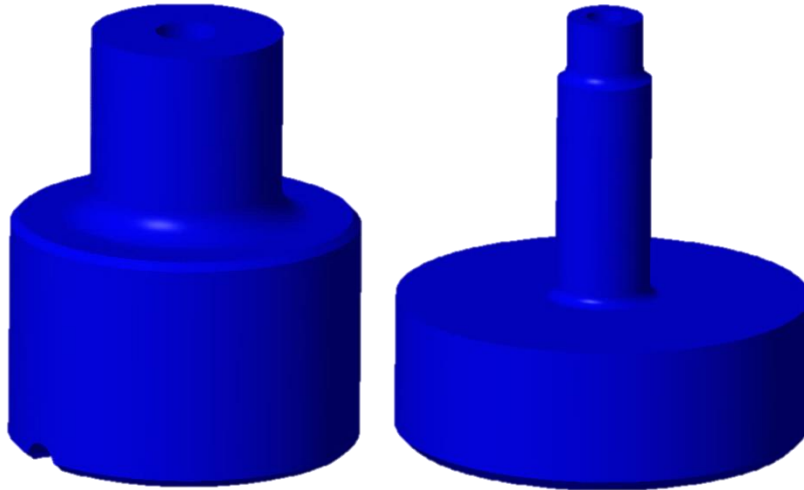


Figure 5.26: Die-Ring punches (a) upper, (b) lower.

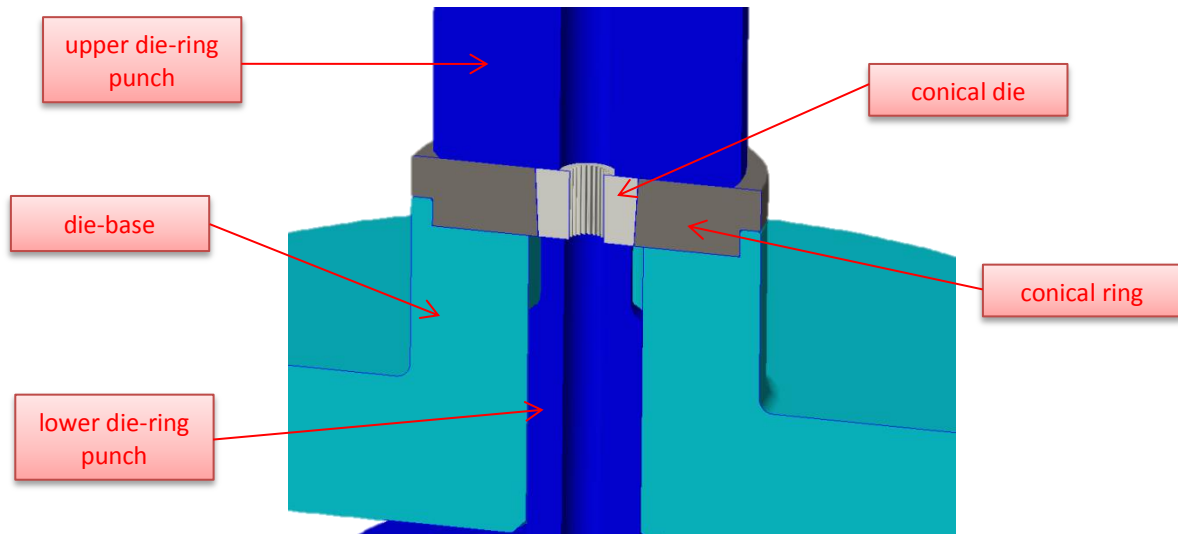


Figure 5.27: Schematic 3D cad related to the die-ring assembly during sintering.

The other two punches designed are important due to fitting and releasing of the die-ring assembly. Respectively, the upper punch generates the fitting, *figure 5.26 (a)*, while the bottom punch, *figure 5.26 (b)*, exerts pressure on the bottom of the die in order to release it from the ring. So, the die will return to its original internal diameter size, thus allowing the estimated clearance and the subsequent ejection of the gear. The main diameters of both punches have been designed according to the sizes of the die-ring assembly, *figure 5.27*. Consequently, the external-diameter sizes have been constrained by the maximum die/ring dimensions, while the internal ones have been designed in order to permit through passage of the inner-gear punches, as described in the last paragraph.

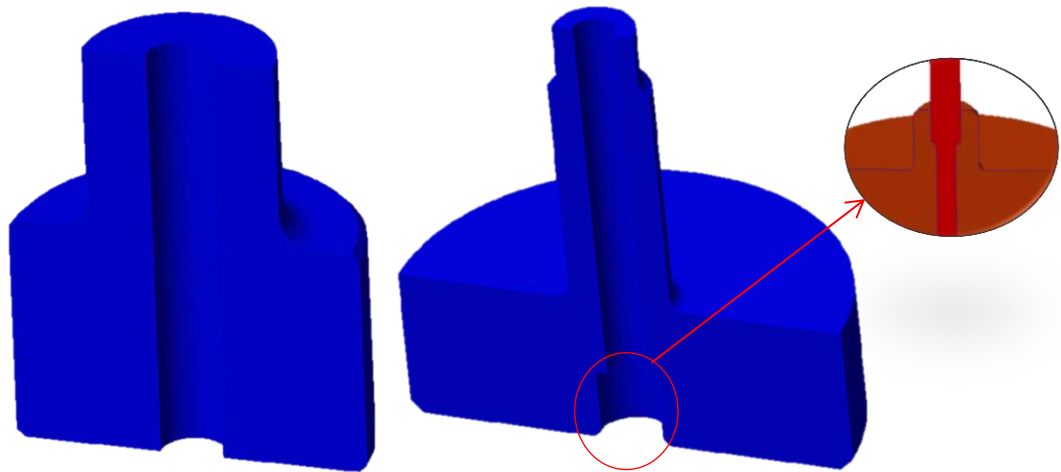


Figure 5.28: Die-Ring punches details (a) upper, (b) lower.

The two punches have an internal hole in order to allow the inner punches access, *figure 5.28 (a) & (b)*. The correct clearance has been designed in order to avoid any friction between the different tools. The axial alignment to the other components has been assured by the cylindrical shape of the parts. It is also possible to see a cylindrical diameter enlargement in the lower punch in order to assure the correct alignment to the cylindrical-shaped component of the bottom gear punch, *figure 5.23 (a)*. If compared to the inner punches, the higher diameter tool values do not generate any buckling risk.

### 5.5.3. Thread Cover

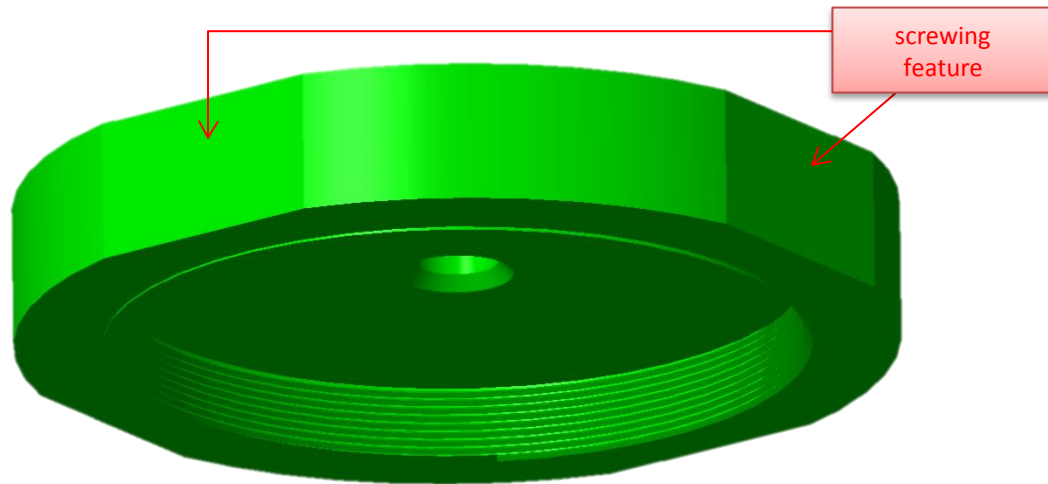


Figure 5.29: Thread cover.

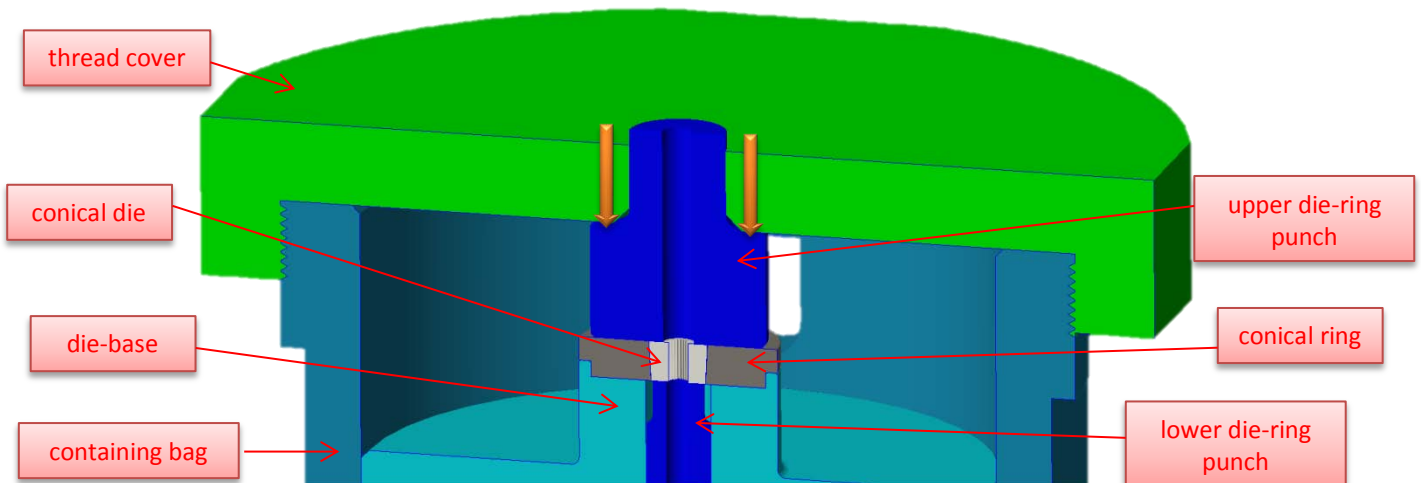


Figure 5.30: Schematic 3D cad related to the die-ring coupling.

The fixing of the whole system has been ensured by an upper cover, *figure 5.29*, screwed on the containing bag. This component has been designed so as to have two main functions. Firstly, the cover exerts pressure on the upper die-ring punch by screwing it to the containing bag, *figure 5.30*. Secondly, it fix the whole die-system during the sintering process, thus ensuring the pressure field on the upper punch and avoiding any elastic release of the die. After sintering, it will be unscrewed in order to take off the upper punches and assemble the ejection ring, see *paragraph 5.5.4*. During the sintering process, the axial alignment is assured by a chamfer on the internal hole and by the cylindrical shape of the assembled tools. The diameter size is constrained by the maximum dimensions allowed by the used press, as already described in the introduction, see *paragraph 5.5*. Screwing feature are designed on the top due to wrench application, *figure 5.29*.

#### 5.5.4. Ejection Ring

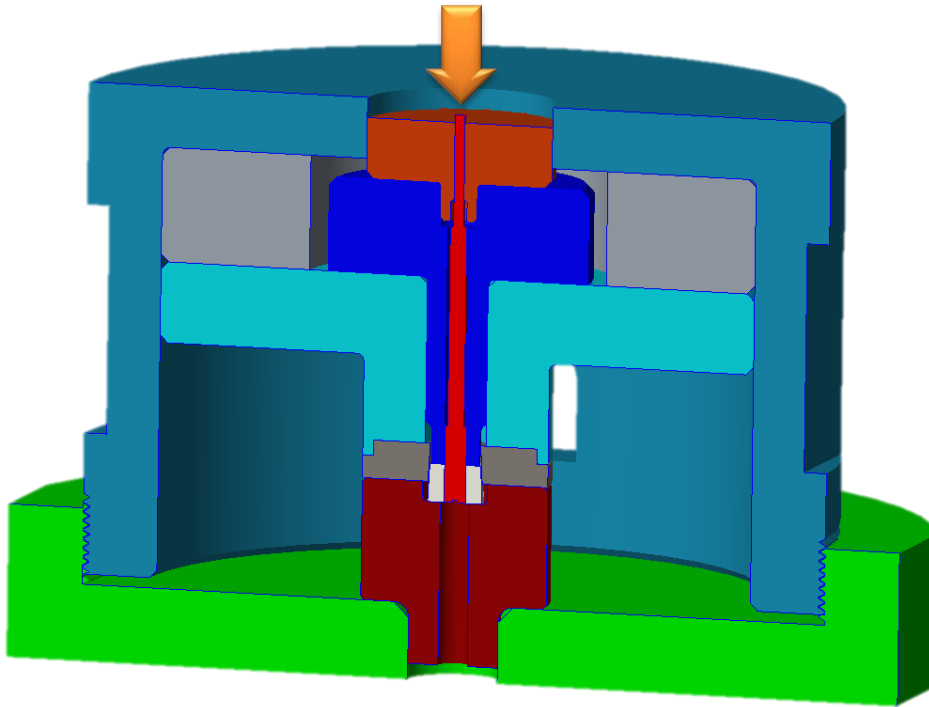


Figure 5.31: CAD assembly for the ejection phase.

After the sintering process, the whole tool system will be rotated to the opposite side in order to exert pressure on the bottom punches due to pressure releasing and the ejection of the gear, *Figure 5.31*. The reason should be considered in the mechanical/hydraulic press characteristics because of their single active element.

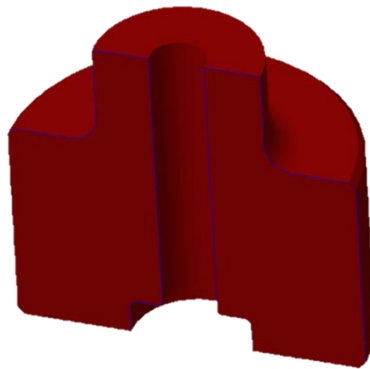


Figure 5.32: Ejection ring model 3D CAD.

In order to fix the internal assembled tools against gravity force, an ejection ring has been designed, *figure 5.32*. As it can be seen from the picture, a diameter enlargement on the bottom is realised in order to allow the ejection of the ring and fix the die position after releasing, in the meantime. Finally, the gear can be ejected from the die. In the same way of the other tools, axial alignment is provided by cylindrical features. On the top of the ring, it can be seen a cylindrical element which fit to the internal hole of the thread cover, *figure 5.29*.

### 5.5.5. Other Tool Components

After an overview of the main tools of the die-system, the remaining components and their respective roles have been described in this paragraph.

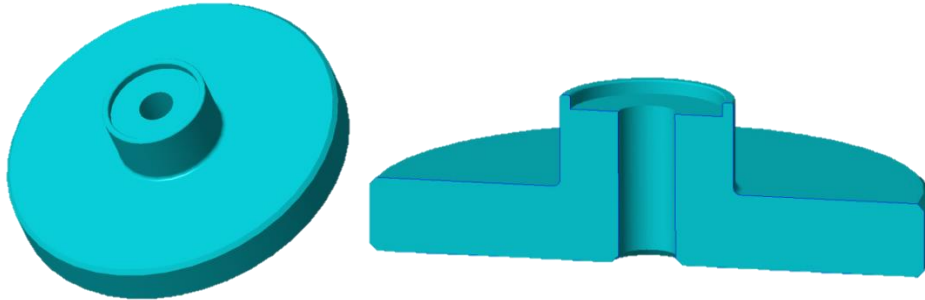


Figure 5.33: CAD model of the die-base (a) and one of its section (b)

The die-base, *figure 5.33*, has been designed in order to place correctly the ring and the heater, see *figure 5.17*, and allow the correct stroke of the two bottom punches. Chamfers and roundings have been designed to make an easier manufacturing and to avoid sharp edges. The tolerances related to the external and internal diameters are designed due to ensure fitting during assembling. The size of the part can withstand high-force values due to reduced pressure because of the large surface. Under process conditions, this component is subjected to high temperature; therefore, so the material should be chosen with the right carefulness.

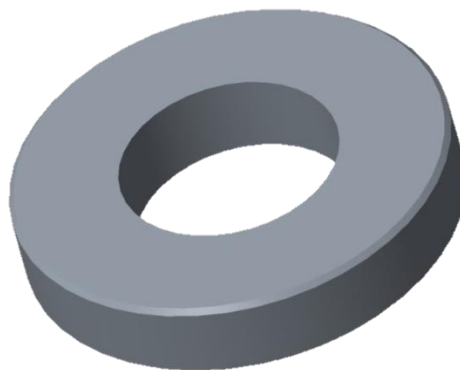


Figure 5.34: CAD 3D model of the bottom ring.

The bottom ring, *figure 5.34*, has been designed due to space needs. It has been assembled above the bottom inner surface of the external bag, see *figure 5.17*. During the designing phase, no particular problems have occurred. The only care should be taken on the tolerances related to the external diameters to avoid any difficulty during assembling.



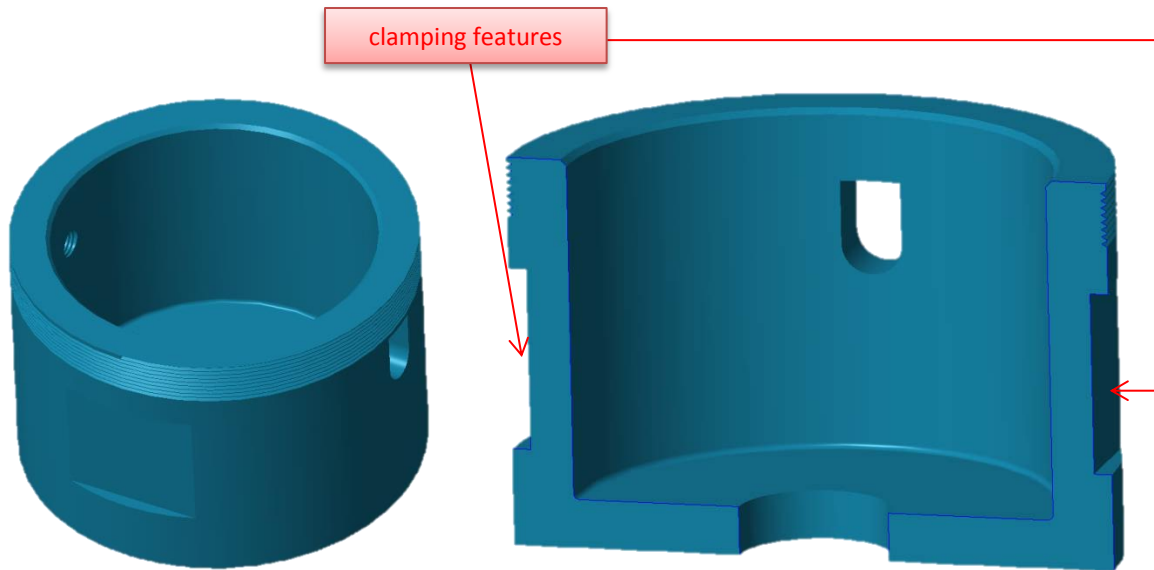


Figure 5.35. CAD model of the external bag (a) and its middle section (b).

The last tool component of the whole system is the containing bag, *figure 5.35 (a) & (b)*. It has been designed to contain all the components into the inside due to safety reasons. The geometry has been designed with the respect of the maximum allowable sizes of the press, as described in *paragraph 5.5*. In the upper side, the thread allows the screwing of the cover. As it can be seen in *figure 5.17*, during the sintering phase the bag should be supported on the base of the press. The central hole on the bottom is designed with the correct thickness in order to fix the position of the bottom punches during the sintering phase. In *figure 5.35 (b)* it can be seen lateral features designed to clamp the bag during the cover screwing. Two holes on the lateral surface of the bag are used to the thermocouple and heater cables.

## 5.6. Forces Estimating

Force analysis is important to estimate the maximum pressure exerted on the single component. Particular attention has been paid to the tools with the smallest surfaces, which have to withstand high pressures. Next paragraph aims at describing the force calculations and the main parameters involved. This phase has been important to the design of the correct height and conicity angle related to the die-ring assembly.

### 5.6.1. Analytical Model on Assembling and Disassembling Forces

Before calculating phase, this paragraph aims at describing the analytical model involved in force estimations. The force required to obtain the forced coupling between the die and the ring, and the force required to release the pressure from the die after the sintering process have been the focus of this model.

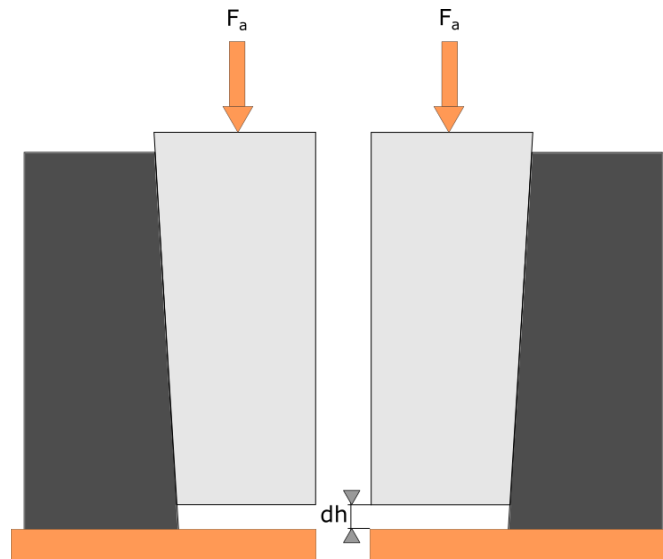


Figure 5.36: Schematic picture of the assembling phase.

The force required in order to assemble the die, *figure 5.36*, is calculated as following (Crivelli 2013):

$$F_a = p_f \pi D_m L \left( \operatorname{tg} \left( \frac{\alpha}{2} \right) + \mu \right) \quad (5.9)$$

where  $p_f$  is the fit pressure,  $D_m$  is the middle section diameter,  $L$  is the height of the fitting surface,  $\alpha$  is the conicity angle and  $\mu$  is the frictional coefficient.

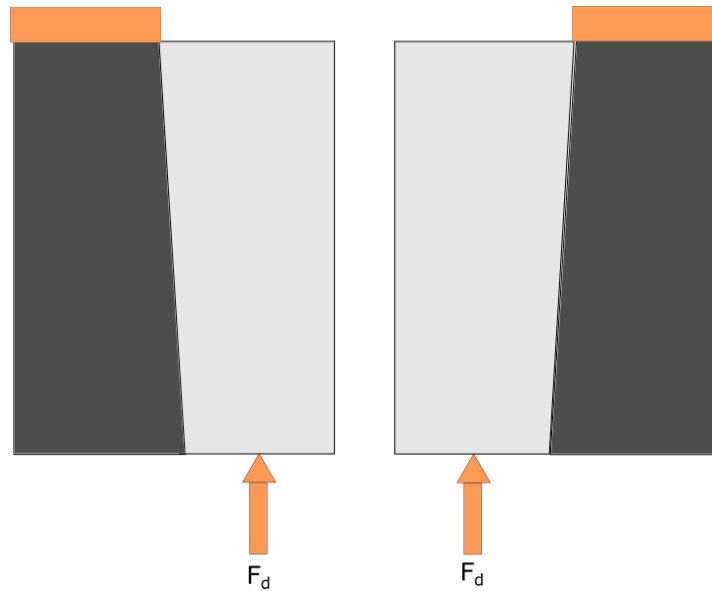


Figure 5.37: Schematic picture of the releasing phase.

The force required due to release of the die, *figure 5.37*, by the ring is calculated as following:

$$F_d = p_f \pi D_m L \left( \operatorname{tg} \left( \frac{\alpha}{2} \right) - \mu \right) \quad (5.10)$$

where the explanation of the different parameters is the same as for *equation 5.9*. It is worth pointing out how the influence of the frictional coefficient can be relevant to the assembly phase. The conicity angle is an essential element due to release of the die, as a cylindrical fit cannot be disassembled without breaking the fitted parts. On the one hand, less forces are required with lower conicity angle. On the other hand, small angles produce less stable coupling compared to higher value of conicity. A trade-off should be reached.

### 5.6.2. Die-Ring Assembling and Releasing

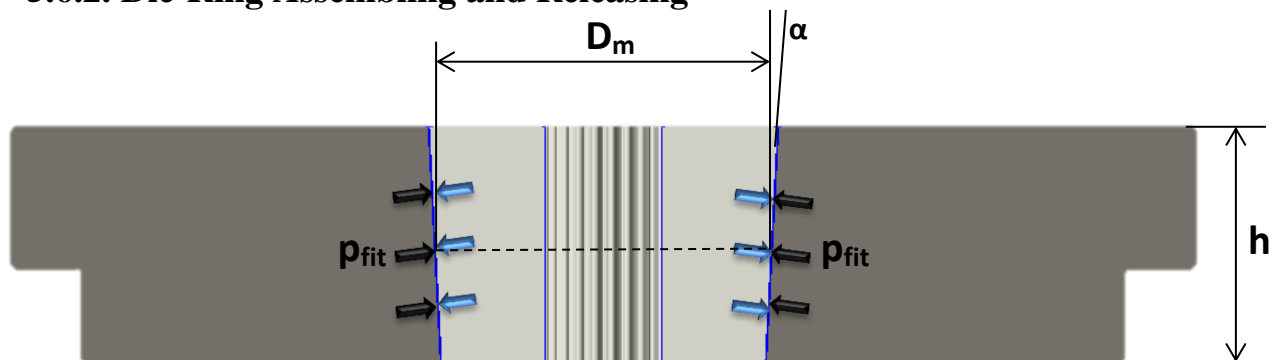


Figure 5.38: Main geometrical sizes related to the die-ring assembly.

The largest force requirements in this project are on the conical fit. According to *equation 5.9 & 5.10*, the assembling and releasing forces are estimated, respectively.

These ones have been analysed below in order to study the influence of the single parameter with regard to the forces. However, the influence of the  $D_m$  and  $p_{fit}$  has not been studied because they have been already set after considerations made in *section 5.4*. Thus, only the influence of the height  $h$ , the conicity angle  $\alpha$ , and the frictional coefficient  $\mu$ , have been studied. The geometrical parameters are shown in *figure 5.38*.

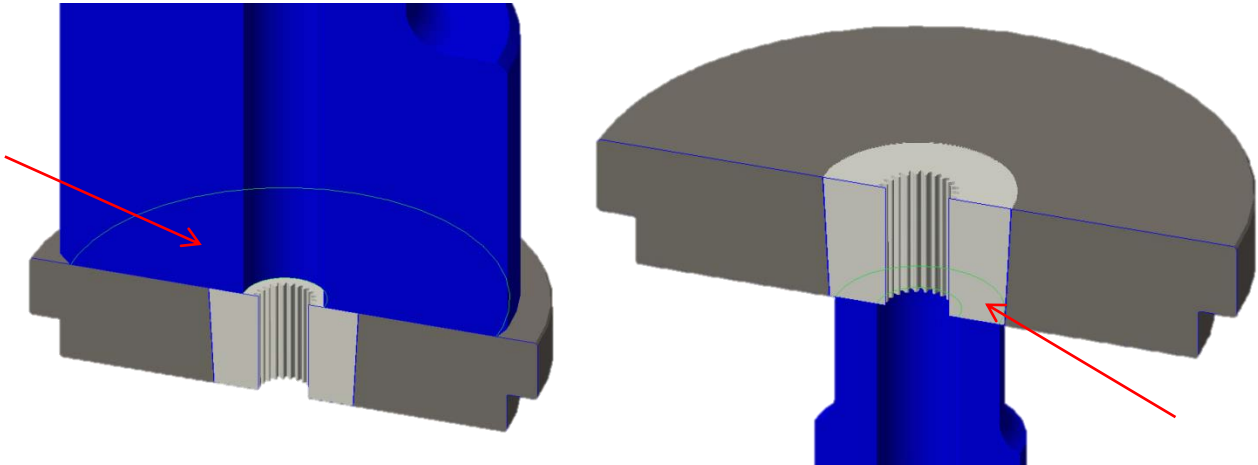


Figure 5.39: On the left, the upper surface considered in pressure estimation; on the right, the lower one.

The *figure 5.39* shows the surfaces considered in pressure estimating. The calculation of them has been done by dividing the force by the value of the proper surface, as indicated by the following equation:

$$p = \frac{F}{A} \quad (5.11)$$

$\mu$	0.5							
$A_{upper}$	36.94	$\text{mm}^2$						
$A_{lower}$	24.13	$\text{mm}^2$						
$p_{fit}$	$D_m$	$h$	$\alpha$	$F_{ass}$	$F_{rel}$	$p_{ass}$	$p_{rel}$	
[MPa]	[mm]	[mm]	[°]	[N]	[N]	[MPa]	[MPa]	
403.66	7.12	30	3	142529.93	128343.77	3858.42	5318.85	
403.66	7.12	25	3	118774.94	106953.14	3215.35	4432.37	
403.66	7.12	20	3	95019.95	85562.51	2572.28	3545.90	
403.66	7.12	15	3	71264.96	64171.89	1929.21	2659.42	
403.66	7.12	10	3	47509.98	42781.26	1286.14	1772.95	
403.66	7.12	8	3	38007.98	34225.01	1028.91	1418.36	
403.66	7.12	6	3	28505.99	25668.75	771.68	1063.77	
403.66	7.12	5	3	23754.99	21390.63	643.07	886.47	

Table 5.5: Forces range depending on the height of the tools.

The first parameter analysed is the height of the tools. Increasing this value the required force will be higher due to expanded contact surface, *table 5.5*. However, if it is too low, the decreased value of the thickness would complicate the alignment of the tools. Thus, the stability of the coupling would be decreased. The value of 5 mm, highlighted on the table, represents a good trade-off to the tools thickness.

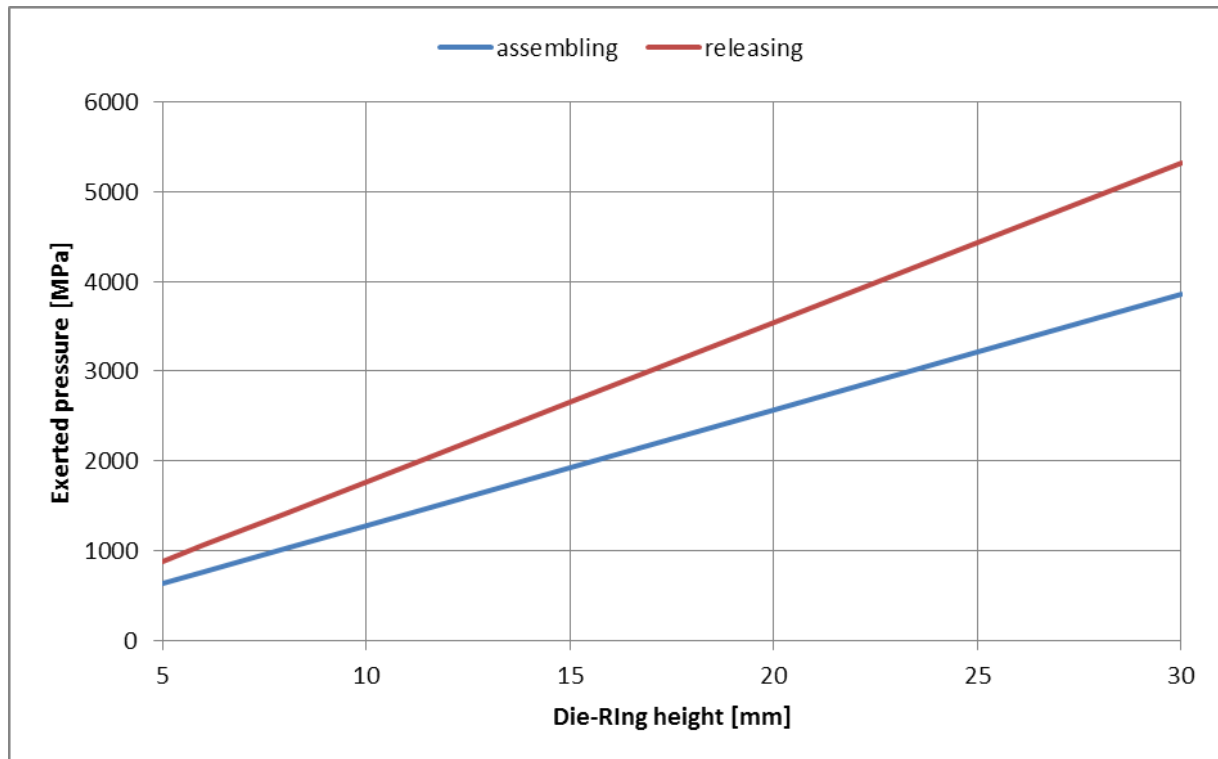


Figure 5.40: Different pressure exerted on the tools at different tools height.

Furthermore, the *figure 5.40* points out how the releasing pressure is higher than the assembling pressure, although the fitting phase requires a higher force. This consideration depends on the size of the different surfaces; a higher value of the area allows less pressure values.

$\mu$	0.5	
$A_{upper}$	36.94	mm <sup>2</sup>
$A_{lower}$	24.13	mm <sup>2</sup>

$p_{fit}$	$D_m$	$h$	$\alpha$	$F_{ass}$	$F_{rel}$	$p_{ass}$	$p_{rel}$
[MPa]	[mm]	[mm]	[°]	[N]	[N]	[MPa]	[MPa]
403.66	7.12	5	10	26522.54	18623.08	717.99	771.78
403.66	7.12	5	9	26125.85	19019.77	707.25	788.22
403.66	7.12	5	8	25729.70	19415.92	696.53	804.64
403.66	7.12	5	7	25334.03	19811.58	685.82	821.04
403.66	7.12	5	6	24938.79	20206.83	675.12	837.42
403.66	7.12	5	5	24543.91	20601.71	664.43	853.78
403.66	7.12	5	4	24149.33	20996.29	653.74	870.13
403.66	7.12	5	3	23754.99	21390.63	643.07	886.47

Table 5.6: Forces range depending on the conicity angle of the conical fit.

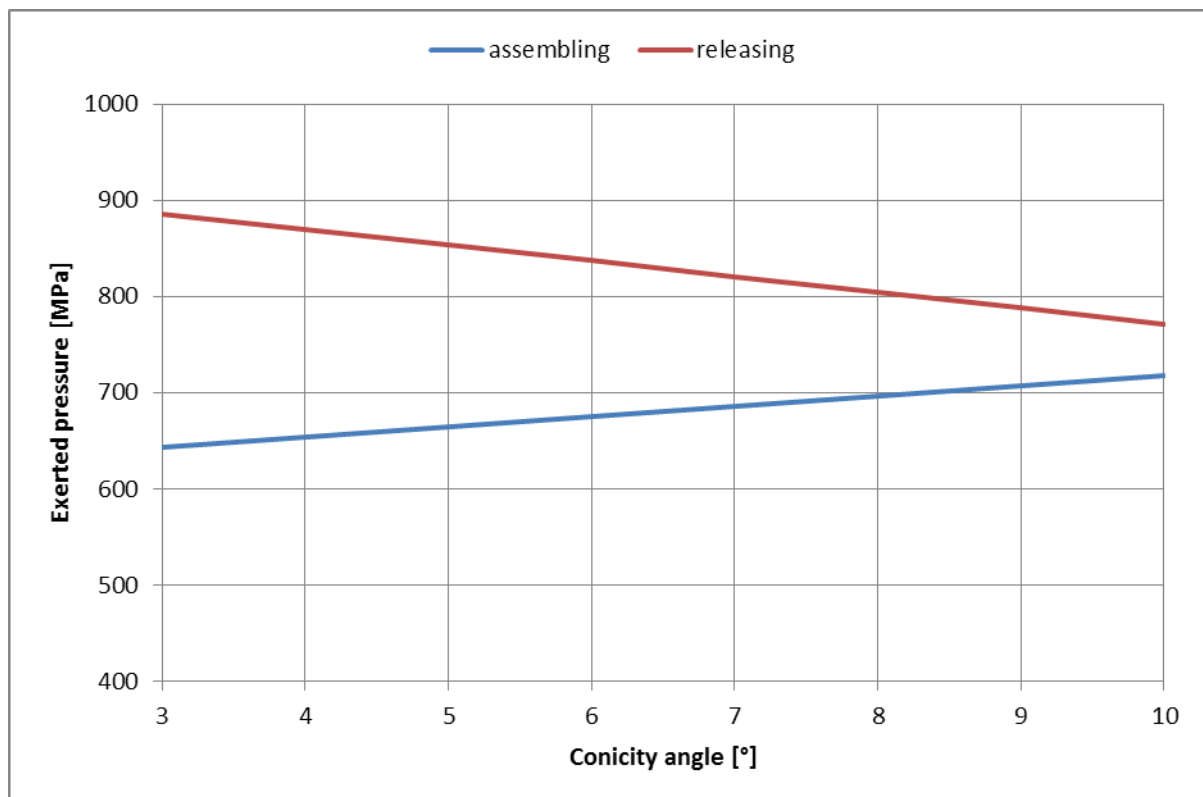


Figure 5.41: Different pressure exerted on the tools at different conicity angle.

Table 5.6 & figure 5.41 show the influence of the conicity angle of the conical fit. The theoretical results show how the releasing pressure will be lower by increasing this parameter. The opposite happens to the assembling one. The value chosen is 3°,

in order to have a good trade-off between the two kinds of pressure. This solution has made reference to the scientific literature (Noveanu & Frunză 2013).

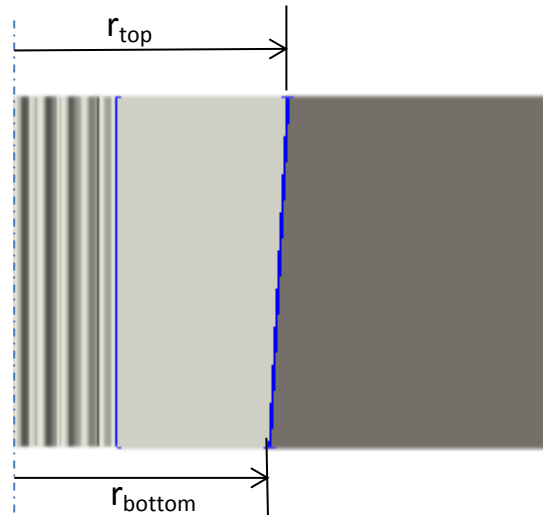


Figure 5.42: Influence of the conicity angle on the interference radius of the tools.

The solution adopted aims also at avoiding too large differences among the various radii in correspondence to the interference radius; because of the sleeve, the radius on the top would be larger than the one at the bottom, *figure 5.42*. As a consequence, different values of compression would be obtained. The solution adopted in this project has been highlighted on the *table 5.6*.

$p_{fit}$	403.66	MPa		
$D_m$	7.12	mm		
$h$	5	mm		
$\alpha$	3	°		
$A_{upper}$	36.94	mm <sup>2</sup>		
$A_{lower}$	24.13	mm <sup>2</sup>		
<b><math>\mu</math></b>	<b><math>F_{ass}</math></b>	<b><math>F_{rel}</math></b>	<b><math>p_{ass}</math></b>	<b><math>p_{rel}</math></b>
	[N]	[N]	[MPa]	[MPa]
0.5	23754.99	21390.63	643.07	886.47
0.45	21497.71	19133.35	581.96	792.93
0.4	19240.43	16876.07	520.86	699.38
0.35	16983.15	14618.79	459.75	605.83
0.3	14725.86	12361.51	398.64	512.29
0.25	12468.58	10104.22	337.54	418.74
0.2	10211.30	7846.94	276.43	325.19
0.15	7954.02	5589.66	215.32	231.65

Table 5.7: Lubrication influence on the assembling/releasing of the conical fit, with fixed geometry of the coupling.

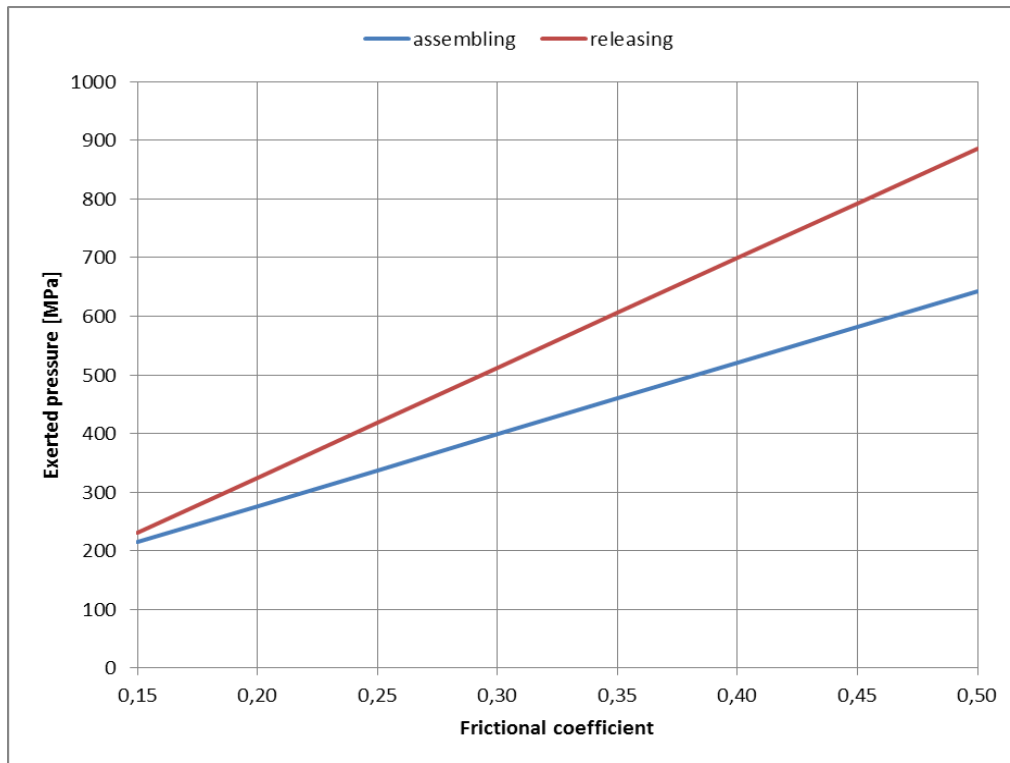


Figure 5.43: Pressure exerted on the tools related to frictional condition.

After defining the most influencing geometrical parameters in required forces during assembling/releasing of the conical fit, *table 5.7 & figure 5.43* show the friction influence related to determined lubrication condition. The geometry of the conical fit has already been defined, as described on the top of *table 5.7*. A correct lubrication decreases the required forces. However, if, on the one hand, the lubrication of the tools is not a problem before coupling, it should be considered the lubricant vaporization due to high temperature achieved during the process, on the other. So, during ejection, controlling the amount of lubrication between die and ring is not possible. On behalf of safety condition, the values of pressure needed have been predicted considering 0.5 as frictional coefficient, as highlighted on *table 5.7*.



### 5.6.2. Compaction Forces and Buckling of the Punches

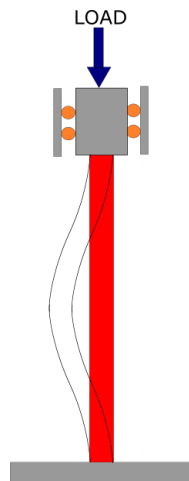


Figure 5.44: Schematic picture of the buckling phenomenon.

The sintered gear has a very small size. As a consequence, the gear punches have a small diameter size, too. Depending on the pressure applied, the main problem should be related to the buckling phenomenon, *figure 5.44*, due to the height of punches. The estimate of the critical buckling force is calculated according to the Eulerian theory (Gere & Goodno 2009):

$$F = \frac{\pi^2 EJ}{(KL^2)} \quad (5.12)$$

where  $E$  is the Young module of the tool,  $J$  is the area moment of inertia of the cross section ( $J=\pi R^4/4$ ),  $K$  is the column effective length factor and  $L$  the length of the tool. The parameter  $K$  depends on the conditions of the end support of the column. In this case both ends are fixed against rotation,  $K = 0.5$  from literature.

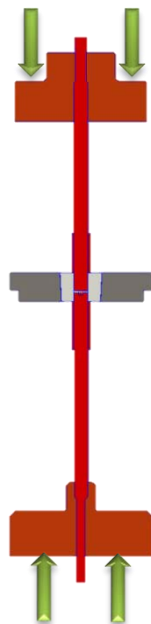


Figure 5.45: Schematic picture related to the buckling of the internal punches

K	0.5	
$R_{\text{circumscribed}}$	1.15	mm
J	1.37	mm <sup>2</sup>
E	190000	MPa
L	35	mm
$P_{\text{critical}}$	8411.21	N
A	4.15	mm <sup>2</sup>
$p_{\text{max}}$	2024.48	MPa

Table 5.8: Critical load before buckling for the gear punches.

Schematically, the buckling phenomenon related to the gear punches is represented in *figure 5.45*. The results showed in *table 5.8* are referred to the longest punch, that is the bottom one. The upper punch has a lower height; so, the  $P_{critical}$  is higher than the last one. Comparing the  $p_{max}$  to the average powder compaction pressure of about 150 MPa, see the end of *paragraph 5.2*, safety operating conditions are achieved.

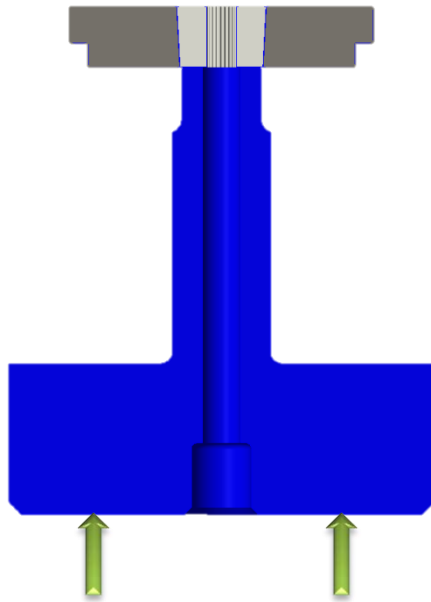


Figure 5.46: Schematic picture related to the buckling phenomenon of the bottom die punch.

K	0.5	
$R_{est}$	3.2	mm
$R_{int}$	1.6	mm
J	77.21	mm <sup>2</sup>
E	190000	MPa
L	24.5	mm
$P_{critical}$	964810.99	N
A	24.13	mm <sup>2</sup>
$p_{max}$	39983.88	MPa

Table 5.9: Critical load before buckling for the bottom die punch.

The same calculations have been done for the bottom die punch, *figure 5.46*, due to reduced diameter value. The results obtained, *table 5.9*, show that the compacting operation to realise the conical fit can be operated in safety condition, because the maximum values allowed result higher than the pressure-estimated values during process, see *table 5.7*. It is worth underlining that the Young's modulus used is referred to an average value of a hot-work steel.

## 5.7. Material Selection

The materials choice needs to satisfy the two main aspects related to the temperature conditions and the maximum strength. The tools should withstand these conditions during process before yielding. Operating condition can achieve temperatures up to 600 °C, as described in *paragraph 5.2*.

### 5.7.1. Die and Ring material

The die and the ring material needs to maintain its properties as much as possible because of their hardness and yield strength. The first constraint is related to thermal expansion. If the die and the ring are made of different material, a difference in thermal expansion may be possible during sintering process. As a consequence, the designed interference, having a tolerance of  $\pm 5 \mu\text{m}$ , may be compromised. The solution adopted aims at overcoming this problem by using the same material for both the tools. The second influencing factor is the operating temperature because of corrosion problem and compromised properties of the material, at high temperatures. In order to avoid corrosion and oxidation, the material research has focused on the field of hot work steels.

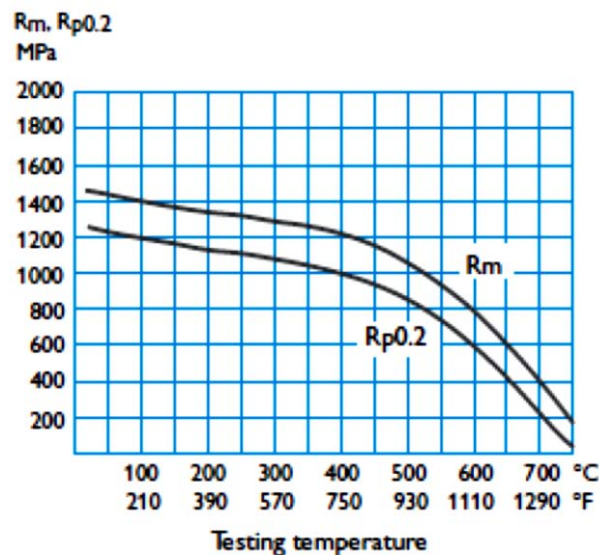


Figure 5.47: Different yield strength values at different temperatures, H13 hot work steel (Bohler Uddeholm H13).

The yield strength of the material is decreased to the higher temperature, *figure 5.47*. This decreasing is connected to the lower hardness achieved during the heating of the tools as hardness and yield strength are strictly correlated (TPPInfo 2006). So, the main focus aims to find one tool material characterised by a good thermal stability under temperature loading condition. A scientific material is the Bohler W360 ISOBLOC.

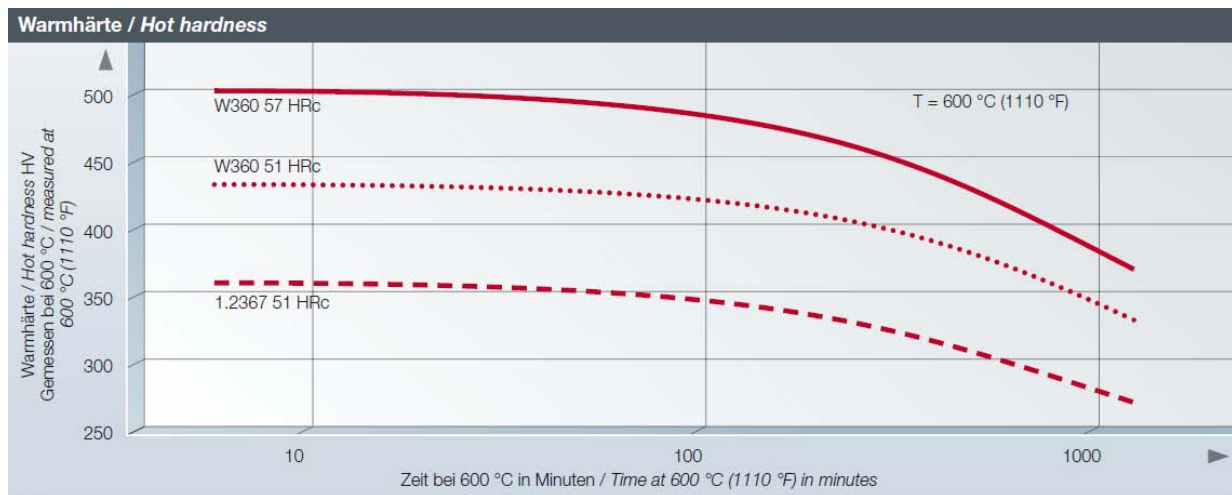


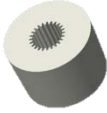



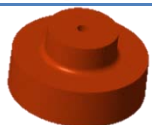


Figure 5.48: Hardness at different operating temperature for Bohler W360 ISOBLOC (Bohler Uddeholm W360 ISOBLOC).

This material is characterised by a high hot-hardness stability at high temperature, *figure 5.48*. The alloy is patented, not classified in AISI designation. The yield strength of the material is not directly reported on the datasheet; but, it can be correlated to another alloy produced by the same company, W302 ISOBLOC, designated as H11/H13 hot-work-tool steel. The yield strength of this material is equal to 1600 MPa (Bohler Uddeholm).

### 5.7.2. Other Components Material

The remaining-material choices have focused on punches and general tools. In forming process, punches require a good compressive strength to avoid any kind of plastic deformation or cracks. In this project, two kinds of punches have been used for die-ring assembling and powder compacting, see *paragraph 5.5.1 & 5.5.2*. Both have been subjected to a high temperature process. The main difference between them is related to the cross sectional area. The estimated powder compaction pressure has resulted to 150-200 MPa, as described at the end of *paragraph 5.2*. This value is lower than the average yield strength of a hot-work steel. However, if during the experiments higher pressure were tested, the choice of a material characterised by a high-compressive yield strength value might result convenient. Among the different materials, the ones selected for the best properties are carbides because of their hardness and compressive strength; in particular, tungsten carbides are characterised by a compressive strength range of 3347-6833 MPa (AZO Materials). The main problem related to this material is the manufacturing as the profile designed, *figure 5.25*, is characterised by small radii, which are difficult to realise. The alternative material studied is in the class of maraging steels. The 18Ni2400 maraging steel is characterised of 2390 MPa yield strength at 56 HRC (INCO databooks). The

compressive strength can be estimated with the relation  $m = \sigma_{oc}/\sigma_{ot}$ , as function of hardness (Bay 1993). The main advantage of maraging steel over the tungsten carbide tool looks at an easier manufacturing process. For die punches, *figure 5.26 (a) & (b)*, the calculated assembling/releasing pressures, see *table 5.7*, allow to use the H13 alloy. This choice represents a good trade-off between cost consideration and material properties. H13 is chosen also for the die-base, *figure 5.33* due to oxidation resistance at high temperature. The remaining components, thread cover, ejection ring, bottom ring, and containing bag, *figure 5.29, 5.32, 5.34 & 5.35*, are made of A514 steel, a high strength steel. They do not require particular consideration, as they are not involved in the high temperature of the sintering process. A summary of the material chosen in this project can be seen in the next table, *table 5.10*.

Component		Material
Conical die		Bohler W360 ISOBLOC
Conical ring		Bohler W360 ISOBLOC
Upper inner punch n.1		Tungsten carbide/18Ni2400 maraging steel
Bottom inner punch n.1		Tungsten carbide/18Ni2400 maraging steel
Upper inner punch n.2		H13 hot work steel
Bottom inner punch n.2		H13 hot work steel
Upper die-ring punch		H13 hot work steel

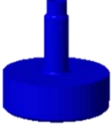
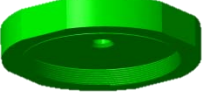


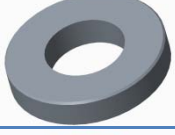

Bottom die-ring punch		H13 hot work steel
Thread cover		A514 steel
Ejection ring		A514 steel
Die-base		H13 hot work steel
Bottom-ring		A514 steel
Containing-bag		A514 steel

Table 5.10: Summary of the tool materials of the conical- system

## 6. Experiments and Results

### 6.1. Overview

As described in the introduction of this thesis, the focus of this project is the reduction of the ejection force after the part sintering. This chapter would show the results obtained in this issue. However, also a preliminary analysis of the main parameters involved during the sintering process has been done. All these parameters, which are temperature, pressure, and holding time, have been studied in a preliminary cylindrical-die set. Then, the analysis on the pre-stress system has been done on a gear-die set. Delays related to the manufacturing and delivery of the tool designed and described in *chapter 5* have determined the use of an alternative solution, based on a similar shape. The pre-stress functional principle of this one is also based on a conical-fit, see *paragraph 5.3*. Thus, the results obtained could be related to the complex design described in the last chapter. With regard to the ejection force, the experimental results obtained with the pre-stress system have been compared to the ones obtained without using any pre-stressed tool. In order to obtain a structure comparison of the sintered parts, the gear die used in these two systems has been the same; in particular, a macro and micro-structure comparison will be shown. The ejection force has been analysed and related to the main-process parameters, which are temperature, pressure, and holding time.

### 6.2. Experimental Set



Figure 6.1: Mechanical press used in the experiments for powder compaction.

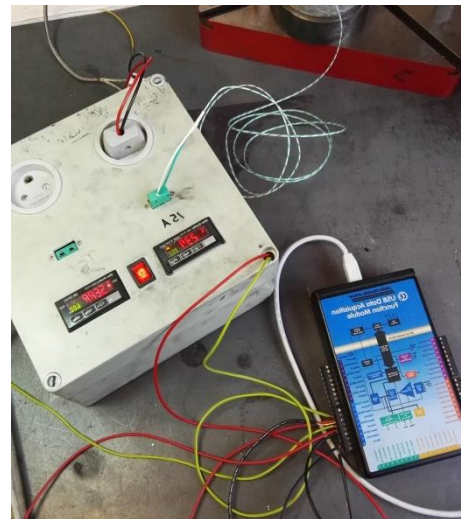


Figure 6.2: Temperature control system on the left (Allen-Bradley 900 TC-32) and computer interface on the right (DataTranslation DT-9800).



Figure 6.3: Plate and system used for the force measurements.

Different mechanical and electronic instruments have been used during the experiments. After filling up of the die, the powder has been pressed by a mechanical press, *figure 6.1*. The process temperature has been controlled by an electronic system of Allen-Bradley®, *figure 6.2*. The sintering temperature is set before the process, using the up and down buttons. The thermocouple measures the instantaneous value of the temperature shown on a digital screen. Relating to this value, the system activates or deactivates the connected heater, in order to reach up and maintain the proper value of temperature. The computer interface by DataTranslation®, *figure 6.2*, has allowed the control and recording of temperature and force during the sintering process. The measurements of the force values have been possible by using a “measurement plate”, *figure 6.3*, connected to the computer interface. A preliminary calibration of the measuring systems has been done before the experiments.

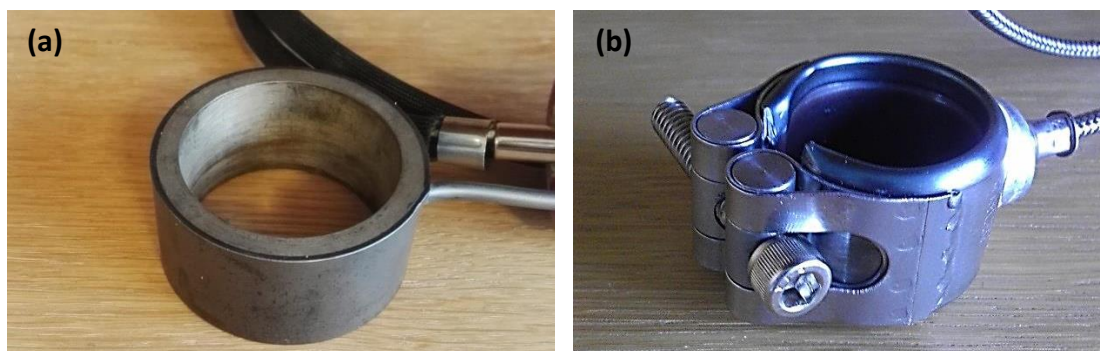


Figure 6.4: Mineral insulated nozzles used in the experiments (Watlov).

Depending on the external radius of the die-system, two kind of heater have been used, *figure 6.4*. The heating direction is radial, as already described in *paragraph 4.2.2*. It should be reminded that during the whole sintering phase, the mechanical press has exerted a defined pressure on the powder, according to a functional principle of the Micro-FAST sintering process, see *paragraph 4.3*.



### 6.3. Parameters Optimising

A preliminary analysis on the influence of the main process parameters has been done. The main purpose of these experiments is to understand how the variation of the single process parameter could influence the micro and macro-structure of the sintered part; the starting data accord to the different-scientific papers studied on micro-manufacturing, see *paragraph 3.4*. The results obtained will be an important reference point to the next-planned experiments concerning the pre-stressed die.



Figure 6.5: On the left, the cylindrical die-set used in these experiments; on the right, a phase of the sintering process.

The tools used in this series of experiments, *figure 6.5*, have been taken from the IPU workshop. They consist of a cylindrical die, an upper and a lower punch. The internal diameter of the die is equal to 4 mm, while its total height is 8 mm. Considering the stroke of the upper punch and the amount of filled powder, the sintered cylinder would have a height of about 3-4 mm.

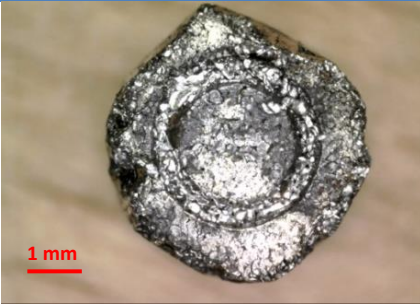
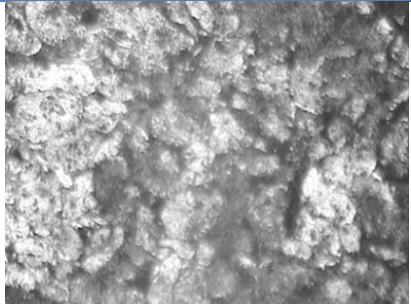

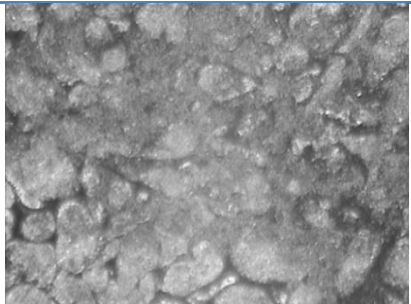

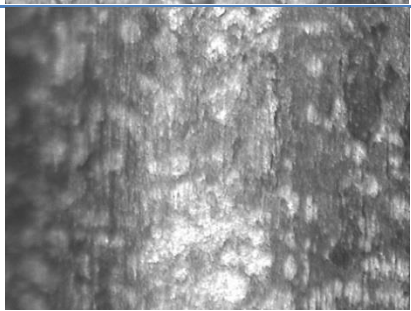
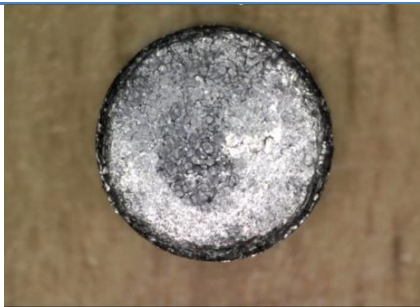
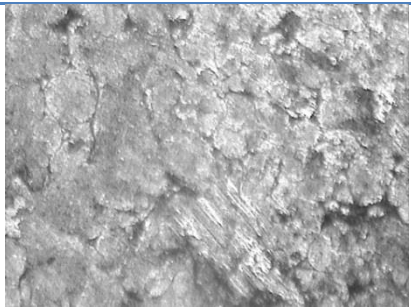

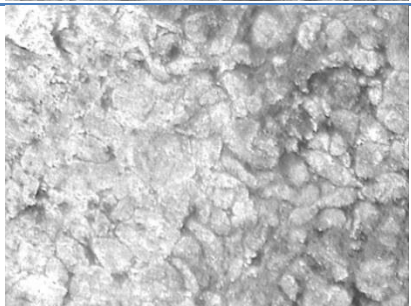
#### 6.3.1. 1<sup>st</sup> Series of Experiments

A first series of experiments have carried out some general results related to the main process parameters, which are time, temperature, and pressure. The starting parameters are based on literature studies, see *paragraph 3.4*, and considerations made in *paragraph 5.2*. It is worth pointing out that this system is not characterised by a shrink-fit.



Figure 6.6: The two microscopes used in this project: the digital one on the left, the optical one on the right.

Next pictures have been obtained using a digital microscope for the macro-structure and the optical microscope for the micro one, *figure 6.6*.

Experimental parameters	Macro-structure	Micro-structure
<p>#1  T: 550 °C  holding time: 40 "  pressure: 103.5 MPa</p>		
		
		
<p>#2  T: 550 °C  holding time: 2' 40 "  pressure: 108.3 MPa</p>		
		

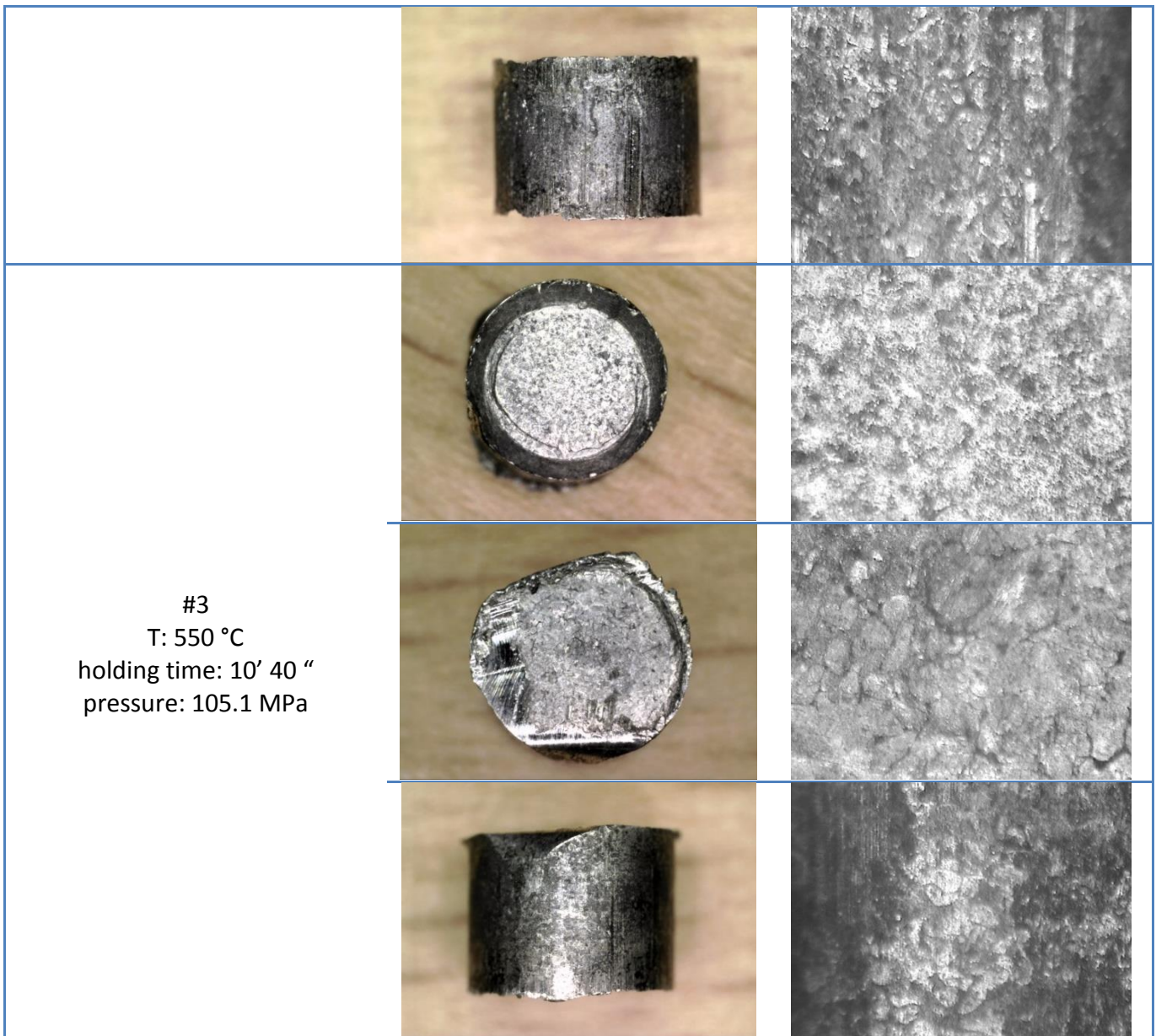
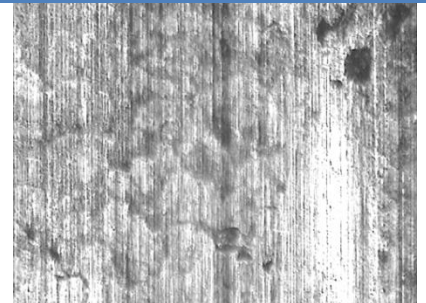
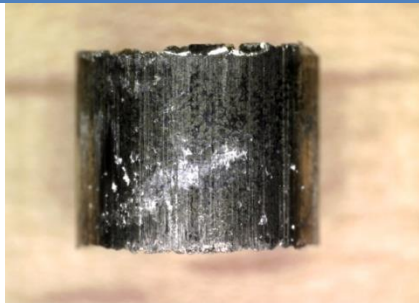
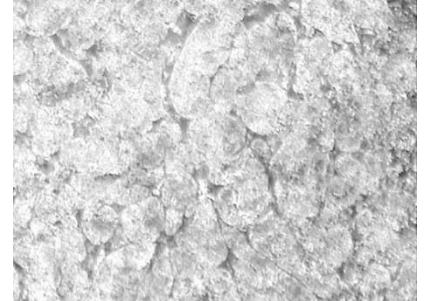
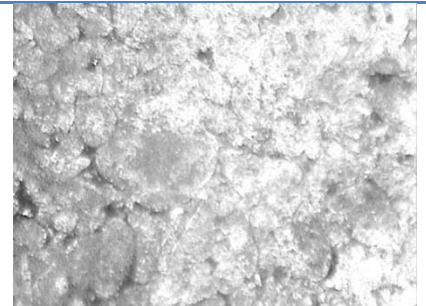
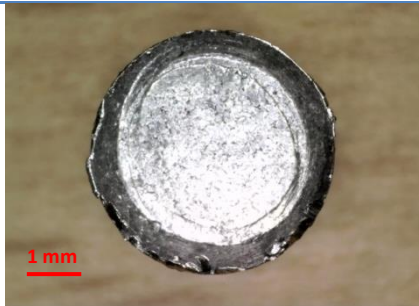


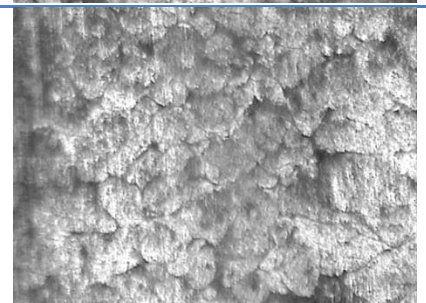
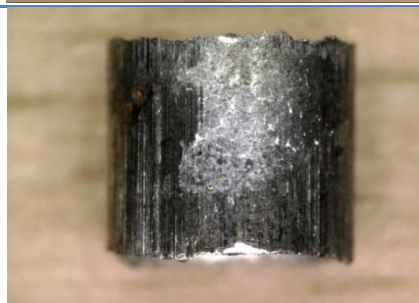
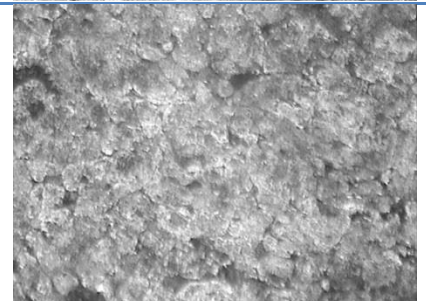
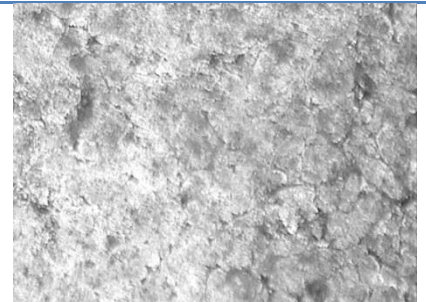
Table 6.1: Holding time influence on the cylinder sintering.

The experiments have been organised in series of three for the single parameter. Macro and micro-structures have been analysed both for the upper and lower side of the cylinders and lateral surface; in particular, particles joining and cracks observation have been the main-analysis objectives. The samples #1, #2 and #3 show the effect of the sintering time, *table 6.1*. Increasing the sintering time, an improved joining among particles has been reached. In sample #1, the boundaries are clearly visible; in these fields, the particles have not been fully melted each other. In sample #2 the boundaries among particles are less evident and even less in sample #3. From these starting experiments, in particular with #1, it is possible to note how the die-wall friction could influence the ejection phase; the parts are damaged and the ejection has resulted difficult, even if the die has been lubricated before.

#4  
T: 450 °C  
holding time: 20'  
pressure: 108.3 MPa  
heating loops: 3 [400;450]



#5  
T: 500 °C  
holding time: 20'  
pressure: 103.5 MPa  
heating loops: 3 [400;500]



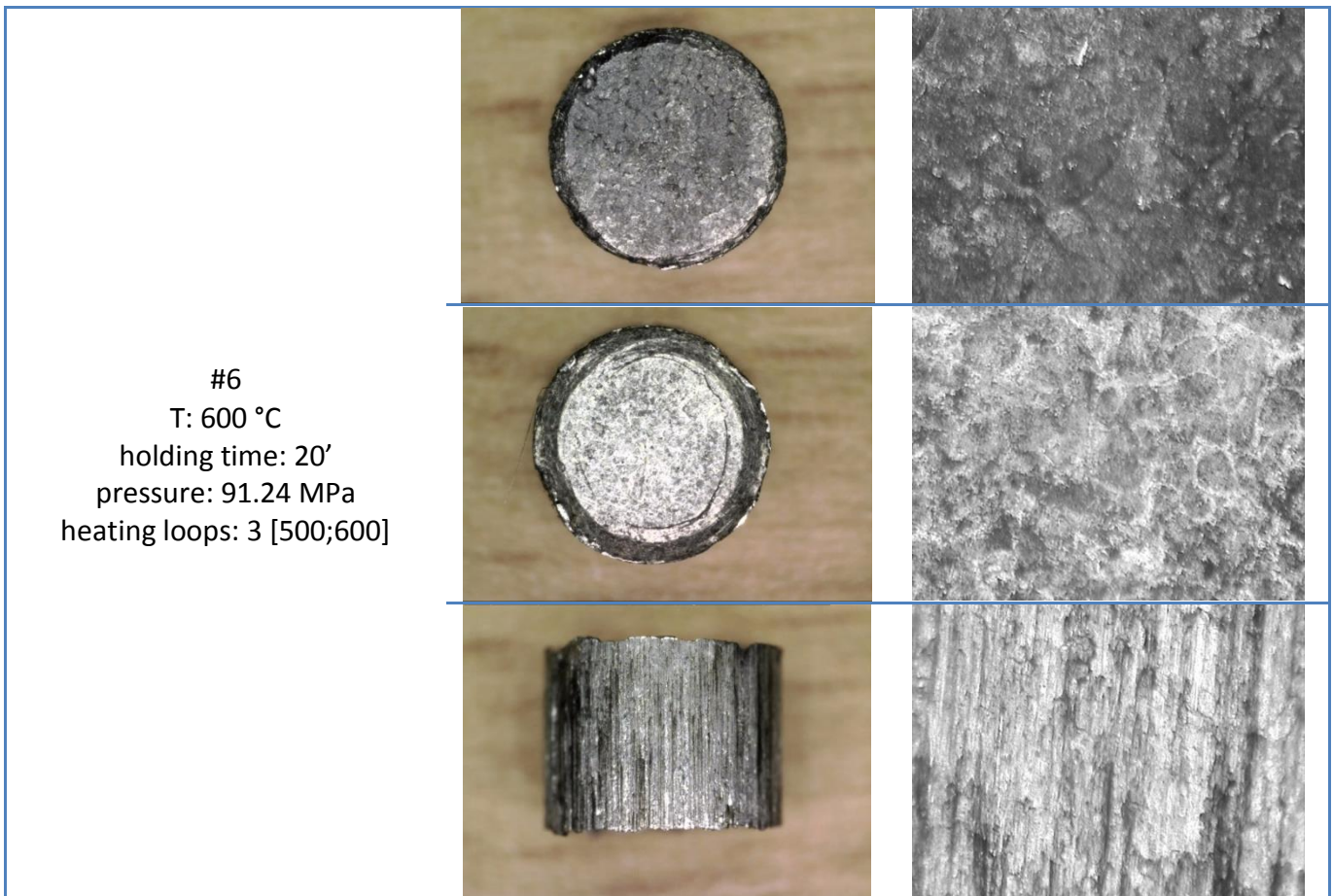
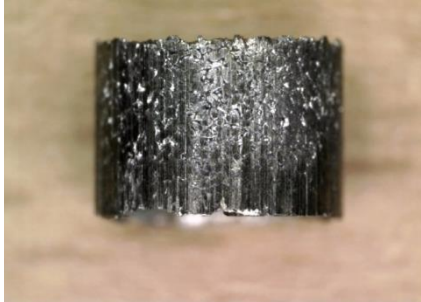
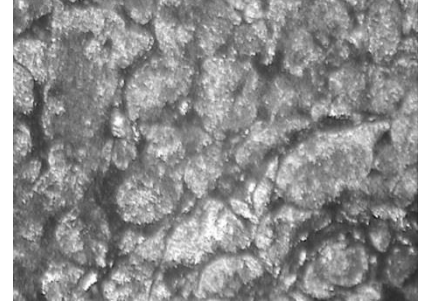
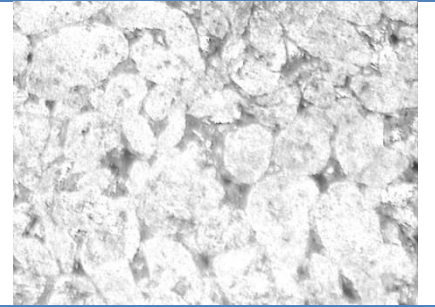
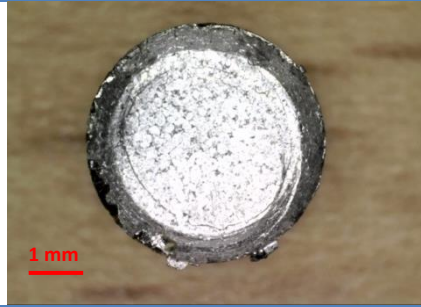


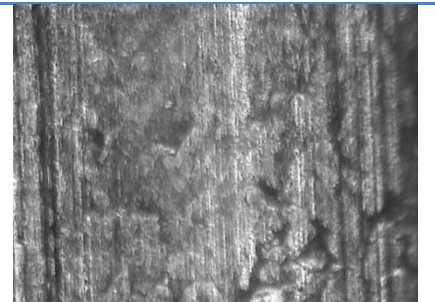
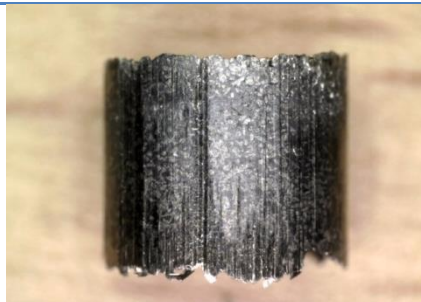
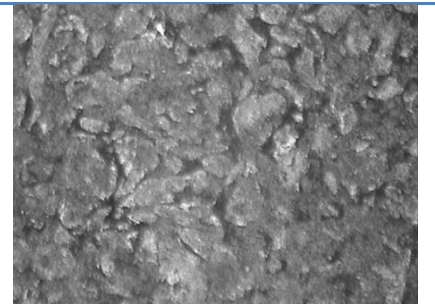
Table 6.2: Temperature influence on the cylinder sintering. The processes have been performed using heating loops.

The second step of this series of experiments would underline the effect of the temperature, *table 6.2*. The temperatures of 450 °C, 500 °C, and 600 °C have been analysed on samples #4, #5, and #6, respectively. The choice of 600 °C as a maximum temperature related to the melting temperature of aluminium, has been motivated in *paragraph 5.2*. Also the heating loops described in theory, see *paragraph 3.3.1*, have been applied. The same considerations of the first step could be done, because the particles melting has been improved with higher values of temperatures. The holding time has depended of the heating loops, because the heater has required time in order to cool and heat the part. Not a large difference can be noted among the two transversal surfaces of the cylinders. Instead, it is interesting to note the lateral surfaces characterised by parallel straight lines; in sample #6, at 600 °C, they are more accentuated. The reasons of these lines would be seen in the geometrical profile of the die or in friction consequences during the ejection phase. In this regard, the increasing of sintering temperature determines an improved-particles joining, on one hand, and an increasing in ejection friction, on the other hand. Because of difficulties in the manual setting of the pressure exerted by the mechanical press, the previous experiments have not carried out exactly with the same value.

#7  
T: 550 °C  
holding time: 5'  
pressure: 151.3 MPa



#8  
T: 550 °C  
holding time: 5'  
pressure: 81.2 MPa



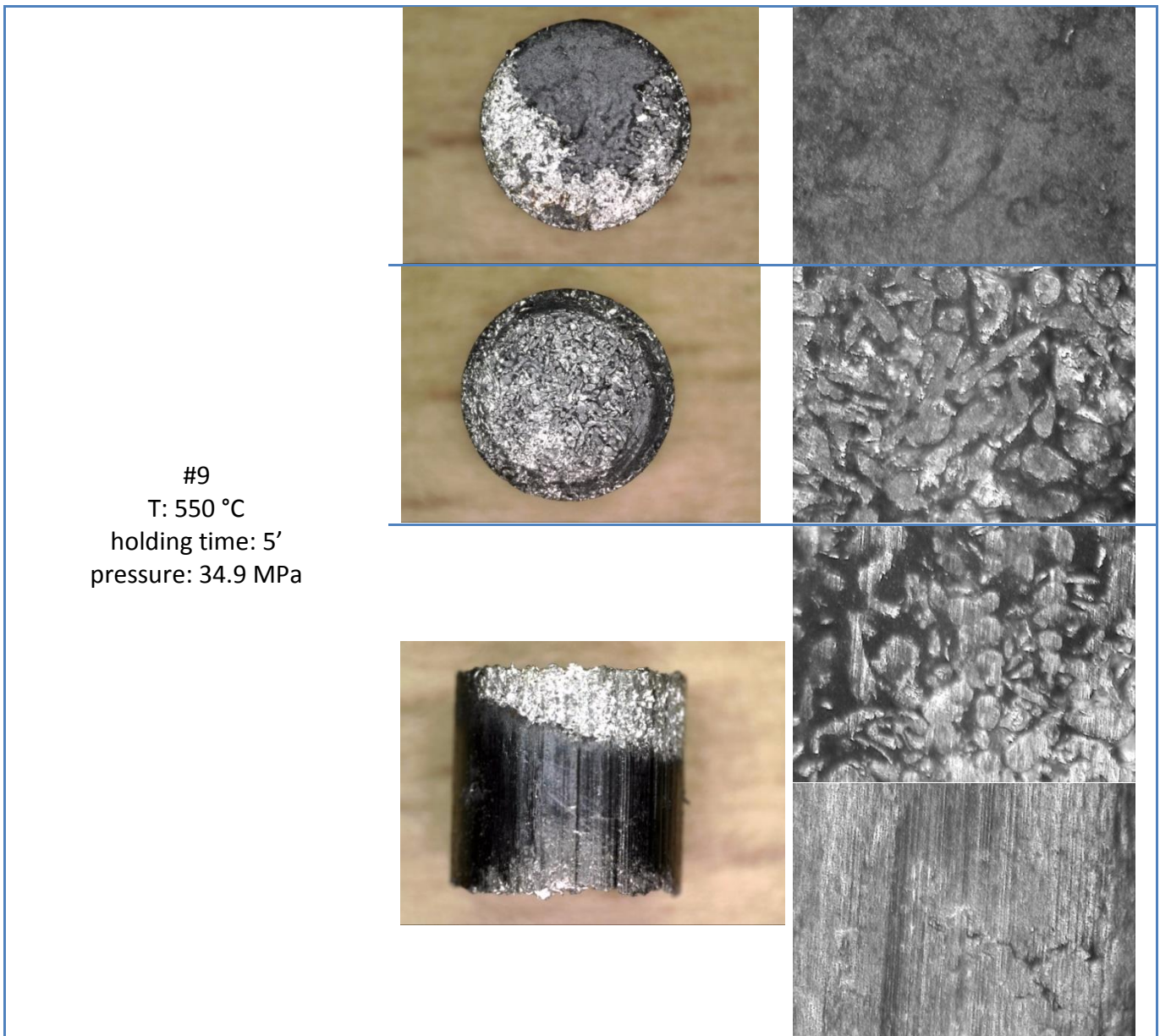


Table 6.3: Pressure influence on the cylinder sintering.

The last step of this series of experiments aims at analysing the influence of the compaction pressure, *table 6.3*. The sample #7 underlines the effect of high pressure on the part. The cylinder has not good sintered; in particular, the lateral surface is characterised by visible cracks/unjointed particles on the upper part. The reason of these ones should be viewed in pressure influence, but also in the sintering time, which in these experiments is less than compared to the last ones, *table 6.2*. The sample #8 seems the best sintered part, compared to the others; the macro-structures analysis shows a high rate of homogeneity, while micro-structure points out a non-complete melting process. Low pressure, sample #9, means high inhomogeneity of the part. In particular, on the lateral surface is clearly visible that particles have not been joined among them, because the pressure applied has not been sufficient to have

a homogeneous compaction of the cylinder. As a summary of this 1<sup>st</sup> series of experiments, concerning particles joining and cracks, samples with sintering temperature over 450-500 °C and holding time over 10 minutes have resulted with the best sintering quality, see #3, #4, #5, and #6. The samples #4, #5 and #6 have been also involved in heating loops, as a proof of the advantages related to these ones, see *paragraph 3.3.1*. The samples #7, #8 and #9 have noted how a higher pressure could result in cracks, while a lower one would not allow a good homogeneity in densification of the part.

### 6.3.2. 2<sup>nd</sup> Series of Experiments

With regard to the melting and densifying of the particles, a second series of experiments aims at further improving in the part quality. The parameter choices should be compared to the 1<sup>st</sup> series of experiments. In particular, the focus is on the holding time and temperature. The compaction pressure has not been analysed because the value of 100 MPa has been considered a good compromise. In the first step, experiments with a holding time over 10 minutes have been analysed. Then, the effect of the temperature has been studied. The influence of the heating loops has no more been analysed, because of the required time.

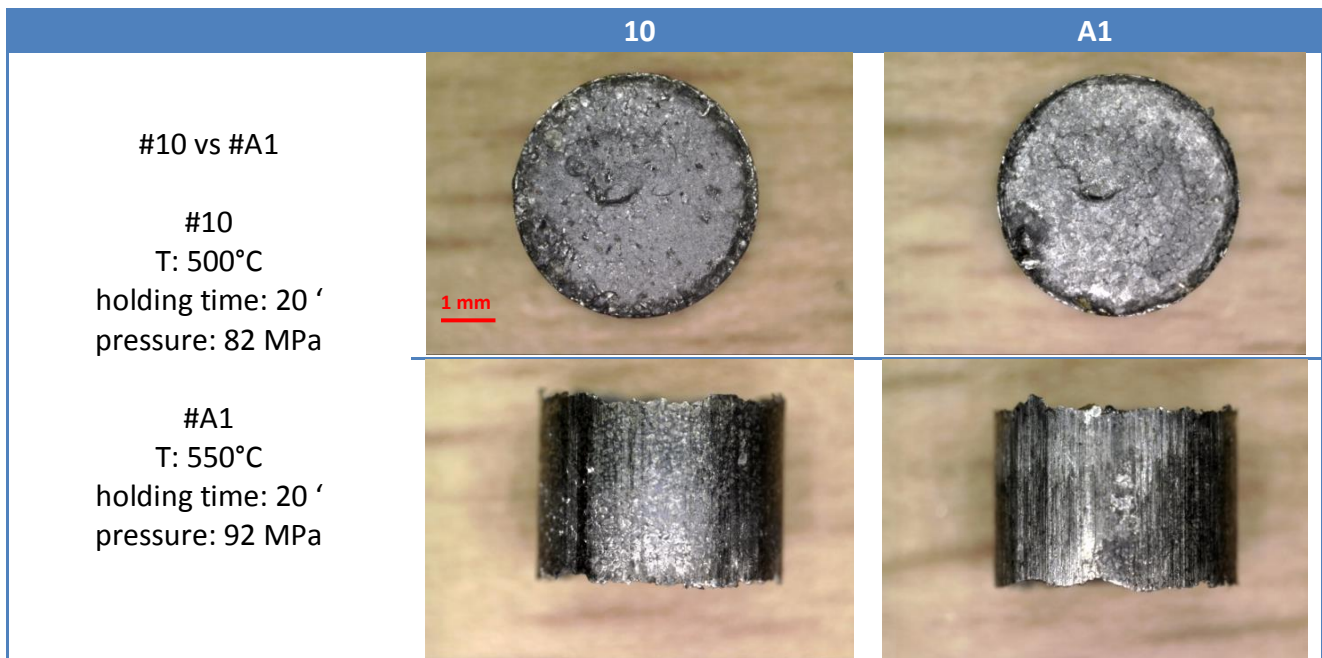
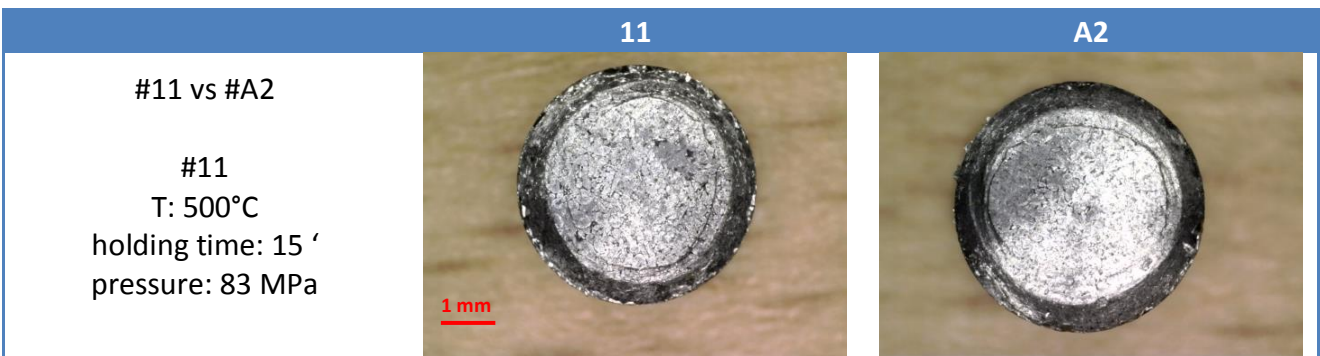






Table 6.4: Macro and micro-structures with 20 minutes of sintering. Temperature comparison.



#A2  
T: 550°C  
holding time: 15 '  
pressure: 92 MPa

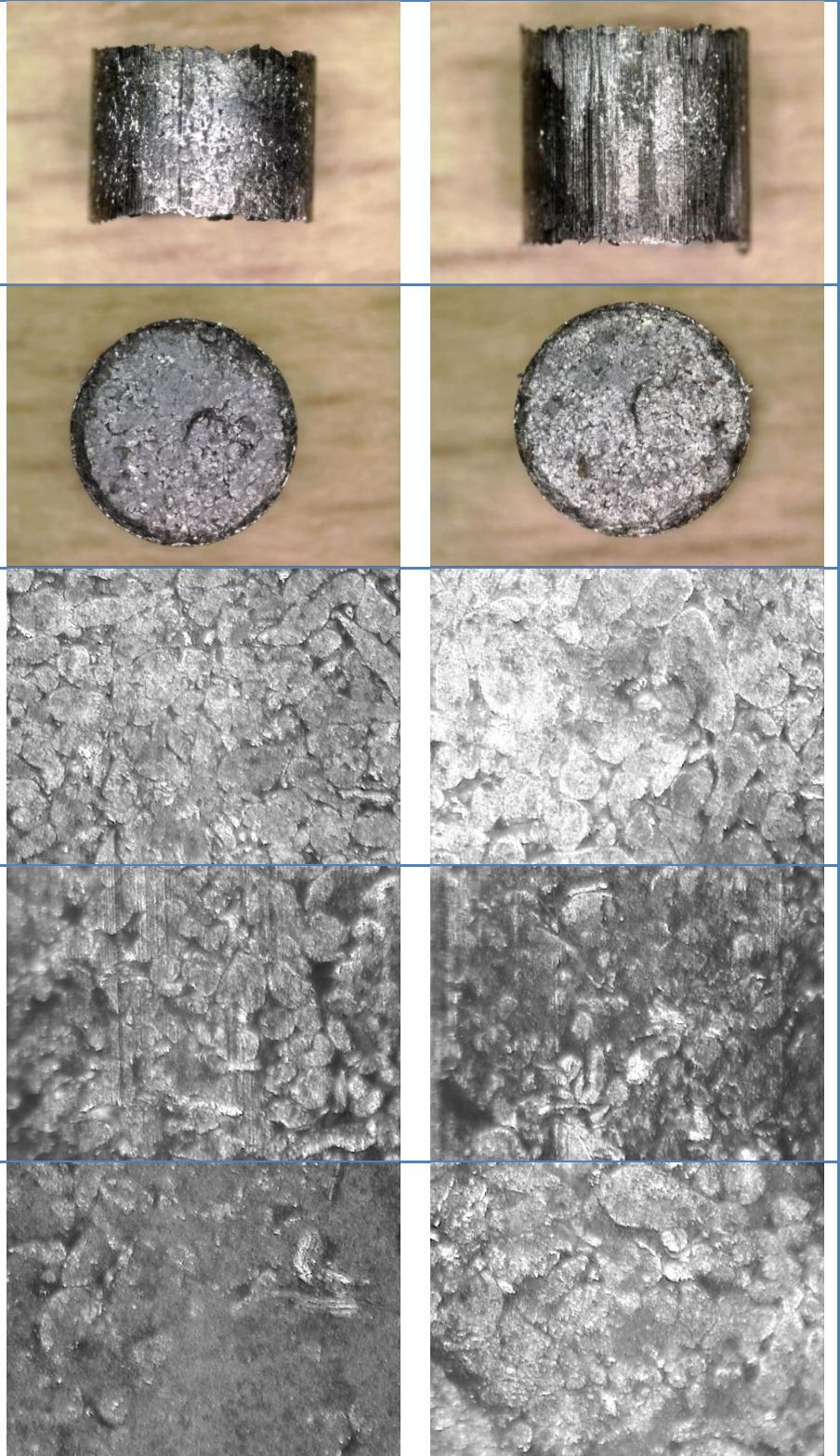
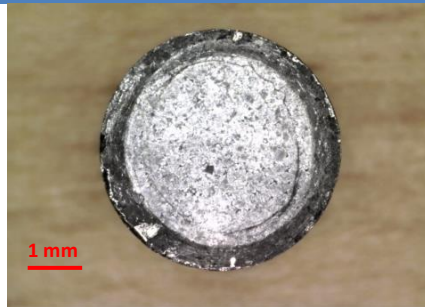


Table 6.5: Macro and micro-structures with 15 minutes of sintering. Temperature comparison.

12

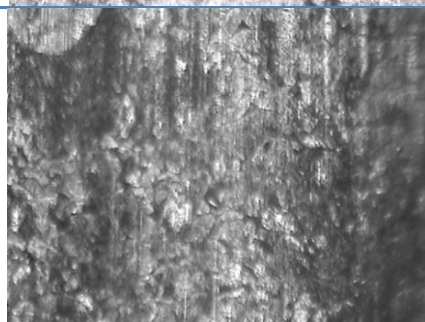
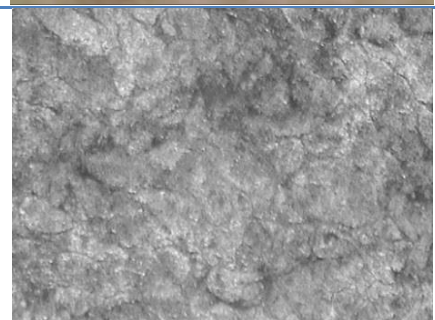
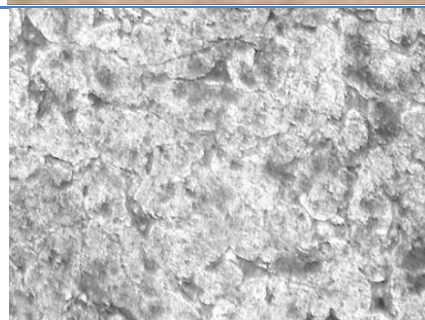
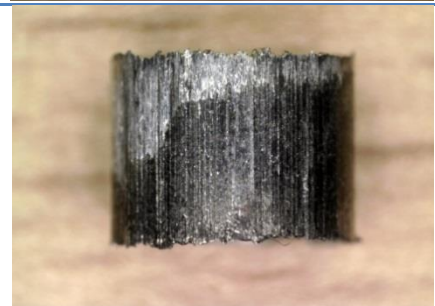
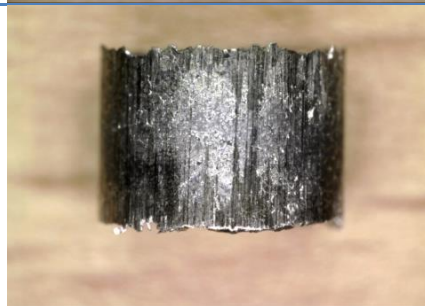
A3



#12 vs #A3

#12  
T: 500°C  
holding time: 25 '  
pressure: 95 MPa

#A3  
T: 550°C  
holding time: 25 '  
pressure: 99 MPa



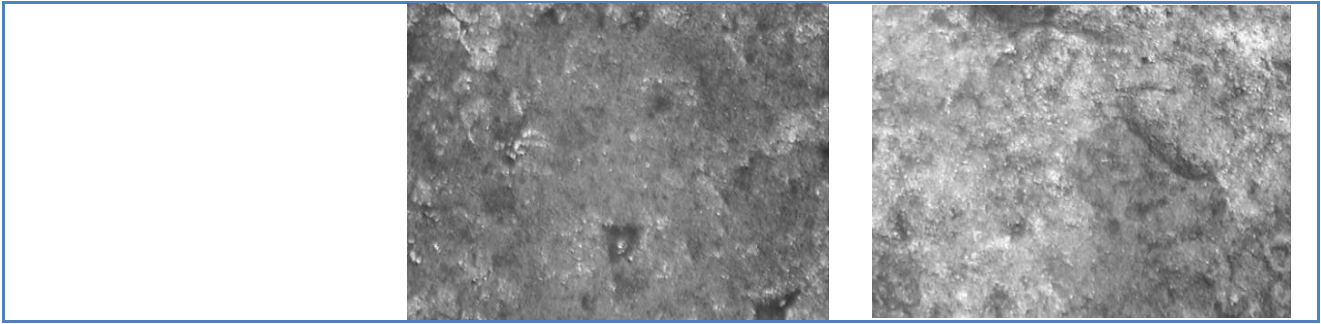


Table 6.6: Macro and micro-structures with 25 minutes of sintering. Temperature comparison

The 1<sup>st</sup> series of experiments has noted how with a holding time less than 10 minutes the part would not be good sintered. Densification has resulted not complete, with clear boundaries among particles. The 2<sup>nd</sup> series of experiments shows how the densifying is increased, in particular on the two opposite surface. The lateral surface is still imperfect. Considering equivalent-process parameters, a comparison between #10 and #5 shows how the heating loops could also improve the densifying related to the lateral surface of the cylinder. The reason of this would be seen in the radial-heating direction and heating-cooling effects. The samples #A1, #A2, and #A3 have been obtained with the same parameters of samples #10, #11 and #12, but with a temperature increase of 50 °C. With a holding time of 15 minutes, *table 6.5*, improvements are not so visible. Over 20 minutes, *table 6.4 & 6.6*, it could be noted how 50 °C have a significant edge in order to achieve a better densification. Especially for sample #A3, a good densification is obtained both for the lateral surface and for the upper and lower side of the cylinder. If the holding time seems the most influencing parameter, pressure has been important, too. In particular, comparing #A2 and #3, it is possible to see how the pressure could decrease the required-holding time, ensuring similar-quality results; in this case, a higher pressure of about 10 MPa has allowed a sintering-time reduction of 4 minutes. All these experiments show how the heater type influences the time of sintering. Scientific papers, see *paragraph 3.4*, have underlined how a Micro-FAST process allows low sintering time, in the order of few minutes. In these experiments, the reason related to the need of an increased time could be seen in the different heating system compared to the one described in literature; the main differences occur in the heating direction and thermal principle concerning the heating production, see *paragraph 4.2.2*.

Temperature [°C]	Time [minutes]	Pressure [MPa]
550	> 15 <small>*possibly using heating loops</small>	90 – 120

Table 6.7: Optimal condition to the cylinder sintering after the analysis of the experiments.

In summary, based on the last experimental considerations, the *table 6.7* shows the standard experiment conditions. A compaction pressure of 90-120 MPa has been a good trade-off, considering the results obtained in the 1<sup>st</sup> series of experiments. Respectively, the optimal values of the temperature and holding time, 550 °C and over 15 minutes, have been seen in the 2<sup>nd</sup> experimental series. Unfortunately, it has not been possible to find an accurate relation among parameters because of influencing factors, such as the amount of powder and lubricant, tool wear, soil, etc. It is worth remembering that these parameters are referred to a micro-aluminium cylinder, about 4 mm of diameter, sintered with the simultaneous applying of pressure and heating. Further experiments have not been done in this field, because the aim of the project has been focused on the ejection force.

## 6.4. Ejection Force Analysis

After the analysis related to parameters optimisation, this chapter wants to prove the advantages related to the pre-stressed die. Considering the variation of the process-parameters involved, several experiments have been done in order to calculate the ejection force at the end of the sintering process. In particular, the same part has been sintered with and without the pre-stressed die, in order to have a comparison of the forces involved. As described in the introduction, the complex tool designed and analysed in the last chapter has not been experimented due to manufacturing delay. However, the experiments have been done with an alternative design, based on the same shrink-fit principle, see *Appendix 3: Technical Drawings*. Thus, the obtained results could be associated to the original model, in order to prove the validity of the concept.

### 6.4.1. Simplified Conical Concept

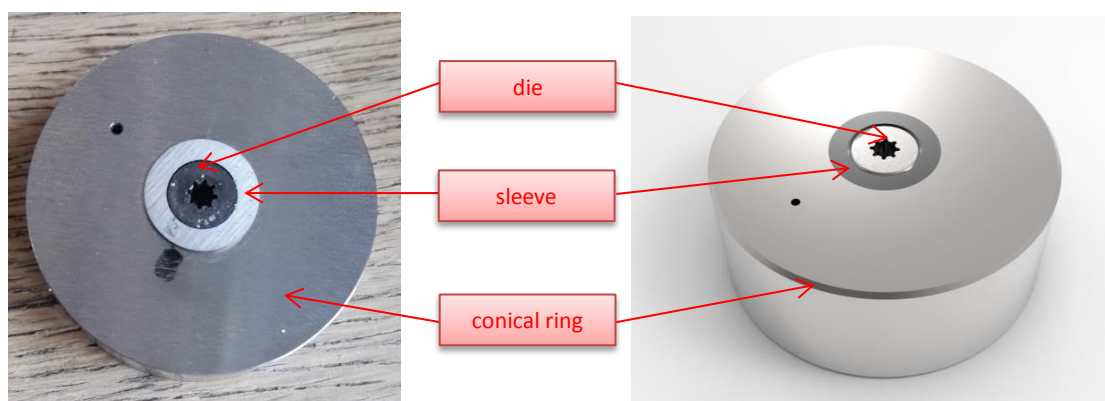


Figure 6.7: Simplified conical concept, based on the shrink-fit model.



Figure 6.8: Die-set for the experimental gears. From left to right, upper punch, die, and lower punch.

As described before, the experiments on the pre-stressed die have been carried out on a simplified concept, *figure 6.7*. The functional principle is based on the conical-fit described in *paragraph 5.3*. This concept consists of a conical ring and a sleeve, designed to fit the die-set already present in the IPU workshop, *figure 6.8*. The internal shape of this one consists of a 8-teeth gear, with an external diameter of 3.5 mm. The height of the sintered gear is approximately 2 mm, depending on the filled powder.

Component	$R_{\text{internal}}$	$R_{\text{external}}$	Thickness
[#]	[mm]	[mm]	[mm]
DIE	1.75	3.99	16
SLEEVE	3.99	6	16
RING	5.975	18	16

Table 6.8: Main geometrical characteristics of the simplified-conical concept.

The external diameter of the ring has been constrained by the diameter of the heater, *figure 6.4 (a)*, while the internal diameter of the sleeve has been designed in order to fit the external diameter of the die. The assembled system is shown in *figure 6.7*. The geometrical sizes of the tools are shown in *table 6.8*. It should be noted that this model was developed only for experimental purpose, in order to have an alternative to the original concept and understand the validity of the pre-stressed die with regard to the ejection force. The main geometrical features have been inspired according to the design of *paragraph 5.4*.

<b>v Poisson</b>	0.3					
<b>E Young</b>	190000	MPa				
<b><math>l_{\phi}</math></b>	<b><math>p_{\text{fit}}</math></b>	<b><math>D_m</math></b>	<b><math>R_{\text{reduction}}</math></b>	<b>conicity <math>\alpha</math></b>	<b><math>F_{\text{assembling}}</math></b>	<b><math>F_{\text{releasing}}</math></b>
[ $\mu\text{m}$ ]	[MPa]	[mm]	[ $\mu\text{m}$ ]	[ $^{\circ}$ ]	[N]	[N]
50	325.71	11.975	-6	3	44345,16	34077,33

Table 6.9: Functional characteristics of the conical fit.

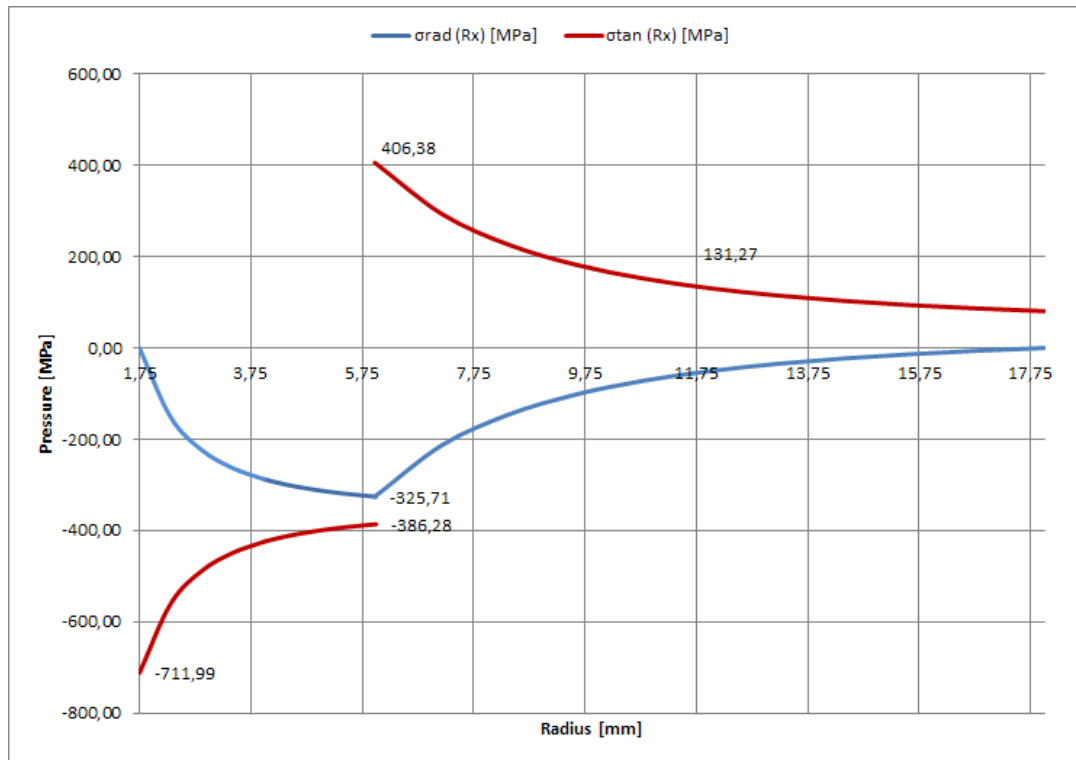


Figure 6.9: Tangential and radial pressure inside the tools.

The main functional characteristics of this simplified concept are shown in *table 6.9*. All the shown results accords to the thick-walled hollow cylinder theory, see *paragraph 5.3.1*. For the purpose of calculating, the Young's modulus  $E$  and the Poisson's coefficient  $\nu$  have been referred to the average value of a steel. The interference value,  $50 \mu\text{m}$ , has been as a trade-off between the design of the original concept and the value of the resulting fit-pressure; the maximum yield strength of the material should not be overcome. According to the theory, see *equation 5.6 & 5.7*, an overview diagram of the tangential and radial pressure field inside the different components is shown in *figure 6.9*. This diagram allows to estimate the maximum pressure that the tools have to withstand; in the calculations, die and sleeve have been considered as a single components. Considering the Von Mises failure strength, the equivalent pressure before failure would be  $\sigma_{eq} = \sigma_{tan} - \sigma_{rad}$ . The calculated value is equal to 732.09 MPa, corresponding to the inner radius of the ring. The H13 steel, already described in *paragraph 5.7.1*, has been chosen as material of the die and sleeve. Instead, the die and punches taken from the workshop are made of Inconel 618 alloy. The forces required to the assembling and releasing of the fitting, *table 6.9*, have been estimated according to the theory described in *paragraph 5.6.1*. For further technical information about this concept, see *Appendix 3: Technical Drawings*.

## 6.4.2. Experimental Procedure

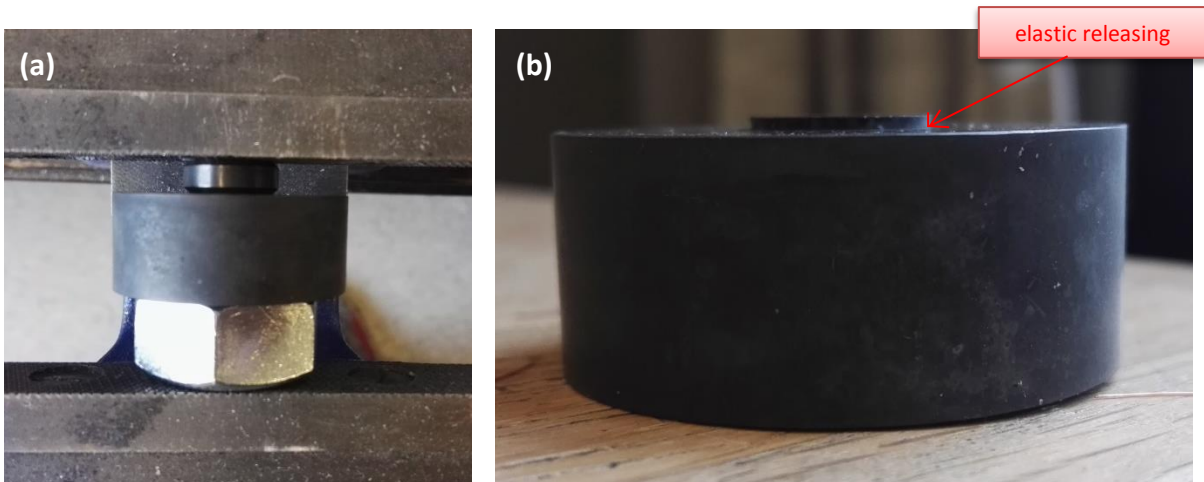


Figure 6.10: On the left, the conical-fit assembling phase; on the right, the elastic expansion of the sleeve after pressure releasing.

Before the gear-sintering process, the conical-fit has been realized. In particular, after the die has been placed inside the sleeve, a pressure has been applied in order to fit the components, *figure 6.10 (a)*. The main problem related to this phase has been in the elastic releasing of the sleeve, *figure 6.10 (b)*. In order to overcome this problem, the sleeve-ring interface has not been lubricated. In this way, the increased value of the frictional coefficient between the two components has reduced the elastic releasing. Unfortunately, this solution has not eliminated the problem. Thus, the maximum reduction has not been achieved.

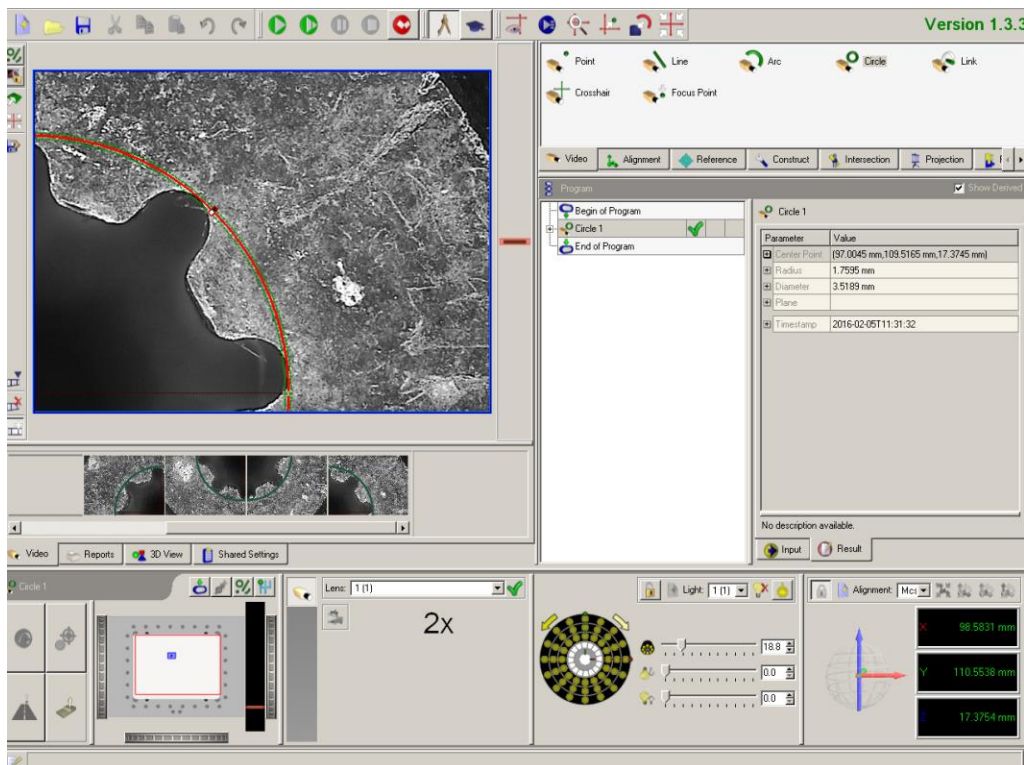


Figure 6.11: Detail of the optical-microscope-software interface used in radius calculations.



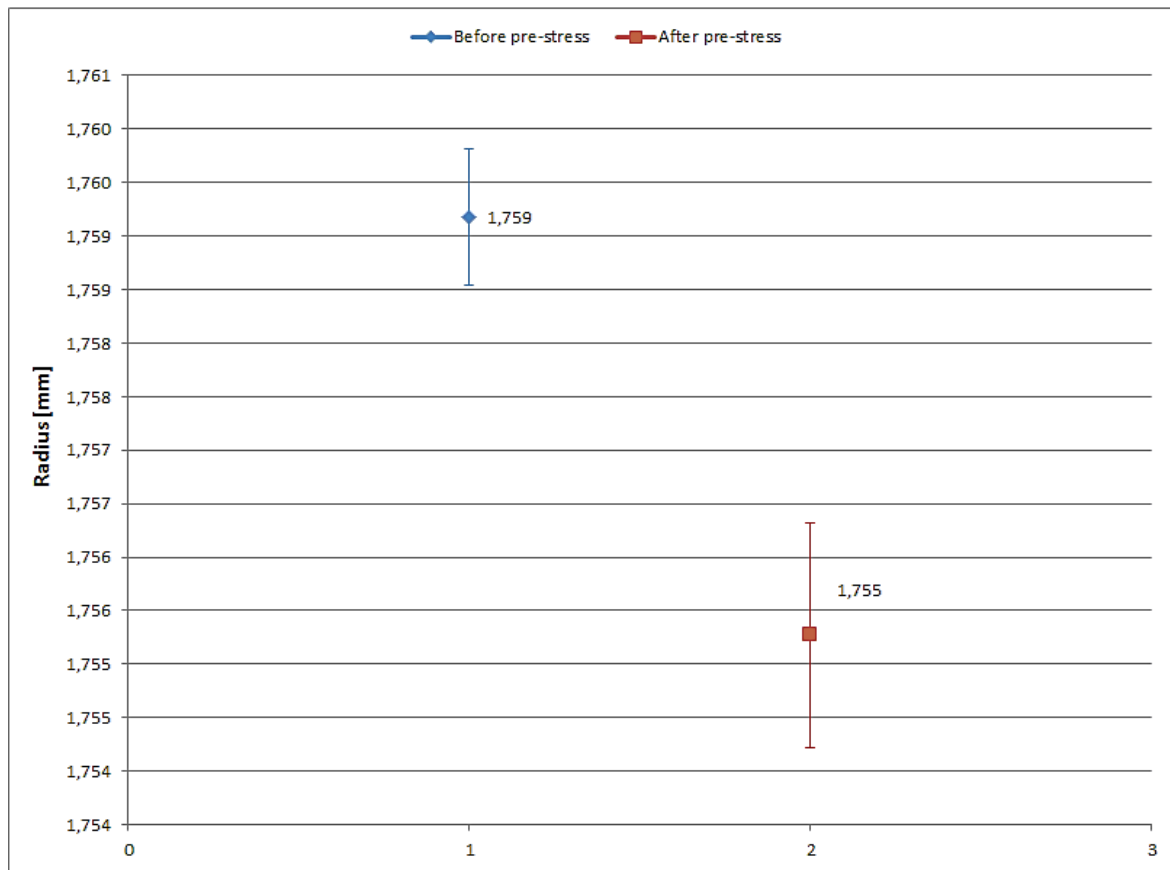


Figure 6.12: Average radius values evaluated before and after die pre-stress.

As a proof of the diameter reduction, 10 radius measurements both before and after compression have been made by using the optical microscopy, *figure 6.6*. The measures have been achieved from the circumscribed circle, *figure 6.11*. The resulting statistical analysis show how the compression has reduced the internal radius of the die, *figure 6.12*. Before compression, the external radius of the die has an average value of 1.759 mm, while after compression it has an average value of 1.755 mm. The resulting-average reduction is equal to 4  $\mu\text{m}$ . This value is lower than the predicted one by 2.5  $\mu\text{m}$ , see *table 6.9*. On the one hand, the thick-walled hollow cylinder model, used to calculate the theoretical value, might have overestimated the value of radius reduction. On the other hand, several-different elements could have influenced this result. For example, the measurement process has been affected by the operator inaccuracy; although the measurement system is very accurate, the manual alignment of the circle used to calculate the radius could have increased the measurement uncertainty. Another influencing element is represented by the interference tolerance required in tools manufacturing; although the value indicated in the drawings is 5  $\mu\text{m}$ , a variation from this could influence the value of the interference, equals to 50  $\mu\text{m}$ . As a consequence, the radius compression could vary from the theoretical value.

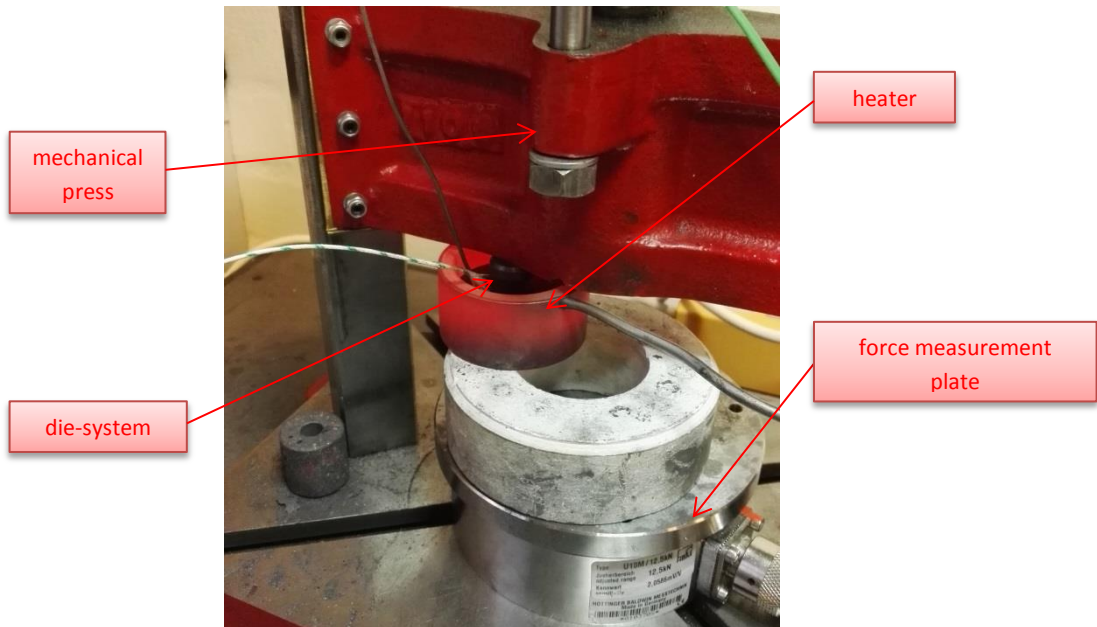


Figure 6.13: Sintering phase of the gear with the pre-stressed die.

The experiments were conducted with the same instruments of the previous ones. The die has filled up with aluminium powder, which has been compacted and heated up to the defined temperature, *figure 6.13*. After the sintering process, the “measurement plate” has measured the force exerted on the gear ejection.

### 6.4.3. Force Analysis: Results and Comparison

As indicated at the beginning of this *paragraph 6.4*, the experimental results on the ejection forces would be compared between the two die system configuration: without and with pre-stress. This choice has been done in order to understand the effectiveness of the pre-stress system, compared to the simple one. Also involving the process parameters analysed previously, which are compaction pressure, temperature, and holding time, three series of experiments have been carried out.

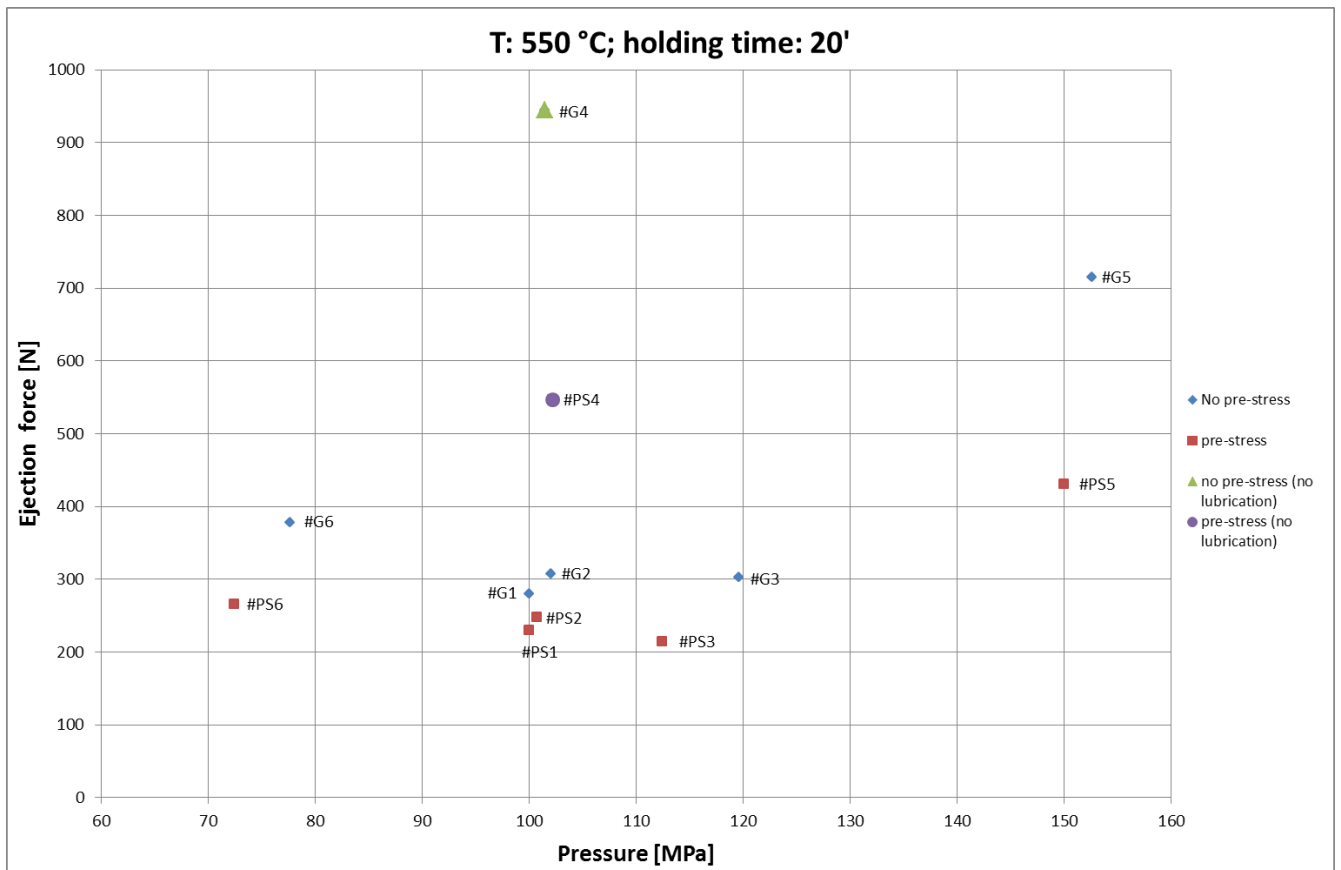


Figure 6.14: Experimental results on force analysis as a function of pressure. Samples from #G1, #PS1 to #G6, #PS6.

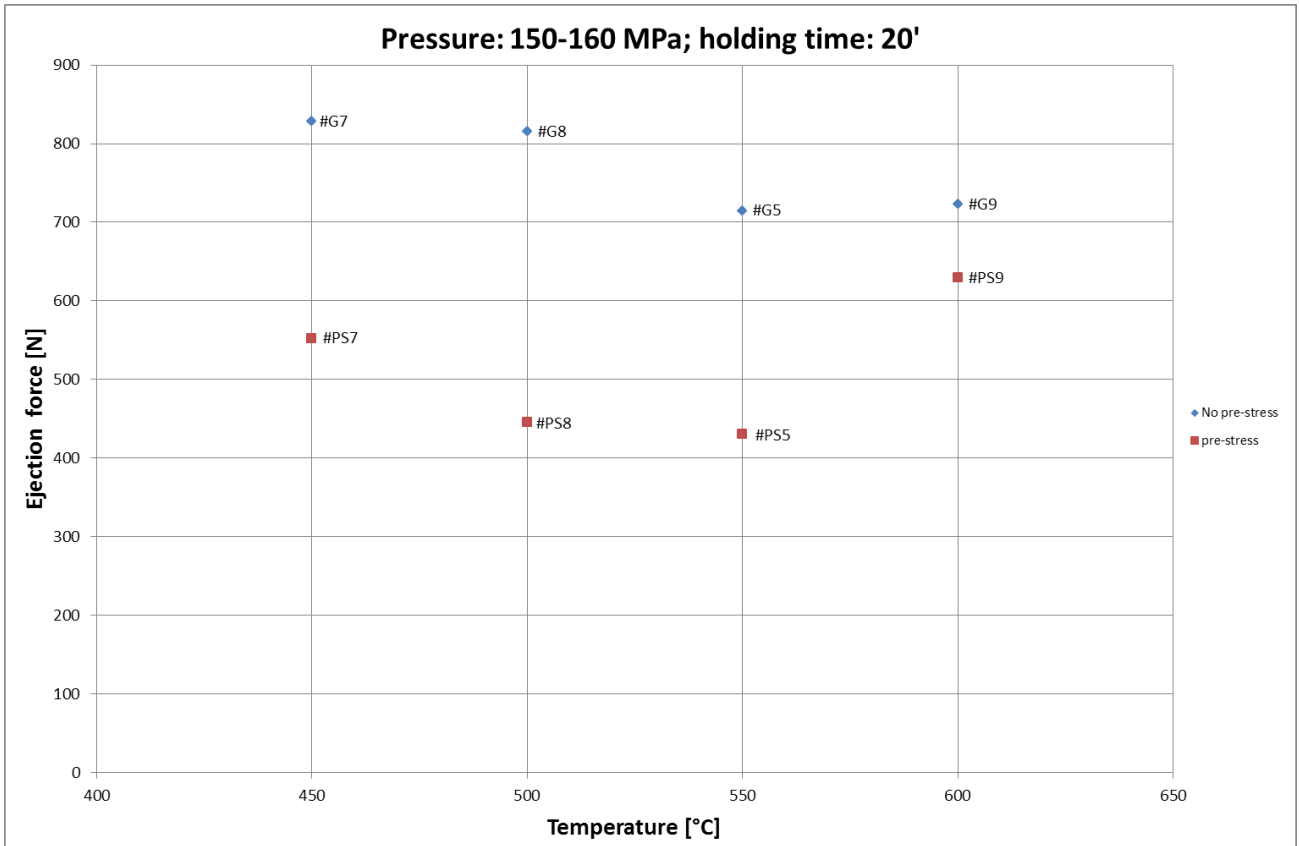


Figure 6.15: Experimental results on force analysis as a function of temperature. Samples from #G7, #PS7 to #G9, #PS9, including the samples #G5, #PS5 from the first series.

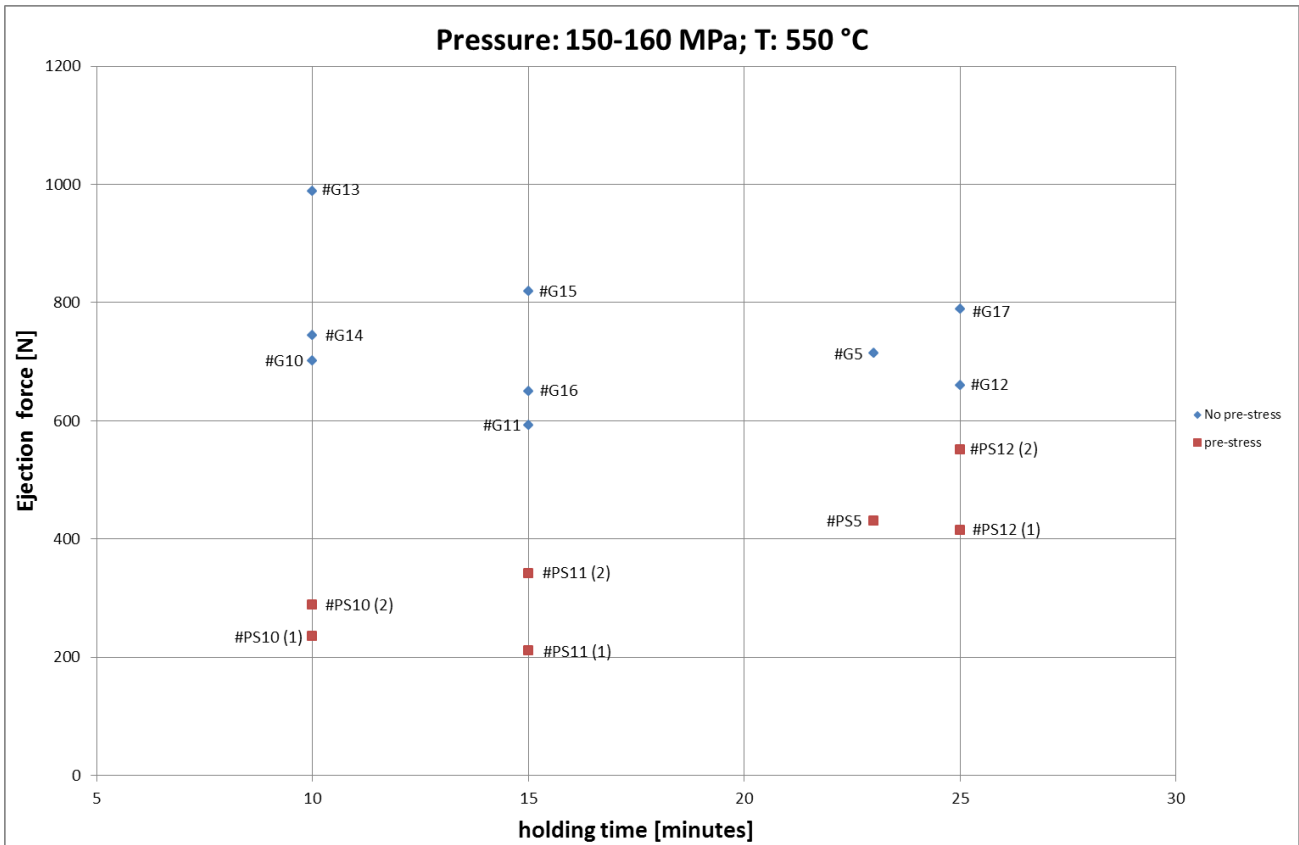


Figure 6.16: Experimental results on force analysis as a function of temperature. Samples from #G10, #PS10 to #G17, #PS12 (2) including the samples #G5, #PS5 from the first series.

The experimental phase has involved the sintering of 32 micro gears. All the experiments have been carried out under lubricated condition. However, also a comparison in unlubricated conditions has been done, samples #G4 and #PS4. The results obtained have pointed out how the measured forces in a pre-stressed die have been lower than the ones related to a simple-die-punch tool, without any compression. The *figures 6.14, 6.15 & 6.16* shows the experimental results concerning the variation of the compaction pressure, temperature, and holding time, respectively.

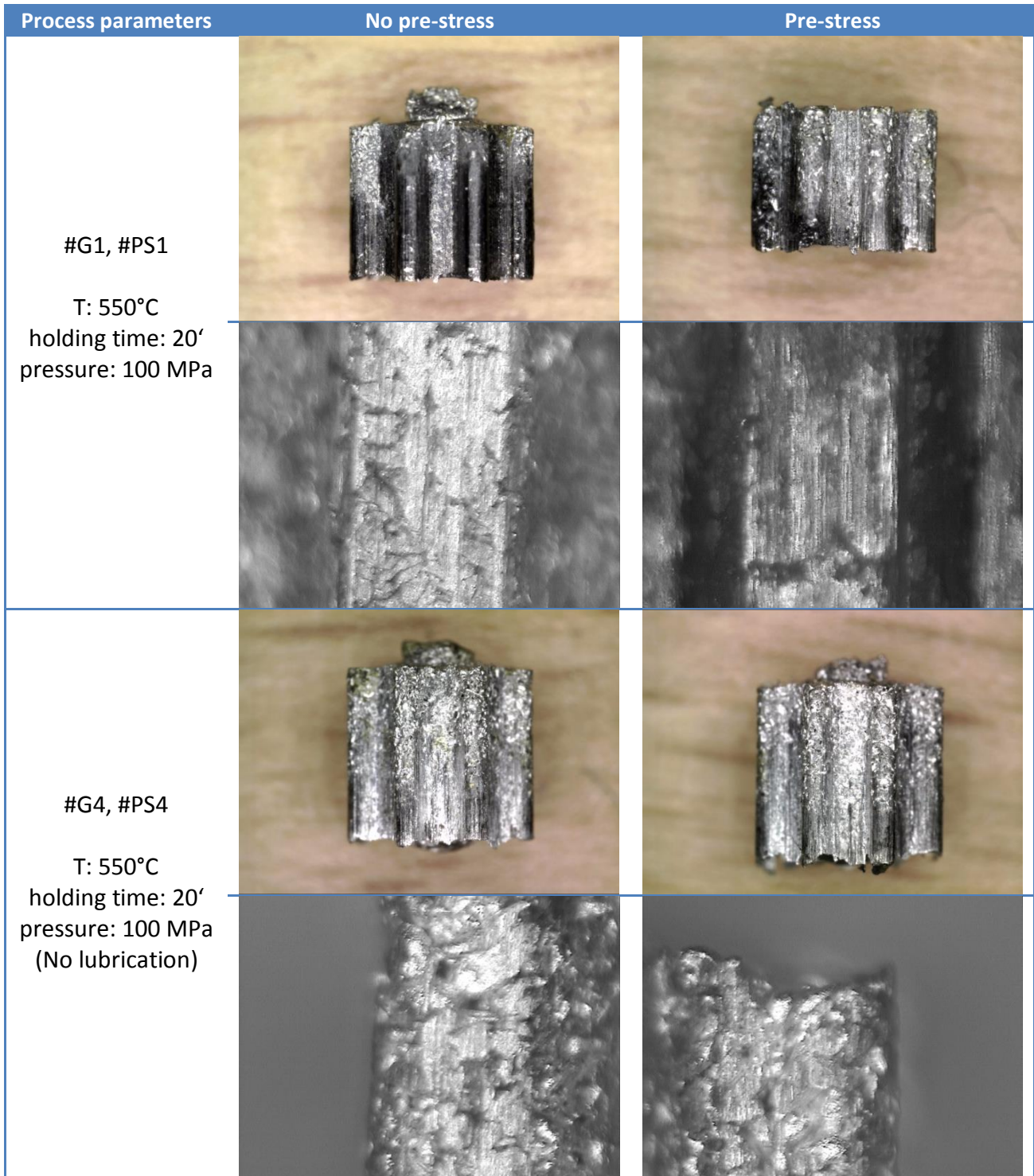
Parameter	PRESSURE	TEMPERATURE	TIME	TOTAL
Percentage reduction of the ejection force	30 %	31 %	53 %	38 %

Table 6.10: Calculations of the percentage reduction of the ejection force.

A summary of the average-percentage reduction of the ejection force is shown in *table 6.10*. Considering the tool system either with or without pre-stress, these results have been obtained comparing the resulting-ejection forces in the same experimental conditions. If considering the variation of temperature and pressure, the percentage reduction of the force has been similar. By contrast, the same percentage as a function of time has been higher. The reason could be seen in the different parameter influence with regard to the ejection force. Due to several influencing factors, such as the amount of lubricants, soil, fed powder, temperature during ejection, etc., establishing an accurate relation between the ejection force and parameters involved has not been possible.

## 6.5. Macro- and Micro-Structure Analysis

Principally, this paragraph aims at analysing the most-relevant-structure differences among the gears analysed previously. In addition, preliminary considerations about lubrication and process parameters have been done.



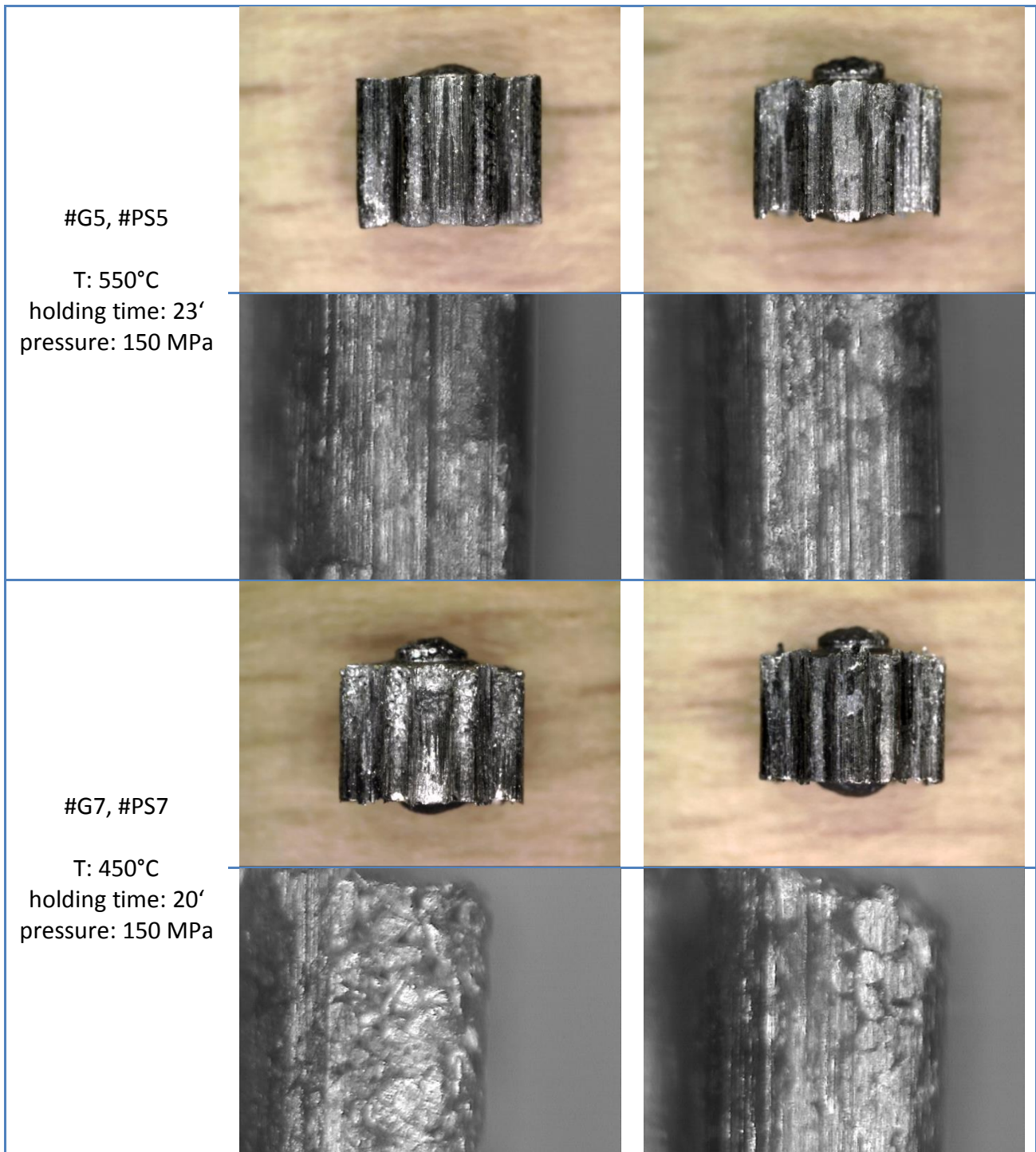
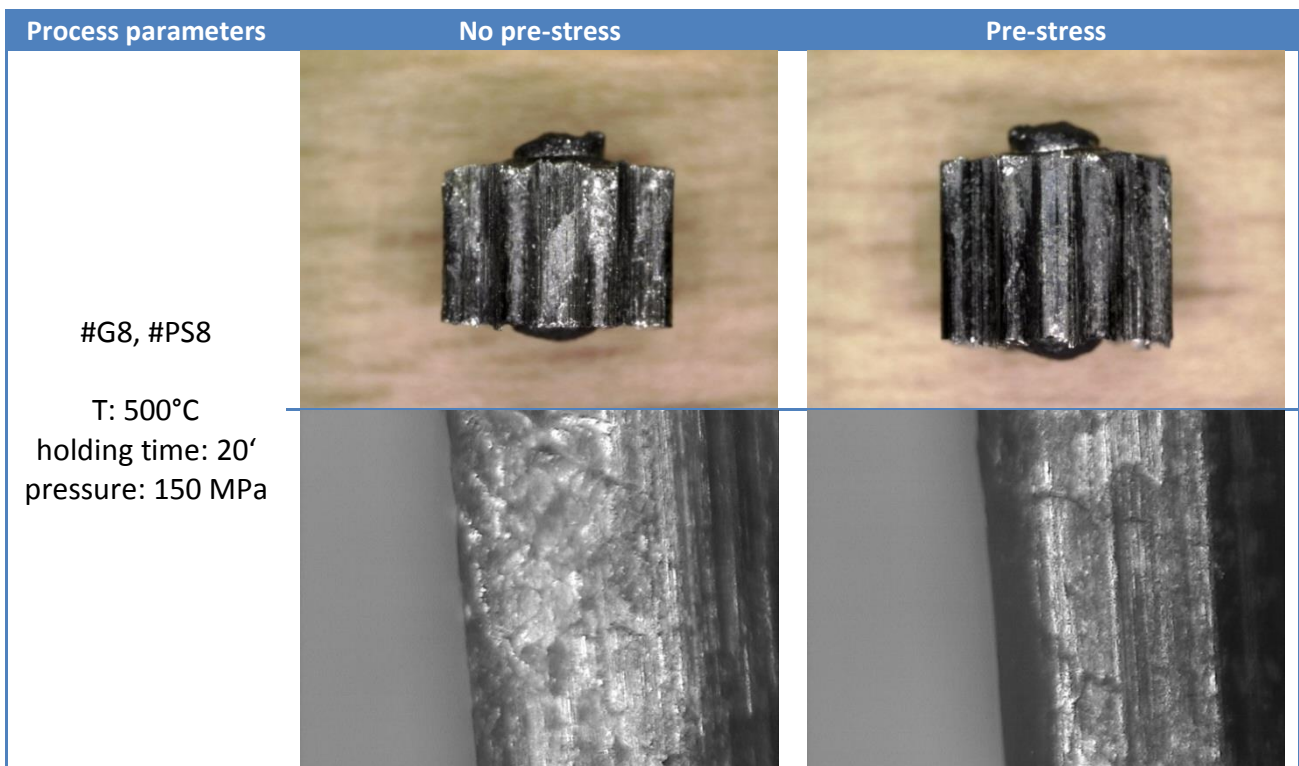


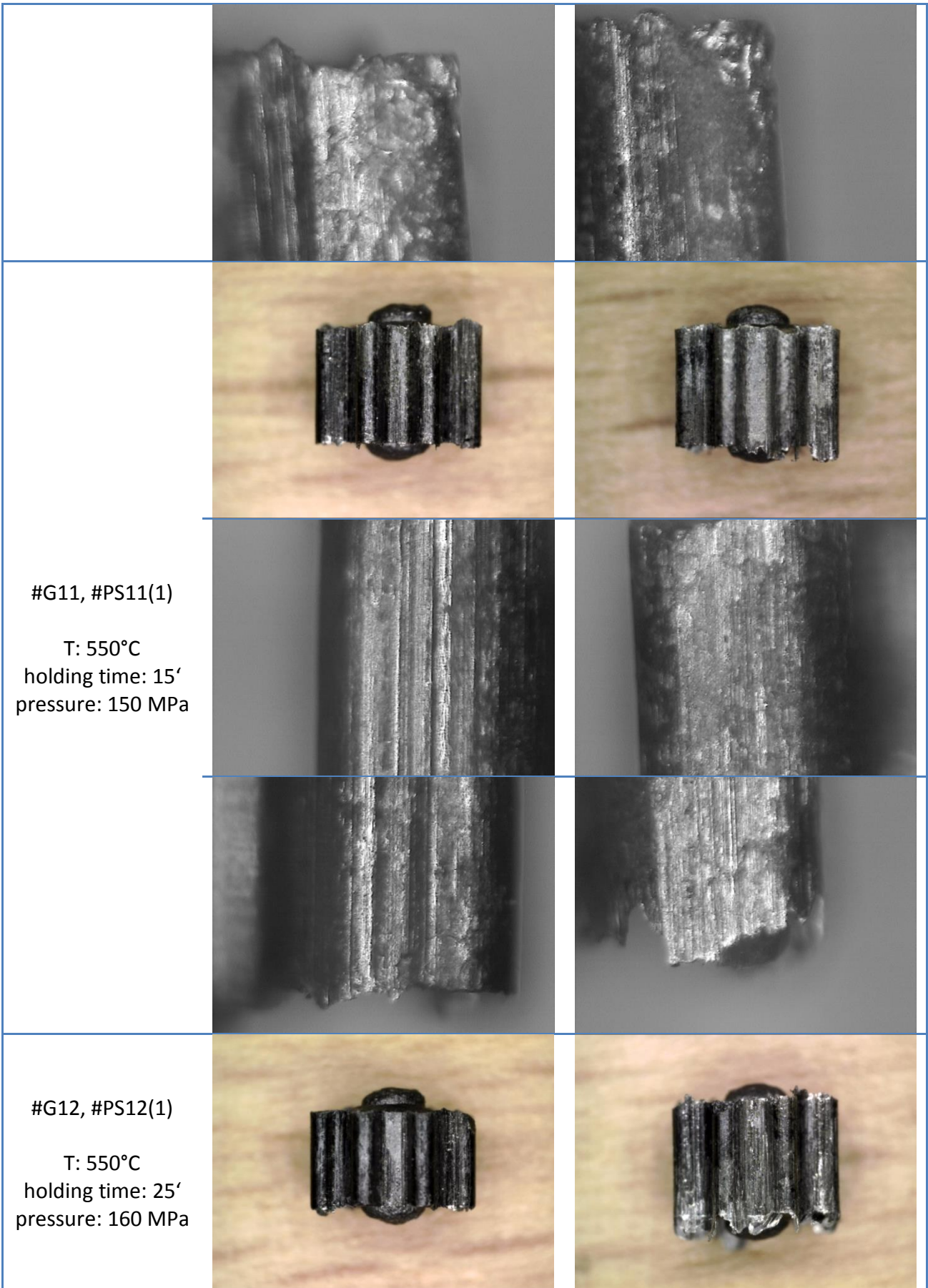
Table 6.11: Macro and micro-structure comparisons between gears manufactured with the two different die-system configurations. In this first table, the purpose is to show the difference between lubricated and unlubricated condition and understand the influence of pressure and temperature.

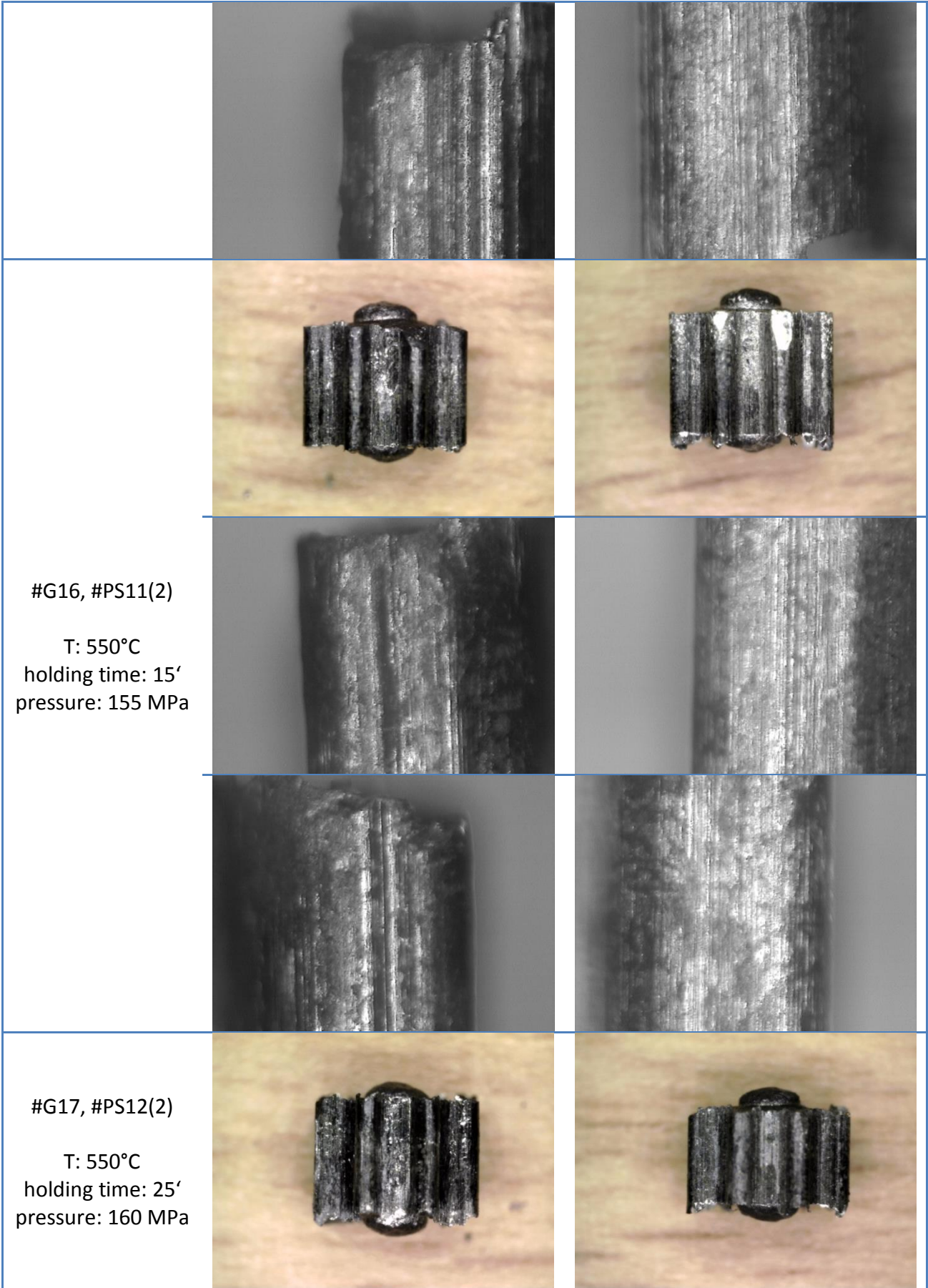
All the sintered samples described in the previous paragraph have been observed on the digital and optical microscopy, *figure 6.6*; in order to summarise the results, only the most relevant-gear structures have been displayed. A preliminary analysis shows the difference between having a sintering process with and without lubrication, #G1, #PS1, #G4, and #PS4, see *table 6.11*. The lubricant has influenced the colour of the gears, shiny grey for the parts sintered without lubricant and smooth black for the

others. However, lubrication allows to decrease the ejection force and the resulting friction, responsible of cracks and bad quality of the final part. A second analysis achieved from the pictures in *table 6.11* concerns two process parameters, which are compaction pressure and temperature. With regard to the particles joining, it has achieved how 100 MPa is not the optimal value, samples #G1 and #PS1. If compared to the considerations made at the end of *paragraph 6.3.2*, this result shows how the optimal compaction pressure depends on the shape complexity of the sintered part. In the cylinder case, 100 MPa have been optimal for a good sintering. In the gear sintering, a better quality is achieved at 150 MPa, samples #G5 and #PS5. The increased die-wall interface could be a reason of the higher-pressure requirement. About temperature, the results obtained in the sintered gears are a proof of the knowledge obtained in cylinder sintering. Compared to the gears produced at 550 °C, #G5 and #PS5, the samples #G4 and #PS4 show how a sintering temperature of 450 °C has not been optimal in the joining process of the aluminium particles. This result has accorded to the one achieved in *table 6.7*.









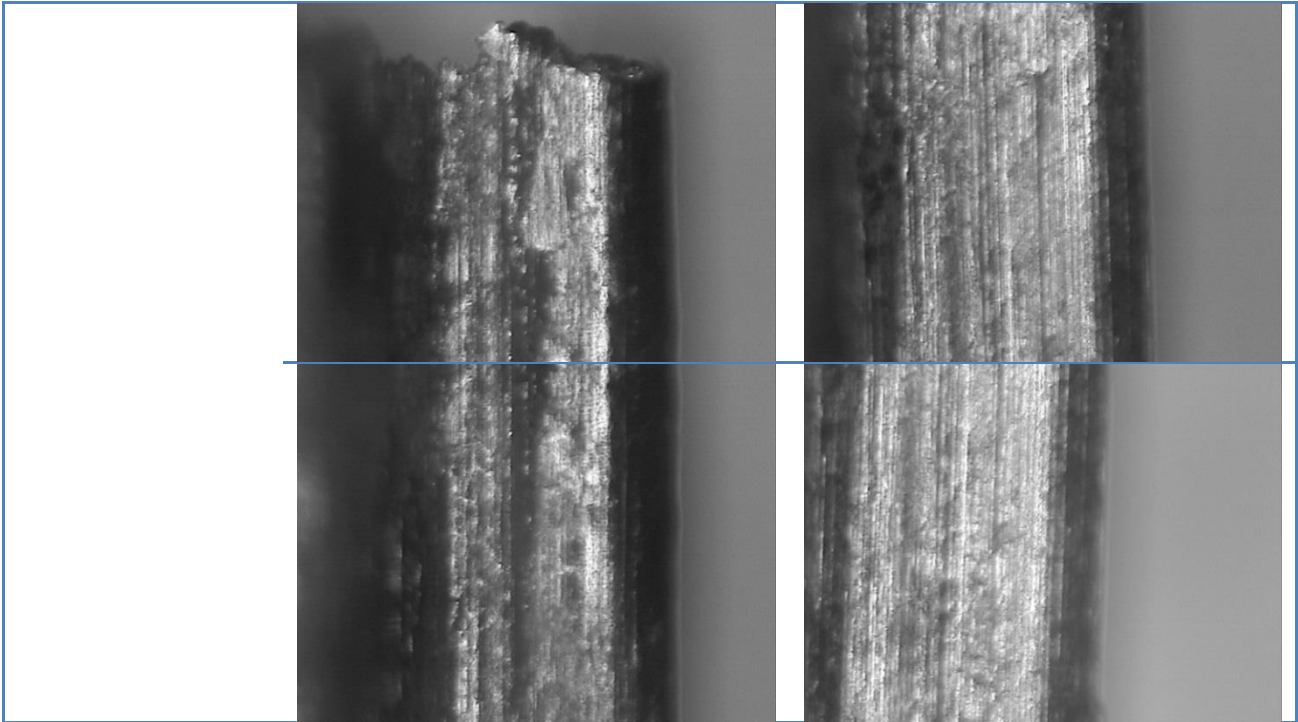






Table 6.12: Macro and micro-structure comparisons between the gears manufactured with the two different die-system configurations. In this second table, the purpose is to show the main differences related to the lateral surface of the sintered gears.

After the previous considerations made about process parameters in gears sintering, the purpose of *table 6.12* is to show the main differences between the resulting shapes in the two different sintering configurations. In order to understand the influence of the ejection force, a visual analysis has been focused on the lateral surfaces. All these experiments have been carried out after having considered the optimisation of the compaction-pressure; the value of 150 MPa was set up. The most interesting considerations regard the shape of the surfaces. Visual analysis on micro-structures have pointed out how the lateral surfaces are characterised by straight lines in the axial direction. In the gears produced without pre-stress, these lines are more marked than the ones characterising the gears manufactured in a pre-stressed die. The reason could be viewed in friction consequences; the pre-stressed die has allowed a reduction of friction during gears ejection, resulting in less-marked lines. In this regard, the *table 6.12* reports the most significant samples. It is worth pointing out how this line differences has been more marked with the increased joining of the aluminium particles; this aspect was not enough clear in the samples described in *table 6.11*, with the exception of samples #G5, and #PS5. Other considerations can be done about generated flash; no particular improvements have been observed in the pre-stress configuration. The reason of this should be viewed in the involvement of other factors not depending on the shrink-fit, such as powder filling, die-punch clearance, etc. As a summary, the main results obtained show that the concept tool

designed and experimented has been an improvement to the reduction of the ejection force and surface quality of the sintered gears, under lubricated condition. Unfortunately, external-influencing factors (soil, wear, amount of lubricant and powder, etc.) have not allowed to determine an accurate relation between the radius reduction, process parameters, and ejection force.

## 6.6. Unlubricated Samples

In this paragraph it will be analysed the manufacturing capability of the pre-stressed die in unlubricated condition, compared to the results in lubricated die described previously. To prevent the sticking between the punches and gear, only the compaction surfaces of the two punches have been lubricated. The parameters choice, which are temperature, pressure, and holding time, is referred to the values obtained by the experience of the previous series of experiments.

Samples	Transversal surface	Lateral surface
<p>#NL1</p> <p>T: 550°C            holding time: 20'            pressure: 150 MPa            ejection force: 973 N</p>		
<p>#NL3</p> <p>T: 500°C            holding time: 20'            pressure: 150 MPa            ejection force: 1800 N</p>		







<p>#NL4</p> <p>T: 500°C holding time: 20' pressure: 150 MPa ejection force: 2887 N</p>		
<p>#NL9</p> <p>T: 550°C holding time: 20' pressure: 130 MPa ejection force: 838 N</p>		
<p>#NLW1 (without pre-stress)</p> <p>T: 550°C holding time: 20' pressure: 150 MPa ejection force: 4500 N</p>		

Table 6.13: Macro-structures comparison about gears manufactured without a lubricated die.

The most interesting-sintered gears are shown in *table 6.13*. As a proof of the consequences related to high friction derived from the absence of lubricant, a visual analysis has pointed out how the lateral surfaces are damaged. This consideration accords to the samples #G4 and #PS4, already shown in *table 6.11*, although these ones have been compacted at up to 100 MPa. The lubricant influence is not only in reducing friction, but also in decreasing the radial pressure generated after powder compaction, according to *paragraph 5.2*, and in cleaning the die-wall surface.



Figure 6.17: Detail of the residual aluminium stuck on upper punch.

Without lubricant, the residual aluminium powder has stuck on the die and punches, *figure 6.17*, generating interference and problem to the following experiments. As a consequence, this problem has influenced the following series of experiments. In order to dissolve the residual amount of aluminium, the use of NaOH has been compulsory after some cycles of

experiments. The sample #NLW1 shows a gear manufactured without pre-stress. Although this sample has been sintered after cleaning of the tools, the ejection force has been higher than the previous ones; furthermore, the punch was difficult to eject from the die. Some other experiments have been carried out, but the wear has produced inaccurate results due to varying mechanical conditions of the tools. In industrial regard, the increased wear could be a serious consequence of the absence of lubricants. Furthermore, the continuous need of tools cleaning might represent a problem; cost increase and reduction of production volumes are the main consequences. Actually, Micro-FAST is also improving a laser die-cleaning technique integrated into the forming-machine (Micro-FAST).

## 7. Conclusions

Based on the functional principles of the Micro-FAST sintering process, this project has investigated on the possibility of reducing the ejection force. The experimental-sintered workpiece has been a micro gear, with a diameter of 3.5 mm. After literature researches and analysis on different models, it is possible to conclude that:

- According to the thick-walled hollow cylinder theory, the pre-stressed solution provided by stress-rings represents a valid problem solving. The main problem related to the pre-stress is on the maximum pressure generated inside the tool components. In this regard, the technological limit is on the yield strength of the tool materials. On one hand, a higher value of pressure means larger diameter compression; on the other hand, increasing the pressure means higher risk of tool component damage. For series production, this limit has to be considered with regard to the number of manufacturing cycles, too. Furthermore, the material has to maintain its mechanical properties in varied condition, such as higher temperature.
- A shrink-fit die system for the experimental sintering of a 24-teeth micro gear has been designed and shown. All the components studied and designed have an important role in the whole system. Great carefulness has been taken in all the dimensions of the tools, trying to take into account all the possible problems related to sintering process conditions (temperature, forces, varied mechanical properties, etc.). Many problems have been encountered because of the small sizes of some components. Unfortunately, this tool could not be tested due to manufacturing delay.
- Based on the designed tool, the functional principle of the pre-stressed die has been tested on a simplified ring-sleeve concept, with similar characteristics. Experimental comparisons show how all the results are in accordance with the purpose of decreasing ejection force. Compared to a simple-die configuration, the ejection force has been reduced by 30-50 %, depending on the process parameters. Due to several influencing elements during sintering, no theoretical estimations have been made on the predicted values of the ejection force. Future works could investigate on establishing a relation between the radial reduction, process parameters, and consequent ejection force, under controlled-experimental condition.
- Experiments on unlubricated dies have been carried out. The sintered components have resulted damaged and with imperfect quality. However, the possibility of

carrying out micro components without lubricants could be realised. The ejection force has been decreased by 36-80% if compared to the one resulting by no pre-stressed die; if compared to the results obtained in lubricated condition, the influence of several elements, like soil, residual aluminium, wear, smaller number of samples, etc., has generated this increased variability. Furthermore, it has to be considered the wear derived by several series of manufacturing cycles; tools have suffered more in unlubricated condition than in the lubricated one. Future works could focus not only on unlubricated system but also in its industrial applicability.

- Considering the process parameters in the aluminium-micro sintering, several experiments were carried out for parameters optimisation. According to literature, the temperature, the compacting pressure, and the sintering time, are the most influencing factors. Cylindrical and gear parts have been investigated. For micro components with similar size, the results show how the optimal compacting pressure depends on the shape complexity of the workpiece. The pressure required in cylinder has been less than the one required to the gear; precisely, 100 MPa for the first and 150 MPa for the second. Time and temperature have not shown this behaviour; both for cylinders and gears, the best results have been achieved with a sintering temperature of 550 °C and a holding time of 20 minutes.



## Bibliography

Yi Qin, 2015, *Micromanufacturing Engineering and Technology*, 2nd edition  
William Andrew Editor, pp 257-275;

GKN, *Aluminium PM Process*. Available from:  
<http://www.gkn.com/sintermetals/capabilities/aluminium-pm/Pages/Process.aspx>;

Colombo, 2000. 'Le fasi della metallurgia delle polveri', *Zincatura a caldo*.  
Available from: [http://www.ing.unitn.it/~colombo/zincatura\\_a\\_caldo](http://www.ing.unitn.it/~colombo/zincatura_a_caldo);

Höganäs, 2000, *Production of Sintered Component*, Handbook for Sintered  
Components;

Micro-FAST, [www.micro-fast.eu](http://www.micro-fast.eu);

Dong Lu, Yi Yang, Yi Qin, and Gang Yang, 2013, *Forming Microgears by Micro-FAST Technology*, journal of microelectromechanical systems, vol. 22, no. 3, pp 708-715;

Jie Zhaoa, Yi Qin, Kunlan Huang, Muhammad Bin Zulkipli, and Hasan Hijji, 2015, *Forming of micro-components by electrical-field activated sintering*, MATEC Web of Conferences 21, 10001;

Z. A. Munir, 2000, *The effect of external electric fields on the nature and properties of materials synthesized by self-propagating combustion*, Mater. Sci. Eng. A, Struct., vol. 287, no. 2, pp. 125–137;

D. V. Quach, H. A. Paredes, S. Kim, M. Martin, and Z. A. Munir, 2010, *Pressure effects and grain growth kinetics in the consolidation of nanostructured fully stabilized zirconia by pulsed electric current sintering*, Acta. Mater., vol. 58, no. 15, pp. 5022–5030;

W. Chen, 1998, *Gleeble System and Application*, 1st ed. New York, NY, USA:  
Gleeble System School;

C. H. Lee and K. Jiang, 2008, *Fabrication of thick electroforming micro mould using a KMPR negative tone photoresist*, J. Micromech. Microeng., vol. 18, no. 5, pp. 055 032-1–055 032-7;

Rockwell Automation, *Bullettin 900-TC Selection GuideI*, Available from: [http://literature.rockwellautomation.com/idc/groups/literature/documents/sg/900-sg001\\_-en-p.pdf](http://literature.rockwellautomation.com/idc/groups/literature/documents/sg/900-sg001_-en-p.pdf);

W.M. Long, 1960, *Radial Pressure in Powder Compaction*, Powder Metallurgy, Volume 3, No. 6, pp. 73-86;

G. Bockstiegel, *The Porosity-Pressure Curve and its Relation to the Size Distribution of Pores in Iron Powder Compacts*, Proceedings of the 1965 International Powder Metallurgy Conference, New York, NY, USA;

Engineers Edge, *Coefficient of friction equation and table chart*. Available from: [http://www.engineersedge.com/coefficients\\_of\\_friction.htm](http://www.engineersedge.com/coefficients_of_friction.htm);

Peng Chen, Gap-Yong Kim, Jun Ni, 2007, *Investigations in the compaction and sintering of large ceramic parts*, Journal of Materials Processing Technology 190 243–250;

Ming Wang Fu, Wai Lun Chan, 2014, *Micro-scaled Products Development via Microforming: Deformation Behaviours, Process, Tooling and its Realization*, Springer, pp 171-172;

Henrik Andresen, Erik Lund, 2008, *Tooling solutions for cold and warm forging applications for automotive and other segments*, Uddeholm Automotive Seminar;

Ehsan Ghassemali, Ming-Jen Tan, Anders E. W. Jarfors & S. C. V. Lim, 2013, *Progressive microforming process: towards the mass production of micro-parts using sheet metal*, Int J Adv Manuf Technol, pp 66:611–621;

Jens Groenbaek , Erik Rlem Nielsen, 1997, *Stripwound containers for combined radial and axial prestressing*, Journal of Materials Processing Technology 71, pp 30-35;

Muammer Koç, Mehmet A. Arslan, 2003, *Design and finite element analysis of innovative tooling elements (stress pins) to prolong die life and improve dimensional tolerances in precision forming processes*, Journal of Materials Processing Technology 142, pp 773–785;

E. Armentani, G. F. Bocchini and G. Cricri, 2012, *Doubly shrink fitted dies: optimisation by analytical and FEM calculations*, Powder Metallurgy vol. n.2;

Yi Qin, 2006, *Forming-tool design innovation and intelligent tool-structure/system concepts*, International Journal of Machine Tools & Manufacture 46 1253–1260;

A.D. Johnson, V. Martynov, V. Gupta, 2001, *Applications of shape memory alloys: advantages, disadvantages, and limitations*, Micromachining and Microfabrication Process Technology VII, Proceedings of SPIE Vol. 4557;

Wenke Pan, Yi Qin, Fraser Law, Yanling Ma, Andrew Brockett, Neal Juster, 2008, *Feasibility study and tool design of using shape memory alloy as tool-structural elements for forming-error compensation in microforming*, Int J Adv Manuf Technol 38:393–401;

Dan Noveanu, 2013, *Researches concerning a new method for obtaining spur gears by metal powder compaction in elastic dies*, Metalurgia, Vol. 65 Issue 4, p35-39. 5p. Diagrams, 5 Graphs;

Dan Noveanu, Dan Frunză, 2013, *Experimental researches and fem simulations of metal powder compaction in elastic dies*, Metalurgia, Vol. 65 Issue 6, p5-9. 5p;

Bruno Atzori, 2001, *Appunti di Costruzione di Macchine*, 2<sup>nd</sup> ed., Libreria Cortina;

Roberto Tovo, 2012, ‘Gusci Spessi’, *Formulario di Costruzione di Macchine*, Versione 3.04, Dipartimento di Ingegneria Università di Ferrara;

Davide Crivelli, 2013, ‘Calettamento Forzato’, *Quaderni di Progettazione*. Available from: <http://www.ilprogettistaindustriale.it/calettamento-forzato/>;

John Gilbert Kaufman, 1999, *Properties of Aluminium Alloys: Tensile, Creep, and Fatigue Data at High and Low Temperatures*, ASM International, pp. 7-15;

Niels Bay, 1993, ‘Cold Forging’, *Advanced Manufacturing Technology, Engineering Economy, and CIM-Oriented Technique in Metal Forming*, TEMPUS-Project JEP 1925 92/2, pp. 91, 95;

James M. Gere, Barry J. Goodno, 2009, ‘Column with Both Ends Fixed Against Rotation’, *Mechanics of Materials, Seventh Edition (SI Edition)*, Cengage Learning, pp. 838-839;

TPPInfo, 2006, ‘Yield Strength Against Hardness’, *Yield Strength and Heat Treatment*, available from: [http://www.tppinfo.com/defect\\_analysis/yield\\_strength.html](http://www.tppinfo.com/defect_analysis/yield_strength.html);

Bohler Uddeholm, *H13 Tool Steel, Material Property*. Available from:  
[http://www.bucorp.com/media/H13\\_data\\_sheet\\_09032013.pdf](http://www.bucorp.com/media/H13_data_sheet_09032013.pdf);

Bohler Uddeholm, *W360 ISOBLOC, Hot Work Tool Steel*. Available from:  
[http://www.bucorp.com/media/W360\\_datasheet.pdf](http://www.bucorp.com/media/W360_datasheet.pdf);

Bohler Uddeholm, *W302 ISOBLOC, Hot Work Tool Steel*. Available from:  
[http://www.bucorp.com/media/BOHLER\\_W302ISOBLOC.pdf](http://www.bucorp.com/media/BOHLER_W302ISOBLOC.pdf);

AZO Materials, *Tungsten Carbide, an Overview*. Available from:  
<http://www.azom.com/properties.aspx?ArticleID=1203>;

INCO databooks, *18 per cent nickel maraging steels Engineering properties*,  
Available from:  
[http://www1.diccism.unipi.it/Valentini\\_Renzo/slides%20lezione%20met.%20meccanica/18\\_NickelMaragingSteel\\_EngineeringProperties\\_4419\\_.pdf](http://www1.diccism.unipi.it/Valentini_Renzo/slides%20lezione%20met.%20meccanica/18_NickelMaragingSteel_EngineeringProperties_4419_.pdf);

Il Progettista Industriale, 2013, 'Molle a tazza', *Quaderni di Progettazione*. Available from: <http://www.ilprogettistaindustriale.it/molle-a-tazza/>.

# **APPENDIX 1:**

## **Spring-Die Design**

## A.1. Spring-Die Design

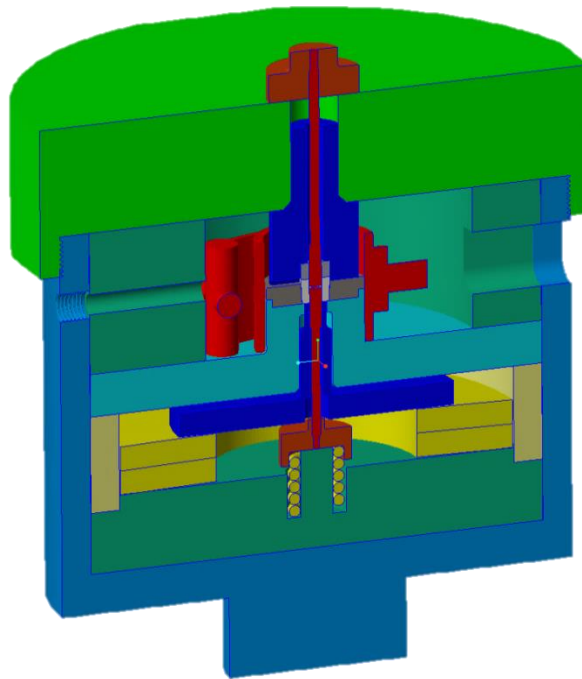


Figure A.1.1: 3D CAD model of a spring-die system.

This appendix aims at describing a different die-system concept. Before designing the model described in *chapter 5*, during the first period spent on this project, the focus has been on the die-system shown in *figure A.1.1*. This die-system has the same functional principle based on die and pre-stress ring. The main difference of this concept has regarded the ejection system.

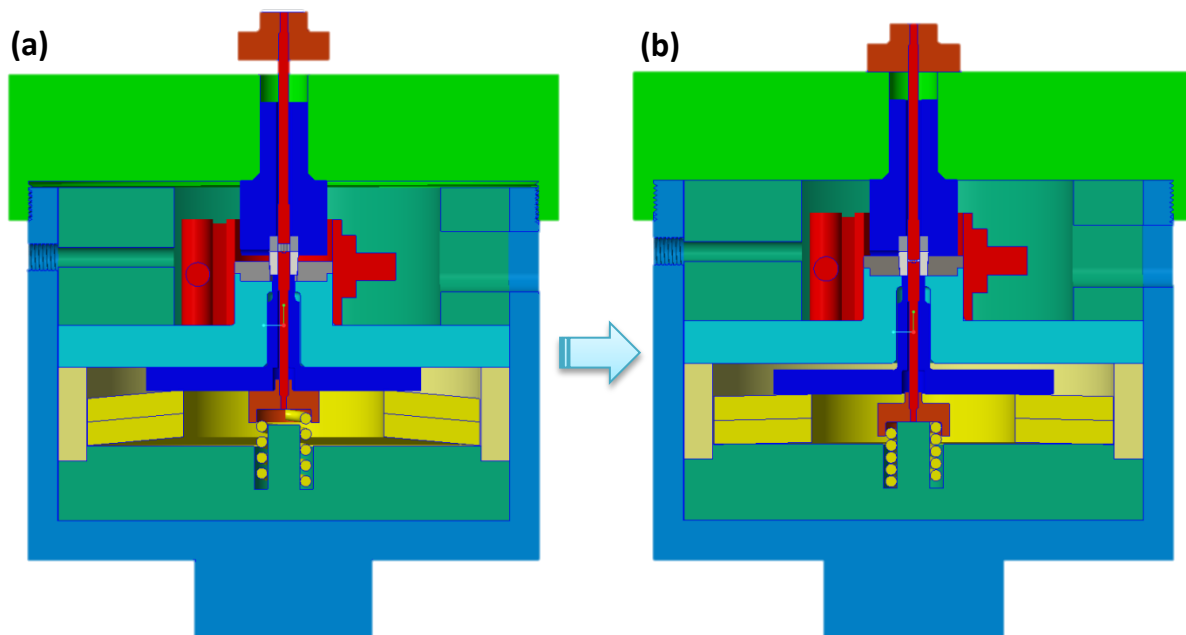


Figure A.1.2: Schematic comparison of the sintering steps, (a) starting system configuration, (b) system configuration during sintering.

The ejection forces are exerted from different springs placed on the bottom side of the system. During the compacting phase, the springs have been compressed from the press, while conical fit is being realised, *figure A.1.2 (a)*. Then, the system is screwed by an upper cover. After realising the pre-compression, due to internal diameter reduction of the die, see *paragraph 4.4.2*, the system is ready for powder compacting and sintering, *figure A.1.2 (b)*. When sintering process is concluded, the system is unscrewed and the part ejected, without rotating the bag. The system does not need a press to exert pressure on the ejection punches. The ejection forces are applied from the compressed springs, which after releasing of the pressure, return to their original shape due the elastic energy collected during compaction phase.

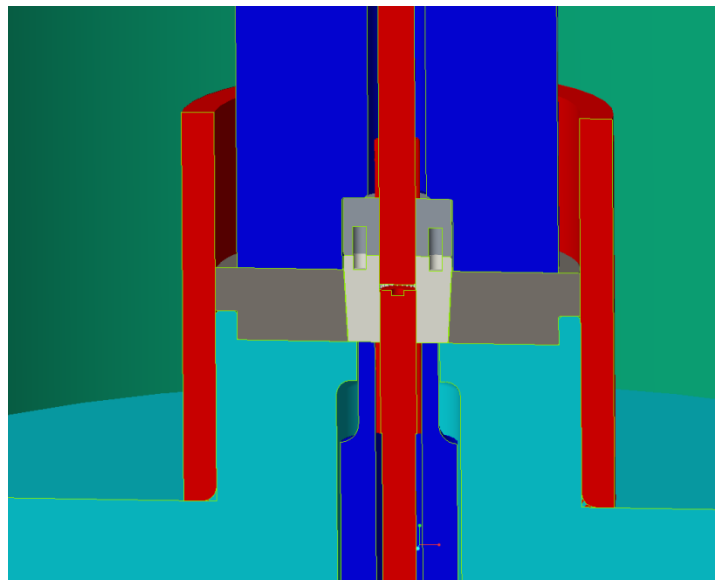


Figure A.1.3: Die-ring fit detail.

The springs selection is based on the required forces in order to release the die and eject the micro gear. In order to assembly and release the die from the coupling with the ring, the forces required to the conical fit, *figure A.1.3*, have been calculated according to *equation 5.9 & 5.10*.

$D_m$	$p_{fit}$	$l_\phi$	$h$	$\alpha$	$\mu$	$F_{assembling}$	$F_{releasing}$
[mm]	[MPa]	[ $\mu m$ ]	[mm]	[ $^\circ$ ]		[kN]	[kN]
7,118	670	60	6	3	0,7	66	-61

Table A.1.1: Geometrical specifications and forces, according to the conical fit.

On *table A.1.1* are shown the main geometrical characteristics of the conical fit, important for the estimations of the required forces. The last two columns show the estimated values of forces. Based on these estimations, the spring system could be designed.

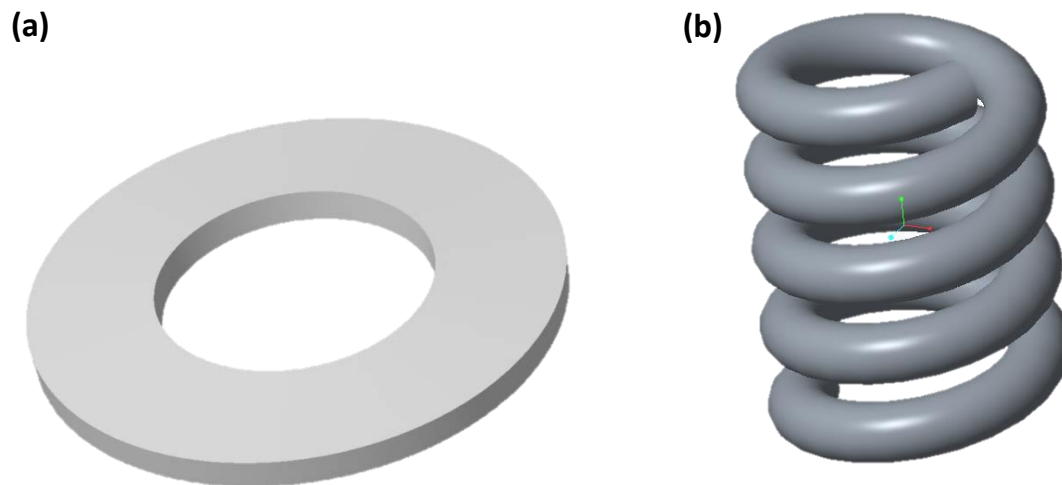


Figure A.1.4: Springs used in the concept, (a) disc spring, (b) compression spring.

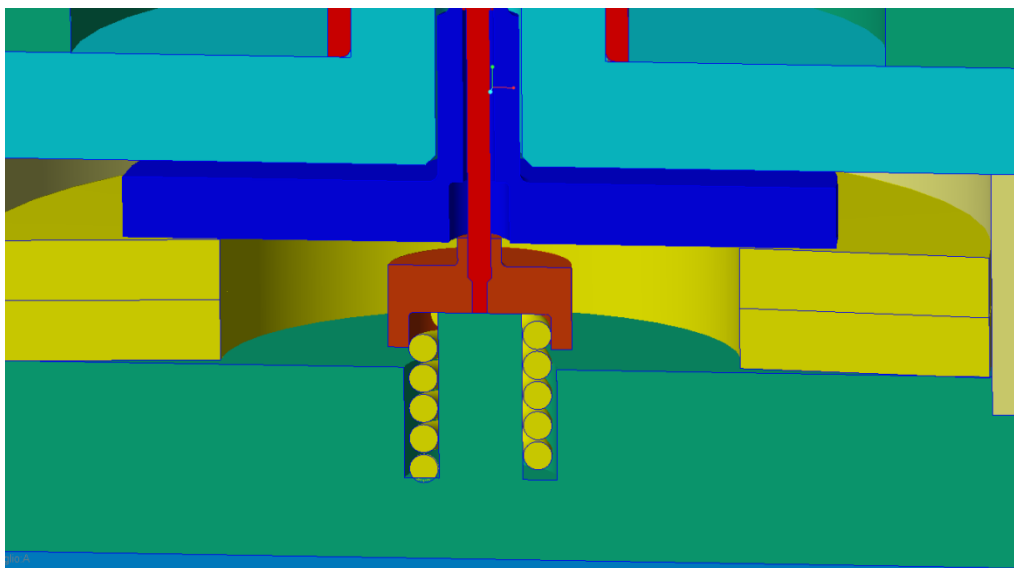


Figure A.1.5: Springs ejection system detail.

The Sodemann springs catalogue (*Note*. Available from: <http://www.molle-industriali.it/negoziario-online>) offers a large variety of solutions to this design. In particular, disc springs have been chosen for the die releasing, *figure A.1.4 (a)*, due to the high-exerted forces related to a minimum stroke; for gear ejection, instead, a compression spring results sufficient to the purpose, *figure A.1.4 (b)*.



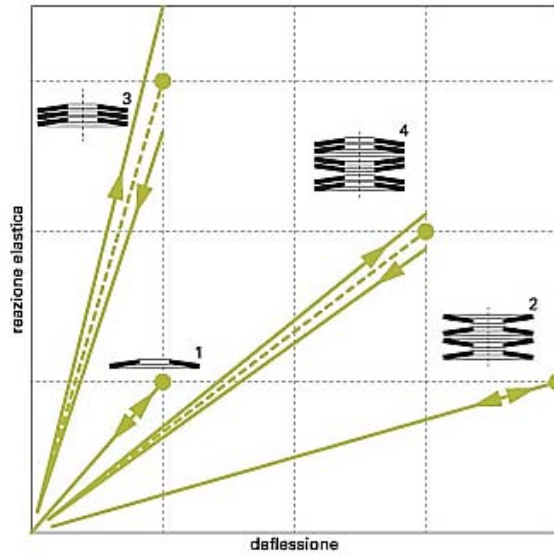


Figure A.1.6: Elastic reaction as a function of spring deflection (Il Progettista Industriale 2013).

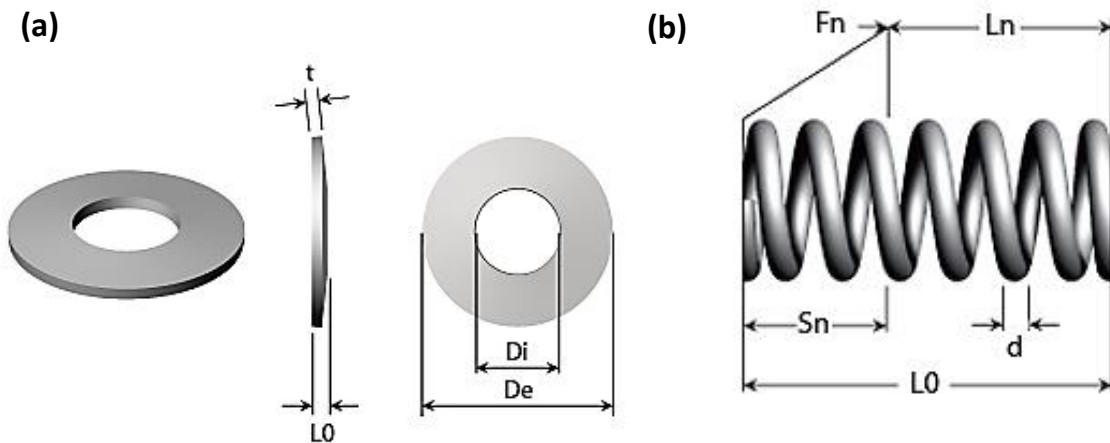


Figure A.1.7: Main geometrical parameters related to (a) disc spring, (b) compression spring. *Note.* Available from: <http://www.molle-industriali.it/negozio-online>.

Disc spring (x2)			Compression spring		
art.code	10019150		art.code	23190	
$D_{\text{external}}$	100	mm	$D_{\text{external}}$	14	mm
$D_{\text{internal}}$	51	mm	$D_{\text{internal}}$	8,4	mm
$L_0$	8,2	mm	$L_0$	20,5	mm
$t$	6	mm	$d$	2,8	mm
			$R$	106,20	N/mm
$S_n$ (stroke)	1,65	mm	$S_n$ (stroke)	4,1	mm
$F_n$ ( $F_{\text{max}}$ )	48022	N	$F_n$ ( $F_{\text{max}}$ )	432,14	N
$F_{\text{required}}$	61000	N	$F_{\text{required}}$	--	N
$F_{\text{exerted}}$	96044	N	$F_{\text{exerted}}$	432,14	N

Table A.1.2: Technical data related to springs and estimation of the exerted forces.

The 3D CAD detail of the spring system can be seen in *figure A.1.5*. From the picture it is visible the parallel configuration of the two-disc springs used in die releasing after sintering. The reason of this choice has to be associated to the higher-elastic reaction associated to an increased stiffness of this kind of configuration, *figure A.1.6*. In this case, if compared to a single spring configuration, this configuration made of two springs generates a double force. Using a disc spring characterised by a larger diameter it has not been possible due to geometrical size constraints. *Figure A.1.7 (a) & (b)* shows the main geometrical parameters related to the springs. The concept is developed considering the correct forces required in order to release the system. The forces exerted by springs result sufficient to the die releasing and part ejecting, *table A.1.2*. It is worth underlining that the compression spring, *figure A.1.4 (b)*, is not so critical as the system is supposed to generate a clearance between the die and the gear after releasing, see *paragraph 4.4.2*. This spring has only to move up the part after being sintered.

$F_{\text{gear}}$	1034	<i>N</i>
$F_{\text{die punch}}$	161536	<i>N</i>
$p_{\text{gear}}$	172	<i>MPa</i>
$p_{\text{die punch}}$	4615	<i>MPa</i>

Table A.1.3: Summary table of the required forces and pressure.

After forces calculation, the total pressure on the punches has been estimated. *Table A.1.3* shows the forces applied respectively on the inner punch for the powder compaction, and on the die punch to the conical fit. Pressures have been estimated relating to the areas of the compacting surfaces of the two punches. When the punches exert pressure on the system, they have to overcome the elastic reaction of the springs. The estimated pressures represent the addition of the compaction and fit components. As it can be seen from the estimated die punch pressure, the value has been shown to be very high. Due to this consideration, it has been preferred to reduce the pressure and avoid springs, which are the main pressure components. Additionally, it has not been possible any considerations regarding fatigue failure related to the springs. So, the model described in *chapter 5* has been developed.

**APPENDIX 2:**

**Datasheets**



Production of Aluminium, Bronze and Copper  
in Powder, Paste and Granules

## TECHNICAL DATA SHEET

**revision n°:** 01 (date 1/06/2010), supersedes n°00 (date 10/01/2008)

**Ident. N°:**

TDS\_S\_AGR\_5945\_v01

**PRODUCT TYPE:** ALUMINIUM GRANULES

**PRODUCT NAME:** 5945

**PRODUCT DESCRIPTION:** Irregular Aluminium Granules

Inspection Criteria	Unit	Lower lim. Value	Upper lim. Value	Test method
Purity of metal	%	99,7	-	
Fineness	µm	42	250	LCI.006.0
Apparent density	g/cm <sup>3</sup>	0,90	1,4	ASTM B212-99

For more information and samples, please contact:

AVL METAL POWDERS nv, Elleboogstraat 7, B-8500 Kortrijk, Belgium, Europe

T +32 (0) 56 22 00 21 - F +32 (0) 56 22 64 14

e-mail: [sales@avlmetalpowders.com](mailto:sales@avlmetalpowders.com)

website: <http://www.avlmetalpowders.com>

VAT BE 0405.375.371 - HR 7 Kortrijk



All data on this technical data sheet are based upon tests and knowledge which our company believes to be currently reliable. Foregoing data is no legal guarantee for specific properties of the product, nor for their suitability for a particular application or process, the liability lies with the buyer. AVL Metal Powders has the right at any time to alter any product data as a result of technical improvements or changes in the manufacturing process.

depart. Name: QC, Stefaan De Forche

**Watlow**

12001 Lackland Rd.

St. Louis, MO 63146 US

**Phone:** 800-893-4022 • **Fax:** 314-878-6814**Email:** inquiry@watlow.com • **Website:** http://www.watlow.com**Code No. MB1A1AN4, Mineral Insulated (MI) Nozzle Heaters****Mineral Insulated (MI) Nozzle Heaters****Performance Capabilities**

- Heater operating temperatures to 1400°F (760°C)
- Watt densities to 230 W/in<sup>2</sup> (35.6 W/cm<sup>2</sup>) available on small diameter nozzle nozzles
- Maximum voltage to 240V

· [SPECIFICATIONS](#) · [OPTIONS](#) · [FEATURES AND BENEFITS](#) · [TYPICAL APPLICATIONS](#)

**SPECIFICATIONS**

Heater Style	Nozzle Heater
I.D.	1 in 25.0 mm
Width	1 in 25 mm
Construction	1 pc
Voltage	240 V
Watts	200 W
Watt Density	122 W/in <sup>2</sup> 18.9 W/cm <sup>2</sup>
Approx. Net Weight	0.1 lb 0.05 kg
Delivery	Stock
Shipping Note	• Stock delivery, same day

**OPTIONS**

Termination	MIN-B-01, Type B Terminal MIN-C, Type C Terminal MIN-E, Type E Terminal MIN-F, Type F Terminal MIN-H, Type H Terminal
Thermocouples Options	Type HDSR, Heavy Duty Strain Relief Type J, Type J Thermocouple Type K, Type K Thermocouple
Wire Options	MIN-LW, Lead Wire MIN-GW, Ground Wire
Ceramic Terminal Cover	MIN-CTC, Ceramic Terminal Cover for Mineral Insulated (MI) Nozzle Heaters
Clamping Options	T-WBN, Tig-Welded Each Nuts L-PT-WBN, Low-Profile Tig-Welded Each Nuts L-PCB, Low-Profile Clamp Bars

## FEATURES AND BENEFITS

### Operating temperatures to 1400°F (760°C)

- Melts resins such as PEEK®, Teflon®, Ultem® and Zytel® safely

### Higher watt densities

- Contributes to faster heat-up and throughput for increased productivity

### High thermal conductivity of MI and low mass construction

- Gives an almost instant response to temperature control
- Eliminates thermal lag and temperature overshoot

### Stainless steel cover and side fold design

- Resists contamination by overflow of plastic or other free-flowing materials

### Permanently attached clamp bars

- Eliminates cumbersome clamping straps, making installation easier

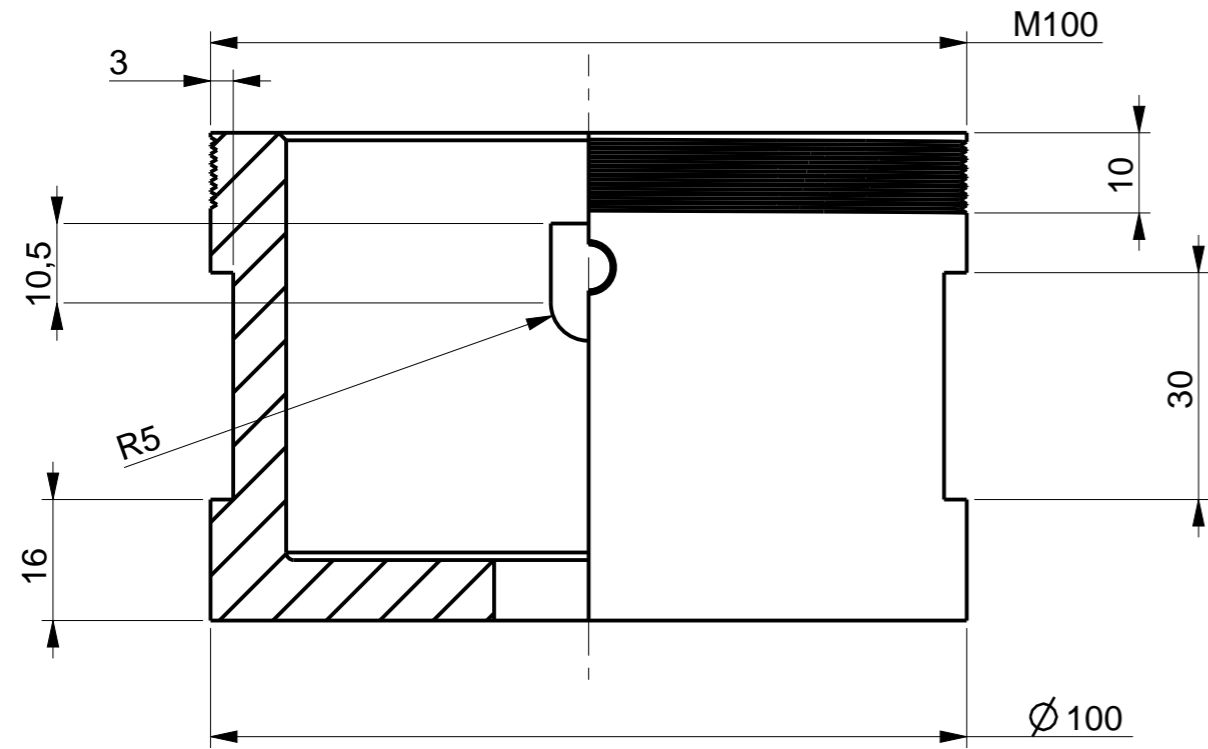
## TYPICAL APPLICATIONS

- Extruders
- Blown film dies
- Injection molding machines
- Other cylinder heating applications

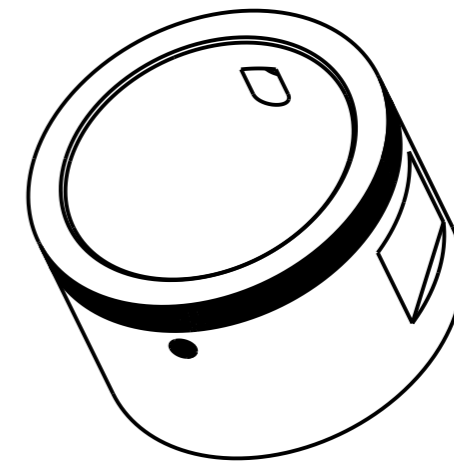
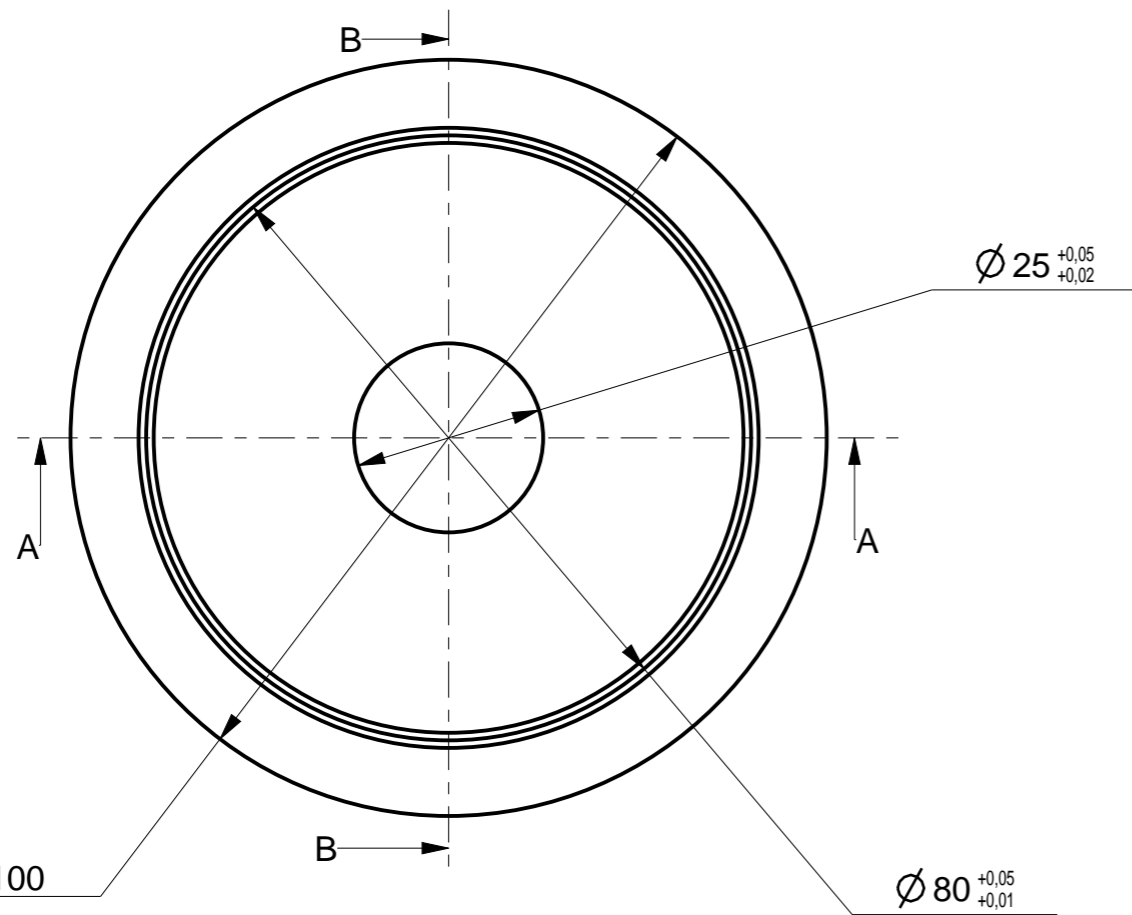
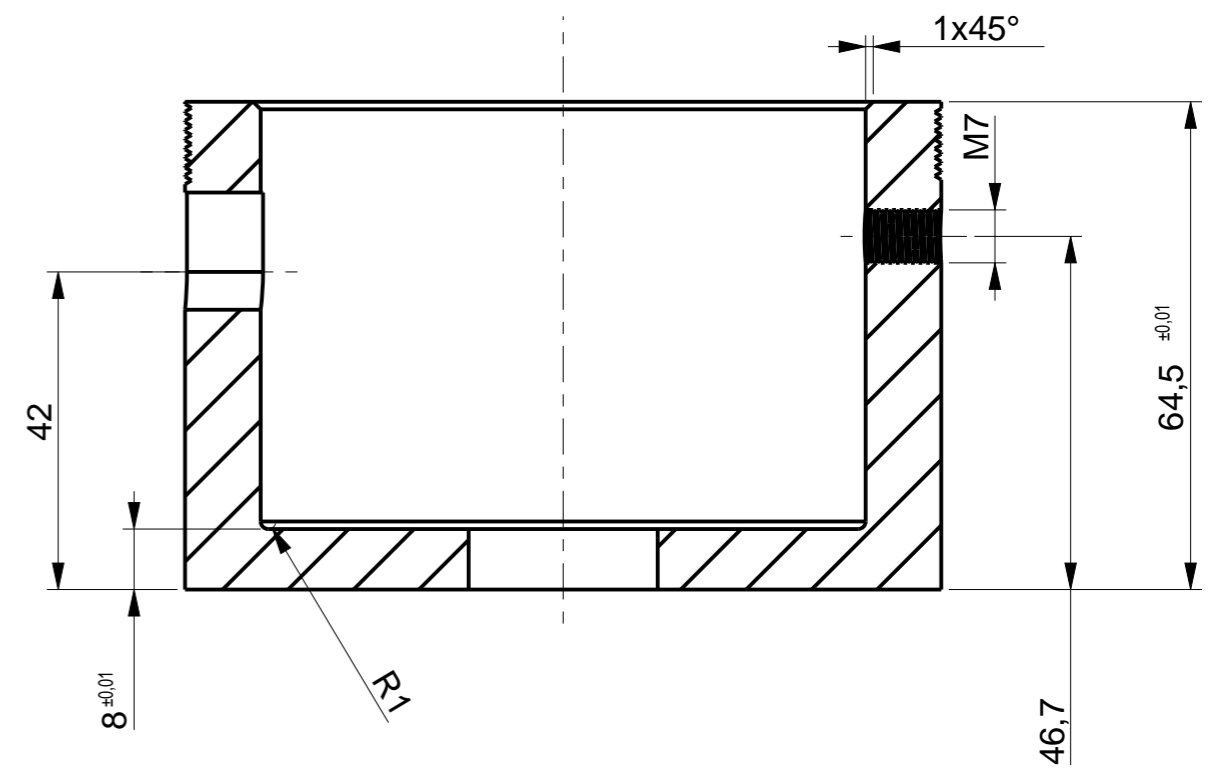
# **APPENDIX 3:**

# **Technical Drawings**


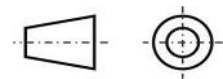
SECTION A-A



SECTION B-B

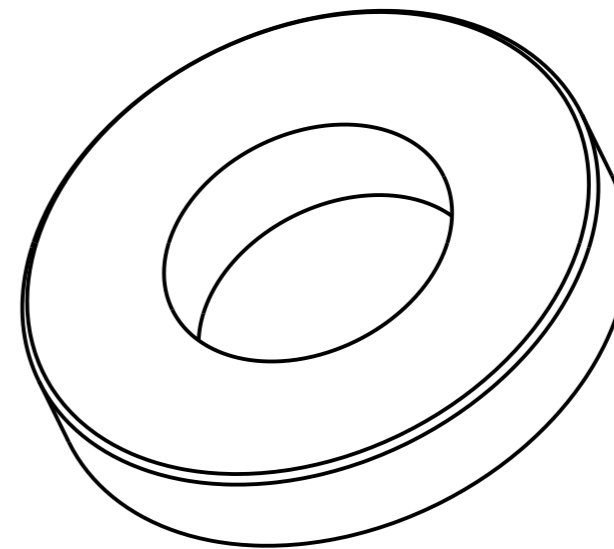
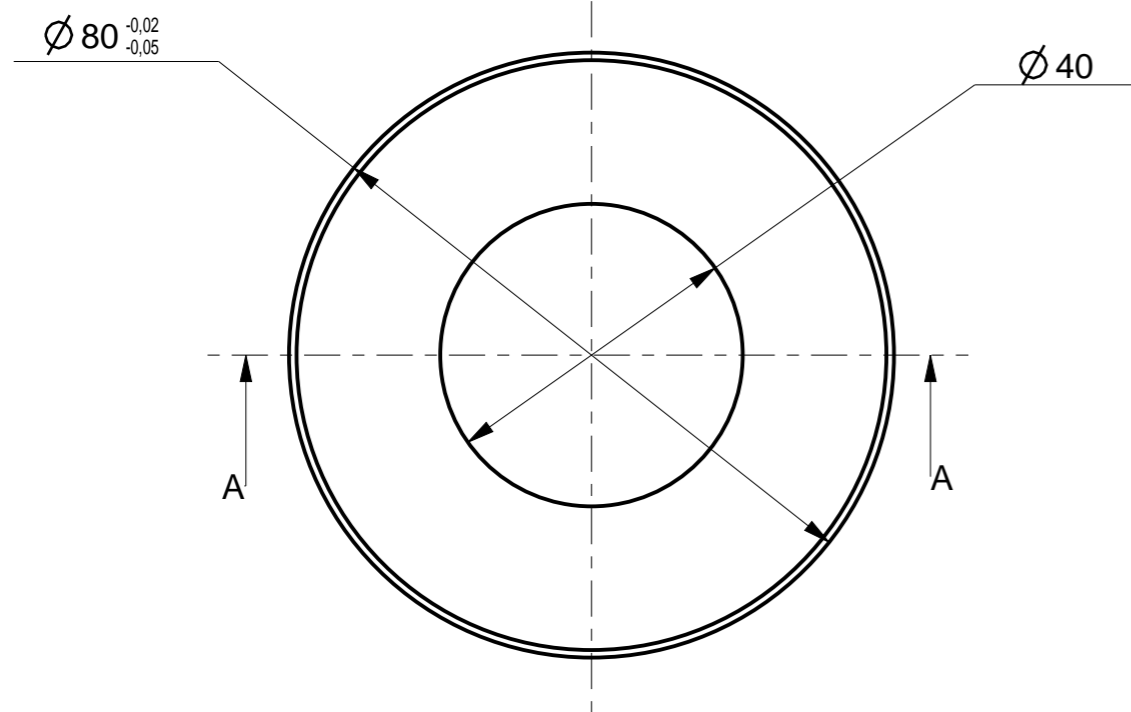
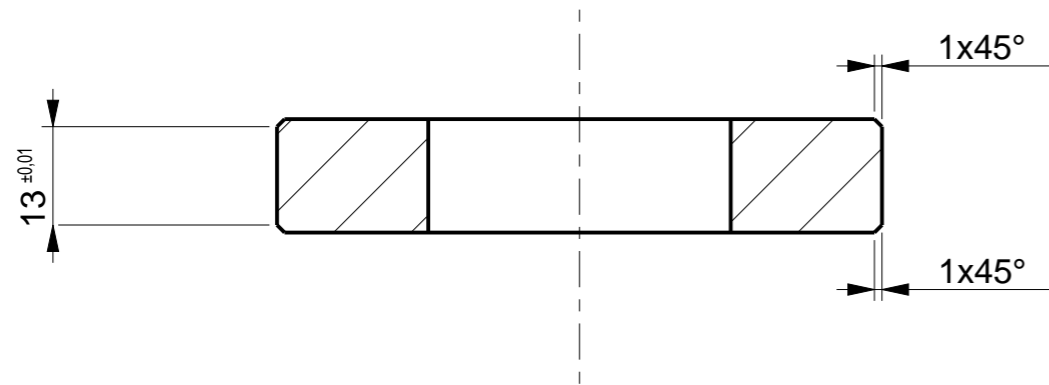



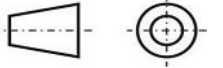
SCALE 0,500

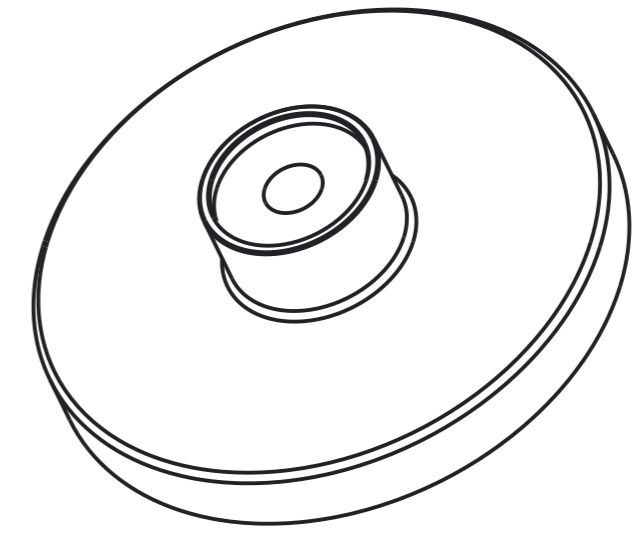
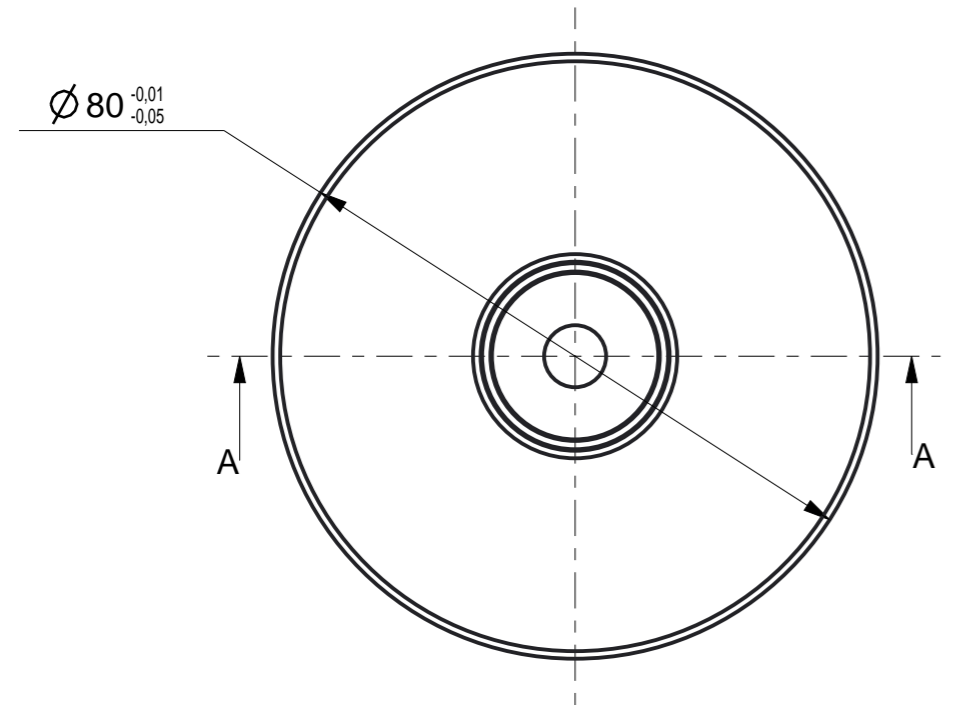
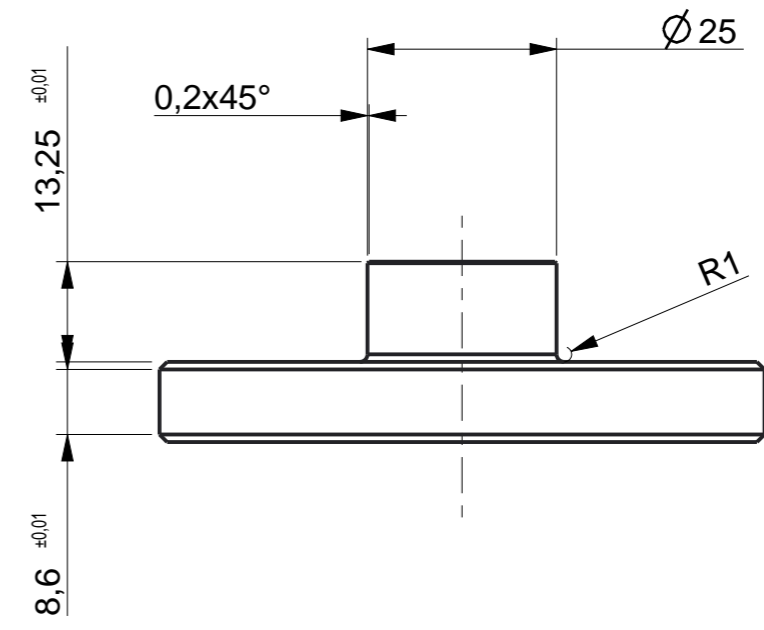
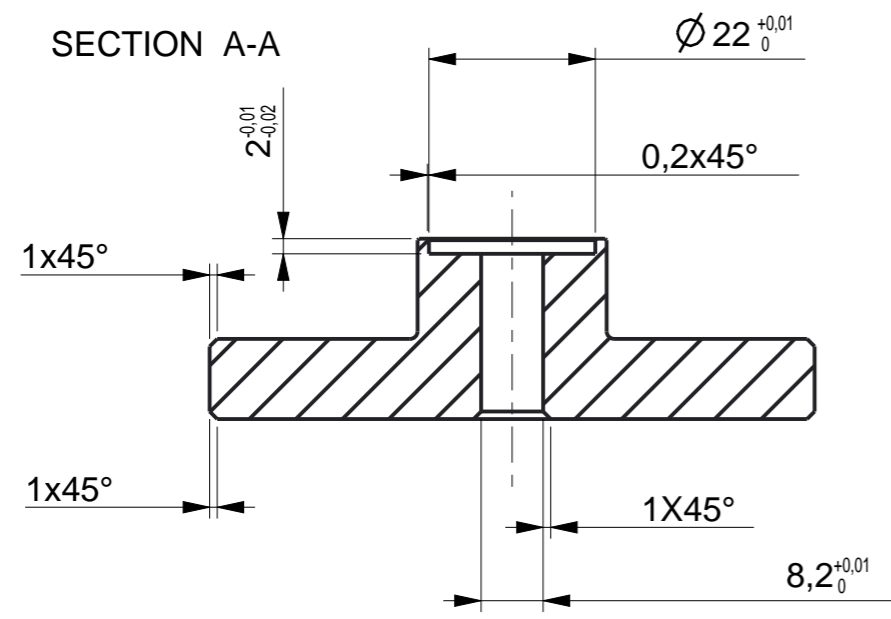
<b>IPU Process Technology</b> Produktionstorvet, Building 425, 2nd floor DK-2800 Kgs. Lyngby Phone: 45 25 46 00, fax 45 88 25 25 www.ipu.dk			Drawing by: EC	Date: Dec-01-15	Revision date:
Project: Micro-gear die system			Name: Bag		
Project number:		Tolerance: ± 0.1 if not specified	Format: A3	Scale: 1,000	
Material: A514 steel		Sheet: 1/12	Drawing number:		




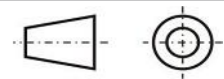
SECTION A-A



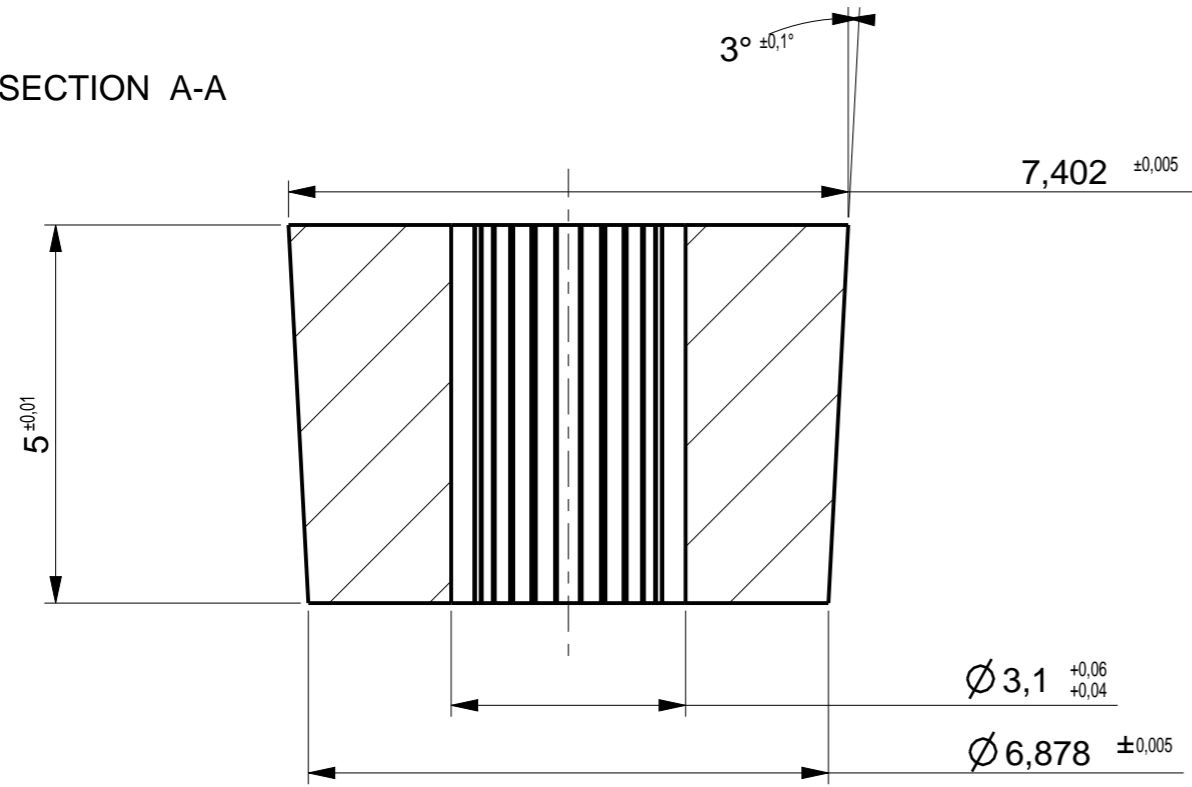
<b>IPU Process Technology</b> Produktionstorvet, Building 425, 2nd floor DK-2800 Kgs. Lyngby Phone: 45 25 46 00, fax 45 88 25 25 www.ipu.dk			Drawing by: EC	Date: Dec-01-15	Revision date:
Project: Micro-gear die system			Name: Bottom ring		
Project number:		Tolerance: $\pm 0.1$ if not specified	Format: A3	Scale: 1,000	
Material: A514 steel		Sheet: 2/12	Drawing number:		



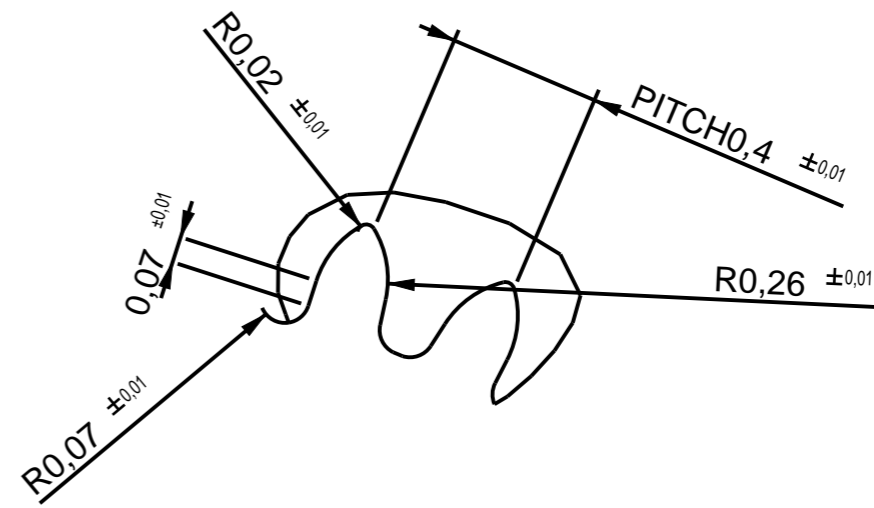
Hardened to 55 HRC ±1

<b>IPU Process Technology</b> Produktionstorvet, Building 425, 2nd floor DK-2800 Kgs. Lyngby Phone: 45 25 46 00, fax 45 88 25 25 www.ipu.dk			Drawing by: EC	Date: Dec-01-15	Revision date:
Project: Micro-gear die system			Name: Die base		
Project number:		Tolerance: ± 0.1 if not specified	Format: A3	Scale: 1,000	
		Material: H13 hot work steel	Sheet: 3/12	Drawing number:	

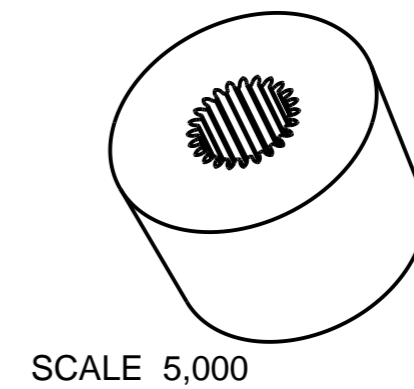
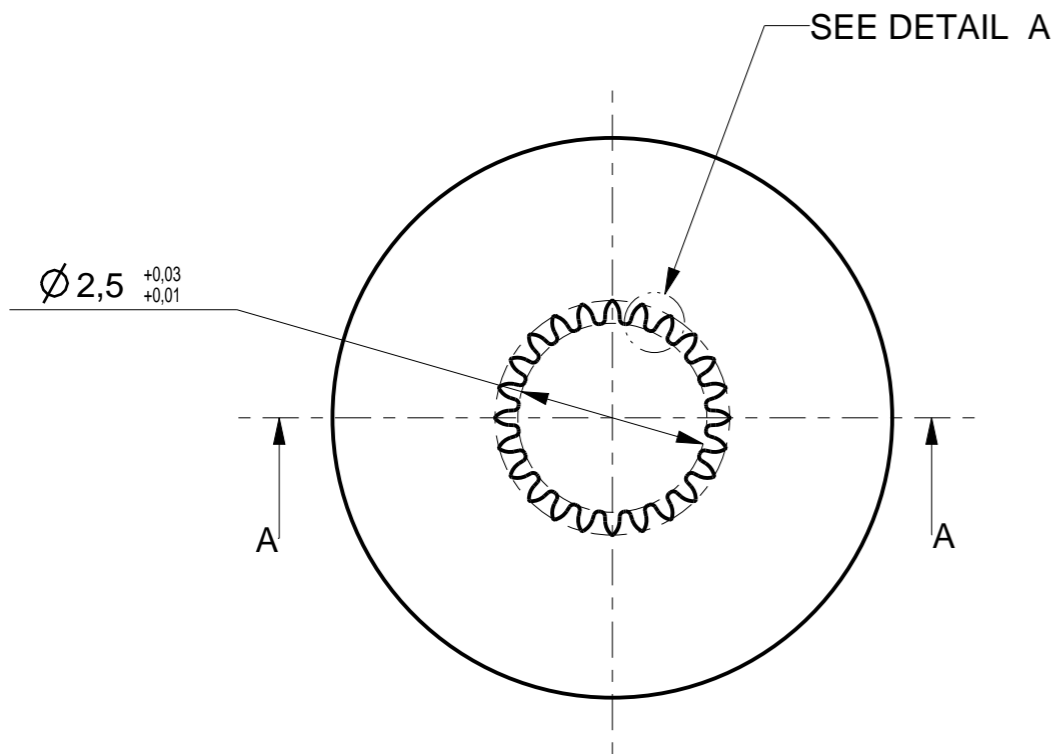
SECTION A-A




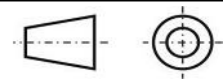
GEAR TEETH x24

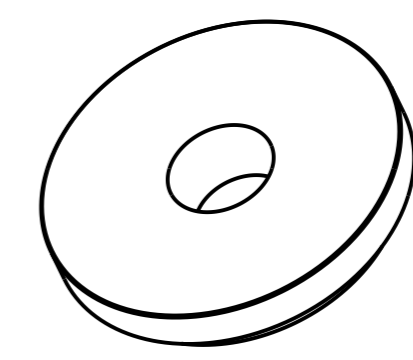
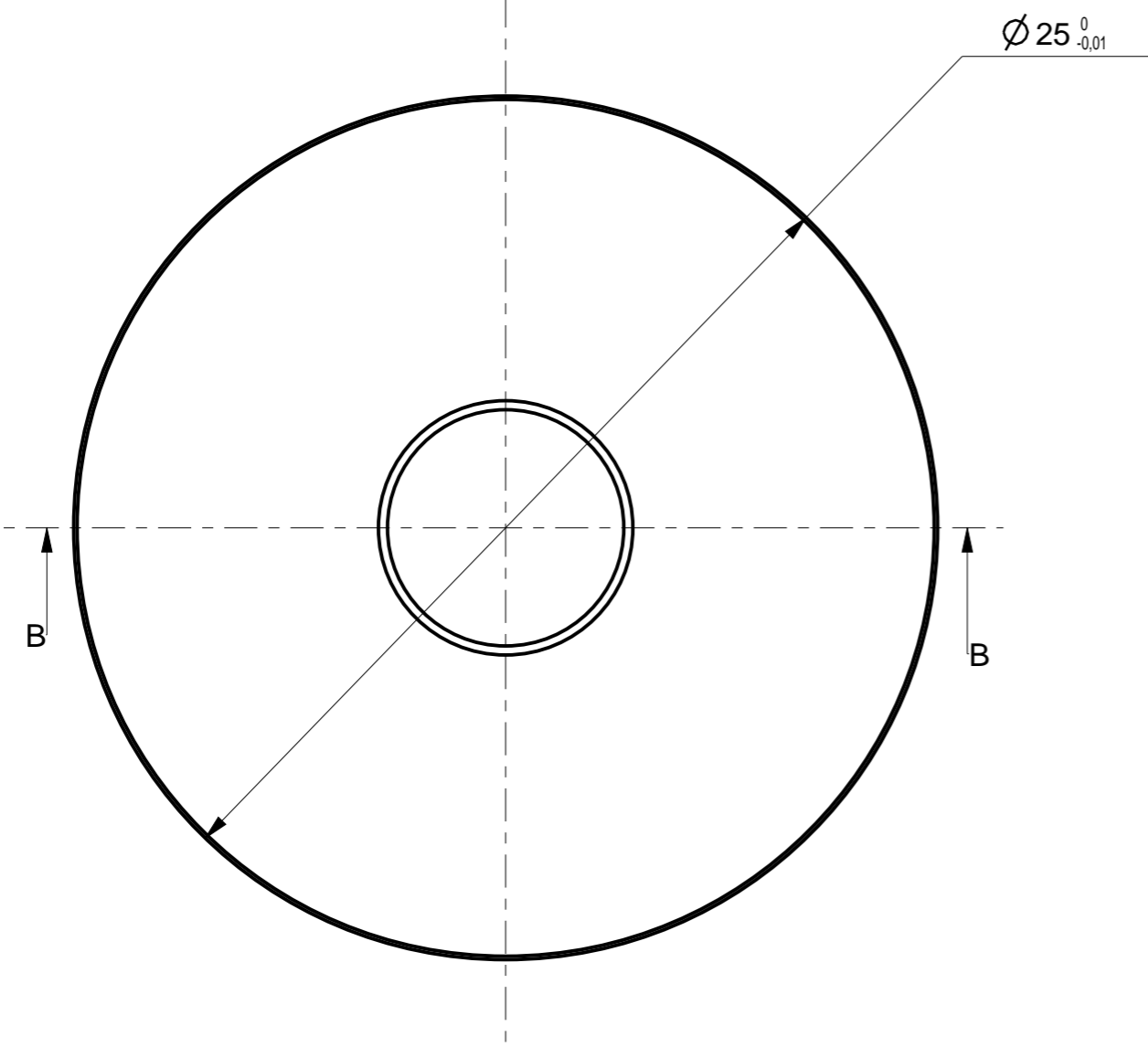
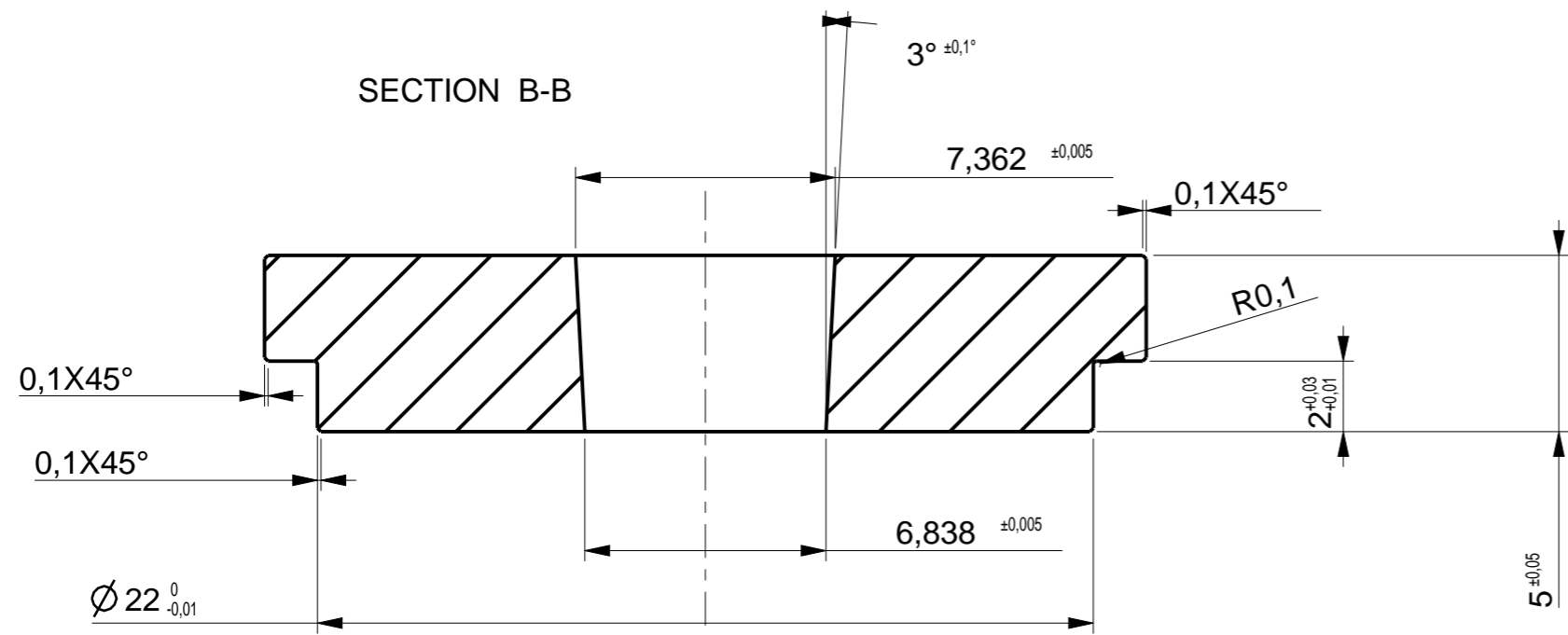


DETAIL A  
SCALE 50,000


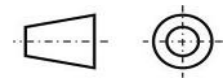


SCALE 5,000

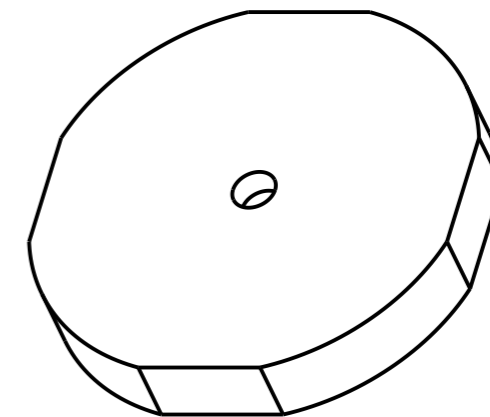
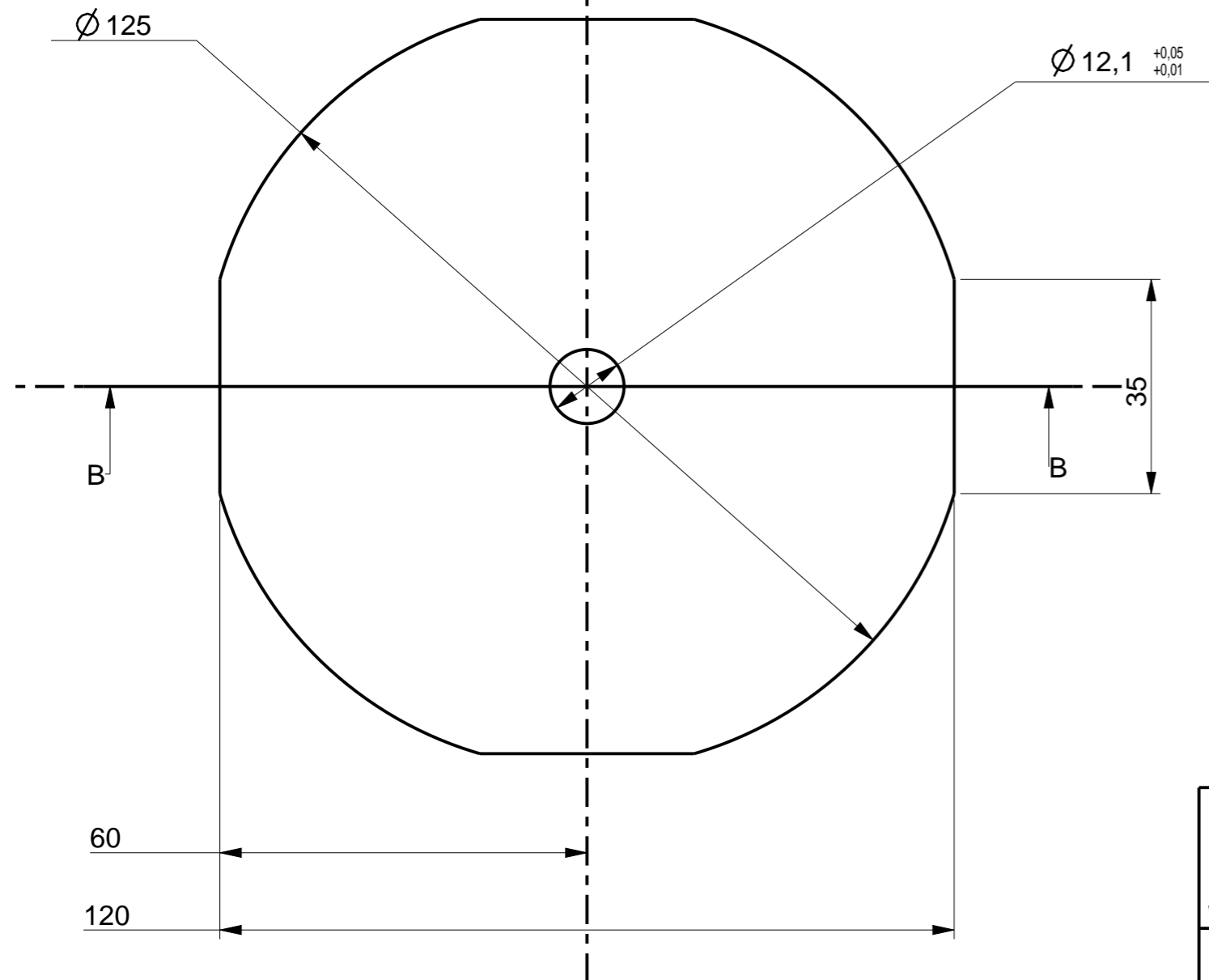
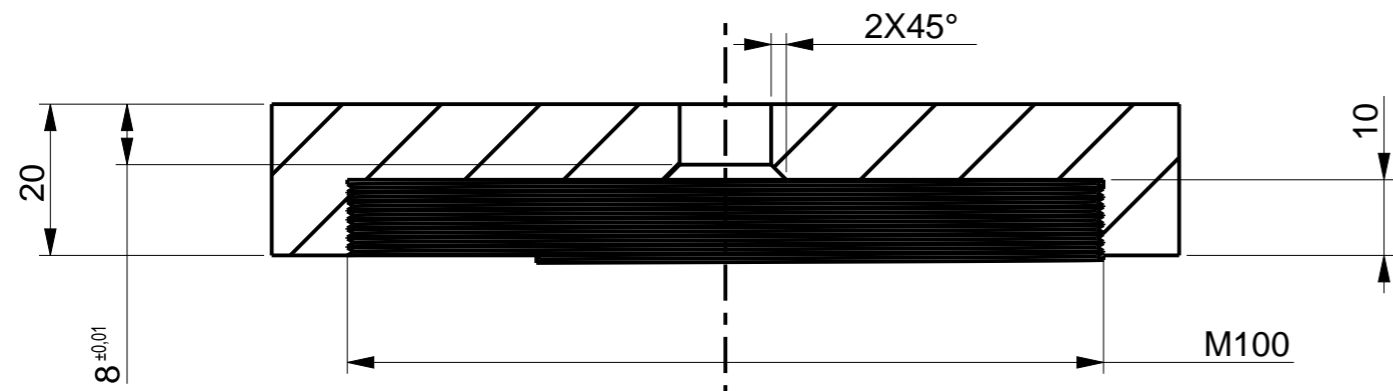
<b>IPU Process Technology</b> Produktionstorvet, Building 425, 2nd floor DK-2800 Kgs. Lyngby Phone: 45 25 46 00, fax 45 88 25 25 www.ipu.dk			Drawing by: EC	Date: Dec-01-15	Revision date:
Project: Micro-gear die system			Name: Conical die		
Project number:		Tolerance: ± 0.1 if not specified	Format: A3	Scale: 10,000	
Material: Bohler W360		Sheet: 4/12	Drawing number:		




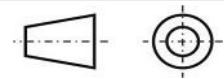
SCALE 2,000

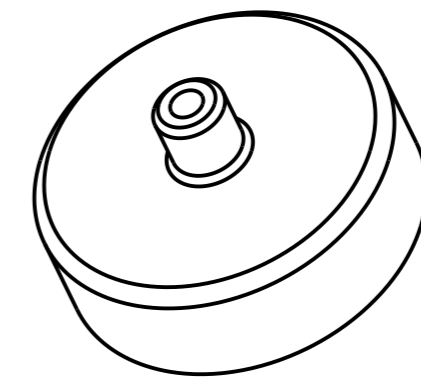
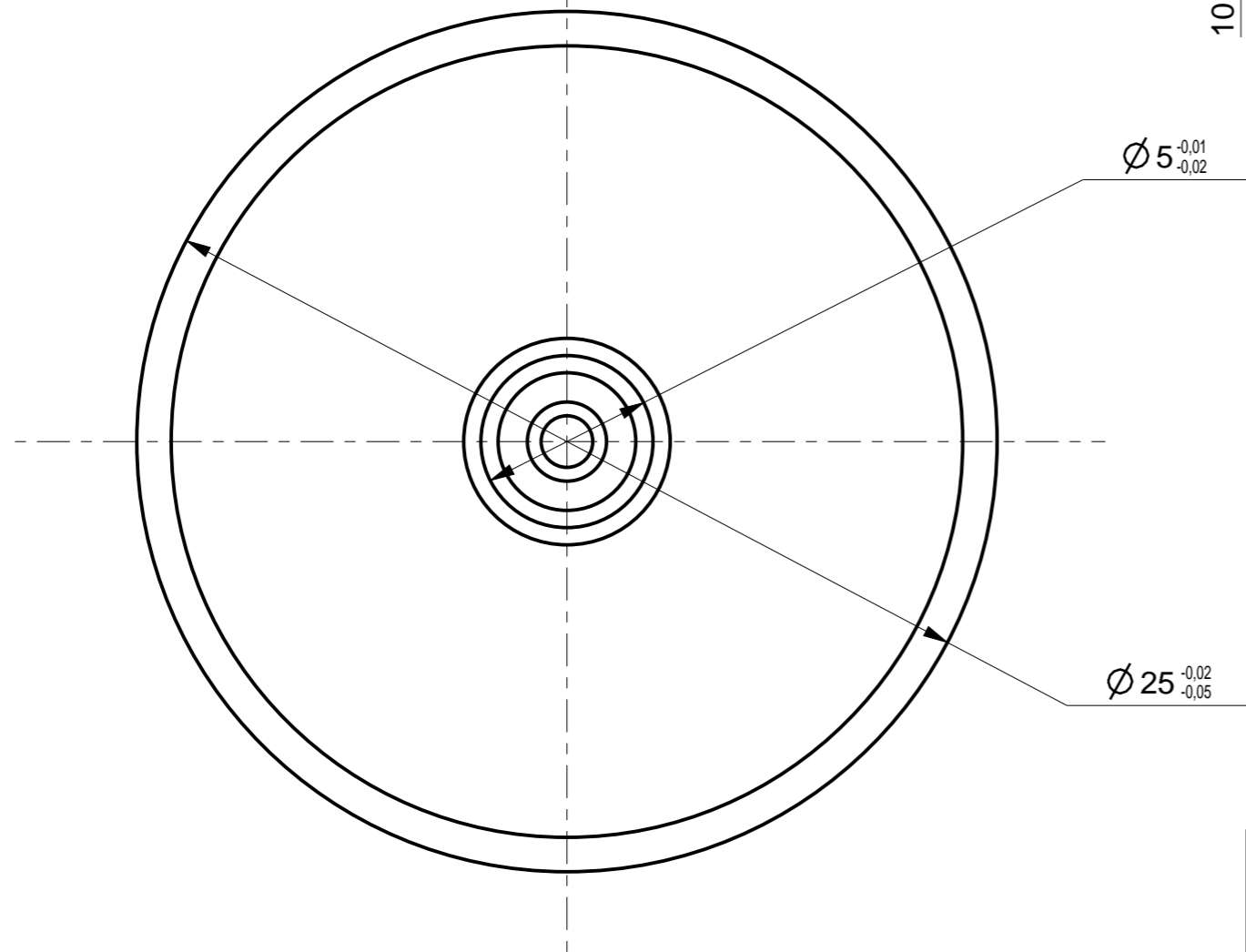
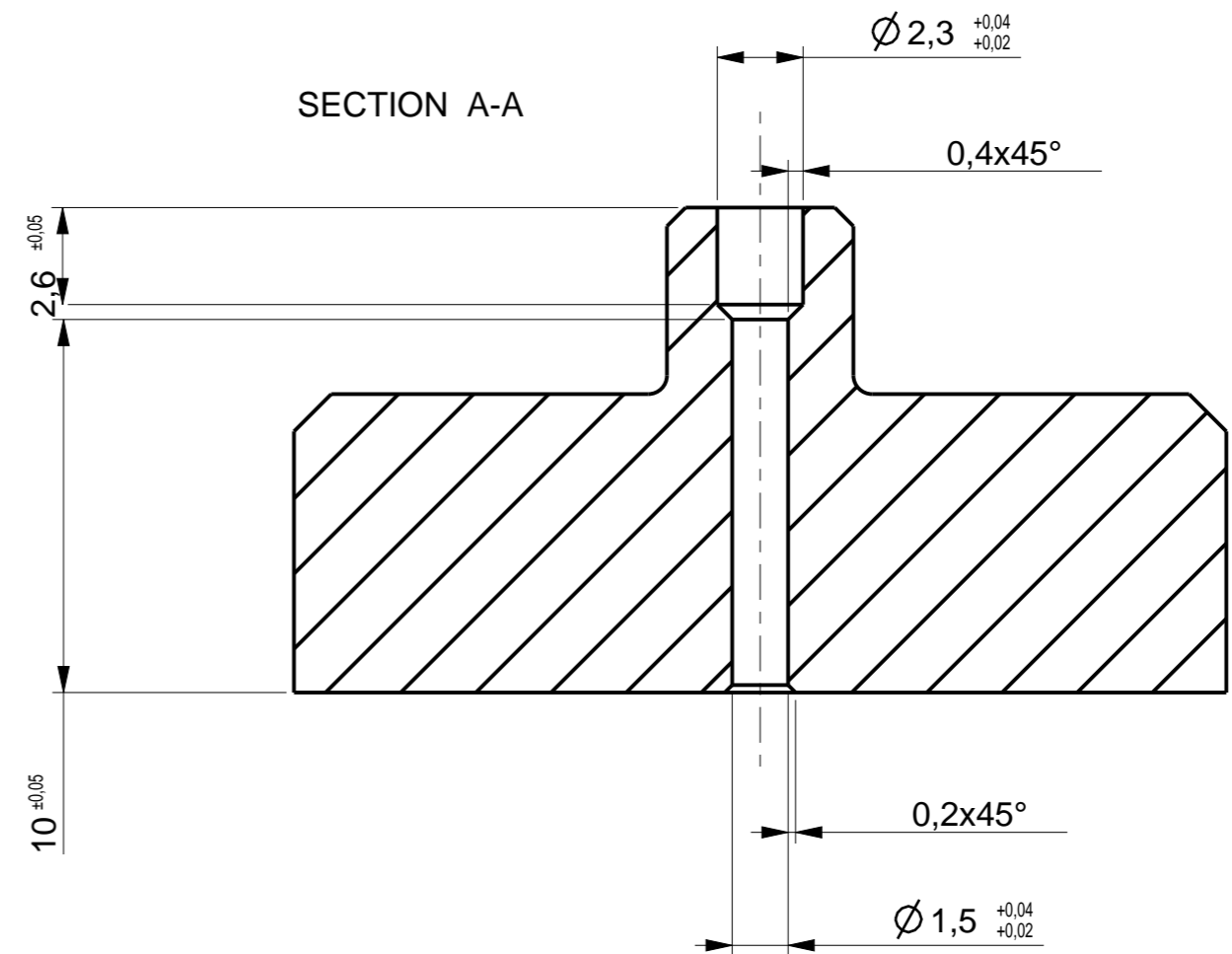
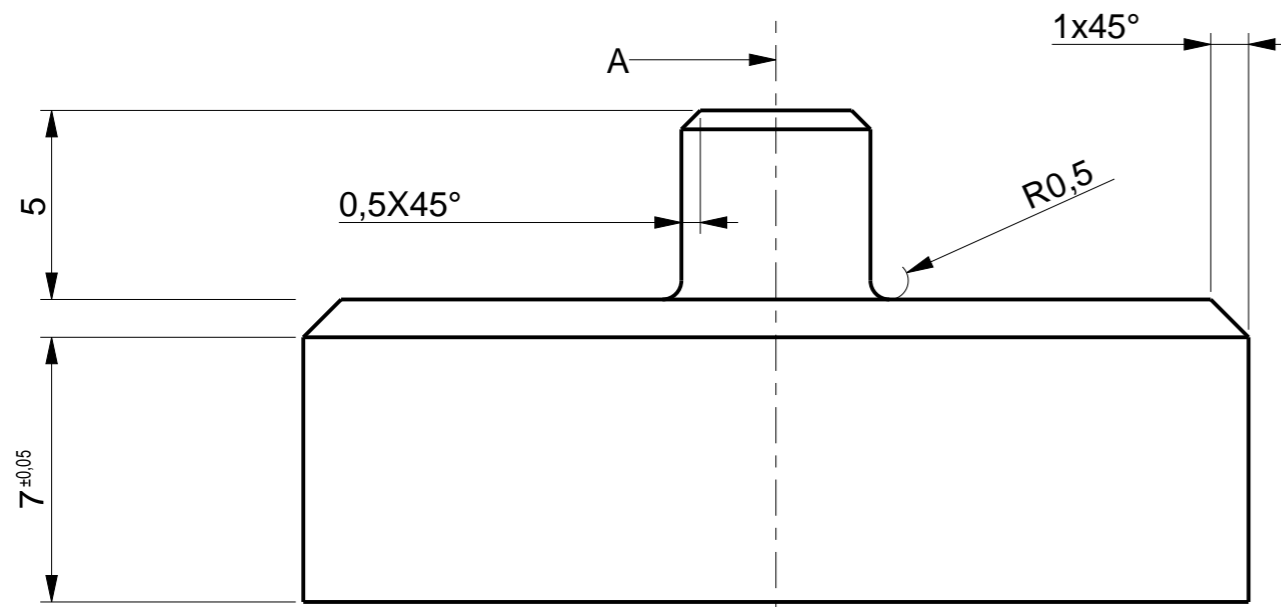
<b>IPU Process Technology</b> Produktionstorvet, Building 425, 2nd floor DK-2800 Kgs. Lyngby Phone: 45 25 46 00, fax 45 88 25 25 www.ipu.dk			Drawing by: EC	Date: Dec-01-15	Revision date:
Project: Micro-gear die system			Name: Conical compression ring		
Project number:		Tolerance: $\pm 0.1$ if not specified	Format: A3	Scale: 5,000	
Material: Bohler W360		Sheet: 5/12	Drawing number:		

SECTION B-B




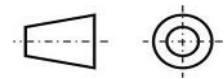
SCALE 0,500

<b>IPU Process Technology</b> Produktionstorvet, Building 425, 2nd floor DK-2800 Kgs. Lyngby Phone: 45 25 46 00, fax 45 88 25 25 www.ipu.dk			Drawing by: EC	Date: Dec-01-15	Revision date:
Project: Micro-gear die system			Name: Screw cover		
Project number:		Tolerance: ± 0.1 if not specified	Format: A3	Scale: 1,000	
Material: A514 steel		Sheet: 6/12	Drawing number:		

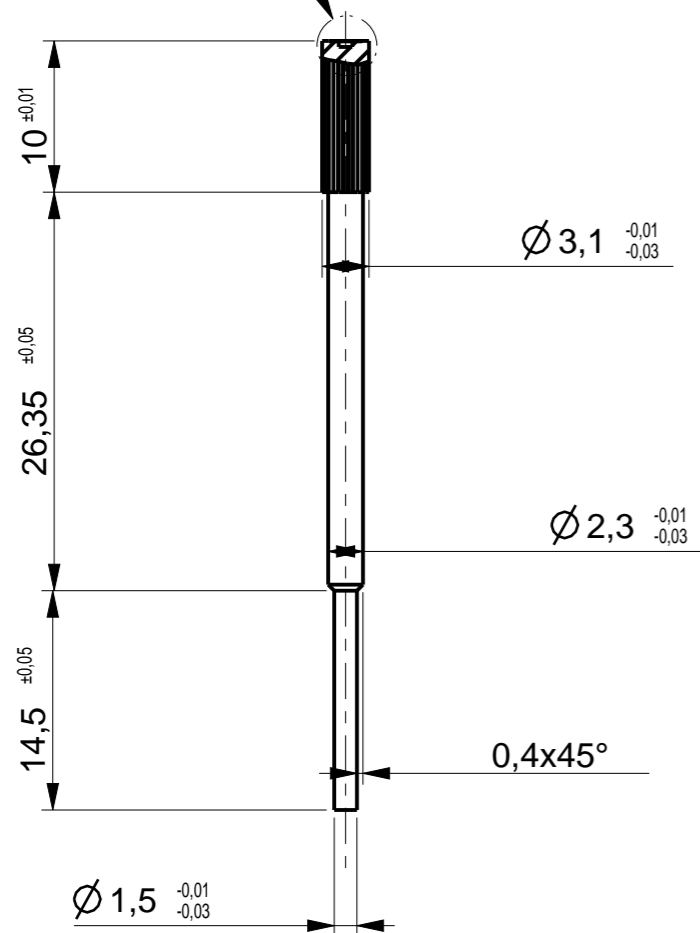


SCALE 2,000

Hardened to 55 HRC ±1

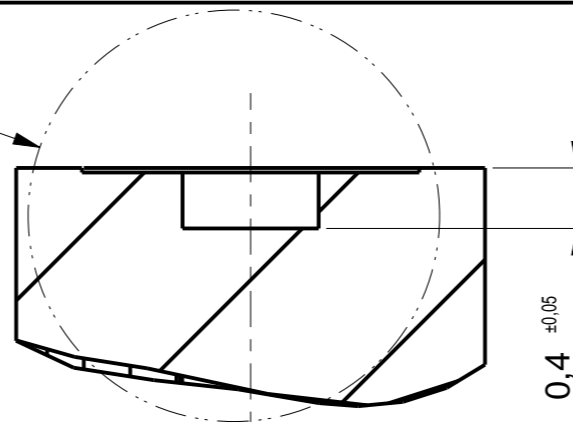
<b>IPU Process Technology</b> Produktionstorvet, Building 425, 2nd floor DK-2800 Kgs. Lyngby Phone: 45 25 46 00, fax 45 88 25 25 www.ipu.dk			Drawing by: EC	Date: Dec-01-15	Revision date:
Project: Micro-gear die system			Name: Bottom inner punch n.2		
Project number:		Tolerance: ± 0.1 if not specified	Format: A3	Scale: 5,000	
		Material: H13 hot work steel	Sheet: 7/12	Drawing number:	

SEE DETAIL C

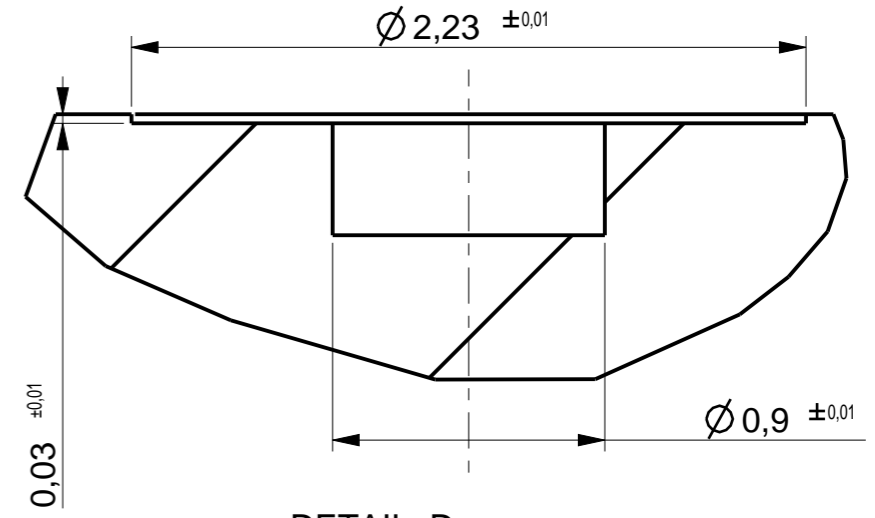


SEE DETAIL D

SECTION A-A

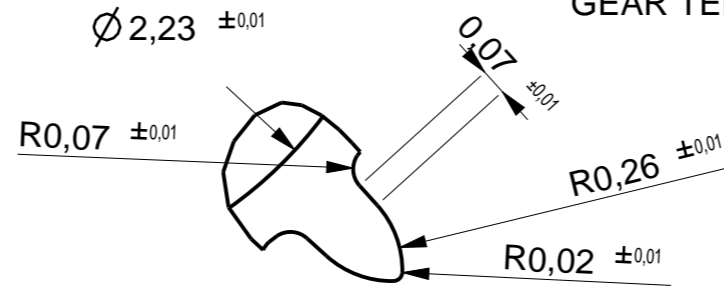


DETAIL C  
SCALE 20,000

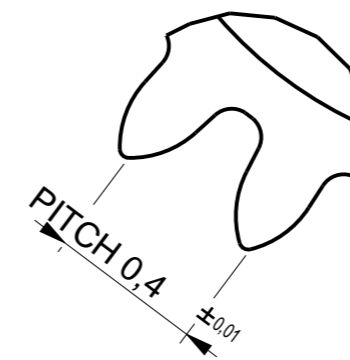


DETAIL D  
SCALE 40,000

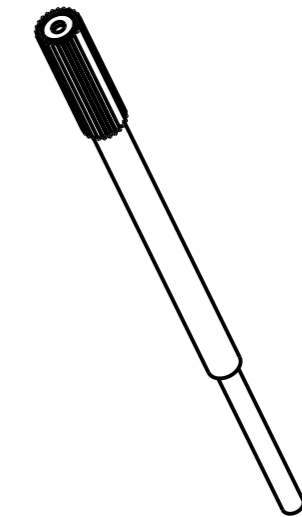
GEAR TEETH x24



DETAIL A  
SCALE 50,000




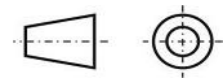
DETAIL B  
SCALE 50,000

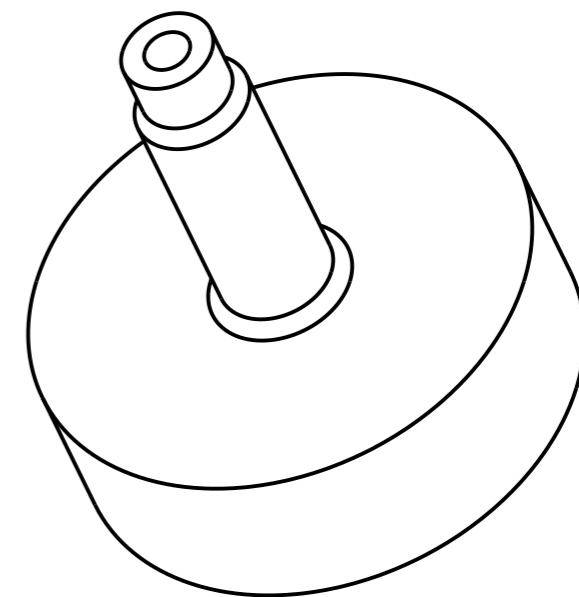
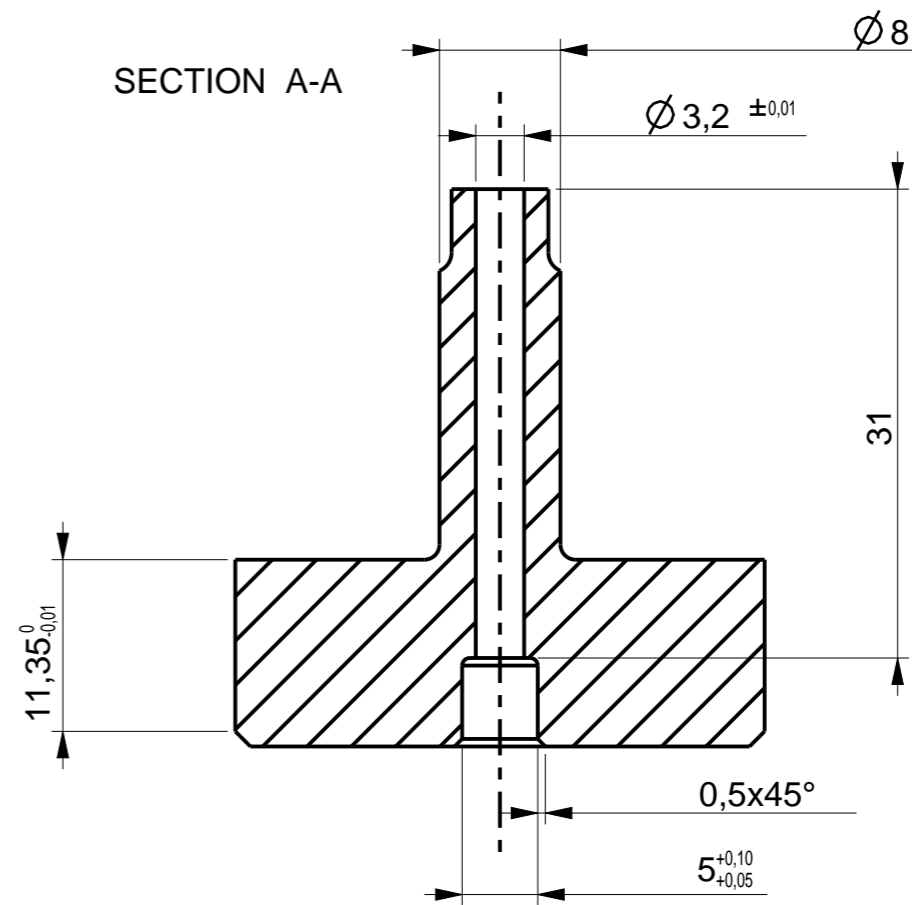
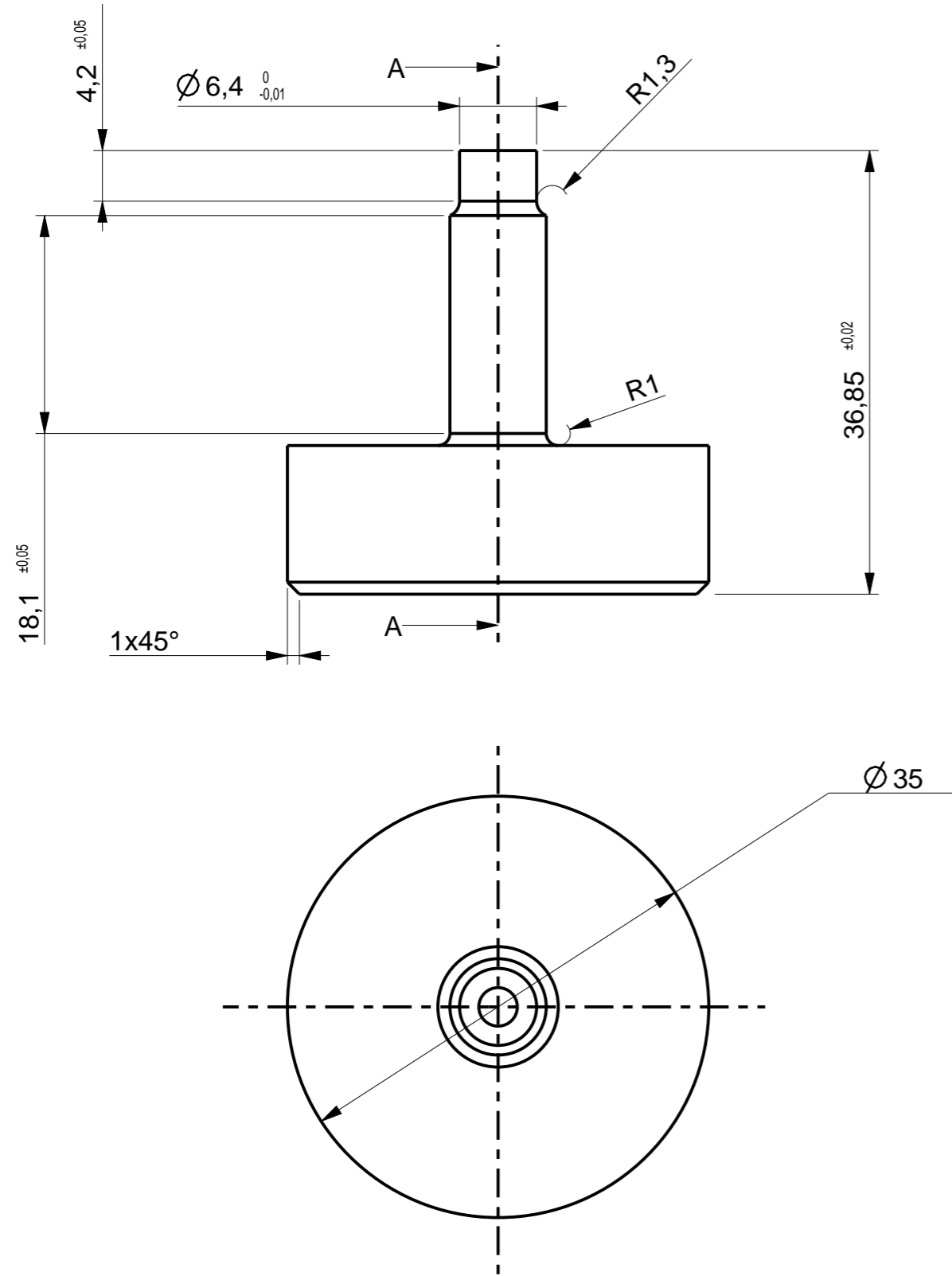


Ø2.5 ±0.01/-0.03


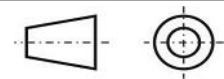
SEE DETAIL A

SEE DETAIL B

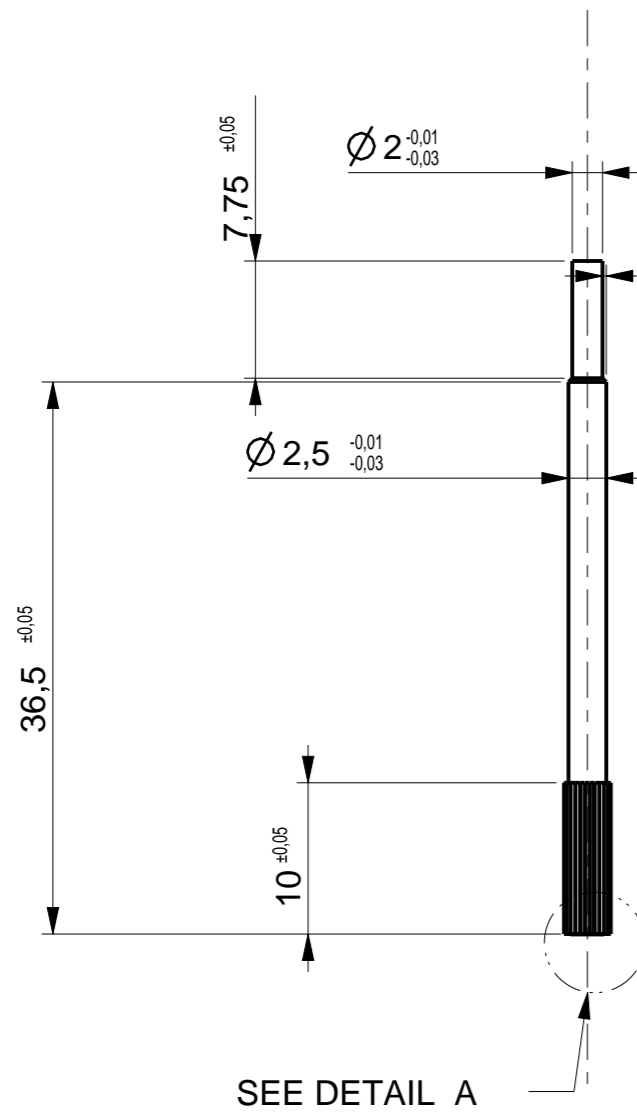
<b>IPU Process Technology</b> Produktionstorvet, Building 425, 2nd floor DK-2800 Kgs. Lyngby Phone: 45 25 46 00, fax 45 88 25 25 www.ipu.dk			Drawing by: EC	Date: Dec-01-15	Revision date:
Project: Micro-gear die system			Name: Bottom inner punch n.1		
Project number:		Tolerance: ± 0.1 if not specified	Format: A3	Scale: 2,000	
Material: Tungsten carbide		Sheet: 8/12	Drawing number:		



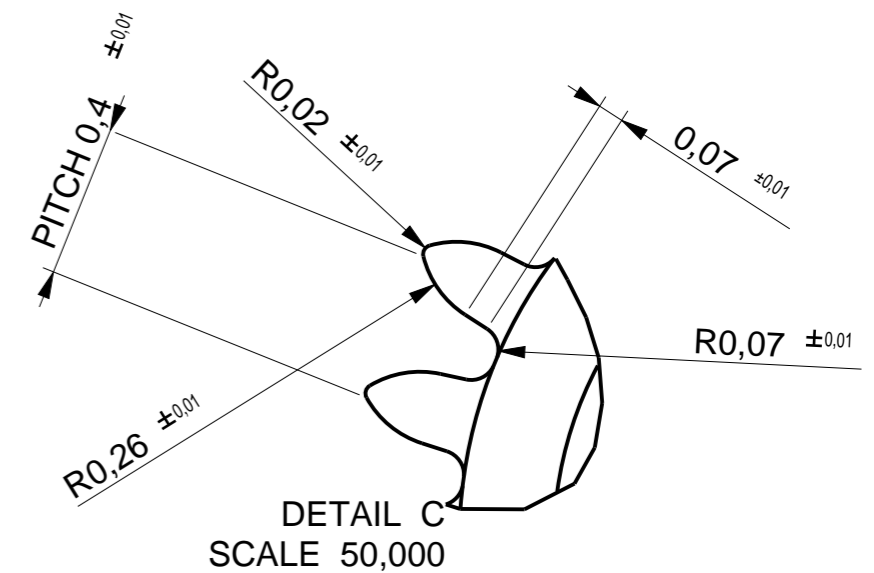
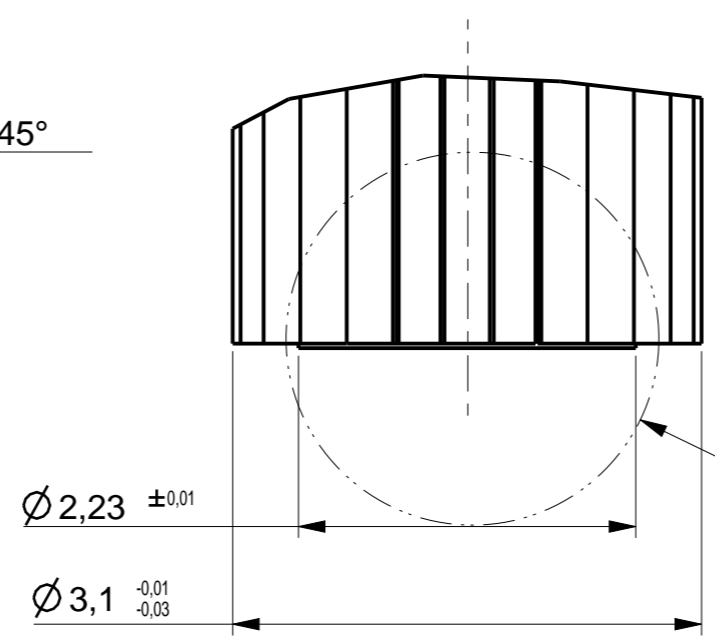
Hardened to 55 HRC ±1

<b>IPU Process Technology</b> Produktionstorvet, Building 425, 2nd floor DK-2800 Kgs. Lyngby Phone: 45 25 46 00, fax 45 88 25 25 www.ipu.dk			Drawing by: EC	Date: Dec-01-15	Revision date:
Project: Micro-gear die system			Name: Bottom die punch		
Project number:		Tolerance: ± 0.1 if not specified	Format: A3	Scale: 2,000	
		Material: H13 hot work steel	Sheet: 9/12	Drawing number:	



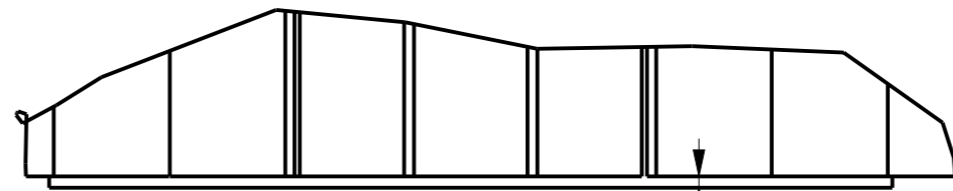


DETAIL A  
SCALE 20,000



DETAIL C  
SCALE 50,000

GEAR TEETH X24

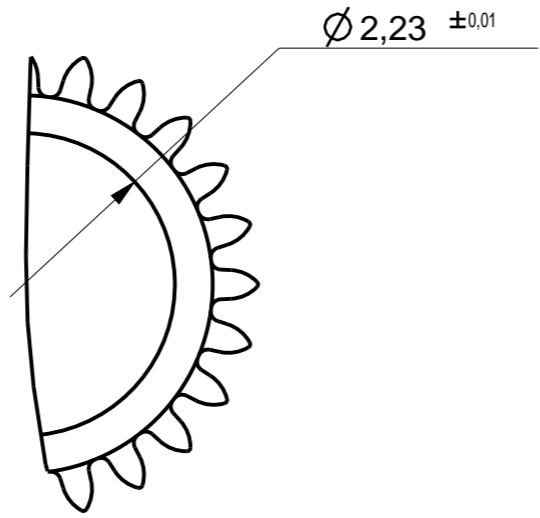


DETAIL D  
SCALE 50,000

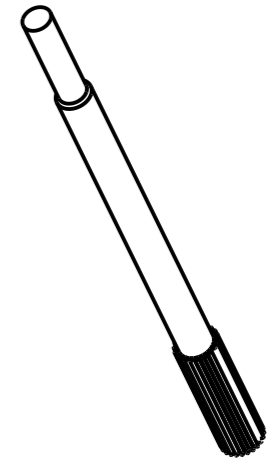
SEE DETAIL A


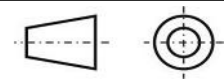
SEE DETAIL C

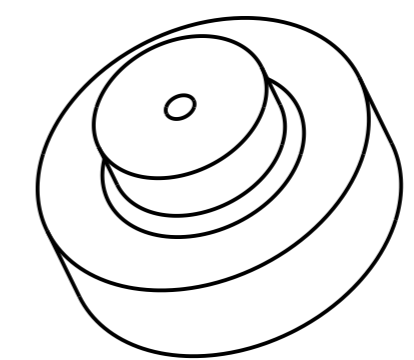
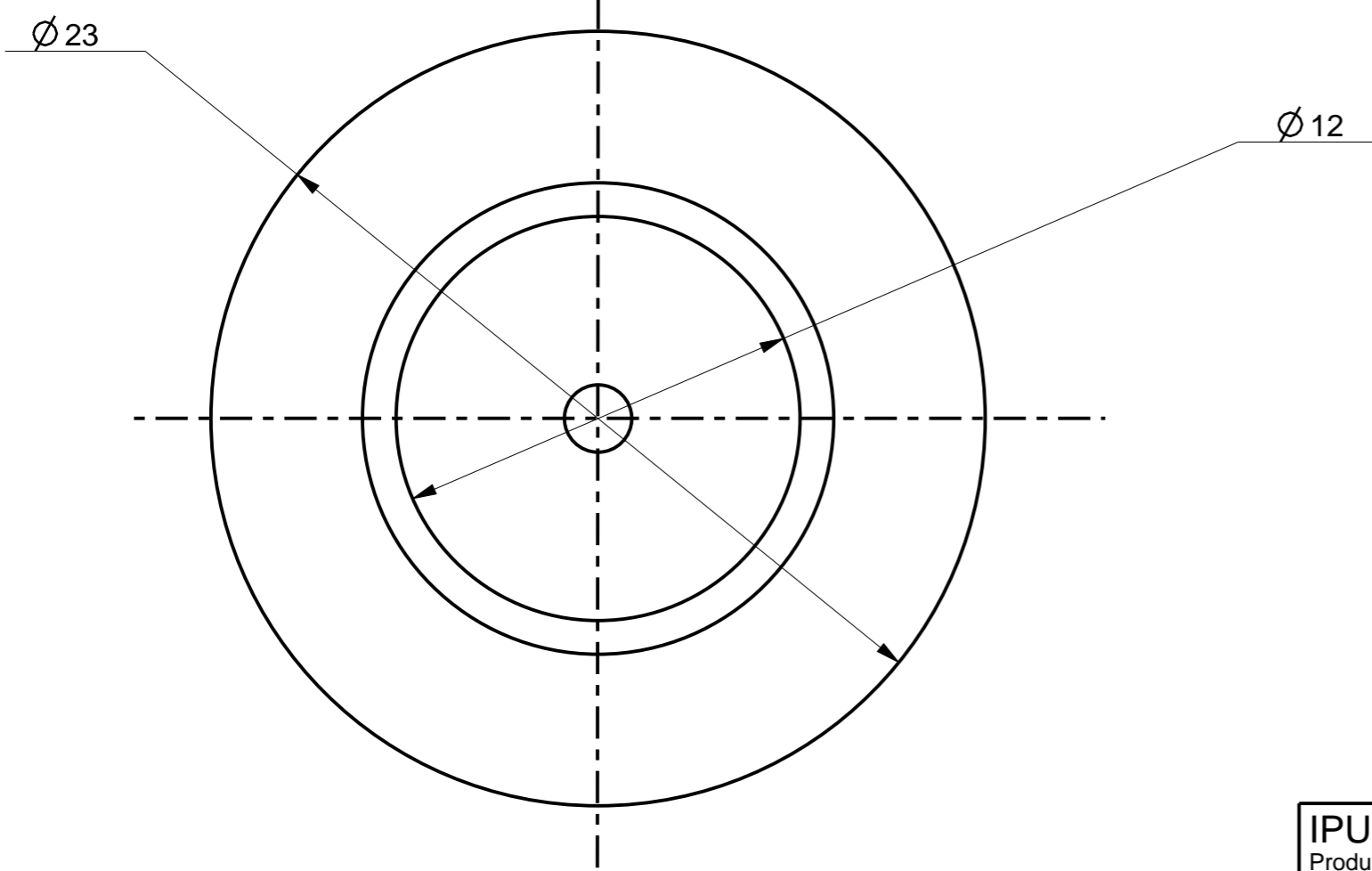
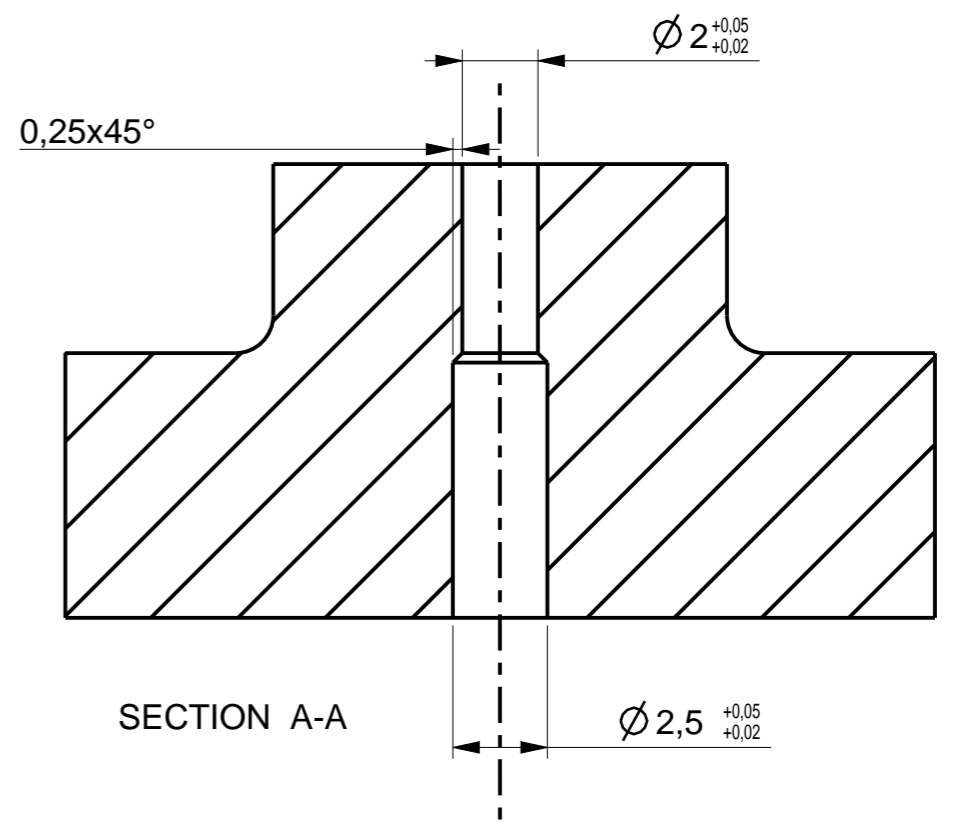
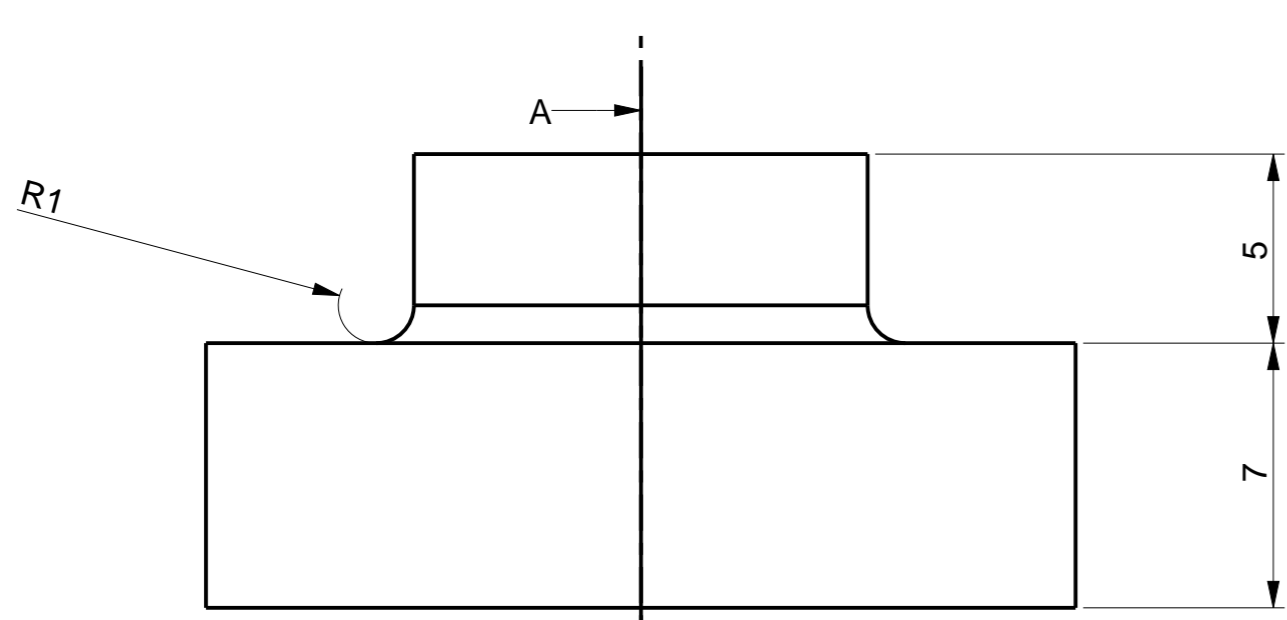
SEE DETAIL B



DETAIL B  
SCALE 20,000


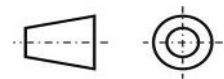


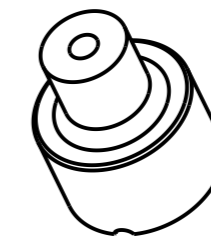
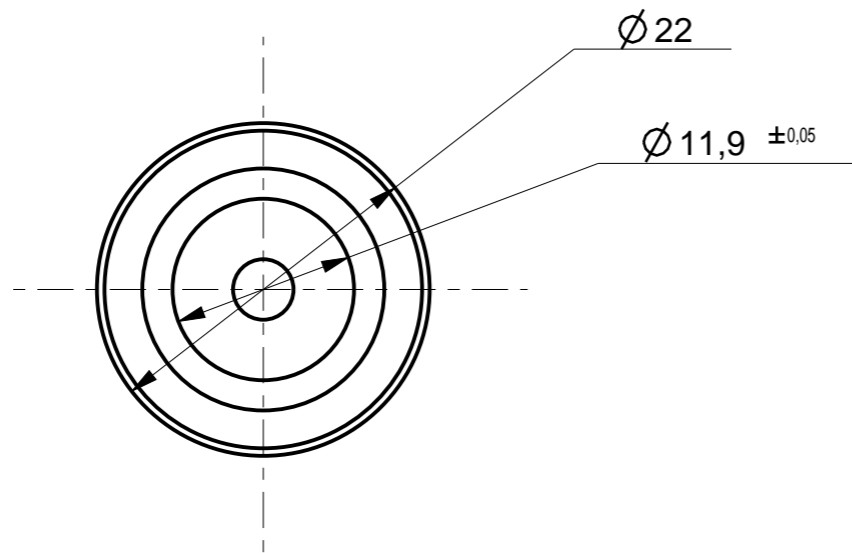
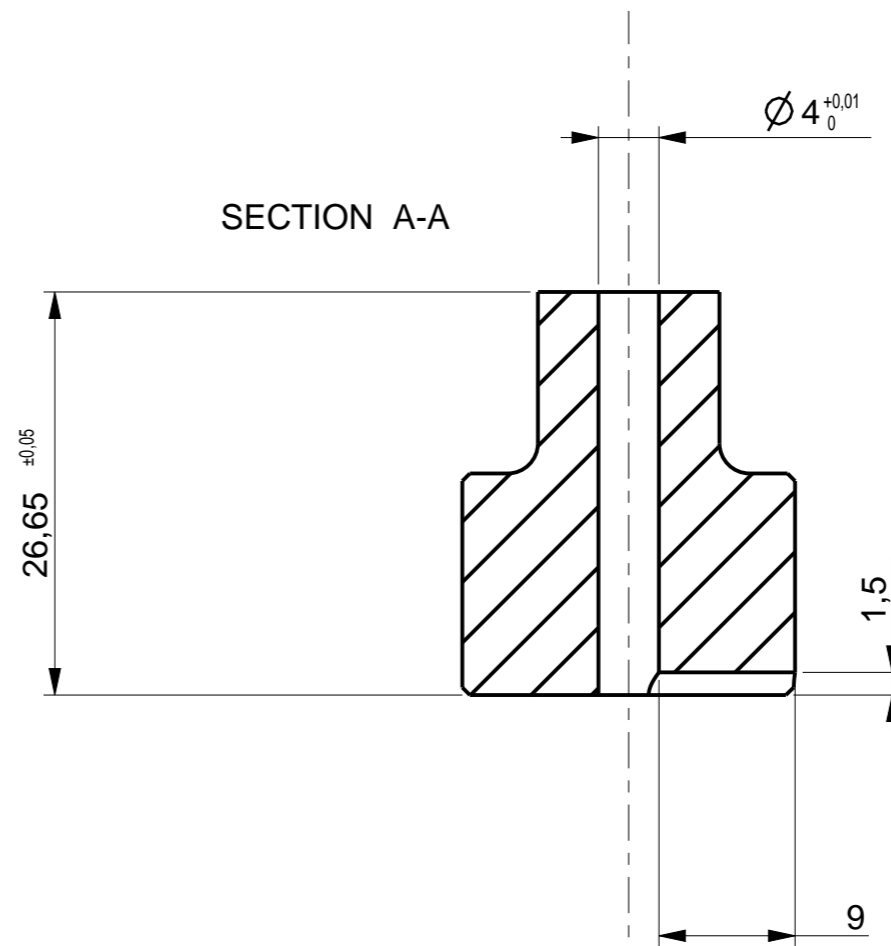
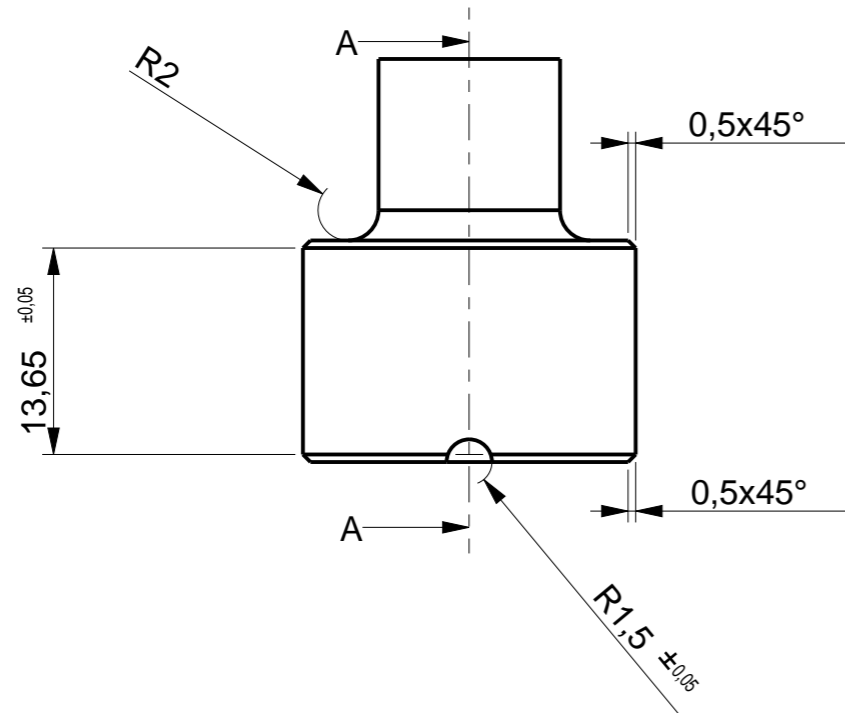
<b>IPU Process Technology</b> Produktionstorvet, Building 425, 2nd floor DK-2800 Kgs. Lyngby Phone: 45 25 46 00, fax 45 88 25 25 www.ipu.dk			Drawing by: EC	Date: Dec-01-15	Revision date:
Project: Micro-gear die system			Name: Upper inner punch n.1		
Project number:		Tolerance: ± 0.1 if not specified	Format: A3	Scale: 2,000	
Material: Tungsten carbide		Sheet: 10/12	Drawing number:		



SCALE 2,000


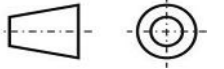
Hardened to 55 HRC  $\pm 1$

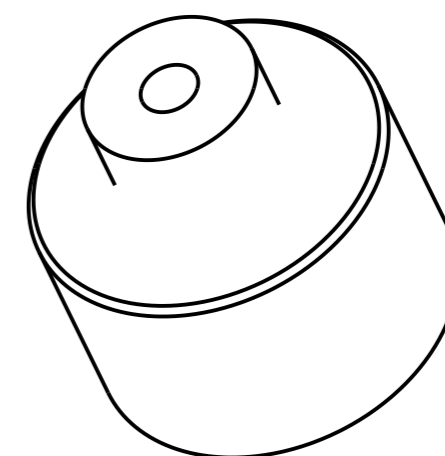
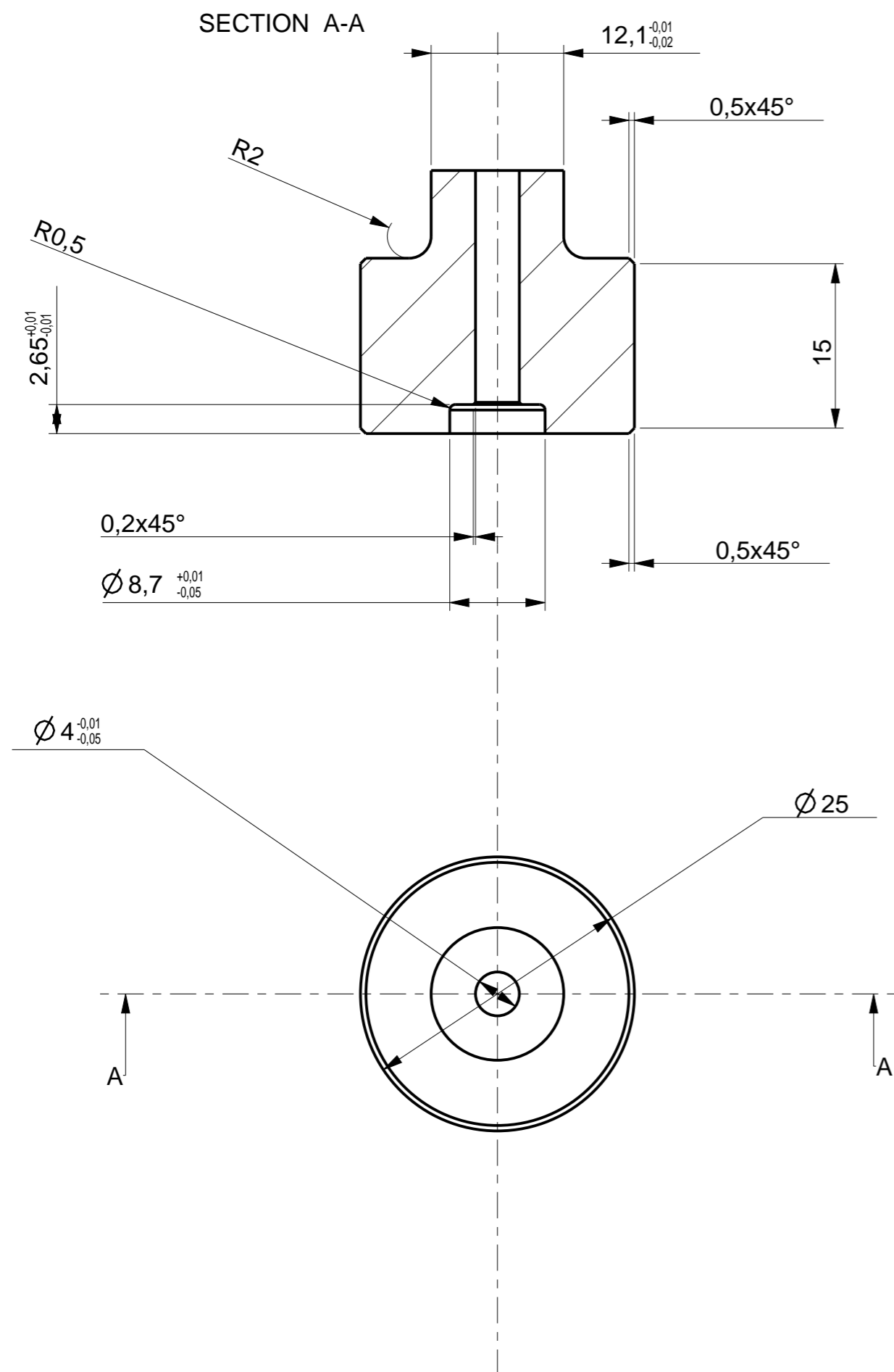
<b>IPU Process Technology</b> Produktionstorvet, Building 425, 2nd floor DK-2800 Kgs. Lyngby Phone: 45 25 46 00, fax 45 88 25 25 www.ipu.dk			Drawing by: EC	Date: Dec-01-15	Revision date:
Project: Micro-gear die system			Name: Upper punch gear n.2		
Project number:		Tolerance: $\pm 0.1$ if not specified	Format: A3	Scale: 5,000	
Material: H13 hot work steel		Sheet: 11/12	Drawing number:		





SCALE 1,000

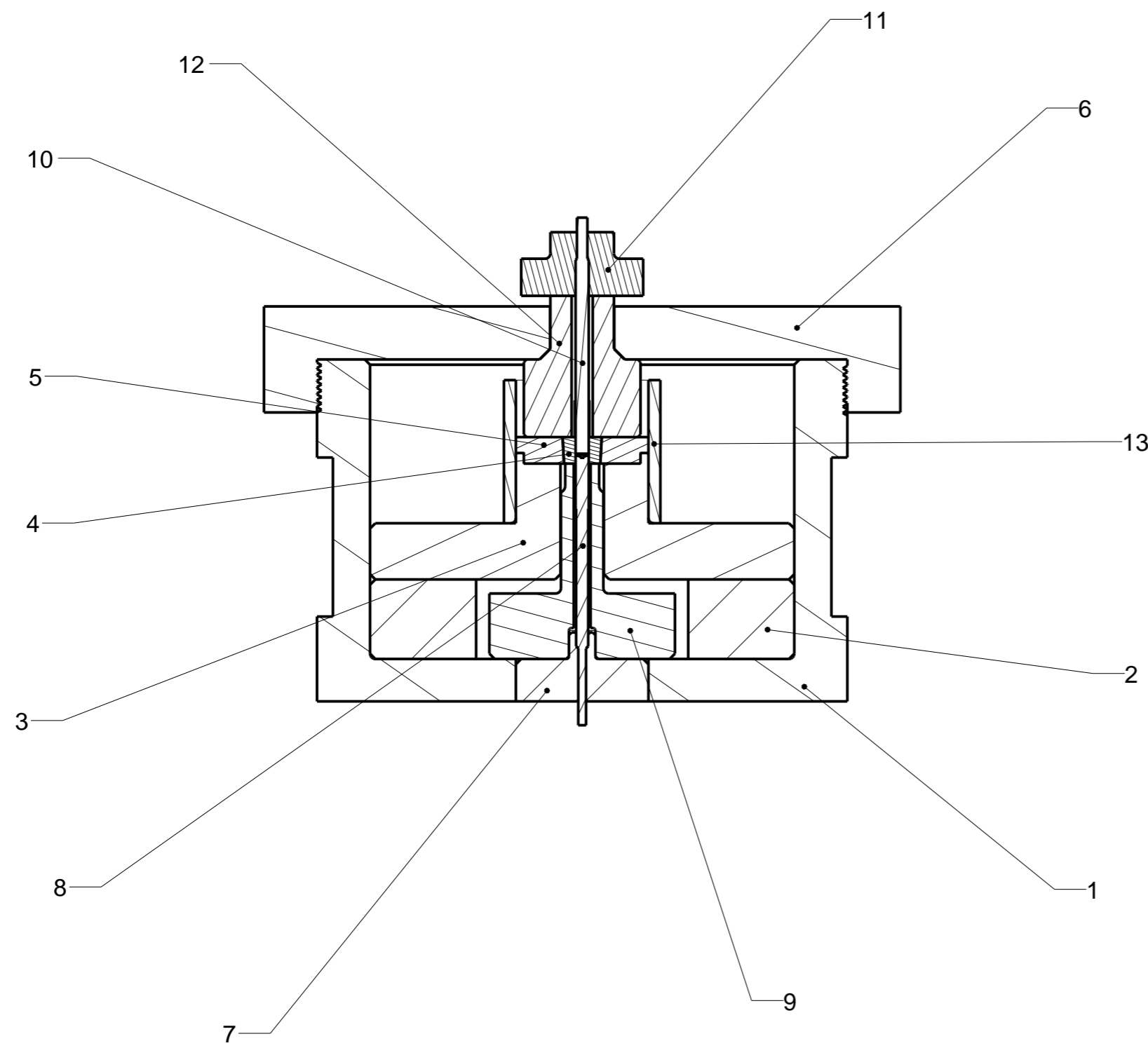
Hardened to 55 HRC ±1

<b>IPU Process Technology</b> Produktionstorvet, Building 425, 2nd floor DK-2800 Kgs. Lyngby Phone: 45 25 46 00, fax 45 88 25 25 www.ipu.dk			Drawing by: EC	Date: Dec-01-15	Revision date:
Project: Micro-gear die system			Name: Upper die punch		
Project number:		Tolerance: ± 0.1 if not specified	Format: A3	Scale: 2,000	
		Material: H13 hot work steel	Sheet: 12/12	Drawing number:	


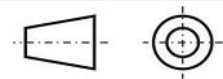


SCALE 2,000

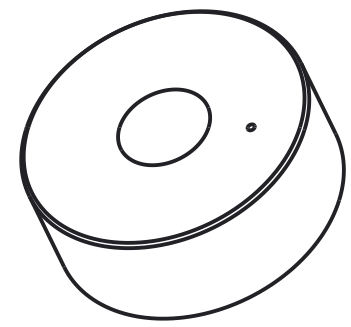
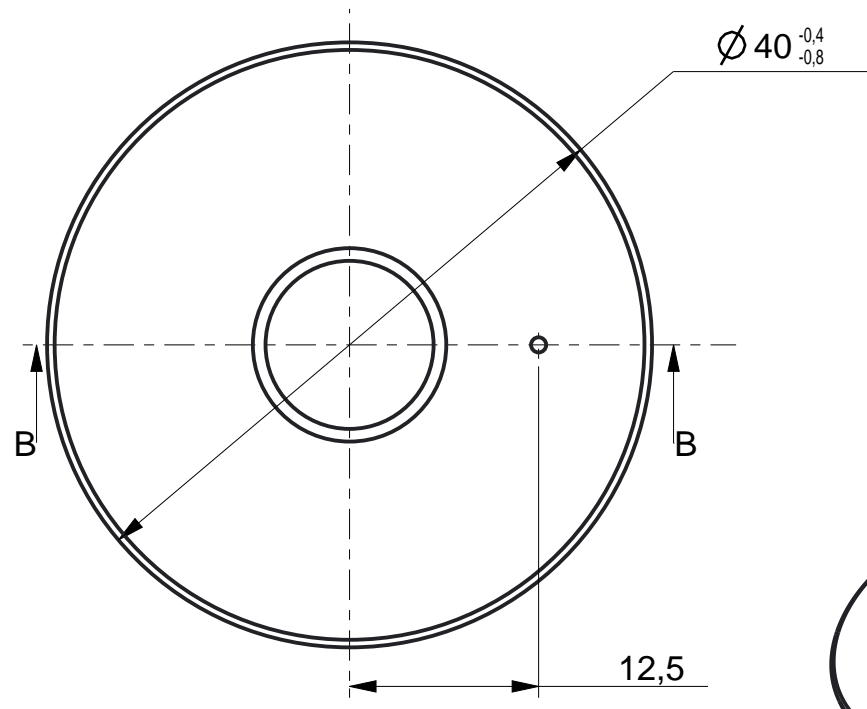
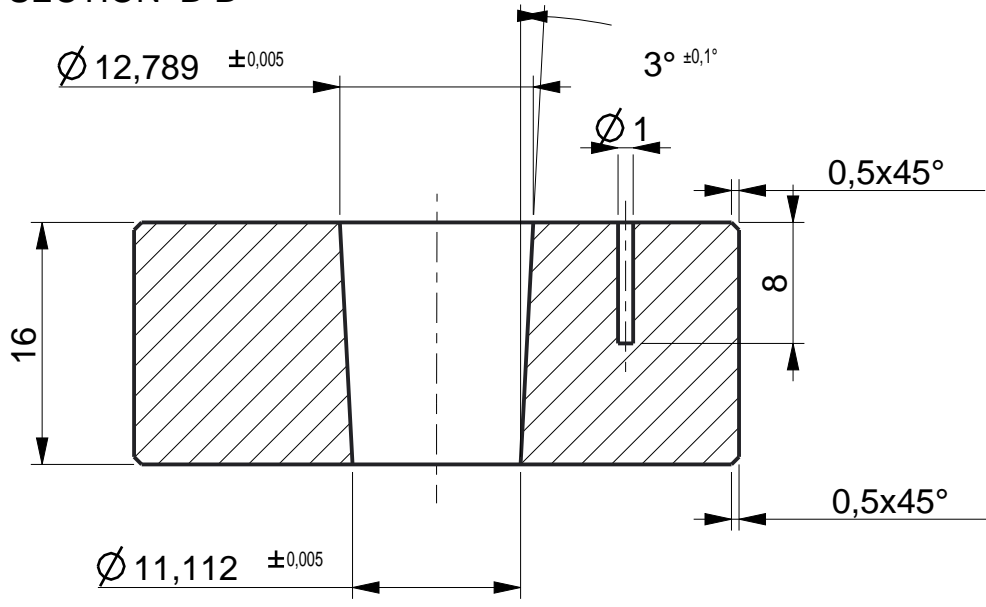
<b>IPU Process Technology</b> Produktionstorvet, Building 425, 2nd floor DK-2800 Kgs. Lyngby Phone: 45 25 46 00, fax 45 88 25 25 www.ipu.dk			Drawing by: EC	Date: Dec-01-15	Revision date:
Project: Micro-gear die system			Name: Ejection ring		
Project number:		Tolerance: ± 0.1 if not specified	Format: A3	Scale: 2,000	
		Material: A514 steel	Sheet: 13	Drawing number:	



ITEM NO	PART	QTY	MATERIAL
1	BAG	1	A514 steel
2	BOTTOM RING	1	A514 steel
3	DIE BASE	1	H13 hot work steel
4	CONICAL DIE	1	Bohler W360
5	CONICAL COMPRESSION RING	1	Bohler W360
6	SCREW COVER	1	A514 steel
7	BOTTOM INNER PUNCH N.2	1	H13 hot work steel
8	BOTTOM INNER PUNCH N.1	1	Tungsten carbide
9	BOTTOM DIE PUNCH	1	H13 hot work steel
10	UPPER INNER PUNCH N.1	1	Tungsten carbide
11	UPPER INNER PUNCH N.2	1	H13 hot work steel
12	UPPER DIE PUNCH	1	H13 hot work steel
13	HEATING NOZZLE	1	
14	EJECTION RING	1	A514 steel



<b>IPU Process Technology</b> Produktionstorvet, Building 425, 2nd floor DK-2800 Kgs. Lyngby Phone: 45 25 46 00, fax 45 88 25 25 www.ipu.dk			Drawing by: EC	Date: Dec-01-15	Revision date:
Project: Micro-gear die system			Name: Assembly drawing		
Project number:		Tolerance: ± 0.1 if not specified	Format: A3	Scale: 1,000	
Material:		Sheet: 14	Drawing number:		

SECTION B-B

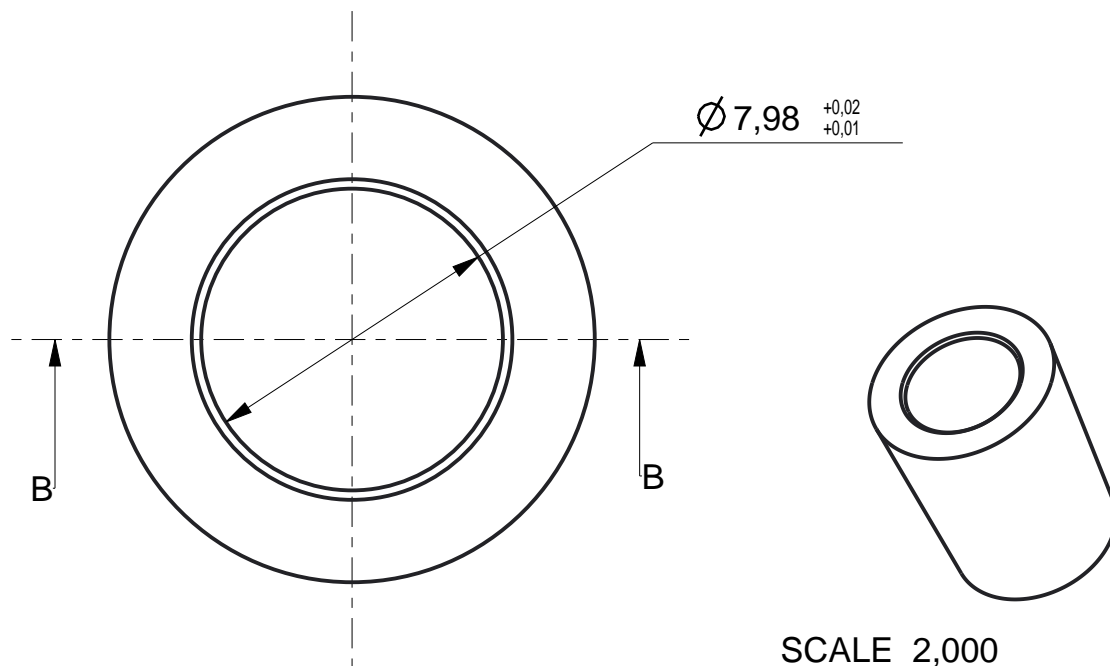
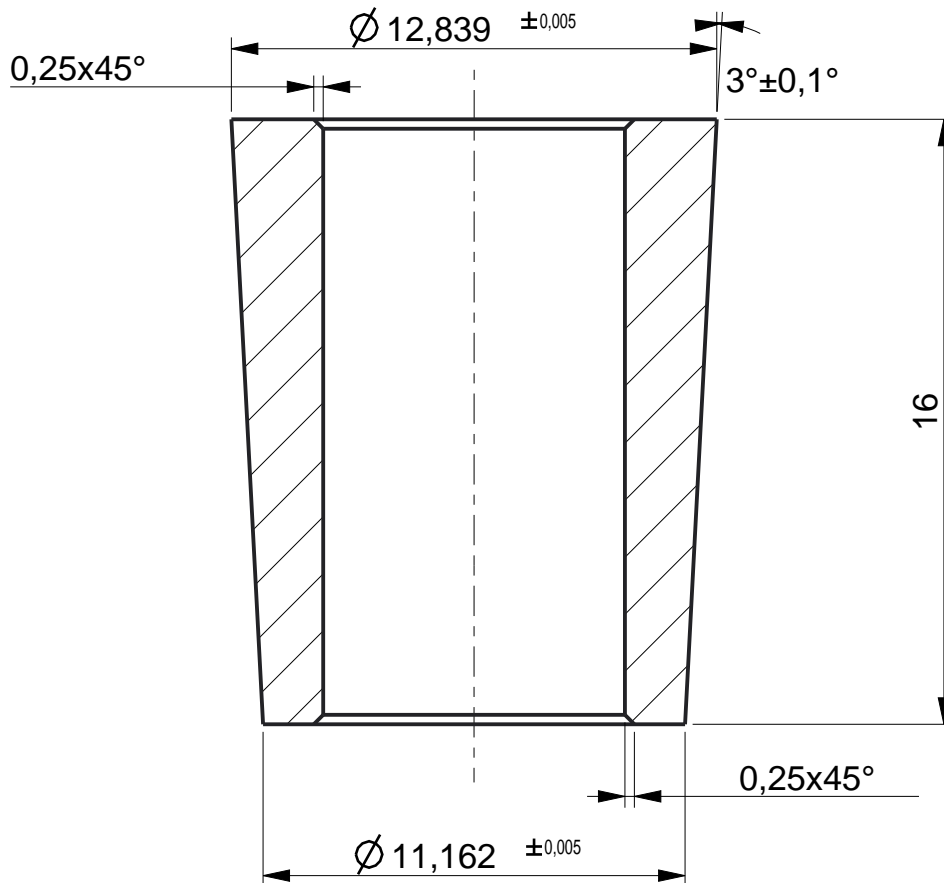


SCALE 1,000

Hardened to  $55 \pm 1$  HRC

<b>IPU Process Technology</b> Produktionstorvet, Building 425, 2nd floor DK-2800 Kgs. Lyngby Phone: 45 25 46 00, fax 45 88 25 25 www.ipu.dk			Drawing by: EC	Date: Dec-07-15	Revision date:
Project: Simplified concept			Name: Conical compression ring		
Project number:		Tolerance: $\pm 0.2$ if not specified	Format: A4	Scale: 2,000	
Project number:		Material: H13 hot work steel	Sheet: 1	Drawing number:	

## SECTION B-B

Hardened to  $55 \pm 1$  HRC

IPU Process Technology

Produktionstorvet, Building 425, 2nd floor  
 DK-2800 Kgs. Lyngby  
 Phone: 45 25 46 00, fax 45 88 25 25  
 www.ipu.dk

Drawing by:  
ECDate:  
Dec-01-15

Revision date:

Name:  
SleeveProject:  
Simplified conceptTolerance:  
 $\pm 0.2$  if not specifiedFormat:  
A4Scale:  
5,000

Project number:

Material:  
H13 hot work steelSheet:  
2

Drawing number: